The University Of Sheffield.

Novel Markers of Human Inflammatory Macrophages

By:

Rehab Alqurashi

A thesis submitted in partial fulfilment of the requirements for the degree of Doctor of Philosophy

The University of Sheffield

Faculty of Medicine, Dentistry and Health

School of Medicine

Department of Infection, Immunity and Cardiovascular Disease

November 2019

Declaration

I declare that, unless specifically stated, the work presented in this thesis is my own. Note that the results presented in chapter 5 (and parts of chapter 2, appendix III) have also been incorporated into the thesis of Kajus Baidzajevas (2019), submitted and examined under the alternative format at the University of Sheffield. Therefore, my work has been presented as part of a manuscript in preparation within this previously submitted thesis, where my contribution and authorship were clearly stated.

Background to this thesis

The work presented in this thesis was produced under the supervision of two different academic supervisors. The first part of my PhD was performed under the guidance of Dr François Guesdon, who then left his post in Sheffield. I therefore moved to the group of Dr Heather Wilson in late 2017 to complete my PhD project. The work I have undertaken in each group has encompassed distinct aspects of macrophage inflammation signalling and polarisation markers to improve our understanding of these processes and how they may relate to chronic inflammatory disease.

Acknowledgements

I would like to thank my supervisors François Guesdon and Heather Wilson for their support, guidance and patience during all stages of this PhD, without your help this thesis would not have been submitted. Special thanks to Endre Kiss-Toth for his precious advices. I also want to thank all my colleagues in our group for their support, especially Kajus Baidzajevas, Laura Campesion, Klaudia Kocsy and Chiara Niespolo. Finally, I would like to thank all technicians and blood donors for the help.

"A special thanks to my family, my mum, my husband and my kids, for their patience, support and love, being in my life is what made me capable of completing this PhD".

"شكر خاص لعائلتي، والدتي، زوجي وأبنائي، على تحملهم، دعمهم وحبهم، وجودكم في حياتي هو ما جعلني قادره على استكمال هذه الدكتوراه".

Table of Contents

List of Figures

List of Tables

List of Abbreviations

ANOVA	Analysis of variance
ATCC	American Type Culture Collection
BSA	Bovine serum albumin
C-terminal	Carboxyl-terminal (-COOH)
CIS	Cytokine-inducible SH2-containing protein
Ct	Crossing threshold
DAMPs	Damage-associated molecular patterns
DAPI	4',6-diamidino-2-phenylindole
DCD	Dermcidin
DMSO	Dimethyl sulfoxide
E2	Ubiqutin ligase enzyme 2
ECL	Enhanced chemiluminescence
EDTA	Ethylenediamine tetraacetic acid
EtBr	Ethidium bromide
FAM	6-carboxyfluorescein
FAM26F	Family with sequence similarity 26, member F
GPS	G protein pathway suppressor
HCL	Hydrogen chloride
HEPES	4-(2-hydroxyethyl)-1-piperazineethanesulfonic acid
hMDM	Human monocyte-derived macrophages
HRP	Horseradish peroxidase
ICC	Immunocytochemistry
IF	Immunoflorescence
IFN g	Interferon-gamma
IFNAR	Interferon-alpha/beta receptor
IFNGR	Interferon-gamma receptor
IHC	Immunohistochemistry
IL	Interleukin
IRF	Interferon regulatory factor
JAK	Janus kinase
LAT	Linker for activation of T cells
LDL	Low-density lipoprotein
Log2FC	log2 Fold Change
LPS	Lipopolysaccharides
M-CSF	Macrophage colony-stimulating factor
M-MLV	Moloney Murine Leukemia Virus
M1	Macrophages type 1
M2	Macrophages type 2
MAPK	Mitogen-activated protein
MHC II	Major Histocompatibility class II
MI	Myocardial infraction

MOPS	3-N-morpholino propanesulfonic acid
Mun	Unpolarised macrophages
MyD88	myeloid differentiation primary response 88
N-terminal	Amine-terminal (-NH2)
NFQ	Non-fluorescent quencher
NMD	Nonsense-mediated mRNA decay
NOS2	Nitric oxide synthesis 2
oxLDL	Oxidised LDL
PAGE	Polyacrylamide gel electrophoresis
PBMC	Peripheral blood mononuclear cells
PBS	Phosphate buffered saline
PCR	Polymerase chain reaction
PIC	Protease inhibitor cocktail
PMA	Phorbol 12-myristate 13-acetate
PPARy	Peroxisome proliferator stimulated receptor PPARy
rh	Recombinant human
RNasin	Ribonuclease Inhibitor
RT	Room temperature
RTqPCR	Real-Time quantitative PCR
SD	Standard deviation
SDS	Sodium dodecyl sulfate
SEM	Standard error of mean
SOCS	Suppressor of cytokine signalling
STAT1	Signal transducer and activator of transcription 1
TAB	TGF- β activated kinase 1 binding protein
TAE	Tris-acetate-EDTA
TAK1	Transforming growth factor beta-activated kinase 1
TAKL	TAK1-like
TBS	Tris-buffered saline
TBS-T	Tris-buffered saline and tween
TGF	Transforming growth factor
TIR	Toll/IL-1R resistance domain
TLR	Toll-like receptor
TNF	Tumour necrosis factor
TPM	Transcript per million
TRAF	TNF receptor associated factor
TRIF	TIR-containing adapter-inducing IFNb
TS	Transcription start site
WB	Western blotting

Abstract

Macrophages play an important role in innate immune responses and in tissue homeostasis, clearing pathogens, dead cells and promoting repair. Macrophages exhibit plasticity, polarising to inflammatory or repair phenotypes, according to their environment. In chronic inflammatory diseases such as atherosclerosis, excessive inflammation occurs without sufficient repair or resolution. Inflammatory macrophages in atherosclerotic plaques, activated by oxidised LDL (oxLDL), pathogens or T-cell derived cytokines are associated with plaque instability, linked to heart attack or stroke. In order to identify how plaque macrophages are altered during atherosclerosis, we need to understand signalling mechanisms and functional markers of inflammation.

We investigated the TLR4/IL-1 inflammation pathway in human macrophages. Firstly, we identified the expression of transforming growth factor (TGF)-β activated kinase-like (TAKL), and its family, comprising several splice variants, to understand how it might be altered in macrophage polarisation. Secondly, we identified the family with sequence similarity 26 member F (FAM26F) to be strongly and specifically upregulated in inflammatory macrophages. Additionally, we identified FAM26F interacting protein partners to explore its function in inflammation. We found that mRNA expression of TAKL-L is up regulated, while FAM26F expression at mRNA and protein levels was strongly elevated, in inflammatory macrophages. In addition, we identified linker of T cell activation (LAT) as a potential FAM26F interacting partner. These findings help to understand inflammation changes in macrophages with future potential to detect changes in vulnerable atherosclerotic plaques.

Chapter 1
General Introduction

1.1. Inflammation

Inflammation is a key response in the body's defence mechanism. It is the means through which the immune system identifies and eliminates harmful pathogens and initiates the healing process. Inflammation can occur acutely or chronically. Acute inflammation is triggered in response to tissue damage as a result of noxious compounds, pathogen invasion. It starts slowly, with mild symptoms within a short period and then may endure for instance in acute pneumonia or cellulitis, followed by a resolution phase. On the other hand, chronic inflammation is also considered as slow, enduring inflammation lasting for many months and even years, where resolution is ineffective or incomplete. Generally, the level and impact of chronic inflammation differs with the cause of the injury and the capacity to overcome the harm or damage and for repair to follow (McKenzie et al., 2014).

Immunologists have defined inflammation as involving two important components. The first one is innate immunity; this depends on granulocytes and complement. Granulocytes are white blood cells containing enzyme-filled granules that normally destroy harmful substances or foreign particles. The complement system, consisting of a cascade of protein fragments that support the innate immune cell response and can be recruited by the adaptive immune system. Adaptive immunity is the second and later response to specifically target pathogens, with a "immunological memory" where specific antibodies to a target are synthesised and available for rapid recruitment upon subsequent infection. This involves white blood cells known as lymphocytes. In this process, the T cells are the main strategists, directing chemicals and cells to alleviate the infectious pathogen. B cells generate antibodies, which recognise specific pathogens and recruit complement to destroy the invading pathogen (Heppner et al., 2015).

Macrophages (from the Greek, "big eaters") function to eliminate microbes, cellular debris and dead granulocytes developed in the immune response. Although macrophages clean up, they also display some innate immune memory where they undergo phenotype re-programming upon exposure to separate pathogens (Fujiwara and Kobayashi, 2005, Prame Kumar et al., 2018).

As pathogens are cleared, suppressor T cells lower the inflammatory reaction, such that the regeneration of the damaged tissue from the immune system can commence. Fibroblasts generate fibrin and collagen, to develop a support for newly synthesised tissue cells. If the damage is massive, collagen and fibrin may become thicker to substitute the new tissue and develop a scar (McKenzie et al., 2014).

As discussed above, inflammation is a defence mechanism that is essential to our health. Often, during acute inflammatory responses, molecular processes successively reduce infection or injury. This is followed by a re-balancing of tissue homeostasis and resolution of the acute inflammation. When acute inflammation becomes unbalanced this can result in a number of chronic inflammatory diseases (McKenzie et al., 2014).

Inflammation is classically described as pain, swelling, redness, loss of tissue function and heat, which originates from local immune, inflammatory and vascular cell reactions to injury or infection. Vital microcirculatory changes take place during the inflammatory process mediating altered vascular permeability, leukocyte recruitment and inflammatory mediator release (McKenzie et al., 2014, Shalapour and Karin, 2015).

Different pathogenic factors, for instance, cardiac infection, tissue damage, can cause inflammation by triggering tissue injury. The causes of inflammation can be attributed to non-infectious and infectious. In reaction to tissue damage, the body starts a signalling cascade that induces repair processes for healing damaged tissues. These signals trigger leukocyte chemotaxis from the main circulation into areas of injury or damage (Shalapour and Karin, 2015). These activated leukocytes secrete cytokines that stimulate inflammatory reactions.

1.1.1. Inflammatory diseases

It is well established that inflammation is a critical host response to infection and injury. However, epidemiological and molecular studies have progressively demonstrated that inflammation is also associated with a wide range of non-infectious diseases, including autoimmune disorders, cancers, and inflammatory disease such as type 2 diabetes, rheumatoid arthritis and atherosclerosis. When inflammation takes place, molecular signals (often cytokines and chemokines) are secreted from the white blood cells into damaged tissue or into the blood leading to an increased blood supply to the area of infection or injury, and therefore to warmth and redness. Some of these chemicals trigger a leak of fluid into the tissue, leading to swelling. For instance, in arthritis, the protective process may as well activate neurones and cause pain. The increased number of cells and inflammatory cytokines within an inflamed joint lead to swelling and irritation of the joint lining and, finally, destruction of cartilage (Tanaka et al., 2014).

1.1.2. Inflammation and Cancer

Inflammation and cancer were linked together since 1863 by Virchow, who noticed that caners generated from chronic inflammation sites. After that many researchers have observed that chronic inflammation is associated with the development of tumorigenesis during the phases of initiation, progression and metastasis (Balkwill and Mantovani, 2001, Coussens and Werb, 2002). Additionally, the work of Kumar, Nicholls, & Wong (2018) offered an explanation that tumour initiation from DNA damage may be triggered by reactive oxygen species produced by immune cells. The role of inflammation in the ensuing processes that result in cancer metastasis is less apparent and may involve signalling and crosstalk between the host immune system and the tumour cells (Prame Kumar et al., 2018). Chronic inflammation triggers cancer through tissue damage and reprogramming of the cell specificity, contributing to modifications in gene expression that promoting tumorigenesis. The persistence of inflammatory proteins sustains an environment in which tumour cells can multiply. Specifically, inflammatory mediators such as chemokines and cytokines, when they persist in the reddened tissue, can proliferate, adjusting their environment to promote survival and cellular transformation (Balkwill and Mantovani, 2001, Coussens and Werb, 2002).

Since chronic inflammation underlies may diseases, it would be appropriate to identify it as a condition that should be managed independently as a preventive treatment. The major concern with targeting inflammation is that this response is fundamental to fighting infection and maintaining tissue homeostasis while chronic dysregulated inflammation is often a result of a loss of homeostasis and inability to repair. Disease is often triggered by environmental and genetic factors. Intrinsically, efforts to relieve chronic inflammation are complicated by the fact that the disease is already initiated and sustained, which is often difficult to reverse.

1.2. Macrophages and their role in inflammation

The inflammatory process is usually tightly controlled, involving both signals that start and sustain inflammation and signals that dampen down the process. An imbalance between the two processes causes dysregulated inflammation, leading to tissue and cellular damage. Macrophages are a key cell type of the mononuclear phagocyte system comprised of cells of bone marrow origin. Monocytes are produced from stem cells in the bone marrow which are distributed throughout the blood stream. Once a monocyte gets out of blood, it differentiates into a fixed or wandering macrophage. Macrophages contain organelles known as phago-lysosomes, which destroy and engulf bacteria. Circulating blood monocytes are recruited into different tissues and then differentiate to macrophages. During the process of inflammation, macrophages have three key functions; immunomodulation, phagocytosis, and antigen presentation through the production of different cytokines and growth factors. Macrophages have an essential role in the initiation, maintenance and resolution of inflammation. During the inflammation process, macrophages are activated and inactivated. Activation is promoted by cytokines, extracellular matrix proteins, bacterial lipopolysaccharide, and other chemical mediators and pathogen patterns (Liu et al., 2014).

Macrophages play critical roles in inflammation, healing and renewal by cleaning up cell debris, activating and resolving inflammation and enhancing fibrosis with key functions in all stages to the response to damage. Tissue damage causes a complex sequence of cellular reactions, beginning from inflammation activated by cell and tissue injury and ensuing healing. By cleaning up cell debris, triggering and addressing the inflammation problem and enhancing fibrosis, macrophages play critical responsibilities, if not all, stages of the reaction to damage or injury. Recent studies on the mechanisms underlying early inflammation and subsequent tissue renewal and repair demonstrated that macrophages coordinate these processes in part by boosting and activating progenitor or stem cells, removing all damaged tissue, restoring extracellular matrix to support angiogenesis. However, macrophages are also implicated in chronic diseases caused by failed resolution of inflammation and excessive tissue damage (Sinder et al., 2015). See figure 1.1 as a summary for macrophage role in inflammation.

Neutrophils and macrophages detect pathogens through cell-surface receptors that can distinguish between the surface molecules showed by pathogens and those of the host. Natural killer cells and cytotoxic T lymphocytes alongside macrophages coordinate the destruction of virus-infected cells. Helper T cells can also identify virus-infected cells and produce multiple cytokines to regulate this process (Chinetti-Gbaguidi et al., 2015, Prame Kumar et al., 2018) . Macrophages are key in priming the immune system during an infection. Macrophages scavenge and destroy pathogens and even infected cells. Macrophages produce signals that coordinate the activation of other types of cells to fight against diseases or infections. The antibodies, produced by adaptive immune cells, recognise antigen which is then overwhelmed and digested by macrophages. On the other hand, white blood cells can secrete chemicals known as antitoxins which engulf the poisons or toxins some bacteria produce especially when they have attacked the body (Chinetti-Gbaguidi et al., 2015, Fujiwara and Kobayashi, 2005) . In addition to this, macrophages play a key role in the process of wound healing when activated by specific cytokines including IL-4 and IL-10. This type of macrophage will generate either polyamines or proline to promote collagen production (Mills and O'Neill, 2016).

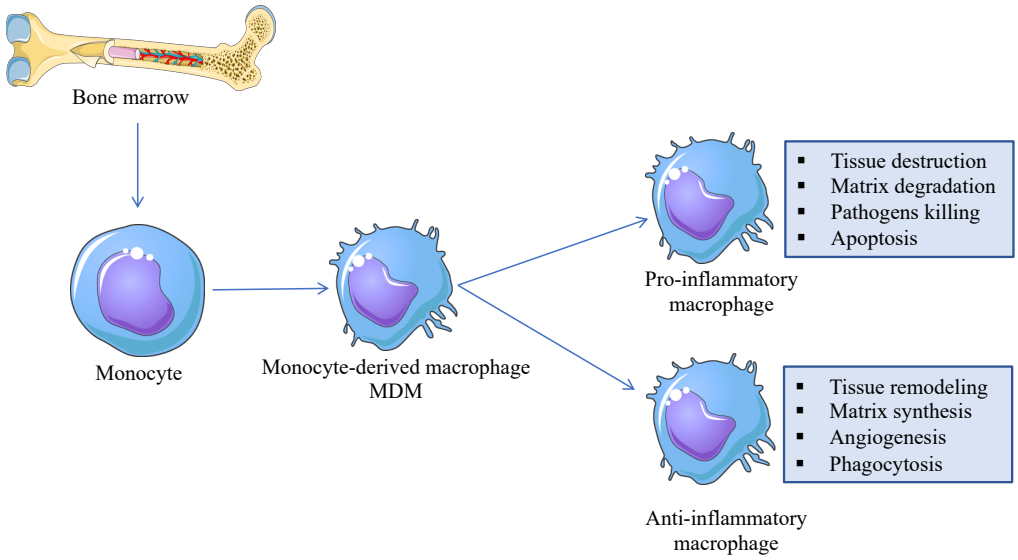

Figure 1.1 Macrophage role in inflammation
The image shows the blood circulating monocyte-derived macrophage (MDM) and the two different types of macrophage (pro-inflammatory and anti-inflammatory). The boxes in the right side shows the roles of macrophages in inflammation, which is a tissue injury or a tissue repair (wound healing) depending on the macrophage phenotype (pro-inflammatory or anti-inflammatory, respectively).

1.2.1. Macrophage activation and polarization

Macrophages have a critical responsibility in the immune system in both innate and acquired immunity. In innate immunity, resident macrophages offer direct protection against foreign substances and organise leukocyte activation. Macrophages also play a role towards the balancing of apoptotic cells, microbes and perhaps neoplastic cell. Macrophages as well work together with T and B cells, through cell-cell interactions. They secrete enzymes, chemokines, cytokines, and arachidonic acid metabolites, and also oxygen radicals in these processes. Macrophage stimulation can either be anti-inflammatory or pro-inflammatory, resulting in tissue damage or resolution, repair and healing. Therefore, macrophages have a vital role in stimulating, ordering and terminating the immune response; they exhibit plasticity to alter phenotype towards inflammatory or repair functions dependent on signals received in their local tissue environment (Murray et al., 2014, Tabas and Lichtman, 2017).

In the past, T cells were regarded as the primary organisers of the immune response while macrophages were just considered effector cells that are only active during acute inflammatory reactions and delayed category hypersensitivity responses. In 1986, Mosmann, Coffman and associates recorded that murine lymphocytes could be classified into Th1 and Th2 cells, based on their individual cytokine production: IL-4 and IFNγ. Moreover, they demonstrated that these cytokines exhibit cross-control characteristics and organise immune responses that are often described as the type I and type II immune response (Mosmann et al., 1986). The cross-talk between adaptive immune cells via cytokine production (such as IL-10, IL-12 and IFNγ) and macrophage polarisation has been described more recently (de Torre-Minguela et al., 2016).

Macrophages are tissue-resident or recruited and specialised phagocytes, which play a critical role in immune-instruction. Activated macrophages have been traditionally grouped into either classically activated M1 inflammatory macrophages or alternatively activated M2 macrophages. The M1 macrophages are pro-inflammatory and have a key responsibility in host defence against diseases or infection whereas M2 macrophages associated with anti-inflammatory responses and tissue restoration, representing the two extremes of the full range of macrophage activation. More recent evidence shows that the M1/M2 paradigm is simplistic since macrophages can polarise to a spectrum of phenotypes and intermediate states between these. M1 and M2 polarisation of macrophages is a finely regulated process involving a group of signalling pathways, posttranscriptional and transcriptional controlling networks (Martinez and Gordon, 2014).

1.2.2. Classically activated M1 macrophages

The M1 phenotype of macrophage is promoted by pro-inflammatory cytokines or microbial products. Interferon-gamma (IFNγ) is the primary the cytokine manufactured from Th1 cells that drives macrophages toward the M1 phenotype. The IFNγ receptor is constituted of the interferon-alpha/beta receptor (IFNAR) and interferon-gamma receptor (IFNGR) chains. The receptor binds to Janus kinase one and two adaptors resulting in signalling and phospho-activation of the signal transducer and activator of transcription 1 (STAT1). IFNγ stimulates the expression of major histocompatibility class II (MHC II), suppresses the suppressor of cytokine signalling 1 (SOCS1), nitric oxide synthesis 2 (NOS2), and IL-12. IFNγ along with LPS signals a strong polarisation of macrophages towards the M1 phenotype, although IFNγ and LPS activate distinct receptors and signalling pathways (Martinez, & Gordon, 2014).

Bacterial moieties are identified by pattern recognition receptors, for instance, Toll like receptors (TLRs). TLR4 is activated by LPS, then this activation stimulates the down-stream signalling starting with Toll/IL-1R resistance (TIR) domain–containing adapter-inducing IFNβ (TRIF) and myeloid differentiation primary response 88 (MyD88) pathways. TRIF activation leads to a cascade of kinase phosphorylation signalling events, which eventually results in the stimulation of transcription element interferon-responsive factor 3 (IRF3). This factor regulates the synthesis and secretion of Type 1 interferons, IFNβ and IFNα which subsequently bind IFNAR with resultant stimulation of STAT1. The other TLR4 MyD88 pathway stimulates NF-kB pathway, a critical transcription element associated with M1 macrophage polarisation. Moreover, MyD88 stimulates activator protein1 through mitogen-activated protein (MAPK) signalling (Hamilton, Thomas. et al. 2014). These pathways control a large number of inflammatory genes including pro-inflammatory cytokines (TNF, IL-12, IL-6 and IL-1β), chemokines (CCL2, ligand 10), antigen-processing molecules and co-stimulatory molecules. Cytokines secreted from stimulated macrophage or other cells activate cytokine receptors, which often regulate pro-inflammatory signalling to promote the M1phenotype (Martinez and Gordon, 2014, Vergadi et al., 2017). See figure 1.2 below for M1 signalling pathways.

1.2.3. Alternatively-activated M2 macrophages

Polarisation of macrophages towards an "M2" phenotype is typically driven by IL-4 and IL-13, which attach to the receptor IL-4α activating various pathways including Janus kinases-1 and 3 (JAK1 and JAK3) signalling which subsequently drives stimulation and translocation of STAT6. Other drivers towards M2 polarisation include interferon regulatory factor 4 (IRF4) and peroxisome proliferator stimulated receptor (PPARy), activated by fatty acid receptors. These upregulate arginase 1, resistin-like- α, CD206 and Ym1 (Bi et al., 2019, Vergadi et al., 2017) (see figure 1.2).

Another cytokine (IL-10) has been found to enhance M2 macrophages. IL-10 binds to IL10R2 and IL10R1. Ligation of IL-10R results in receptor auto phosphorylation inducing the stimulation of the transcription factor STAT3, in turn activating SOCS3, which down-regulates pro-inflammatory cytokines signalling pathways (Chuang et al., 2016, Vergadi et al., 2017).

M2 macrophages is the tissue remodelling/repairing phenotype by secreting cytokines including TGFβ and IL-10. Targeting M2 macrophages may contribute as a potential treatment strategy in atherosclerosis (Bi et al., 2019).

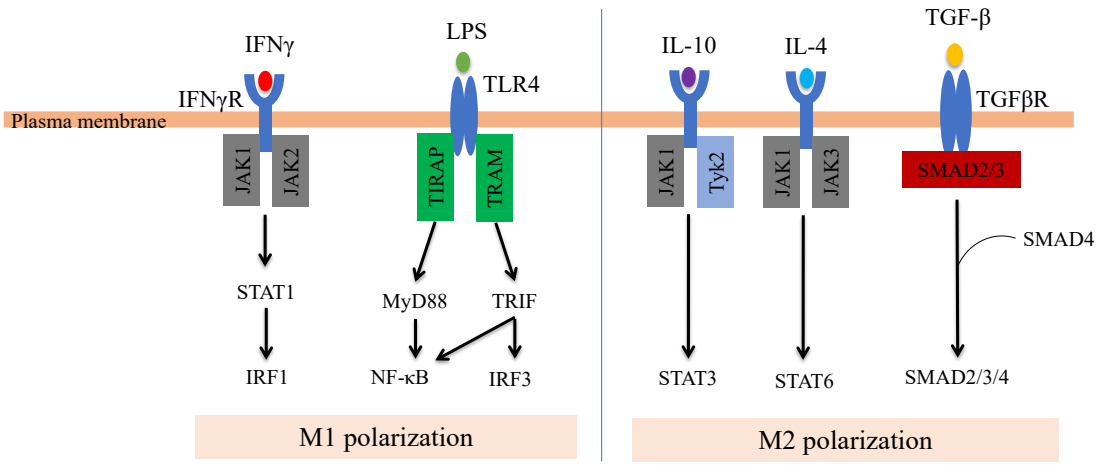

Figure 1.2 M1 and M2 polarization signalling in immune response
This image shows the activation process of pro-inflammatory (M1) and anti-inflammatory (M2) macrophage signalling pathways in immune response, which can be activated by different receptors. This picture shows the widely used polarization agents; IFNγ and LPS for M1, IL-10, IL-4 AND TGF-β for M2. The down-stream signalling then leads to the activation of transcription factors and induce different genes expression.

1.3. Atherosclerosis

Atherosclerosis was identified as a cholesterol storage inflammatory disease and it is the most common cause of coronary and cerebrovascular diseases. Inflammation responses are found to mediate all atherosclerosis stages (initiation, progression and complications from loss of plaque stability). Clinical studies had found a potent link between inflammatory cytokines as prognostic markers with patients of acute coronary syndrome. Atherosclerosis is also described as a chronic and deteriorating disease affecting medium and large-sized arteries. Atherosclerotic plaque rupture or vessel occlusion results in acute myocardial infarction (MI) or stroke (Libby et al., 2002).

The initiation of atherosclerosis (atherogenesis) is due to accumulation of low-density lipoprotein (LDL) cholesterol into the sub-endothelial intima. LDL accumulates in areas of disturbed blood flow and low shear stress, which leads to endothelial cells activating to a proatherogenic phenotype. Activated endothelial cells express adhesion molecules promoting interaction with circulating monocytes, which transmigrate across the arterial wall, differentiating to macrophages. Arterial macrophages engulf LDL and become foam cells (Libby et al., 2002, Moore et al., 2013) (see figure 1.3).

Various environmental risk factors (including smoking and high sugar diet) cause high blood pressure by disrupting endothelial cell activity and also promoting atherogenesis. The critical role of LDL in the progression of atherosclerosis has led to the development of effective lipid-lowering therapies, which have reduced cardiovascular diseases. Reduction in smoking and hypertension has resulted in a fall in cardiovascular disease burden. The role of inflammation in the process of atherogenesis has been reported over recent years. Lipid deposition into the arterial wall enhances inflammation activating a systemic and local immune response. Despite lipid-lowering treatments there is still a need to dampen inflammation, particularly to reduce the risk of plaques becoming vulnerable to rupture (Moore et al., 2013, Jaipersad et al., 2014). Most recently the anti-inflammatory therapy, canakinumab, which is an anti-interleukin1 beta antibody, was found to be effective in the treatment of coronary atherosclerosis (Ridker et al., 2017), although this has yet to be approved for licencing.

1.3.1. Monocyte/macrophage role in atherosclerosis

Blood monocytes are recruited to the atherosclerotic plaque, which then differentiate to macrophages within the artery wall. Cellular production of chemokines and cytokines, including CCL-2 and MCP-1 appear to play a critical role by recruiting circulating monocytes into the plaque. Interestingly, mouse atherosclerosis models have shown that a specific subset of monocytes are differentially recruited into the atherosclerotic plaque. Specifically, monocytes expressing high levels of Ly6Chi, seem to be the most dominant suppliers to plaque macrophages in mice. The human equivalent of $Ly6Chi^{+}$ monocytes are the $CD14^{+}CD16^{-}$ classical subset of monocytes, which have a proinflammatory role, although these monocytes have been previously recorded to define cardiovascular occurrences. The intermediate $CD14^{hi}CD16^{+}$ monocyte subset has been identified as the main subset involved in promoting atherosclerosis (Schober et al., 2015, Chinetti-Gbaguidi et al., 2015).

The stimulation of immune cell pattern recognition receptors in the arterial wall is thought to initiate atherogenesis. The damage-associated molecular patterns (DAMPs) that promote macrophage inflammation include cholesterol crystals and heat shock proteins, although pathogen priming is often required to initiate this process. Recent evidence also demonstrates that LDL in the subendothelial space is a key DAMP involved in activating inflammation. Oxidised (ox-LDL) are identified by a number of pattern recognition receptors in particular, Toll-like receptor 4 (TLR4). TLR4 is highly associated with human atherosclerosis (Jaipersad et al., 2014, Camaré et al., 2017), it is an essential stimulus of the innate immunity and it is known to bind to lipopolysaccharide (LPS). TLR4 is expressed in many cells such as dendritic cells, macrophages, neutrophils, B cells and mast cells (Garay-Malpartida et al., 2011).

In plaque macrophages, an imbalance has been found to occur between cholesterol uptake and efflux, causing an intracytoplasmic build-up of cholesteryl lipid droplets. This results in the development of lipid-laden foam cells, which are typically seen in atherosclerotic plaques. Cholesterol crystals can also stimulate the inflammasome, which may cause cell death by apoptosis or necrosis (Tall et al., 2002). Inflammasomes are known to recruit multiprotein complexes, receptors and sensors, that activate caspase-1 and lead to the expression of pro-inflammatory cytokines such as IL-1β and IL-18, and proteolytic cleavage and cell death (Schroder and Tschopp, 2010).

Macrophage necrosis results in the growth of the necrotic core in the atherosclerotic plaque. The necrotic core is primarily constituted of cellular debris, and lipid components and thus is extremely thrombogenic. It is separated from the arterial lumen by a fibrous cap. A rupture of the fibrous cap starts a process of intraluminal thrombosis, which leads to acute events including MI and stroke. Thinning and rupture of the fibrous cap seems to be more probable with higher foam cell numbers, upregulation of T-cells, and inflammatory activation (Tall et al., 2002) (see figure 1.3).

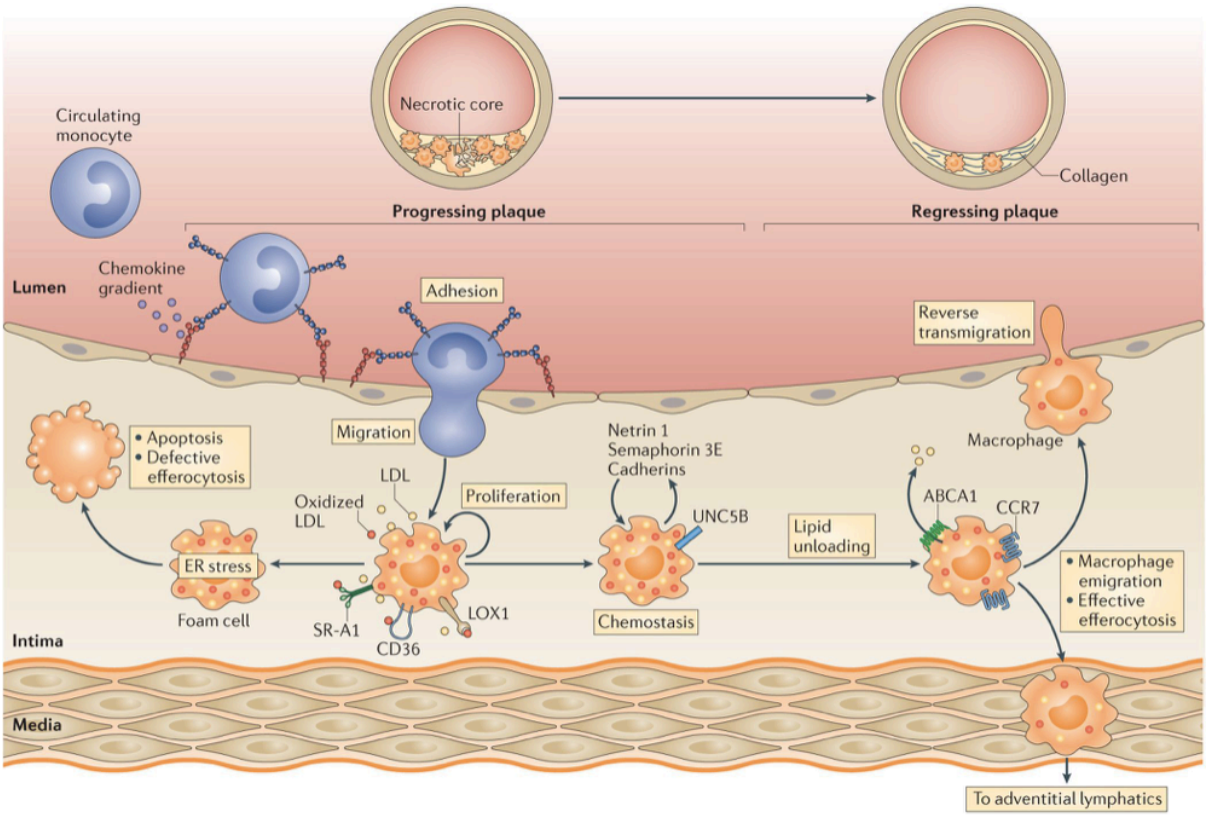

Figure 1.3 Macrophage in atherosclerotic plaque formation (Moore et al., 2013)
The image represents a schematic illustration of plaque progression in the artery wall, which happens as a result of monocyte/macrophage differentiation and activation into inflammatory foam cells. It shows the imbalance in lipid metabolism in lipid-laden macrophage, which leads to LDL and ox-LDL accumulation and endoplasmic reticulum (ER) stress and resulting in apoptosis/necrosis, that causes the collagen building up and plaque formation.

1.3.2. Atherosclerotic plaque neoangiogenesis

The development of a lipid-rich necrotic core in the arterial wall in the process of atherogenesis essentially brings the development of a hypoxic environment. The physical reaction to hypoxia is an intricate genetic process resulting to the development of new blood vessels, termed neoangiogenesis, and concentrated neoangiogenesis occur in the atherosclerotic plaque. Significant to note, highly neovascularised artery regions seem to be more susceptible to rupture and ultimately contributes to acute MI or stroke. Intraplaque haemorrhage is an complex process leading to established atherosclerotic plaques becoming highly vulnerable to rupture and therefore extremely unstable (Jaipersad et al., 2014).

Lymphocytes within the plaque supply more phospholipid and cholesterol, triggering the development of the necrotic core and promoting inflammation. Inflammation as such has been demonstrated to have a critical role in the neoangiogenesis process and particularly macrophages have been demonstrated to be central in the development of new blood vessels. In the surrounding region, innate immune cells secrete proangiogenic factors, including VEGF, FGF and MMPs, activating endothelial outgrowth, and breakdown of the extracellular matrix to allow new vessel growth. The new blood vessels seem characteristically dysfunctional, often allowing blood outflow into the vessel wall, promoting plaque progression, new hypoxia, and more angiogenesis. The connection between hypoxia, macrophage plaque progression, and neoangiogenesis has been seen in human histological studies, and less so in animal models of disease (Moroni et al., 2019, Tabas and Lichtman, 2017). Additionally, a recent study suggested that $CD168^{+}$ has role in developing plaque angiogenesis, via non-lipid related mechanism, by elevation the expression of vascular cell adhesion molecule (VCAM) that is associated in increasing macrophage density (Guo et al., 2018).

In addition to macrophage and lymphocytes, there are other cell types that are also involved in the vulnerability of atherosclerotic plaque. Studies had identified many T cells, few B cells, NK cells and mast cells, while the most dominant cells were the smooth muscle cells in the fibrous cap, and monocyte-derived macrophages in the lipid core (Jonasson et al., 1986, Rekhter and Gordon, 1995). It has been found that these inflammatory cells contribute in the atheroma development and promote replication of smooth muscle cells which leads to an increase in lesion size (Hartman and Frishman, 2014). Therefore, studying the interaction between these different cell types is useful in understanding the pathogenesis of atherosclerosis.

1.3.3. Macrophage phenotypes in atherosclerosis

The objective of this section is to assess the current evidence on the role of macrophages and monocytes in human atherosclerosis in relation to plague features, patient diagnosis and the potential opportunity to use macrophage phenotype labelling as biomarkers of disease.

Many studies observed a strong link between inflammatory "M1" macrophages in human atherosclerotic plaques associated with disease. Moreover, most recent studies show lower numbers of M2 macrophages within plaques susceptible to rupture. M1 macrophages were demonstrated to be enhanced in the regions of plaque more susceptible to rapture, whereas M2 were found in higher numbers in stable regions of the plaque (Tabas and Lichtman, 2017, Newby Andrew, 2008). Histological studies of the plaque show that carotid artery plaques have a larger proportion of M1 macrophages compared to femoral artery plaques with less disease (Stöger et al., 2012, Cho et al., 2013). Moreover, a recent study exploring 110 human aortic plaques demonstrated that both M1 and M2 subgroups are connected to advanced atherosclerosis and susceptible plaques (de Gaetano et al., 2016). However, most of the available evidence on the role of macrophages and monocytes in atherosclerosis is from animal studies. Therefore, to study the human proinflammatory macrophage role in atherosclerosis, we require a marker that is specifically expressed in M1 and not in other macrophage subtypes. Moreover, its expression has to be conserved in other species to carry out and compare, *in vitro* and *in vivo,* experiments to study the role of M1 macrophages in atherosclerosis.

1.4. TAK1-like (TAKL) gene as a potential new macrophage marker

The TAK1-like (TAKL) gene was first discovered in 2001 (Reymond et al., 2001). It is homologous to a regulatory domain of Transforming growth factor (TGF)-β activated kinase (TAK1), but unlike TAK1, TAKL does not have a protein kinase domain. The gene is located on human chromosome 21 and is also known as C21orf7 in human and ORF63 in mouse. It encodes several alternative transcripts and can potentially produce four different proteins.

The partial homology of some TAKL proteins to the kinase TAK1 and some experimental results suggests that they could participate in the TNF Receptor-Associated Factor (TRAF) / TAK1 signalling pathway, which controls immune and inflammatory responses (Chung et al., 2002, Xie, 2013).

The expression of TAKL has been studied by several groups (Reymond et al., 2001, Li et al., 2004, Taira et al., 2005, Kilpinen et al., 2010). The gene is expressed in all tissues tested in both mouse and humans (Reymond et al., 2001), in mesenchymal, adult and differentiating stem cells (Taira et al., 2005), in several carcinomas-derived cell lines (Li et al., 2004) and in lymphomas (Kilpinen et al., 2010). Interestingly, TAKL appears to be most strongly expressed in neutrophils (Li et al., 2004) and in monocytes/macrophages (Reymond et al., 2001). Finally, an unpublished preliminary study carried out in the group of one of my co-supervisors (Dr F. Guesdon) prior to the beginning of this project has shown that expression of certain TAKL mRNAs is dramatically induced in an *in vitro* model of macrophage differentiation based on the THP-1 monocytic cell line. This suggested that some TAKL mRNA variants might be expressed specifically in monocytes or macrophages and could be used as differentiation markers if assays that could detect them without cross-reacting with other, more ubiquitously expressed mRNA variants.

1.4.1. Structures of alternative TAKL mRNA variants

A systematic study of the structure of the human TAKL gene, C21orf7, and of its alternative transcripts was carried out by Dr Guesdon and collaborators (Ellis et al., unpublished). The results identified 17 exons in the C21orf7 gene and showed that it can produce 14 alternative transcripts that altogether allow it to encode four different proteins, called TAKL-1 to TAKL-4 (Figure 1.4).

The systematic analysis of the 5' ends of all human TAKL cDNA clones available in GenBank suggests that C21orf7 has five alternative transcriptions start sites (TS), numbered TS I to TS V from the 5' to the 3' end of the gene (Figure 1.4).

The transcripts that originate from TS I are alternatively spliced to produce 7 or 8 mRNA variants (variants A, B, C, E, F, G, M and possibly I, whose 5' end has not been identified, Figure 1.4). Two of these mRNA variants (A and E) encode the TAKL-3 protein and another (TAKL-F) encodes TAKL-4 but the others are either predicted to undergo nonsense-mediated decay (NMD, variants B, C, and M) or have incompletely known sequences that do not allow prediction of their products (variants G and I).

The next transcription start site, TS II, which is at the 5' end of exon 7, is responsible for transcription of variants H and N which are both predicted to undergo NMD, and perhaps also the incompletely sequenced variant I.

The mRNA variants that originate from TS III and TS IV all encode the TAKL-1 protein. TS III is located at the 5' end of exon 10. It initiates transcription of variant D and is by far the most frequently cloned C21orf 7 mRNA variants, which suggests that it is the default product of the gene in most tissues (See Figure 1.4 and (Ellis et al., unpublished). TS III may also be the transcription start site of variant J (Figure 1.4). TS IV is at the 5'end of exon 12 and produces variant K.

The last transcription start site, TS V, is at the 5'end of exon 14 and produces variant L, which encodes the TAKL-2 protein. Based on the statistics of its representation in EST libraries, it appears to be the second most frequently cloned mRNA variant of C21orf7 (Figure 1.4).

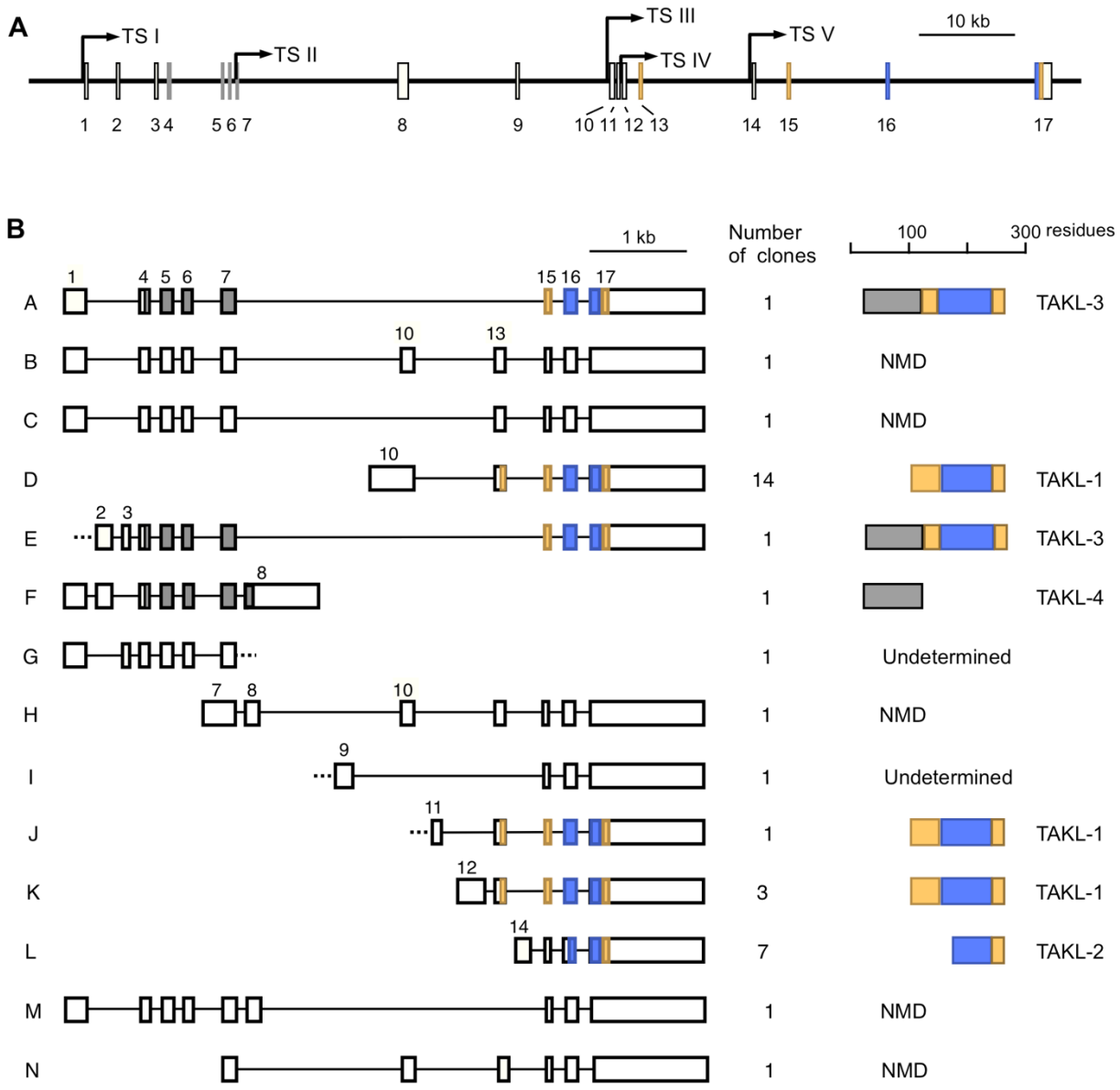

Figure 0.4 Structure of TAKL gene and its mRNA variants (Ellis et al., unpublished)

(A) Structure of the TAKL human gene, C21orf7; the white bars represent the exons, blue bars for the coding regions homologous to the TAB 2/3 binding domain of TAK1, yellow bars for regions that are similar to TAK1 but not including in TAB2/3 binding domain and grey bars for coding regions that are not similar to any protein. Exons numbers are included, and the bent arrows shows the alternative transcription start sites (TS).

(B) Structures of mRNA and protein variants encoded by the human TAKL gene; TAKL mRNA variants (A to N) are represented on the left-hand side. Grey bars show the open reading frames, yellow and blue bars are as in panel A. The number of cDNA clones of each mRNA variant is indicated as has been found in GeneBank. The different predicted protein product of each TAKL variant is shown in the right-hand side, except for variant G because it has an incomplete sequencing or for mRNA predicted to be subjected the nonsense mediated decay (NMD).

1.4.2. Structures of TAKL proteins

In spite of its large number of alternatives transcripts, the human TAKL gene (aka C21orf7) only encodes four alternative predicted proteins called TAKL-3 to TAKL-4.

The last two exons of C21orf7 are strongly homologous to exons 16 and 17 of the TAK1 gene, which are the exons encoding the TAB2/3 binding domain of the kinase (Dempsey et al., 2000). The two homologous exons of TAKL form the 3' ends of the open reading frames of TAKL-1, TAKL-2 and TAKL-3 and the predicted sequences of these proteins therefore include a domain structurally similar to the TAB2/TAB3-binding domain of TAK1. However, TAKL-4 does not contain the TAB 2/3 binding domain (Figure 1.5). This suggested that TAKL-1, TAKL-2 and TAKL-3 could be able to associate with the TRAF complex components TAB2 and TAB3 in a manner similar to the kinase TAK1 (Reymond et al., 2001, Ellis et al., unpublished). However, in contrast to TAK1, the TAKL proteins does not have a kinase domain and their functions in TRAF complexes would be expected to be different from those of TAK1 (Ellis et al., unpublished).

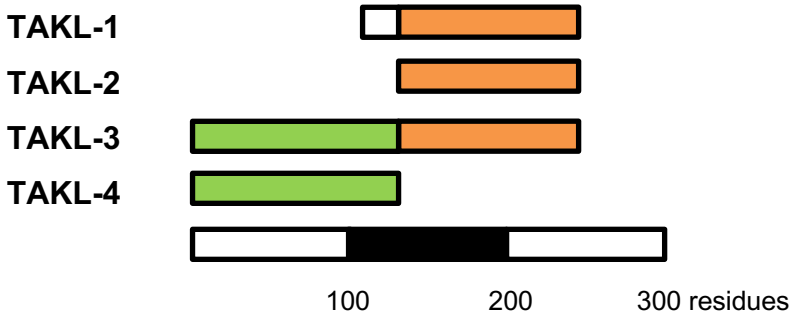

Figure 0.5 Structure of TAKLs isoforms (Ellis et al., unpublished)
The orange boxes represent TAB 2/3 binding domain and the green boxes represent unknown function domain. TAKL-1, 2 and 3 all possess the TAB 2/3 binding domain and TAKL-4 is the only TAKL that does not contain this domain.

1.4.3. Functions of TAKL proteins

To the best of our knowledge, no detailed study of the functions of TAKL proteins as yet been published. However, unpublished findings of Dr Ellis in Dr Guesdon's lab have shown that TAKL-1 and TAKL-3 can both bind to the TAB2 and TAB3 adaptor proteins and then the resulting dimers can associate to TRAF2 or TRAF6 complexes whereas TAKL-4 was unable to do so, as expected given its lack of TAB2/3-binding domain, (Ellis et al., unpublished). Unfortunately, TAKL-2 was not included in these experiments as its cDNA had not yet been cloned (Dr Guesdon, personal communication). Over-expression of TAKL-1 in transfected cells was found to inhibit partially signalling by IL-1β, LPS and TNF-α, suggesting that TAKL-1 has an inhibitory role in TRAF mediated signalling pathways (Ellis et al., unpublished).

TAKL-3 has been shown by two genome-wide protein association screens to associate with two inhibitors of signal transduction pathways, the G-protein pathway suppressor 2 (GPS2) (Rual et al., 2005), and the SOCS family member, CIS (Wang et al., 2011). However, the ability of the other TAKL proteins to bind GPS2 or CIS was not investigated in these studies.

GPS2 and CIS are both known to inhibit TAK1-based signalling. GPS2 attaches to the E2 ubiquitin-conjugating enzyme which is required for the formation of K-63 ubiquitin chains. Although it is primarily known as a nuclear regulatory protein, it can also associate to TRAF2/6 and inhibit the cytoplasmic signal transduction mechanisms of TNFα (Cardamone et al., 2012). CIS inhibits the signal transduction of IL-1β, TGF1β and TNFα (Chen et al., 2011). Specifically, CIS binds to phospho-tyrosines in the activated cytokine receptors and inhibit IL-1-TAK1 signalling pathway (Frobøse et al., 2006).

The presence of a TAB2/TAB3 binding domain in three TAKL proteins and the ability of at least one of them (TAKL-3) to associate with the two inhibitors of TAK1-based signalling, CIS and GPS2, suggest that TAKL-3 and perhaps also TAKL-1 and TAKL-2 may be implicated in the negative control of TAK1 activity by recruiting these inhibitors to TRAF complexes (Ellis et al., unpublished).

1.4.4. Could TAKL-L be a maker of macrophage differentiation?

Shortly before this project began, an experimental study of the expression TAKl/C21orf7 in various human cell lines, primary leukocytes and tissues was carried out by S. Kumar and I. Tzani in Dr Guesdon's group. The study used real-time PCR methodology with two different TAKL mRNA assays.

The first assay called "TAKL-all" aimed to measure the overall expression of all C21orf7 mRNA variants used a probe and primers set targeting exons 16 and 17, which are present in almost all C21orf7 mRNA variants (Figure 1.4). The results obtained with this assay are summarised in Appendix II. Briefly, they showed that C21orf7 was expressed in all tested cells and tissues, but its expression level varied very strongly between samples. Established cell lines showed much lower levels of C21orf7 mRNAs than primary peripheral blood leukocytes and differentiated tissues, with the lowest levels found in the THP-1 monocytic cell line (See Appendix II, Figure 1). The results also showed that the expression of C21orf7 could be up regulated in the Jurkat and THP1 cell lines by treatments that induced their activation or differentiation (See Appendix II, Figures 2, 3 and 4). The most dramatic increase (peaking at more than 900-fold) was found during PMA-induced macrophage differentiation of THP1 cells (Figure 1.6).

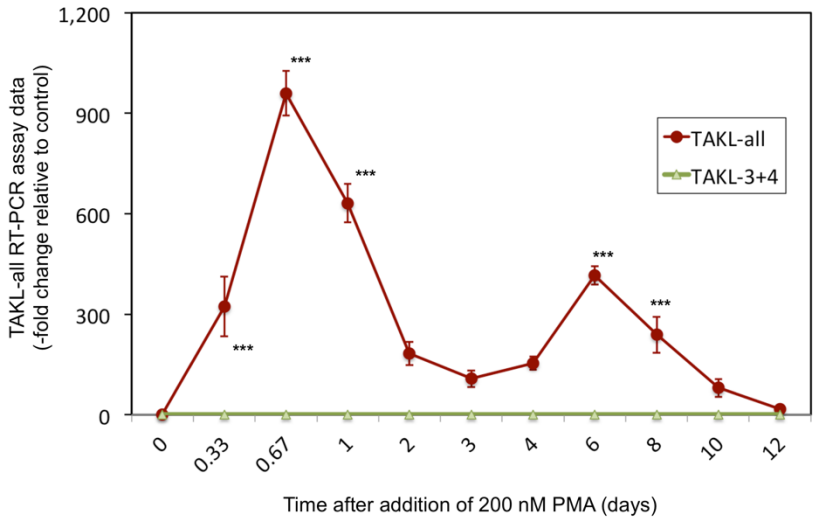

Figure 0.6 Expression of TAKl mRNAs during PMA-induced macrophage differentiation of THP1 cells (Unpublished data from Kumar & Tzani, reproduced from Appendix II, Figure 4)

THP1 cells were induced to differentiate into macrophages by a 3-day exposure to phorbol 12-myristate 13-acetate (PMA, 200 ng/ml) followed by a rest period of 9 days in culture medium without PMA. The cell suspension was aliquoted immediately after addition of PMA into samples that were then incubated for times varying from 8 hours (0.33 day) to 12 days. Samples taken prior to PMA addition (shown at 0 day on the graph) were also taken for reference. After RNA extraction and first strand cDNA synthesis, TAKL expression was assayed with the TAK-all assay and the TAKL-3/4 assay as described in "Materials and Methods". The data were analysed by the comparative method (ΔΔCt) using β-actin mRNA as normaliser and the first strand cDNA preparation from unstimulated THP1 cells (day 0 sample) as reference. The data shown are the means ± SEM of triplicate assays.

Interestingly, no increase in C21orf7 expression was detected when the same THP1 samples were assayed with another set of probe and primers that targeted exons 4, 5, 6 and 7 (Figure 1.5). These exons are only present in the C21orf7 mRNA variants which originate from the first transcription start site, TS I and encode the TAKL-3 and TAKL-4 proteins, but are absent from the mRNA variants encoding TAKL-1 or TAKL-2, which are produced by the alternative transcription start sites, TS III to TS V (Figure 1.4). This indicated that the increased expression of C21orf7 during macrophage differentiation did not result from a general activation of all the gene's transcription start sites, but from a more specific activation of expression of TAKL-1 or TAKL-2 coding mRNAs.

This data thus strongly suggested the hypothesis that a strong increased expression of specific TAKL mRNA variants could be used as makers of macrophage differentiation. Testing this hypothesis was one of the aims of my project.

In conclusion, we tested two potential M1 markers in this research. Firstly, TAK1-like (TAKL) because of its mRNA expression level that is found to elevate under monocyte/macrophage differentiation conditions in monocytic THP-1 cell line (previous data in Dr Guesdon group). Secondly, we identified the family with sequence similarity member 26 F (FAM26F) as a specific M1 marker which raise at both levels of mRNA and protein in human and mouse (data in Dr Wilson group).

1.4.5. TAK1/TAKL and cancer

As explained previously there is an important relationship between inflammation and cancer (section 1.1.2). There are many studies which have linked the transforming growth factor β-activated kinase 1 (TAK1) with cancers, and we hypothesized that TAKL (the inactive form of TAK1) could inhibit TAK1 and help in improving cancer treatments.

Deletion or decreasing TAK1 expression is related to malignant tumors. A recent study has noticed that there are low expression levels of MAP3K7 gene in prostate tumor cells compared to normal prostate cells. It has been suggested that MAP3K7 may function as a tumor suppressor on prostate cancer cells (Kluth et al., 2013).

Several studies have implicated TAK1 as a target in cancer therapy. For example, it has been highlighted that targeting TAK1 could be effective in breast cancer therapy. They have used small interfering RNA (siRNA) to inhibit different genes such as TAK1, tumor necrosis factor receptor associated factor 6 (TRAF6) or a regulator of TAK1 called TAK1-binding protein2 (TAB2) and they have found that inhibition of TAK1, TRAF6 or TAB2 may offer a useful therapeutic goal for breast cancer cells (Martin et al., 2011). That is because suppression of TAK1, TRAF6 or TAB2 enhance activity of camptothecins (CPT) which is an anti-tumor drug that damages DNA by inhibiting the enzyme topoisomerase 1 (Top 1). TAK1 contributes in sensitizing cancer cells to cytotoxic agents such as CPT which makes TAK1 an impressive tumor therapeutic target (Martin et al., 2011). Interestingly, it has been found that TAK1 inhibition, by 5Z-7-oxozeaenol, promotes the efficacy of chemotherapy treatment on different neuroblastoma cell lines in vivo and in vitro (Fan et al., 2013). In addition, TAK1 inhibition promotes apoptosis and enhances sensitivity of KRAS dependent colon cancer cells (Singh et al., 2012). Furthermore, using the oral inhibitor of TAK1 (LYTAK1), this sustained the antitumor activity of pancreatic cancer cells (Melisi et al., 2011).

Targeting TAKL and maybe using a TAK1-inhibitor in cancer therapies is an interesting area for future studies.

1.4.6. TAKL and FAM26F: potential signalling link

In this research, one of our aims was to study the signalling pathways of the two proteins (TAKL and FAM26F) to understand the reason for mRNA up-regulation in inflammatory macrophages (stimulated with IFNγ and LPS). High mRNA levels of TAKL and FAM26F in $M^{IFN\gamma+LPS}$ has been reported in previous data in Dr Guesdon's and Dr Wilson's groups (Ellis et al., unpublished, Hadadi, 2015, Baidžajevas, 2019), and these findings were confirmed in this project using many experimental tools (see chapter 3 and 4).

Interestingly, Baidžajevas has studied IFNγ and LPS pathways (both canonical and non-canonical TLR4 signalling) (see figure 1.7). The data showed that siRNA knockdown of STAT-1 and TICAM1 in IFNγ and LPS signalling, respectively, lower FAM26F mRNA expression level after IFNγ and LPS stimulation (see results in appendix III). Currently there are no studies relating the signalling pathways of TAKL and FAM26F. We hypothesise that both genes are linked to TLR4 signalling, from the previous data of FAM26F, it has been found that it is activated by the non-canonical pathway (TICAM1-IRF3 signalling), while TAKL might be activated by the canonical pathway (MyD88-NF-κB signalling), similar to TAK1 pathways. TAK1 can be activated by the same canonical TLR4 pathway of FAM26F (MyD88-NF-κB), more future studies are required in order to understand TAKL signalling pathway and function.

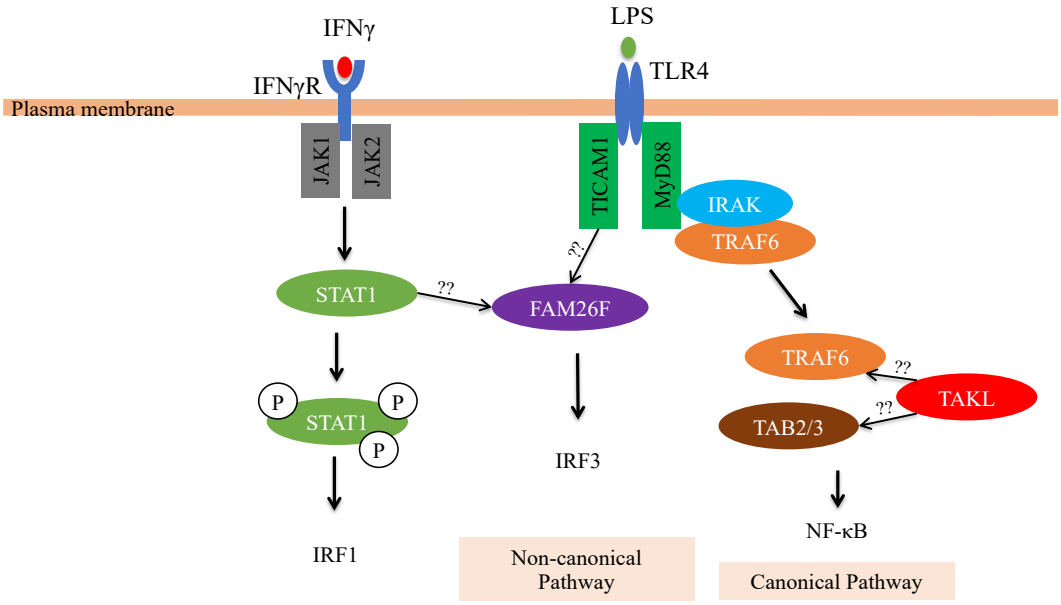

Figure 1.7 Potential TAKL and FAM26F pathways through IFNγ and LPS signalling
This image shows the activation process of pro-inflammatory (M1) macrophage signalling pathways after stimulation with IFNγ and LPS. The down-stream signalling then leads to the activation of transcription factors and induce different genes expression. TLR4 signalling cab be activated by two pathways either the canonical (MyD88-NF-κB) or the non-canonical (TICAM1-IRF3) signalling. The potential link of TAKL and FAM26F to these pathways as shown in this figure as a result of our preliminary data, and more studies are required to understand their signalling and function.

1.1. Aims of this thesis

Here we have introduced the role of inflammation in macrophage biology. In this thesis we have explored human inflammatory macrophages by testing the following hypotheses:

1. Specific TAKL variants show altered expression between monocytes, macrophages and in differently polarised macrophages.
2. Inflammatory signalling pathways show altered expression and can be delineated according to macrophage polarisation.

As outlined in the results of chapter 4 and the introduction to chapter 5, we identified a potential macrophage inflammatory phenotype marker, therefore we investigated the following hypotheses:

3. FAM26F is a marker for M1 macrophages and therefore is detected in a specific inflammatory population of macrophages in diseased atherosclerotic plaques.
4. FAM26F plays a role in inflammation by interacting with proteins related to its immune function.

Chapter 2
Materials and Methods

2.1. List of Reagents

Reagent	Catalogue number	Vendor
10 mM dNTPs	U1511	Promega
10x MOPS electrophoresis buffer	L-13279	Fisher Bioreagents
4-12% Bis-Tris gel	NP0321	Invitrogen
5x M-MLV buffer	M531A	Promega
Absolute methanol	M/4000/17	Fisher Scientific
Blue/orange 6x loading dye	G190A	Promega
Bradford 1x dye reagent	5000205	BioRad
Bradford reagent	B6916	Sigma
Ca2+ ionophore A23187	C7522	Sigma
$CD14^+$ microbeads, human	130-050-201	Miltenyi Biotech
ECL select western blotting detection reagent	RPN2235	GE Healthcare
Ficoll-Paque PLUS	17-1440-03	GE Healthcare
Formaldehyde solution 37/41%	F/1501/PB15	Fisher Scientific
Heat-inactivated foetal bovine serum (HI-FBS)	10500064	Gibco
Hi-Res standard agarose powder	AGD1	Geneflow
Hyperladder 25bp	BIO-33057	Bioline-Life Science
L-glutamine	BE17-605E	Lonza
LS columns	130-042-401	Miltenyi Biotech
M-MLV reverse transcriptase	M1701	Promega
Nano-flow liquid chromatography	U3000 RSLCnano	ThermoFisher
Penicillin/streptomycin	15140-122	Gibco
Phorbol 12-myristaye 13-acetate (PMA)	P8139	Sigma
PKH26	MINI-26	Sigma
PKH67	MINI-67	Sigma
proliferation dye CPD eFluor 670	65-0840	ThermoFisher
ProLong Gold Antifade Mountant with DAPI	P36931	Invitrogen
Protease inhibitor cocktail 100x (PIC)	P-8465	Sigma
Puromycin	A11138-03	Gibco
Random primers	C1181	Promega
Recombinant human rh M-CSF	300-25	Peprotech
RIPA lysis buffer 10x	20-188	Merck Millipore
RNA loading dye	R4268	Sigma
RNasin	N251A	Promega
RPMI 1640	31870-025	Gibco
RPMI 1640 medium supplemented with GlutaMax	61870010	Gibco
TaqMan gene expression master mix	4369016	ThermoFisher
Tri Reagent	T9424	Sigma
Ultra-low endotoxin heat-inactivated FBS	S178B	Biowest

2.2. Cell culture

2.2.1. THP-1 cells culture

THP-1 cells are human monocytic cell line, derived from the peripheral blood of acute monocytic leukaemia patients. These cells were obtained from the American type culture collection (ATCC), and cultured in an RPMI 1640 medium supplemented with GlutaMax and with 10 % of heat-inactivated foetal bovine serum in standard plastic tissue culture flasks (Thermo Fischer) kept vertically at 37ºC in an atmosphere supplemented with 5% CO_2. Cell density monitored by counting the cells using the hemocytometer (Hawksley). The cultures were maintained in growth phase by diluting them down to a density of 250-300×10^3 cells/ml culture medium, whenever their density reached or exceeded 1×10^6 cells/ml.

2.2.2. In vitro monocytic differentiation by the PMA-rest treatment

- **Principle:**

Differentiation of THP-1 cells into macrophages was induced by the procedure established by Daigneault et al. (2010), called "PMA-rest". This consists of a 3-day incubation in the presence of 200 nM phorbol 12-myristaye 13-acetate (PMA) followed by a 7-day "rest" period in culture medium without PMA. Exposure to PMA stops cell division and causes most cells to adhere to the culture flask plastic within a few hours. This is followed by gradual expression of various monocyte differentiation markers over the 10-days period of the PMA-rest treatment (Daigneault et al., 2010).

- **Procedure:**

Suspension-growing THP-1 cells were collected from their culture medium by centrifugation (1,000xg, 5 minutes) and the differentiation was initiated by suspending the cell pellet in fresh culture medium supplemented with 200 nM PMA. This cell suspension was dispensed in 75 cm^2 tissue culture flasks so that each flask contained 8×10^6 cells. The volume of the culture was then adjusted to a total of 25 ml /flask by adding the appropriate amount of PMA-containing medium and the flasks were laid horizontally in the incubator to facilitate adherence to the plastic of differentiating cells. After three days, the rest period was started by removing the PMA-containing medium was removed, washing the cells once in sterile PBS and feeding the cells with 25 ml/flask of culture medium without PMA (Daigneault et al., 2010). See Figure 2.1, section 1 for a brief model of illustration for this procedure.

2.2.3. Human blood monocytes isolation from healthy donors

The blood was collected by venepuncture from healthy donors (Ethical approval: University of Sheffield, SMBRER310), it was mixed gently 9:1 with 3.8% trisodium citrate dehydrate. The procedure of separating the peripheral blood mononuclear cells (PBMCs) from the whole blood was done using the Ficoll-Paque PLUS method. Erythrocytes were lysed in lysis buffer (155 mM NH_4Cl, 10 mM $KHCO_3$, 0.1 mM EDTA) at room temperature RT for 5 minutes. To purify monocytes, $CD14^+$ microbeads and LS columns were used as 10 µl of beads per $1x10^7$ of PBMCs for 15 minutes at 4 °C. See Figure 2.1, section 2 for a brief model of illustration for this procedure.

2.2.4. Macrophage culture and polarisation

The monocytes were cultured in RPMI 1640 supplemented with 10% ultralow endotoxin heat-inactivated FBS, 1% L-glutamine, 1% penicillin/streptomycin. To differentiate $CD14^+$ monocytes *in vitro* to monocyte derived macrophages (MDMs), 100 ng/ml recombinant human rh M-CSF was added to a fresh culture media, and seeded as 1×10^6 in 3 ml of media per well in 6 well plate (3516, Costar), for 7 days at 37 °C**,** 5% CO_2. After a week of differentiation, the media was replaced with fresh complete media with the polarising agents for 24 hours as in Table 2.1.

Table 2.1 Macrophage polarisation conditions

Macrophage phenotype	Polarising agent	Concentration	Catalogue number	Manufacturer
Unpolarised (M^{un})	None	-	-	-
M1-like ($M^{IFNϒ+LPS}$)	rh IFNϒ	20 ng/ml	300-02	Peprotech
	LPS from E. coli, Serotype R515	100 ng/ml	ALX-581-077-L002	Enzo Life Sciences
M2a-like (M^{IL-4})	rh IL-4	20 ng/ml	200-04	Peprotech

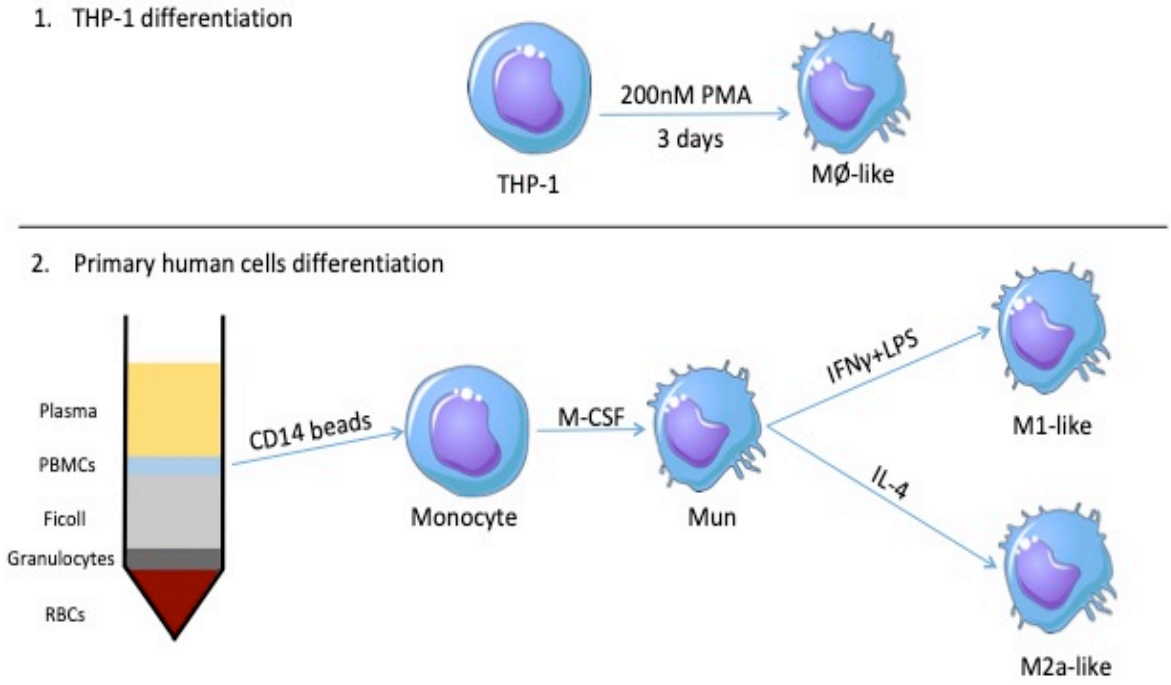

Figure 2.1 Cells differentiation procedures

1. Outline model of THP-1 cell line differentiation by PMA.
2. Outline model of PBMCs and CD14+ monocytes isolation, then differentiation by M-CSF and finally macrophage polarisations by INF and LPS to M1 like macrophages or IL-4 to produce M2a-like macrophages.

2.2.5. Culture of Jurkat and THP-1 (FAM26F overexpression cell line)

Jurkat cells (T-cell model) and FAM26F-THP-1 stable cell line (macrophage model) were cultured and activated to be used in the cell-cell interaction experiments (see section 2.10).

Jurkat cells were obtained from ATCC, and cultured at the same density (250-300×10^3 cells/ml) as THP-1 cells in RPMI 1640 medium supplemented with GlutaMax and with 10 % of heat-inactivated foetal bovine serum in standard plastic tissue culture flasks (Thermo Fischer) at 37 °C in an atmosphere supplemented with 5% CO2. The cultures were maintained in growth phase by diluting them down to a density of 250-300×10^3 cells/ml culture medium, whenever their density reached or exceeded 1×10^6 cells/ml.

THP-1 cells (control and FAM26F-3XFLAG) were cultured in the same conditions and density as Jurkat cells except that they were supplemented with 2 μg/ml of puromycin, as this stable cell line was generated and selected using puromycin. In the co-culture experiments, puromycin was not added because it could kill the non-resistant Jurkat cells.

- **Jurkat cell activation**

Jurkat cells were activated with 100 nM PMA for 20 h followed by centrifugation at 1,200 rpm for 5 min and treatment with 2 μM Ca2+ ionophore A23187 for 4 hours, followed by a 20-hour resting period in fresh media.

- **PMA stimulation of THP-1 (FAM26F overexpression cell line)**

Suspension-growing THP-1 cells were collected from their culture medium by centrifugation (1,000xg, 5 minutes) and the differentiation was initiated by resuspending the cell pellet in fresh culture medium supplemented with 2 μg/ml of puromycin and 0.5 μM PMA for three hours at 37°C and 5% CO2 incubator. This cell suspension was dispensed in 75 cm^2 tissue culture flasks so that each flask contained 8×10^6 cells. After 3 hours of PMA treatment, the media was replaced with fresh complete media with 2 μg/ml of puromycin. This was followed by a PMA-rest period, of 24 hours from PMA addition, then the medium was
removed and replaced with a new fresh medium containing 2 μg/ml of puromycin and the polarising agents, as previously explained in table 2.1, for 24 hours.

2.3. Preparation of samples

2.3.1. Preparation of cell samples for gene expression studies by RT-qPCR

These samples were prepared in Tri Reagent, this reagent is a monophase solution mixture of phenol and guanidine thiocyanate, which can inhibit RNase activity and is mainly used to isolate RNA and DNA from the biological samples (TRI Reagent Protocol, Sigma). Different procedures were used for cells in suspension and adherent cells.

Suspension-growing THP-1 cells were collected by centrifugation (1,000 x g, 5 minutes) and washed two times by suspension / centrifugation with sterile cold phosphate–buffered saline (PBS) (Thermo Fischer). After removal of the last PBS supernatant, the cell pellets were re-suspended in 1 ml / million cells of Trizol. Adherent cells, such as THP-1 cells undergoing PMA-rest treatment or human peripheral monocytes and macrophages, were washed twice in cold PBS and Trizol (1 ml per million cells) was added directly onto the cells after removal of the last wash. The cells were then scrapped manually from their plastic substrate using cell scraper (CSC-211-023, Biofil) and the resulting suspension were collected. All Trizol cell suspensions were frozen at -80 °C immediately after collection and stored at that temperature until they were used for RNA isolation.

2.3.2. Preparation of cell samples for protein expression studies by Western blotting

The adherent macrophage-like cells (PMA-treated THP-1 cells or in vitro-differentiated human peripheral blood monocytes and macrophages) were washed two times with cold PBS, and detached using cells scraper (CSC-211-023, Biofil). Cells suspension in PBS is then centrifuged for 5 minutes at 1500 rpm to remove all medium residues that interfere with western blot. Cells were lysed in Laemmli lysis buffer (2% SDS, 5% β-mercaptoethanol, 10% glycerol in 60 mM Tris-HCL, pH 6.8) or RIPA lysis buffer 10x supplemented with 10 µl / ml protease inhibitor cocktail 100x (PIC). Lysates were vortexed to completely lyse the proteins. Protein concentration then measured using Bradford reagent, to prepare WB samples at the concentration of 15 µg/µl. Samples then can be stored at -20°C, and can exposed to just one freeze-thaw cycle before boiling at 95°C for 5 minutes. Boiling step should take a place before loading samples into the gel.

2.4. Real time-qPCR

2.4.1. RNA isolation

This was done using the standard procedure developed in the laboratory based on the manufacturer instructions for the TRI Reagent. The solution of RNA-Trizol was mixed several times by pipetting and incubated at 15-30 °C for 5 minutes to fully homogenise the suspensions and allow dissociation of proteins from RNAs. Samples were centrifuged at 3000 rpm for 10 minutes to keep the sediment, then 200 µl of chloroform was added per 1 ml of lysate and incubated at room temperature for 2-3 minutes, then centrifuged at 12000 rpm and 4 ºC for 15 minutes. This chloroform step will separate the mixture into three phases: a lower red phase contains proteins and interphase contains DNA and an upper colourless phase contains RNA. The upper transparent phase was carefully transferred to a new tube (500-550 µl). The next step was mixing the samples with 500 µl of isopropanol by inverting the tubes to precipitate the RNA, then incubated at 15-30 ºC for 10 minutes and centrifuged at 1200 rpm and 4 ºC for 10 minutes. The pellet of RNAs was then washed with 1 ml of 75% ethanol in DEPC-treated water. RNA samples were vortexed and centrifuged at 12000 rpm and 4 ºC for 5 minutes. After centrifugation, almost 75% of ethanol was removed except 100 µl of RNA sample, and centrifuged again at 12000 rpm for 1 minute. Then, the leftover ethanol was removed and the RNA pellet was left to dry in air for 20 minutes. RNAs were dissolved in 20 µl of DEPC-treated water by pipetting few times and then heated at 55-60 ºC for 10 minutes. Finally, the RNA was quantified using a ND 1000 Nanodrop Spectrophotometer (Thermo Scientific). The instrument software (ND-1000 V3.8.1) gave directly the sample's absorbance at 230, 260 and 280 nm, the equivalent RNA or DNA concentration as appropriate to the type of preparation and the 260/280 and 260/230 ratios. If the 260/280 ratio was from 1.8 to 2.0 that indicates the RNA sample is free of proteins and 260/230 should be more than 1.5 to indicate that the RNA is free of phenol (Trizol).

2.4.2. Assessing RNA quality by agarose gel electrophoresis

0.5g of Hi-Res standard agarose powder was dissolved in 36ml of water and 5ml of 10x MOPS electrophoresis buffer using a microwave, then 9ml of formaldehyde solution 37/41% was added. After that, the gel was poured into the cassette with the combs and left to set for 15-20 minutes. 2 µl of RNA loading dye was added to 2 µl of RNA and heated to 65°C for 2-5 minutes. Next, the gel cassette was loaded into the tank with 1x MOPS solution. 4 µl of RNA mixture was loaded to the lanes and the gel was run at 80 V for 30 minutes. Images were taken under UV light activation by Biorad Chemi Doc gel system.

2.4.3. Synthesis of 1st strand cDNA

Firstly, the reaction mix was prepared from 6 µl of 5x M-MLV buffer, 6 µl of 10 mM dNTPs, 0.9 µl of random primers, 0.75 µl of RNasin, 2 µg of RNA preparation and 9 µl of RNAse-free water. The mix was heated up at 70°C for 5 minutes to allow denaturation and then 1.2 µl of the enzyme M-MLV reverse transcriptase (M1701, Promega) was added. The total volume in each tube was then 30 µl. The tubes were centrifuged for 1 minute to ensure collection of all mixture components and put in the Eppendrof RT-PCR machine. The PCR program was as in Table 2.2. The RNA tubes were centrifuged again for 1 minute and then stored at 4°C.

Table 2.2 RT-PCR Program

Cycle	Temperature	Duration
Pre-warm	23°C	5 minutes
Reverse transcription	42°C	120 minutes
Enzyme activation	95°C	5 minutes

2.4.4. Principle of RT-PCR reaction monitoring using labelled probes

We used the real-time PCR technology commercialised by ThermoFisher Scientific under the brand name TaqMan. TaqMan assays are sets of three synthetic oligonucleotides. The first two are the forward and reverse PCR primers and the third is the probe, which is a reporter oligonucleotide covalently linked to the fluorescent dye, 6-carboxyfluorescein (FAM), at the 5' end and a non-fluorescent quencher (NFQ) at the 3' end. During PCR, each time a new cDNA molecule is synthesised, the DNAse activity of the polymerase hydrolyses one copy of the probe, thereby separating the FAM dye from its quencher and allowing it to fluoresce (Figure 2.2). Thus, in RT-PCR a fluorescent signal is generated that allows the real-time monitoring of PCR product molecules production (amplicons) as the reaction progresses (Real-time PCR handbook, ThermoFisher).

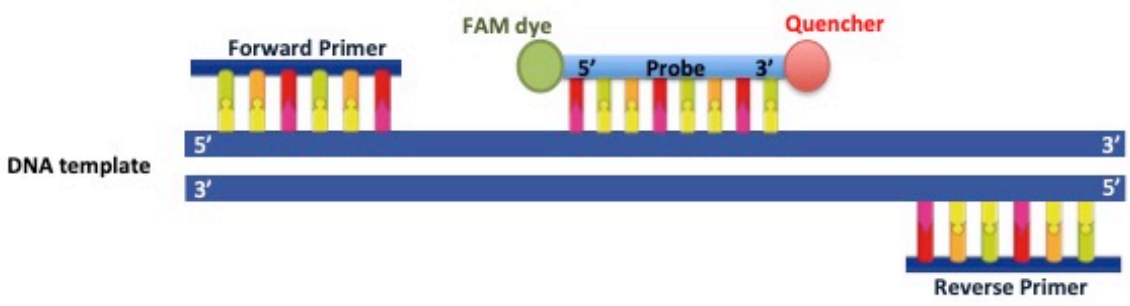

Figure 2.2 TaqMan assay primers and probe. Adapted from the Real-time PCR handbook (ThermoFisher)

The TaqMan probe has a specific sequence that can attach in between the two primers (Forward and Backward). The Reporter dye represented by the green circle, which is attached to the 5' end of the probe. The red circle is the quencher that is attached to the 3' end and, in addition to quenching the dye's fluorescence, also blocks the unwanted probe extension by the DNA polymerase.

If one assumes 100% efficiency of the amplification reaction, the amount of amplicon produced is expected to increase by a factor of two at each cycle, leading to an exponential increase in fluorescence. The raw data generated by the real time PCR instrument is a set of curves where each curve shows the fluorescence in each amplification reactions on the assay plate (y axis) plotted against the cycle number (x axis). Progress curves are normally plotted using a logarithmic scale for the y axis so that when they appear to be straight lines when the fluorescence increases exponentially as expected for a successful PCR reaction. In practice, however, the progress curves look like sigmoid curves (Figure 2.3). This is because the exponential phase is preceded by an initial phase during which the fluorescence signal remains lower than the detector noise and is followed by a plateau when the reaction becomes inefficient.

The list of all the probes that have been used and the expected size of RT-PCR products are shown (Table 2.3 and 2.4). The reactions also contained the TaqMan Universal PCR master mix, containing the DNA polymerases and nucleotides.

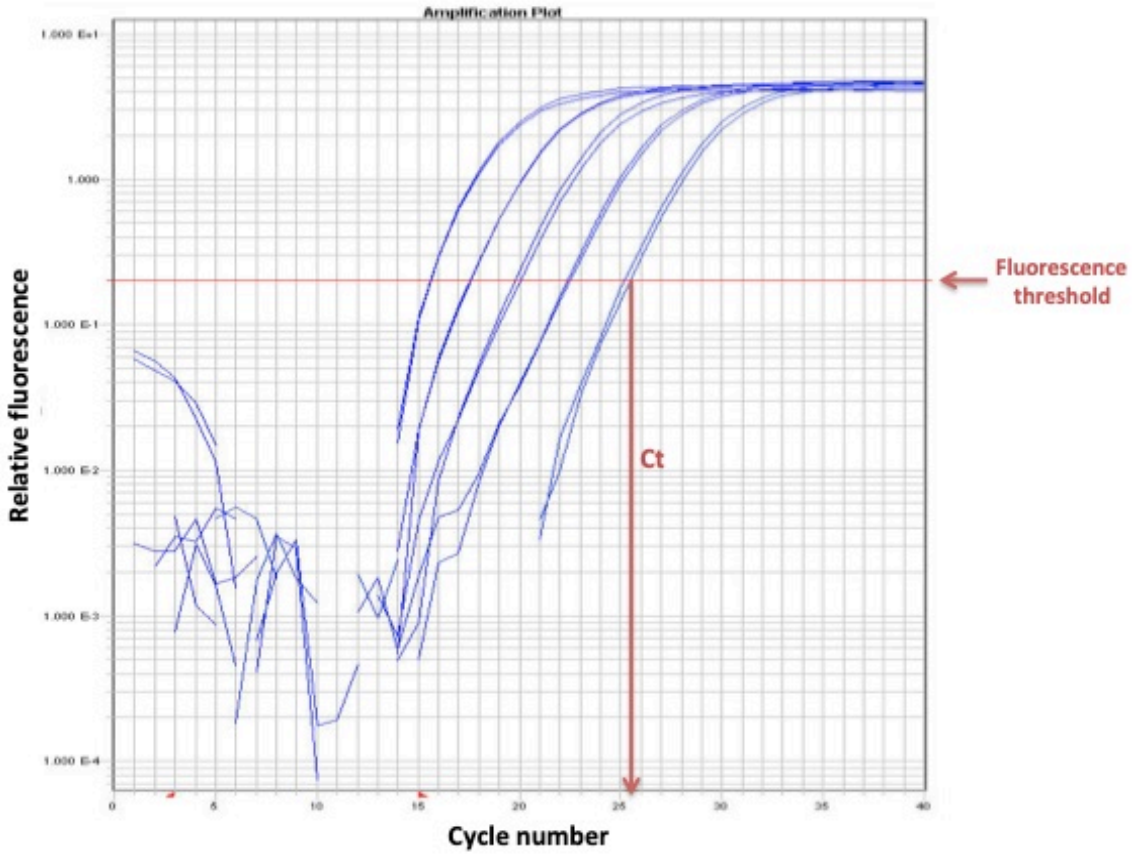

Figure 2.3 Amplification curve of RT-qPCR
These progress curves were generated by the TAKL-all assay using serial dilutions of the positive control plasmid (IMAGE 5185447) to produce a standard curve. Each dilution was assayed in duplicate. Each curve represents the fluorescence signal (y axis) produced in one reaction against the cycle number (x axis). The red horizontal line is the threshold, which was set as 0.2 in most experiment. The vertical red line represents the Ct, which is the point when the progress curves cross the threshold line.

2.4.5. Standard and custom-designed TAKL TaqMan assays

- **Monitoring overall gene expression with pre-designed probes:**

To monitor the expression of TAKL and other genes of interests, we relied primarily on commercially available sets of assays that have been pre-designed by ThermoFisher Scientific to monitor the expression of most protein-coding genes. Several such assays are usually available for each human gene, and we used two main criteria for selecting our pre-designed probes. First, we selected pre-designed assays that amplified a junction between two consecutive exons of the target mRNAs. This is because unlike single-exon assays, they would only amplify the mature spliced mRNAs but not its un-spliced RNA precursors or contaminating genomic DNAs. Second, in order to measure the total expression of a gene, we usually used the gene transcripts maps and sequences from the ENSEMBL database [*Database URL: http://www.ensembl.org/index.html*] to check that the exon junctions selected were present in all alternative mRNAs of the gene of interest. For example, the overall expression of the TAKL gene was measured with a pre-designed assay, called here TAKL-all (Table 2.3, Hs00963407_m1) that targets the boundary between the last two exons of the gene, which are present in all TAKL mRNAs (Figure 1.4).

- **Monitoring the expression of specific TAKL mRNA variants:**

To monitor specifically the TAKL mRNA variants encoding each of the 4 alternative protein products, several assays with different target exons are needed (Figure 2.4 and Table 2.3 and 2.4). For example, as TAKL-1 is encoded by three alternative mRNAs (D, J and K) three different assays are needed to measure the expression of all TAKL-1 coding mRNAs. Therefore, determining the expression of all TAKL mRNA variant by RT-PCR is costly and time consuming. The details of all TaqMan assays (pre-designed and custom) are in Table 2.3 and 2.4.

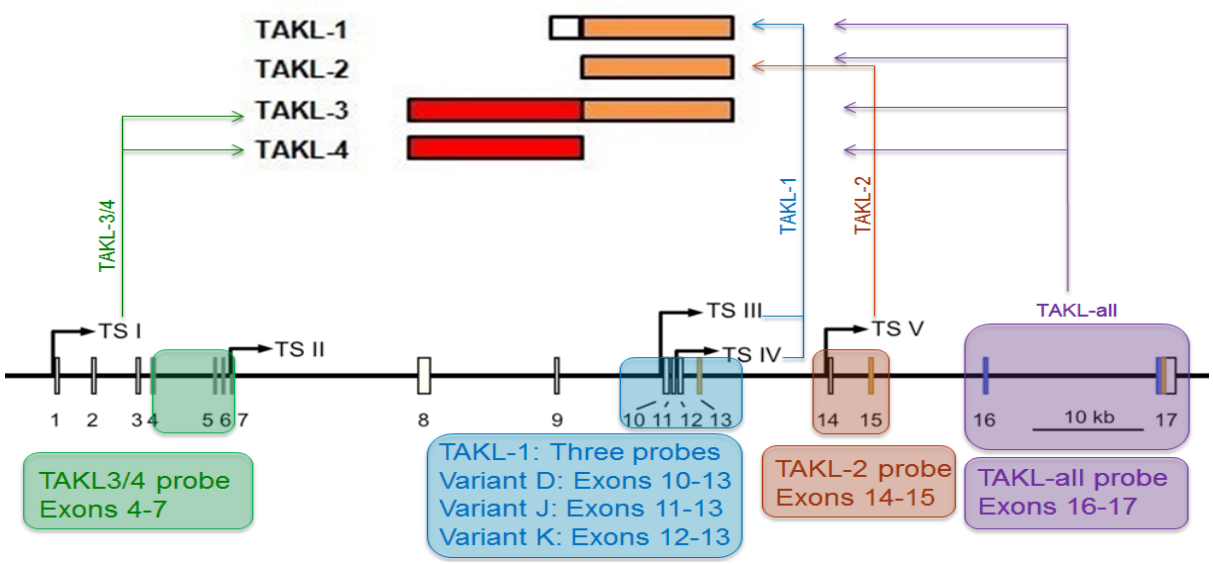

Figure 0.4 RT-PCR probes for TAKL mRNA variants. Adapted from (Ellis et al., unpublished)
The purple bar on TAKL gene map shows the assay that targets exon 16 to 17 and measures all TAKL mRNA variants. The red bar shows the assay that targets exon 14 to 15 which is specific for TAKL-2 variant. The blue bar shows the three assays, which targets the alternative variants of TAKL (D, J and K). The green bar shows the assay that targets TAKL-3/4.

Table 0.3 Pre-designed TaqMan assays and plasmid cDNAs used as technical controls

- IMAGE cDNA plasmids were obtained from commercial suppliers, and the other plasmids were cloned in the lab by a previous member of Dr. Guesdon's group.
- Some plasmids were used as controls for more than one assay (e.g. IMAGE 5185447)
- There was no positive control plasmids for some assays such as β-actin, β2M, IL-8 and OAZ1.

Target mRNA variants	Protein(s) encoded by target(s)	Target exons	Assay ID ThermoFisher catlogue	Plasmid cDNA used for positive control reactions	Amplicon length (bp)
β-actin	β-actin	E1 only	Hs99999903_m1	N/A	171
β2-microglobulin	β2M	E3-E4	Hs00984230_m1	N/A	81
CISH	CIS1	E2-E3	Hs00367082_g1	YFP-CIS1	64
GPS2	GPS2	E8-E9	Hs00409956_g1	GPS2-PD27	150
IL-8	IL-8	E1-E2	Hs00174103_m1	N/A	101
OAZ1	OAZ1	E3-E4	Hs00427923_m1	N/A	122
TAB2	TAB2	E3-E4	Hs00248373_m1	CFP-TAB2	68
TAB3	TAB3	E5-E6	Hs01087551_m1	CFP-TAB3	60
TAKL-all variants	TAKL-1, TAKL-2, TAKL-3, TAKL-4 and NMD	E16-E17	Hs00963407_m1	IMAGE 5185447	76
TAKL-D	TAKL-1 and NMD	E10-E13	Hs00963405_m1	IMAGE 5185447	67
TAK1-all variants (a,b,c,d)	TAK1-a,b,c and d	E9-E10	Hs01105682_m1	GFP-TAK1-b	135
TAK1-a and TAK1-b	TAK1-a and TAK1-b	E16-E17	Hs01105673_m1	GFP-TAK1-b	113
TLR4	TLR4	E3-E4	Hs00152939_m1	pcDNA3.1-TLR4	89
TRAF6	TRAF6	E6-E7	Hs00371512_g1	GFP-TRAF6	64

Table 2.4 Custom TaqMan assays designed to assay individual mRNA variants and plasmids used as technical controls

- The target exons are the two exons recognised by the forward and reverse primers, respectively. The numbering of TAKL exons in this table is based on the analysis of the gene that has been done by Dr Guesdon and collaborators (Figure 5) and is different from the exon numbering of Thermofisher website, in which some TAKL exons are missing.
- IMAGE Clone cDNA plasmids were constructed by Clontech Laboratories, and the others were cloned in the lab by a previous group in Dr. Guesdon lab.

Target mRNA variants	Protein(s) encoded by target(s)	Target exons	Assay ID assigned by ThermoFisher	Plasmid cDNA used for positive control reactions	Amplicon length (bp)
TAKL-I	TAKL-2	E9-E13	AJRR90Q	IMAGE 4247492	96
TAKL-J	TAKL-1	E11-E13	AJFASAI	IMAGE 4244723	111
TAKL-K	TAKL-1	E12-E13	AJHSOMY	IMAGE 5185447	92
TAKL-L	TAKL-2	E14 -E15	AJGJQGQ	IMAGE 4247492	104
TAKL-3/4	TAKL-3, TAKL-4 or NMD	E4-E7	AI6RNHO	YFP-TAKL-3 YFP-TAKL-4	234
TAK1-c and TAK1-d	TAK1-c and TAK1-d	E15-E17	AJ70L9L	GST-TAK1-c	69

Table 0.5 Plasmids used for determination of reaction efficiencies

Plasmid name	Cloned cDNA	Plasmid size (bp)	Plasmid molecular weight (Da)
YFP-CIS1	CIS-1	7,011	4,332,351.12
GPS2-PD27	GPS2	7,218	4,460,223.90
CFP-TAB2	TAB2	7,211	4,455,644.20
CFP-TAB3	TAB3	6,870	4,245,037.31
GFP-TAK1-b	TAK1 splice variant b	6,695	4,136,888.86
GST-TAK1-c	TAK1 splice variant c	8,179	5,053,643.00
IMAGE 4244723	TAKL-J	5,542	3,424,014.29
IMAGE 5185447	TAKL-D and TAKL-K	6,140	3,793,672.41
IMAGE 4247492	TAKL-L and TAKL-I	5,431	3,349,255.05
YFP-TAKL-3	TAKL-3	6,961	4,301,369.28
YFP-TAKL-4	TAKL-4	6,646	4,106,718.07
pcDNA3.1-TLR4	TLR-4	7,949	5,166,850
GFP-TRAF6	TRAF6	6,296	3,890,374.73

2.4.6. Real time qPCR assay procedure

- **Reaction mixes:**

Reactions were carried out in standard 384-well plates (785290, Greiner/Bio-one). All reactions were carried out in duplicate or in triplicate on the same plate.

Each individual real-time PCR reaction mix had a total volume of 20 µl and contained 10 µl of TaqMan gene expression master mix, 5 µl of sterile water, 1 µl of assay mix (probe and primers) and 4 µl of template.

The templates were either first strand cDNA preparations in the case of experimental samples or, for calibrations and positive controls, preparations of plasmids containing cloned cDNAs of the target mRNAs. The IMAGE clones were purchased from the Human Genome Mapping Project Resource Centre (HGMP-RC) at Hinxton, Cambridge, while other plasmids had been constructed by previous members of Dr Guesdon lab (see table 2.5 for details). Sterile water was used instead of template in negative controls.

The TaqMan probes were purchased from ThermoFisher. They were described in the previous section and are listed in Table 2.3 and 2.4.

- **Procedure:**

After pipetting of all reaction components in the appropriate wells of the assay plate, the wells were sealed with an adhesive transparent plastic cover (E2796-9795, Polyolefin star seal, Starlab). The real-time RT-PCR reactions were carried out on an ABI 7900 HT instrument according to instructions from TaqMan gene expression assays protocol of Applied Biosystems.

The reactions used the standard cycling parameters recommended by the manufacturer. In the first stage of each cycle, the temperature is raised to 95°C to allow the denaturation for the double-stranded cDNA. Then in the next stage, the temperature is decreased to 60°C to allow the annealing of primers and probe to their targets. When the polymerase reaches the probe, it cleaves the probe and the FAM reporter dye will separate from the quencher. The PCR cycles will then be repeated 40 times (Table 2.6).

Table 0.6 Standard settings for PCR cycles

Initial Step		**PCR Cycle 40 repeats**	
50°C for 2 min	95°C for 10 min	**Denaturation**	**Annealing and Elongation**
		95°C for 15 sec	60°C for 1 min

2.4.7. Data collection (determination of Threshold and Ct values)

For each experiment, the first step in the analysis is to use the instrument software (The 7900 SDS v2.4.1) to set a fluorescence value called threshold, which is represented by a horizontal line on the progress curves plot (Figure 2.3). The value of the threshold is chosen so that the horizontal line crosses all progress curves when they are in their exponential phases. This determines for each reaction a numerical value called Ct (Crossing threshold), which is the cycle number at which the threshold is crossed. Once the desired threshold value is set, the instrument software allows saving of the corresponding Ct values data set in formats that can be read by data processing applications such as Microsoft Excel

The Ct number is the basic numerical data used to determine the expression levels of the target mRNA by both the relative and the absolute quantitation methods of analysis. In order allow comparisons and statistical determinations between different experiments, we used the same threshold value of 0.2 to generate all our Ct data.

It is important to note that Ct values are inversely related to expression levels. A sample containing lower levels of the target cDNA will give a higher Ct values than a sample containing higher amounts. This is illustrated by experiments in which a single sample is subjected to serial dilutions (Figure 2.3).

2.4.8. Checking assay specificity by DNA agarose gel electrophoresis

This was carried out to check the specificity of each Real-time PCR assay. Samples were taken from randomly chosen wells of assay plates after reactions had been completed and were analysed by electrophoresis on agarose gel. The aims were to check that the reactions contained a single product of the expected size.

Electrophoresis was done on 3% of agarose gels in 1x Tris-acetate-EDTA (TAE) buffer. The stock of 50x TAE was prepared from 242 gm of Tris base, 57.1 ml of acetic acid, 100 ml of 0.5M EDTA and adding distilled water to 1 litre and the pH was adjusted to 8.0. Then, 1x TAE was prepared by diluting the stock 50-fold. The final step was adding 0.5µg of ethidium bromide for each ml of gel.

Each sample was prepared by adding 5 µl of the blue/orange 6x loading dye to the chosen 20 µl-reaction directly on the assay plate and transfering the reulting mix to a well of the gel. Molecular weight standards were from 8µl of the hyperladder 25bp. Gel images were taken by the Biorad Chemi Doc gel system and then exported as jpg files from the ImageLab software. Sizes of amplimers were determined relative to the hyperladder DNA fragments. The sizes of

the actual products were compared to the expected sizes (Table 2.5) to check the products were correct.

2.4.9. Preparation of plasmids used as positive controls

Plasmid constructs containing cloned cDNAs of some of our mRNAs of interest were used as positive control template for real-time PCR reactions and to determine the efficiency of the assay reactions against known amounts of template copies. The plasmids were obtained commercially or had been constructed previously by other members of Dr Guesdon's group and are listed in table 2.5. They were maintained in transformed E.coli cultures and purified by other members of Dr Guesdon's group using standard methods.

The concentrations of the purified plasmid preparations were determined using the Nanodrop spectrophotometer as already described for RNA preparations in section 2.3.1.

2.4.10. Determination of assay efficiency parameters using linear regression on standard curves data

The efficiency parameters of all the assays for which a cloned cDNA template was available were determined by carrying out real-time PCR assays on serial dilutions of the positive control plasmids. For these assays, the plasmids were subjected to 4-fold serial dilutions over 5 orders of magnitudes (from 10 ng / µl to 1.53E-04 ng/µl). This generated raw data similar to those shown in Figure 6, with regularly spaced sets of progress curves separated by an interval of about 2 Ct values (as each 4-fold dilution requires two additional amplification cycles to reach the threshold). To analyse the results, the amounts of template used in each reaction (in ng / µl) were converted into zeptomoles (1 zmole = 10^{-21} moles) and the log10 of these values were determined.

The analysis of these data is based on the observation that because the amount of product augments exponentially, the Ct values should be expected to decrease in direct proportion to the log of the amount of template in the reaction. In other words, when the data is represented on a plot where the Ct values are represented on y axis and the log of the amount of template is measured on the x axis, the data points should be expected to fit as a straight line. The data were therefore analysed by linear regression to determine the slope and Y-axis intercept of the best fitting line and the correlation coefficient. For a perfectly efficient reaction where the amount of product increases by a factor of 2 at each cycle, the slope of the line should in theory

be 3.49. The slope and intercept of the best fitting line were used for absolute quantitation analysis of our experimental data. The slope (a) is also the value from which we can calculate the amplification factor (AF) and the efficiency (e) of the reaction by the following formulas:

$AF = 10^{-1/a}$ and $e = (AF-1) \times 100$

2.4.11. Analysis of RT-PCR gene expression data by comparative quantitation (ΔΔCt method)

- **Normalising genes and calibrating samples:**

For most experiments, including all those carried out at the beginning of the project for exploratory purposes, processing of the data was done by an approach called comparative, or relative, quantitation. This is a very widely used method in which results from experimental samples (e.g. PMA-treated cells) are compared to both a normalising housekeeping gene from the same sample and a calibrator sample (e.g. untreated cells). This method is popular because it does not require precise calibration of the assay against accurately known amounts or a reference template such as a cloned cDNA.

In all our experiments, the normaliser (designated in the following equations as N) was β-actin. The calibrators (reference samples, designated in the following equations as C) were exponentially growing untreated THP-1 cells.

- **Method:**

The first step is the normalisation of raw Ct values to the normaliser mRNA, which is assumed to be expressed at constant levels in all samples. For each experimental sample X, the Ct values for the mRNA of interest (RoI) were normalised to the level of β-actin in the same sample using the equation:

$$\Delta Ct_X = Ct_{RoI} - Ct_N.$$

The ΔCt value thus expresses the amount of target cDNA in the sample relative to its amount of β-actin cDNA. Because β-actin expression is assumed to be constant, this normalisation should remove from the data the effect of any non-biological varaiations that may have been introduced by experimental error, such as for example an accidental partial loss of material during RNA extraction.

The second step determines the expression of the mRNA of interest in a test sample X relative to its expression in the calibrator sample C (untreated cells) by calculating the difference between the ΔCt values of the two samples. This difference, called ΔΔCt, is calculated for each individual sample by the formula:

$$\Delta\Delta Ct_X = \Delta Ct_X - \Delta Ct_{C\text{-}Av}$$

Were $\Delta Ct_{C\text{-}Av}$ is the average of all the replicates ΔCt_C determined in the same assay plate.

- **Statistical analyses:**

The statistical analyses were carried out on individual ΔΔCt values of test samples by calculating means and SEMs of replicates. Statistical significance of differences between sets of replicates were determined by one-way ANOVA test.

Finally, to convert the ΔΔCt-based results to relative expression levels RE (equivalent to -fold change relative to Calibrator) the mean values were converted by the formulae:

$$RE = 2^{-\Delta\Delta Ct}$$

The same exponential transformation has to be applied to the upper and lower limits (mean ± SEM). Because this transformation is not linear, the error bars shown on the graphs are not symmetrical (Figure 3.6A).

To take one example, in the data shown in figure 3.6A for TAKL-all at day 1, the average ΔΔCt was -12.958 and the SEM was 1.52. The limits on the ΔΔCt mean value are therefore -12.958+ 1.52 = -14.478 and -12.958-1.52 = -11.438, which are symmetrical relative to the mean. But the exponential transformations give the results of $2^{-(-12.958)}$ = 7,958 for the mean, $2^{-(-11.438)}$ = 2,774 for the lower limit and $2^{-(-14.478)}$ = 22,834 for the upper limit.

2.4.12. Analysis of RT-PCR gene expression data by absolute quantitation

This analysis method was used to determine the absolute amounts of template cDNA in samples in zeptomoles and to derive from this the absolute level of expression of the target mRNA, expressed in number of copies per cell.

The first step was to determine for each Ct value (measured on the Y axis of the standard plot) the corresponding value (x) on x axis of the plot. This conversion was done using the equation:

$x = (Ct-b)/a$

Where a and b correspond respectively to the slope and the Y-axis intercept of the best-fitting line determined by linear regression of the efficiency measurement data as described in section 1.3.10.

The second step was to convert x into the absolute quantity of template T in the reaction (expressed in zmoles = 10^{-21} moles) using the formula

$T = 10^x$

The final step was then to convert T into the corresponding number of molecules of mRNA of interest per cell using the formula

$N = T \times 602 / (4 \times C)$

Where N is the number of copies of mRNA per cell, 602 is the factor converting T zmoles into the number of template copies in the reaction (it is the Avogadro number 6.02×10^{23} multiplied by 10^{-21}), 4 is the number of µl of sample used in our standard reaction mix and C is the number of cells per µl of sample.

The value of C varied between individual 1st strand cDNA samples. It was calculated from the number of cells used for RNA extraction (N), the total volume of the RNA preparation (VR), the volume of the sample of RNA preparation used in the first strand cDNA synthesis reaction (vS) and the total volume of the latter (30 µl). Although care was taken to adjust the scale the RNA preparations to the number of cells (see section 2.3.1), the concentration of RNA varied significantly between individual preparations. The value of vS needed to be adjusted within the range 1 – 6 µl to provide all 1st strand cDNA synthesis reactions with the required 2 µg of RNA (section 2.3.3). These adjustments in the value of vS were the main cause for the variations of the value of C between samples. In practice, C varied within the range 3,500 to 20,000 cells/µl.

2.5. Wester Blotting

2.5.1. Gel electrophoresis and electro-transfer onto PVDF membrane

Cell lysates were prepared as described and heated up to 95ºC for 5 minutes, as previously mentioned in section 2.2.2. Heating step is considered to denature the proteins and reduce the disulfide bonds. The lysates were then loaded onto 4-12% Bis-Tris gel, and ran at 150V for 80 minutes. Then, proteins were transferred from the gel to a PVDF membrane that had been wetted by immersion in absolute methanol before being soaked in transfer buffer. The transfer took place in the same buffer, at 35V and Amp, for 1 hour.

2.5.2. Immunodetection of proteins of interests

After transfer, the membrane was washed in Tris buffered saline (Sigma) with 0.1% Tween (TBS-T), (3 times, 1 minute per each wash), and then blocked in 5% milk in TBS-T (0.1% Tween in TBS). The membrane was then exposed to the primary antibody (Table 2.7A) diluted to the desired concentration in 5% milk in TBS-T and incubated overnight at 4°C. After washing extensively in TBS-T (3 times, 5 minutes per each wash), the membrane then was exposed to the secondary HRP-linked antibody (Table 2.7B) diluted at 1:2000 in the blocking buffer and incubated for 1 hour at room temperature. The membrane was then washed again in TBS-T (3 times, 5 minutes per each wash).

ECL select western blotting detection reagent were used to detect the HRP-linked antibodies. Images were taken by Biorad Chemi Doc gel system, colorimetric detection was used to detect the marker and Chemiluminescent hi-resolution to detect the antibody bands and then the two images were merged and exported as a jpg file from the ImageLab software.

Table 0.7 List of WB antibodies

- The rabbit anti TAKL antibody was raised against a synthetic peptide from the TAKL-1, TAKL-2 and TAKL-3 sequence (CQIAEEYHEVKKEI), corresponding to a fragment of the human sequence that is fully conserved in the mouse and rat homologues (Ellis et al., unpublished).

A. Primary antibodies				
IgG	**Concentration**	**Incubation**	**Catalogue number**	**Manufacturer**
Anti-TAKL	1:100	Over night, 4°C	Custom made 217D	Innovagen
Mouse anti-β-actin	1:2000	1 hour, RT		
Mouse monoclonal anti-Flag M2	1:15000	1 hour, RT	F1804-50UG	Sigma
Mouse monoclonal anti-LAT	1:100	Over night, 4°C	14-9967-82	Invitrogen
Rabbit polyclonal anti-DCD	1:1000	Over night, 4°C	PA5-13677	Invitrogen
Rabbit polyclonal anti-MARCKS	1:2000	1 hour, RT	Ab51100	Abcam
B. Secondary antibodies				
Polyclonal goat anti-mouse-HRP	1:2000	1 hour, RT	P0447	Dako
Polyclonal goat anti-rabbit-HRP	1:2000	1 hour, RT	P0448	Dako
Polyclonal goat anti-rabbit-HRP	1:2000	1 hour, RT	7074S	Cell Signalling

2.6. Bioinformatics

2.6.1. RNA sequencing (Baidžajevas, 2019)

Polarised MDM from 8 separate donors were lysed in extraction buffer from the ARCTURUS PicoPure RNA Isolation Kit (ThermoFisher) and incubated at 42°C for 30 minutes, followed by centrifugation at 3,000 g for 2 minutes. Supernatants were stored at -80°C, until total RNA was extracted using the RNA isolation kit according to the manufacturer's protocol. Total RNA integrity was assessed using an Agilent Bioanalyzer with RNA Intigrity Number (RIN) ≥ 8.5, cDNA libraries were prepared using 2 ng of total RNA and 1 μl of a 1:50,000 dilution of ERCC RNA Spike in Controls (Ambion) using SMARTSeq v2 protocol (Picelli et al., 2014). The length of the cDNA libraries was determined using a DNA High Sensitivity Reagent Kit on the Perkin Elmer Labchip. All samples were subjected to an indexed pair-end sequencing run of 2 × 51 cycles on Illumina HiSeq 2000 (16 samples/lane).

RNA-Seq data in FASTQ files were obtained and mapped using STAR (Dobin et al., 2012) against build 38 of the human genome. The number of reads per gene was counted using feature counts, part of subread package (Liao et al., 2013), using annotations from GENCODE (v 24). Log2 RPKM values were computed using edgeR in R (v 3.1.2) (Robinson et al., 2009), and also the differential gene expression analysis for each of the cell types were performed using edgeR with unpolarised macrophage samples as the reference. Differentially expressed genes were identified using False Discovery Rate (FDR) of < 5% (Benjamini and Hochberg, 1995), and fold change log2 FC > log2(1.5) when compared to unpolarised macrophages.

2.6.2. Pathway analysis

the databases that has been used were STRING, GENEMANIA and Reactome. Additionally, for protein expression and RNA transcripts variants, we used ENSEMBL, Human Protein Atlas and UniProt.

2.7. Immunocytochemistry studies on human monocyte-derived macrophage

Human MDMs were fixed with 4% paraformaldehyde in PBS (Sigma) for 30 minutes, then permeabilised with 0.1% Triton in PBS (Sigma) for 15 min and blocked with 2% BSA–PBS for 45 min. Primary antibodies (Table 2.8A) in 1% BSA-PBS (at 4°C, overnight), followed by 3 times PBS washes. Then incubated in secondary AlexaFluor antibodies (Table 2.8B) in 1% BSA-PBS (in dark at RT for 1 hour), followed by 5 times PBS washes. Coverslips were mounted using the ProLong Gold Antifade Mountant with DAPI, stained slides then left to dry in dark overnight at RT. Images were taken using the Leica AF6000 microscope and intensities of the fluorescence signal were adjusted according to the isotype antibody controls using Leica LAS AF Lite (v 2.6.3, Leica). Then the integrated densities of regions of interest in cells (fluorescence positive areas) were measured using ImageJ (v 1.52p).

2.8. Immunohistochemistry studies (IHC) on human carotid artery sections

Carotid artery samples were collected from consented patients after endarterectomy surgery (study ethics approval STH18222). Tissues were placed in 10% formalin and decalcified in 0.5M EDTA pH 8 for 7 days. After that tissues were cut into 3 mm thickness regions and embedded in paraffin. The blocks then were cut by the blade into sections of 4-5μm in thickness. Section then placed in a water bath of 40-45°C, then the floating sections were collected by glass slides. For immunofluorescence staining, sections were dewaxed in xylene for 10 minutes, rehydrated in descending concentrations (100%, 95%, 70% and 50%) of ethanol, rinsed 2 minutes in each concentration. Then H2O2 was used to block endogenous peroxidases (at RT for 10 minutes), and dipped in water, antigen retrieval step was performed in 10 mM citric acid (at 95°C for 20 minutes), followed by 20 minutes cooling at RT. Permeabilisation step then was done (only with anti-FAM26F sections), using 0.1% Triton (at RT for 15 minutes). 5% of goat serum in 1% BSA-PBS was used to block the unspecific binding (at RT for 30 minutes). Sections then incubated with primary antibodies (Table 2.8A) in 1% BSA-PBS (at 4°C, overnight). Washed by PBS (3 washes, 5 minutes each), and the incubated in secondary AlexaFluor antibodies (Table 2.8B) in 1% BSA-PBS (in dark at RT for 1 hour). PBS washes were done again in dark, coverslips were mounted using the ProLong Gold Antifade Mountant with DAPI, stained slides then left to dry in dark overnight at RT. Images were taken using the Leica AF6000 microscope. Fluorescence signal intensities were adjusted according to the isotype antibody controls using LAS AF Lite (v 2.6.3, Leica).

Table 0.8 Antibodies used in ICC and IHC staining on carotid artery sections

A. Primary antibodies			
IgG	**Concentration**	**Catalogue number**	**Manufacturer**
Mouse monoclonal anti-CD68	4 μg/ml	M0814	Dako
Mouse monoclonal anti-CD86	1:50	Ab213044	Abcam
Rabbit polyclonal anti-FAM26F	1:20	HPA017948	Sigma
Rabbit polyclonal anti-MR	1:50	Ab64693	Abcam
B. Secondary antibodies			
Polyclonal goat anti-mouse-AF488	2 μg/ml	Ab150113	Abcam
Polyclonal goat anti-rabbit-AF647	2 μg/ml	Ab150079	Abcam

2.9. Co-immunoprecipitation

Macrophage–like IFNγ+LPS control and FAM26F–3×FLAG THP–1s were collected and washed in PBS before lysis in 50 mM Hepes–NaOH (pH7.5), 100 mM NaCl, 1 mM EDTA (pH8), 0.5% Triton–X100, 10% glycerol (wash buffer) supplemented with 1% (v/v) Nonidet™ P40 (NP40, Roche), 1 mM dithiothreitol, protease inhibitors (Sigma, 1:100 dilution), 10 µg/ml RNase A. Cells were sheared using a needle and syringe before centrifugation at maximum speed for 5 min to separate the supernatants. Bradford assays were performed following the manufacturer's protocol to quantify total protein content in the supernatants. 50 µl of FLAG–agarose beads were washed in wash buffer before blocking in wash buffer supplemented with 1% (w/v) BSA (Sigma) for 2 hours at 4 °C with agitation before removal of supernatant by centrifugation at 2,500 g for 1 min and washing. Equal amounts of control and FAM26F–3×FLAG protein was loaded onto the beads and the volumes were adjusted with wash buffer, followed by incubation for 2 hours at 4 °C with agitation. The unbound fraction was then removed before washing the samples in wash buffer lacking detergent or glycerol. Bound proteins were eluted in 1 M arginine (Sigma) at pH 3.5 followed by neutralisation with 1.5 M Tris–HCl at pH 8.8. Coomassie blue staining, western blotting and mass spectrometry were used to test the samples for presence of specific proteins.

2.10. Mass spectrometry of co-immunoprecipitation

The mass spectrometry was performed, analysed and written by Caroline Evans (Mark Dickman lab, Chemical Engineering, University of Sheffield) as follows:
LC MS/MS was performed and analysed by nano-flow liquid chromatography coupled to a hybrid quadrupole–orbitrap mass spectrometer (Q Exactive HF, Thermo Scientific). Peptides were separated on an Easy–Spray C18 column (75 µm x 50 cm) using a 2–step gradient from 97% solvent A (0.1% formic acid in water) to 10% solvent B (0.1% formic acid in 80% acetronitrile) over 5 min then 10% to 50% B over 75 min at 300 nL/min. The mass spectrometer was programmed for data dependent acquisition with 10 product ion scans (resolution 30,000, automatic gain control 1×10^5, maximum injection time 60 ms, isolation window 1.2 Th, normalised collision energy 27, intensity threshold 3.3×10^4) per full MS scan (resolution 120,000, automatic gain control 106, maximum injection time 60ms) with a 20 second exclusion time.

MaxQuant (version 1.5.2.8) software was used for database searching with the *.raw MS data file using standard settings. The data for searched against the Homo sapiens Uniprot proteome database (taxa id: 9606, downloaded 25 November 2018, 73101 entries), using the following settings: Digestion type: trypsin; Variable modifications: Acetyl (Protein N–term); Oxidation (M); fixed modifications: carbamidomethyl (C); MS scan type: MS2; PSM FDR 0.01; Protein FDR 0.01; Site

FDR 0.01; MS tolerance 0.2 Da; MS/MS tolerance 0.2 Da; min peptide length 7; max peptide length 4600; max mis–cleavages 2; min number of peptides 1.

2.11. Cell interaction assay

THP–1 and Jurkat cells were labelled with the fluorescent membrane dyes; PKH26 and PKH67 respectively before treatment with PMA. PKH staining was done according to the standard procedure based on the manufacturer instructions (Sigma), as follows:

Cells suspension in medium without serum (5×10^5/ml) was centrifuged at 1500 rpm for 5 minutes, then the pellet of cells was suspended in 500µl of diluent C. The dye solution was prepared by adding 2µl of the PKH dye (26 or 67) to 500µl of diluent C, then the equal volumes of cells suspension and dye solution was mixed together and incubated for 5 minutes with periodic mixing. Staining was stopped by adding equal volume (1ml) of 1% BSA for 1 minute, then cells were centrifuged at 1500 rpm for 10 minutes, resuspended and washed in complete medium (3 times) to remove the unbound dye.

Both cell types were then differentiated and activated or polarised as described in their culture methods. Macrophage–like IFNγ+LPS control and FAM26F–3×FLAG THP–1s were co-cultured 1:1 with activated Jurkats in culture media without puromycin and imaged using the Leica AF6000 microscope. Fluorescence signal intensities were adjusted using LAS AF Lite (v 2.6.3, Leica). Overlapped or in-contacted cells were considered as attached.

2.12. Flow cytometry

Jurkat cells were washed in PBS and centrifuged at 1500 rpm for 5 minutes. Then they were stained with viability dye (Propidium Iodide, PI) to define live/dead cells, and after that the cells were washed in FACS buffer and centrifuged at 1500 rpm for 5 minutes. Next, staining was performed using proliferation dye CPD eFluor 670 or PKH67. Samples were analysed using BD FACS-Diva (v 8.0.1).

Chapter 3

Expression of TAKL mRNA variants in differentiating monocytes and macrophages

3.1. Introduction

The aim of the work presented in this chapter was to test the hypothesis that the expressions of certain mRNA variants of the TAKL gene were up regulated during differentiation of monocytes into macrophages and during polarisation of macrophages. This hypothesis was firstly based on an analysis of TAKL variants sequences in EST databases which found that TAKL-D is the variant expressed in most human tissues [Ellis et al., unpublished manuscript in appendix I], and secondly on preliminary laboratory observations made by former members of Dr Guesdon's group that the expression of TAKL was strongly increased in an *in vitro* model of macrophage differentiation of the monocytic cell line THP1 [Unpublished data by S. Kumar and I Tzani, shown in Fig. 3 of appendix II].

Differentiated macrophages are derived from blood-circulating monocytes and the produced macrophage phenotypes provide special different immune functions according to the tissue stimuli as was previously explained in chapter one.

The THP-1 cell line can be induced to differentiate into macrophage-like monocytes by a treatment involving transient exposure to 200nM phorbol 12-myristaye 13-acetate (PMA)**.** Treating suspension-growing THP-1 cells with PMA for 3 days and following by a 7-day period in culture without PMA leads the cells to attach to the plastic, stop dividing and differentiate to a state where they express several markers typical of monocyte-derived macrophages (Daigneault et al., 2010). Some macrophage characteristics, which are related to differentiation, have been demonstrated by Daigneault et al. in PMA-treated THP-1 cells such as increased number of mitochondria and lysosomes. The greater number of cytoplasmic organelles may be associated to significant kinetic functions. Additionally, cytokines responses are increased in PMA-differentiated THP-1 cells especially in IL-1β, TNF-α and LPS pathways (Daigneault et al., 2010).

We used this THP-1 model of differentiation to carry out a detailed exploration of the changes in expression of TAKL as well as of other genes encoding components of the TLR-TRAF-TAK1 signalling pathway. In these experiments THP-1 monocytic cell line was stimulated by PMA for 3 days, and RNA samples were collected before, during and in the 7-day differentiation period following the treatment.

After using this in vitro model to identify the TAKL mRNAs that were most likely to function as possible markers of macrophage differentiation, we used monocyte-derived macrophages (MDMs) differentiated *in vitro* from peripheral blood mononuclear cells (PBMC) using the macrophage colony-stimulating factor (M-CSF). Macrophages where then treated with

different cytokines to induce macrophage polarisation into M1 and M2-like macrophages. LPS and IFN-ϒ treatment was used for M1 cells and IL-4 treatment for M2 cells.
The expression of TAKL variants were assessed in THP-1 and MDM cells in order to examine the effect of differentiation on the expression levels.

3.2. Summary of aims and techniques

The main aims of the work presented in this chapter were:

- To check the specificity of these assays and determine the efficiencies of the Real-time PCR assays, especially the custom-designed assays targeting specific TAKL mRNA variants.
- To characterise the changes in expression levels of TAKL mRNA variants in the THP-1 cell line-based model of macrophage differentiation and to attempt the detection of the corresponding TAKL proteins by immunoblotting.
- To use other real-time PCR assays to explore if the expression of other genes encoding components of the TLR signal transduction pathway is also altered in this differentiation model.
- To study the expression of the possible differentiation markers identified in the THP-1 model during in vitro macrophage differentiation and polarisation of human peripheral blood monocytes.

3.3. Assessing the quality of RT-qPCR assays

3.3.1. Assessing RNA samples quality

Two sets of THP1 samples were collected: RNAs and protein lysates. Samples were isolated before PMA treatment (Time zero), during PMA stimulation (8 hours, 16 hours, 1 day, 2 days and 3 days) and during the resting period in medium without PMA (after 3 days to 12 days of PMA exposure). The same sets of samples, RNAs and protein lysates, were collected from human monocyte-derived macrophages (hMDMs), which were as follows: unpolarised macrophages, M1 and M2 phenotypes (M^{un}, $M^{IFN\gamma+LPS}$ and $M^{IL\text{-}4}$, respectively).

All RNA samples were assessed for quality by electrophoresis (Figure 3.1), when 18s and 28s rRNA bands appeared clearly, RNA samples were considered intact, not degraded and of suitable quality. Then, the best quality RNA samples were selected for cDNA synthesis and RT-qPCR assays.

In figure 3.1, the 18s and 28s bands appeared in all RNA samples that has been tested, additionally we selected the best quality RNAs depending on the strength of the bands.

As an example, from the PMA-untreated THP-1 RNAs (Figure 3.1A), we selected samples 2 and 6 for cDNA synthesis. While RNA samples after 16 hours and 3 days of PMA treatment (Figure 3.1B) and MDM samples (Figure 3.1C), were with a high quality and all had been used for cDNA synthesis.

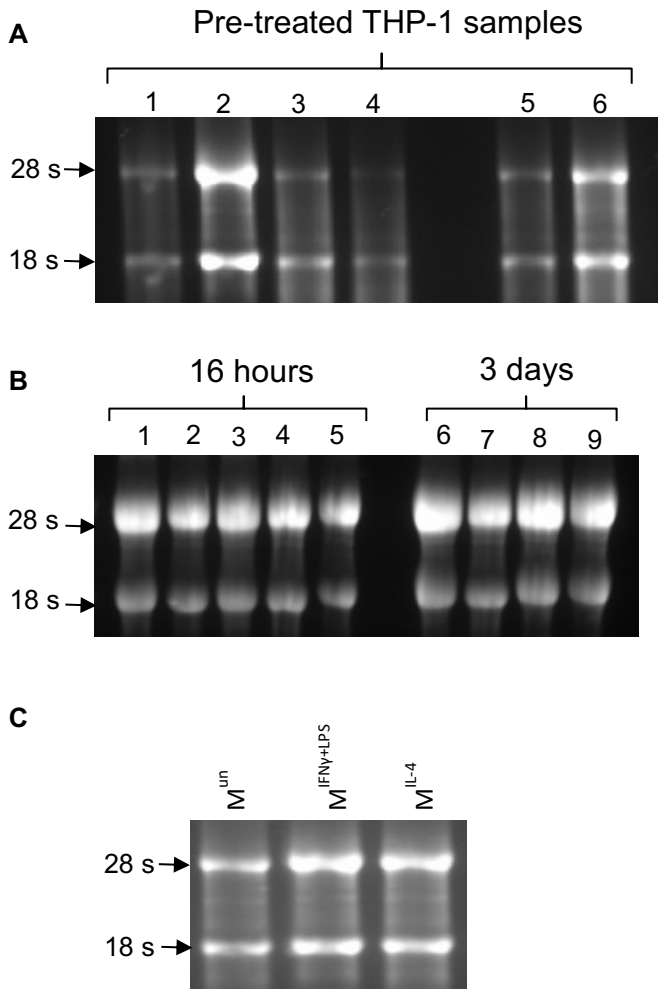

Figure 0.1 Assessing the quality of RNA samples by agarose gel
RNA samples separated by 1% agarose gel to select those suitable for 1st strand cDNA synthesis to use in RT-PCR assays. (A) RNA samples from PMA-untreated THP-1 cells (1, 2, 3, 4, 5 and 6). (B) RNA samples that were isolated after 16 hours (1, 2, 3, 4 and 5) and 3 days (6, 7, 8 and 9) of PMA treatment. (C) RNA samples from human primary unpolarised macrophages (M^{un}), the polarised isoforms M1-like ($M^{IFN\gamma+LPS}$), and M2-like (M^{IL-4}).

3.3.2. Size determination of RT-qPCR products

To check if the TaqMan probes were detecting the target cDNAs specifically, the size of RT-qPCR products amplified from THP-1 cDNA preparations was examined using gel electrophoresis. All assays that have been tested were detecting the correct size products (Figure 3.2). TAKL probes that worked with THP-1 samples were as follows: TAKL-all, TAKL-1-D, TAKL-2-L, TAKL-3/4.

Exceptionally, TAKL-1-J and TAKL-2-I which were attaching to the positive plasmids and their band sizes were in the expected size when tested on the gel (Figure 3.2D), but not working with THP-1 samples, so that could be because these variants are not expressed by THP-1 cells. In addition, TAKL-1-K did not work with any qPCR assay, and all TAKL variants are custom probes designed by Thermofisher software, so the sequence of primers was chosen automatically by the software. Designing new primers for TAKL-1-K might solve this limitation, but it is a time-consuming process. That can be considered as a future work for this variant.

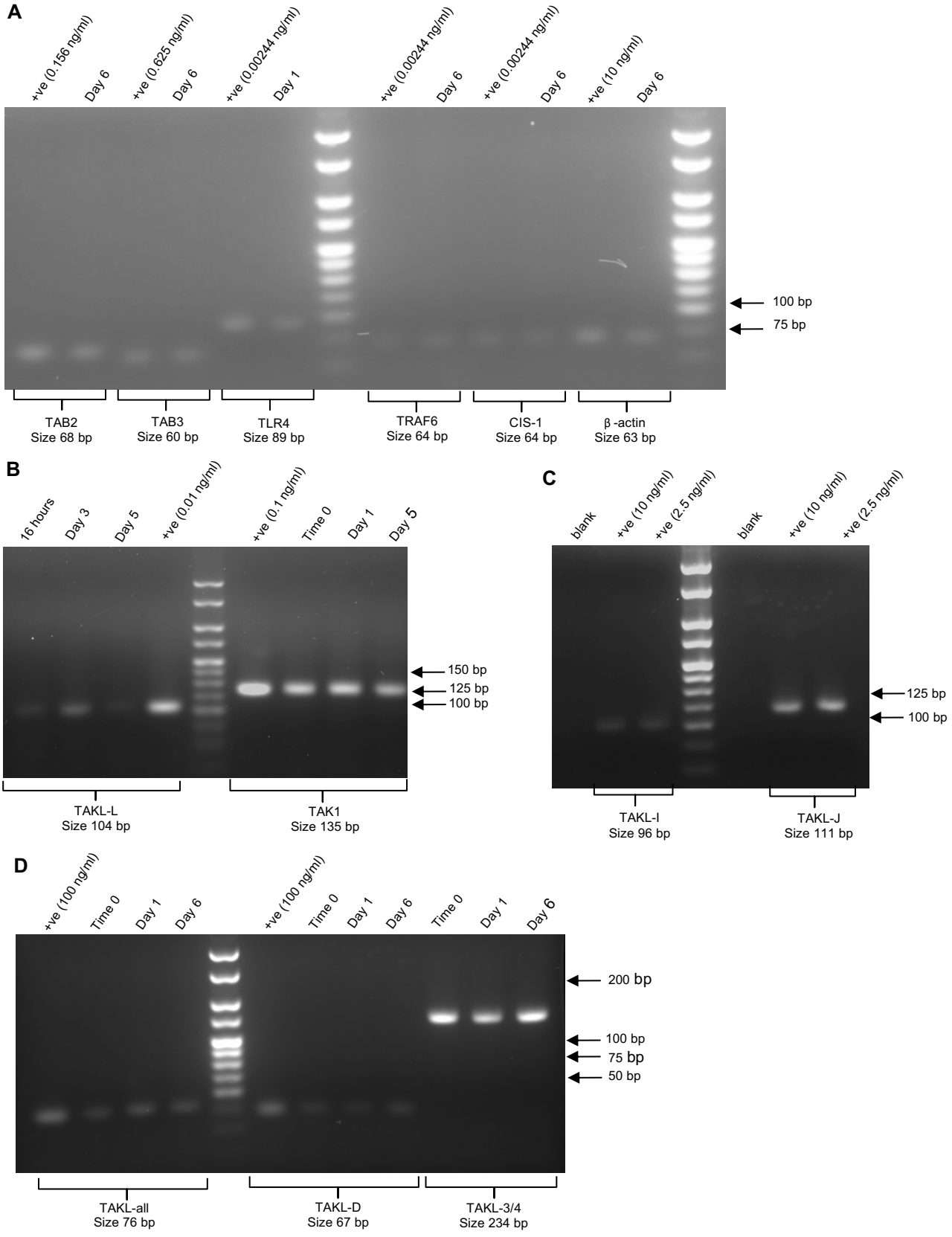

Figure 0.2 Determination of RT-qPCR products sizes

Positive plasmid controls (+ve), and THP-1 time course samples (day stated above respective gel) from RT-qPCR assays were presented on 3% agarose gels. The blue/orange 6x loading dye ladder (Promega) was used in all gels. The expected sample sizes are shown at the bottom of each gel. (A) PCR products from the following assays: TAB2, TAB3, TLR4, TRAF6, CIS-1 and β-actin. (B) PCR products from the following assays: TAKL-L and TAK1. (C) PCR products from the following assays: TAKL-I and TAKL-J. (D) PCR products from the following assays: TAKL-all, TAKL-D and TAKL-3/4.

3.3.3. Calibration of TaqMan RT-qPCR assays

We produced calibration curves for all TaqMan assay for which a cloned cDNA template was available (Table 2.5). The calibration data was generated by carrying out assays on serial dilutions of the cDNA and the data were analysed as described previously in section 2.3.10. The resulting plots are shown in Figures 3.3 and 3.4. The correlation coefficients, slopes and intercepts of the best fitting lines and the efficiencies of the reactions are shown in the corresponding tables below the figures.

To interpret the results, it is important to note that the efficiency is the important parameter for determining the suitability of the assay to the comparative method of analysis. The acceptable efficiency range for comparative quantitative analysis is considered to be 100% ± 10%. This is because the ΔΔCt calculation used for comparative analysis is only valid if the target gene and normaliser gene assays have similar efficiencies. Efficiencies outside the 100% ± 10%range would be too different from the efficiency of the β-actin normaliser assay, which has been optimised by ThermoFisher to be very close to 100%.

Unlike the comparative method of analysis, the absolute quantitation method takes in account the actual efficiency of the assay because it uses the slope and the Y axis intercept of the calibration curve in its calculations. Therefore, it can in principle correct for lower efficiencies than the comparative method.

The results show that the TAKL-All, TAKL-D, TAKL-L and TAKL-I assays had efficiencies within the acceptable range for comparative analysis (Figure 3.3). However, the efficiencies of the TAK-1 and TAKL-J assays were outside the 100% ± 10% range, and these assays cannot be expected to provide accurate quantitative results when analysed by the comparative method. Nevertheless, the TAK1 assay whose efficiency is 80% may still be able to generate reliable quantitative data when analysed by the absolute method. In the case of the TAKL-J assay, it is likely that the calibration curve itself is unreliable because the very high efficiency of 149 % is physically impossible and likely to result from experimental error. This interpretation is also supported by the relatively low value of the correlation coefficient (0.96).

Figure 3.4 shows the efficiency of other assays (TAB2, TAB3, TRAF6, CIS1 and GPS2) was lower than 80%. These poor efficiencies seem genuine since the correlation coefficients were close to 0.99 (Figure 3.4). Therefore, these assays cannot be expected to provide accurate quantitative results by the comparative quantitation method. Like the TAK1 assay, they may provide more useful results if analysed by the absolute quantitation methods.

It is worth pointing that in principle, it would also have been possible to determine the efficiencies of the assays for which we did not have a cloned cDNA template, such as the IL-8, β-actin, β2M and OAZ assays. This is can be done by assaying serial dilutions of a biological sample instead of a purified cDNA template. The reasons why this was not attempted were as follows. First, although the results would have allowed us to determine the efficiencies of these assays, they would not have provided us with the parameters needed for absolute quantitation since the absolute amount of template in the biological sample used a standard was unknown. Second, these assays had been used reliably by many other researchers (Dheda et al., 2004, de Jonge et al., 2007) and were considered trustworthy by our colleagues, so there was no strong reason for checking efficiencies.

A

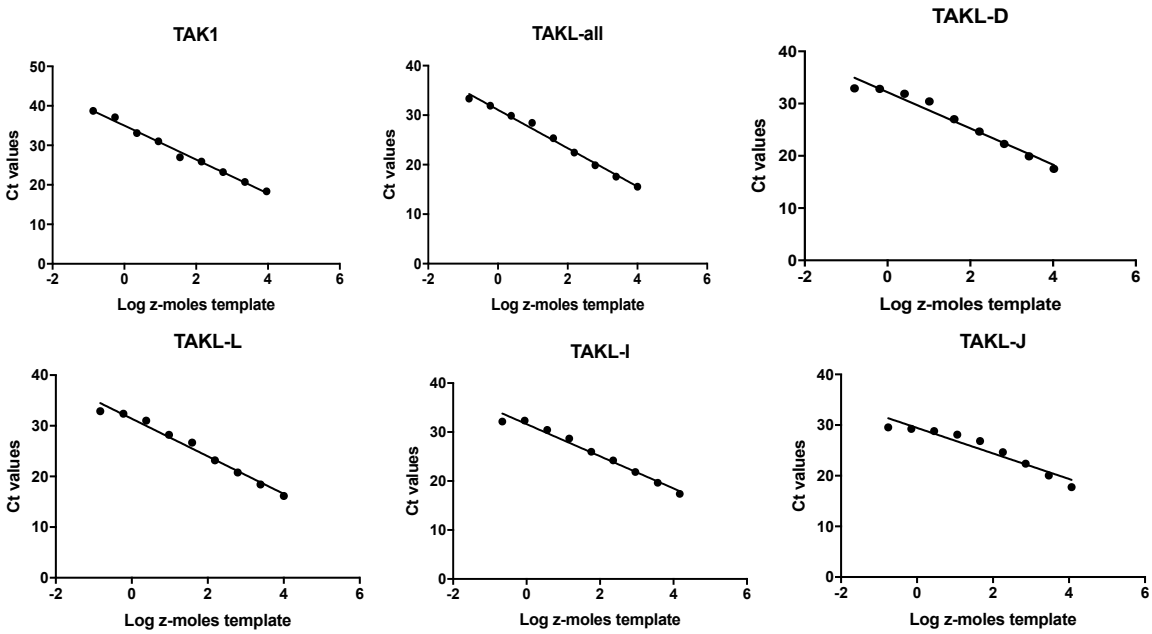

B

Genes	Probe ID	Template	Correlation	Slope	Intercept	Efficiency
TAK1	Hs01105682_m1	TAK1-a/pcDNA4	-0.996	-3.919	34.30	81.3%
TAKL-All	Hs00963407_m1	YFP-TAKL2	-0.9958	-3.625	30.91	89.5%
TAKL-D	Hs00963405_m1	IMAGE 4244723	-0.9824	-3.327	31.56	100.1%
TAKL-L	AJGJQGQ	YFP-TAKL2	-0.9908	-3.381	30.79	99.4%
TAKL-I	AJRR90Q	IMAGE 814105	-0.9903	-3.285	31.63	101.55%
TAKL-J	AJFASAI	IMAGE 4244723	-0.9613	-2.523	29.46	149.07%

Figure 3.3 Calibration curves for TaqMan probes 1

(A) Calibration curves for TaqMan probes targeting TAK1, TAKL-All or TAKL variants (D, L, I or J) with serial 4-fold dilutions. On the X axis, the log (10) zeptomoles (10^{-21} moles) template against Ct values on the Y axis. Data shown are in duplicates, except. The results were analysed by linear regression. (B) The resulting parameters (correlation, slope, amplification factor and efficiency) shown in the table at the bottom. The amplification factor and efficiency are calculated from the slope by the qPCR efficiency calculator on ThermoFisher website.

A

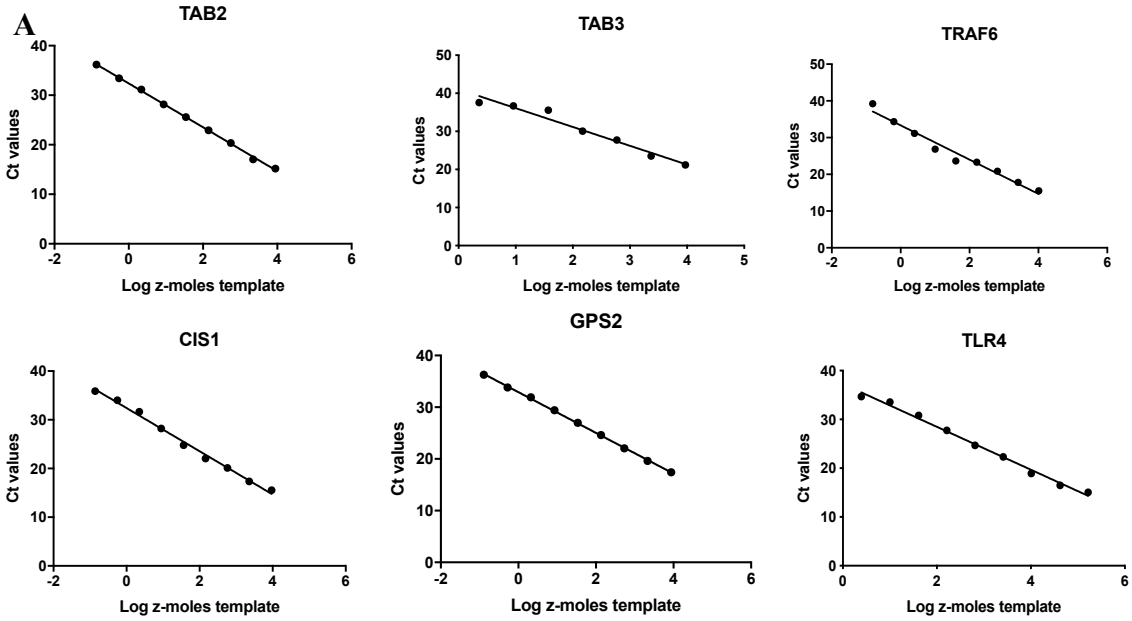

B

Genes	Probe ID	Template	Correlation	Slope	Intercept	Efficiency
TAB2	Hs00248373_m1	CFP-TAB2	-0.9995	-4.426	32.39	68.25%
TAB3	Hs01087551_m1	CFP-TAB3	-0.9823	-4.941	41.04	59.36%
TRAF6	Hs00371512_g1	GFP-TRAF6	-0.9853	-4.663	33.34	63.86%
CIS1	Hs00367082_g1	YFP-CIS1	-0.9968	-4.441	32.42	67.95%
GPS2	Hs00409956_g1	GPS2-PD27	-0.9997	-3.939	32.92	79.42%
TLR4	Hs00152939_g1	TLR4-pcDNA3.1	-0.9965	-4.398	37.27	68.79%

Figure 3.4 Calibration curves for TaqMan probes 2

(A) Calibration curves for TaqMan probes targeting TAB2, TAB3 or TRAF6, CIS1, GPS2 or TLR4 with serial 4 fold dilutions. On the X axis, the log (10) zeptomoles (10^{-21} moles) template against Ct values on the Y axis. Data shown are in duplicates and analysed by linear regression. (B) The resulting parameters (correlation, slope, amplification factor and efficiency) shown in the table at the bottom. The amplification factor and efficiency are calculated from the slope by the qPCR efficiency calculator on ThermoFisher website.

3.3.4. Comparing the expression of β-actin to other housekeeping genes

A housekeeping gene is a gene that is transcribed and expressed continually in all cell types. It is used as an expression reference point in qPCR assays to normalise the expression of other variable genes.

Data where normalised to housekeeping genes in each RT-qPCR experiment: β-actin, β-2microglobulin (β-2M) and Ornithine Decarboxylase Antizyme 1 (OAZ1) were assessed in THP-1 time course assays and two genes (β-actin and GAPDH) were used in hMDMs assays. Previously used genes were β-actin in THP-1 assays and GAPDH in hMDMs and other genes (β-2M and OAZ1) were tested for the first time in this project on these macrophage-like cells to optimise the optimal housekeeping gene to use on macrophages under stimulation conditions. All these genes are housekeeping genes used as standard references for normalisation of RT-PCR data by many investigators (Dheda et al., 2004, de Jonge et al., 2007). However, because of the possibility that the expression of some of these genes might have been altered during differentiation processes studied in this work, we assessed the behaviour of several of these genes in each experimental system.

Ct values were plotted against PMA time course samples from THP-1 qRT-PCR assays (Figure 3.5). Normalising data to β-actin or β-2M was always giving a similar interpretation of expression results for all time course samples (Figure 3.5); so selecting one of them was depending on having Ct value result for each sample replicate, in order to increase the samples number. OAZ1 data was slightly different (Figure 3.5) and it has been used for some of the qPCR assays but not all of them.

In conclusion these results showed that expression of all three housekeeping genes β-actin, β-2M and OAZ1 showed no strong variations during the PMA-induced differentiation of THP-1 cells. Our data suggests that in this system, the expression β-2M might be slightly more stable than that of the other two genes, which both exhibited minor fluctuations between time zero and day one. However, the β-actin results still showed very good stability as they remained very close to those of β-2M at almost all time points. Therefore, in order to be able to compare our results with earlier data generated by other researchers using β-actin we decided to carry on using the latter as our normaliser gene.

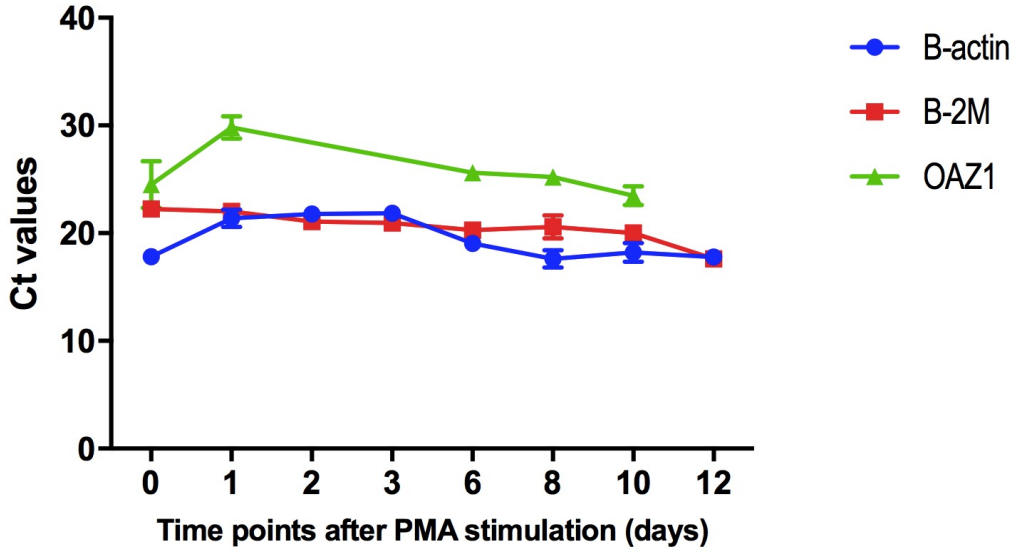

Figure 3.5 Assessing housekeeping genes

Three housekeeping genes (β-actin, β-2M and OAZ1) Ct values were measured over time follows PMA stimulation to determine the housekeeping gene of choice for PCR data normalisation. Ct values are on the X axis and THP-1 time course samples on the Y axis. β-actin and β-2M linear curves are similar, while OAZ1 curve is slightly higher.

3.4. Assessing the expression of genes of interest in THP-1 cells by the comparative quantitation analysis method

3.4.1. Expression of TAKL mRNA variants

The overall expression of TAKL mRNAs was determined by TaqMan RT-qPCR using the TAKL-all probe. The samples were cDNA preparations from THP-1 cells at different times during and after PMA treatment, starting from PMA-untreated samples (Time zero) and ending with 12 days samples after PMA treatment. The expressions of the kinase TAK1 and β2-microglobulin mRNAs were also measured. The data were analysed using the ΔΔCT method to normalise them to the β-actin mRNA levels and express the results relative to the level of expression at time zero. The data was analysed statistically using one-way ANOVA. Significance test was then calculated comparing all time points to PMA untreated THP-1 samples (baseline level), (see the table in Figure 3.6E).

The results (Figure 3.6A and B) suggested that expression of TAKL was dramatically elevated on the first day of PMA treatment (51.592- fold stimulation). This was followed by a decrease at day 2, 3 and 6 of PMA stimulation, and a decrease at day 8 (0.628- fold). The differences between the expression levels of TAKL-all at day 0 (baseline level) and each of the maximum levels (at day 1, 2, and 3) were statistically significant ($P < 0.0001$) and the second elevation level at day 6 was also statistically significant ($P = 0.003$).

Interestingly, the mRNAs encoding the kinase TAK1 were also activated following PMA stimulation. This increase was represented in two peak points, the first peak was at day 2 and 3 and it was statistically significant ($P = 0.0005$ *and* $P = 0.0035$, respectively). The second peak was at day 8 but it was not statistically significant (Figure 3.7).

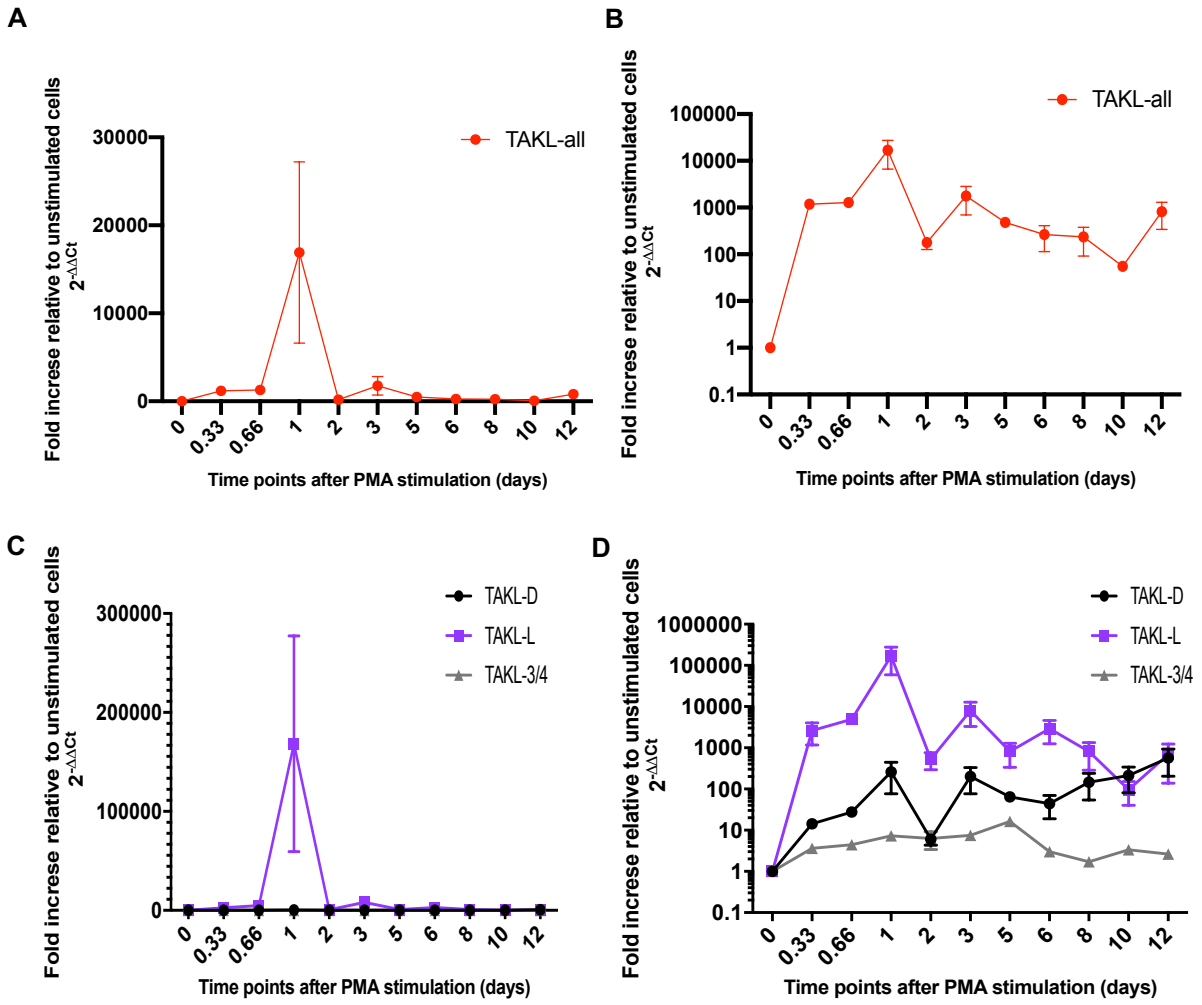

E

Time points Days	TAKL-all		TAKL-D		TAKL-L		TAKL-3/4	
1	****	*P* <0.0001	Ns		**	*P* =0.0023	*** *	*P* =0.0001
2					****	*P* <0.0001		*P* <0.0001
3							ns	
6	**	*P* =0.0030			Ns			
8	ns							
10	****	*P* <0.0001	***	*P* =0.0002				

Figure 3.6 RT-qPCR assay of TAKL-all and TAKL variants mRNAs expression during the PMA-induced macrophage differentiation of THP1 cells

(A) Expression curve of TAKL-all transcripts mRNA relative to its level in non-stimulated THP1 cells. (B) Same data of A, except that the Y axis was represented as log10. (C) Expression curves of individual TAKL mRNA variants; TAKL-D, TAKL-L which encoding TAKL-1, TAKL-2, respectively, and of all the mRNA variants encoding TAKL-3 and TAKL-4 proteins. (D) Same data of C, except that the Y axis was represented as log10. (E) Data were normalised to β-actin by the ΔΔCt method and are means ± SEM of n=4, and statistically analysed using one-way ANOVA and the table represents the significant elevations with *P* values for each variant among the time course samples comparing to PMA-untreated THP1 cells.

A

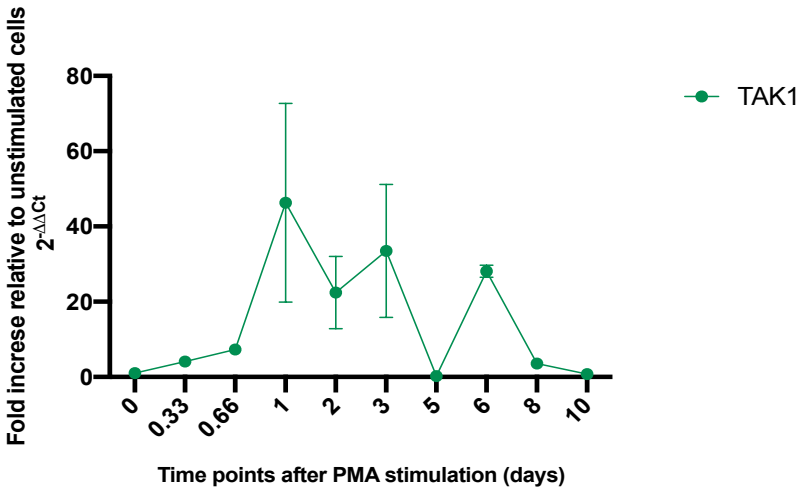

B

Time points Days	TAK1	
0.33	*	*P* =0.0174
0.66	****	*P* <0.0001
1	ns	
2	***	*P* =0.0005
3	**	*P* =0.0035
5	ns	
6		
8		
10		
12		

Figure 3.7 RT-qPCR assay of TAK1 mRNAs expression during the PMA-induced macrophage differentiation of THP1 cells

(A) Expression curves of TAK1 relative to their expression level in non-stimulated THP1 cells. Data were normalised to β-actin by the ΔΔCt method and are means ± SEM of n=4. (B) The data was statistically analysed using one-way ANOVA and the table represents the significant elevations with *P* values for each gene among the time course samples comparing to PMA-untreated THP1 cells.

Specific TaqMan RT-qPCR probes were used for individual TAKL mRNA variants to determine which variants were responsible for the successive increases seen at days 1, 2 and 3 of the differentiation process. The results (Figure 3.6) show that expression of the mRNA encoding TAKL-L was strongly activated at day 1 (83- fold, $P = 0.0023$), day 2 (169- fold, $P < 0.0001$) and day 3 (201- fold, $P < 0.0001$). We also assayed one of the mRNA variants encoding TAKL-1 (mRNA variant D) and all the mRNAs variants encoding TAKL-3 and TAKL-4 together. The TAKL-D assays showed two high activation peaks at day 5 (64- fold), which was not statistically significant from control values, and at day 10 (211- fold $P = 0.0002$). The TAKL-3/4 mRNAs levels show a low increase at day 1 (11- fold $P = 0.0001$) and day 2 (7- fold, $P < 0.0001$). Although these increases were very small compared to that seen with TAKL-D and TAKL-L.

These findings are consistent with a bioinformatics analysis of the TAKL EST data available in GenBank that has been done by others in Dr Guesdon (see Figure 1.4 and section 1.5.1) and which showed that TAKL-D and TAKL-L have been much more frequently cloned than the other TAKL mRNA variants in all the human cDNA libraries that have been used in EST projects. This EST data analysis therefore strongly suggest that TAKL-D and TAKL-L are the main products of the TAKL gene.

It is also important to note that in addition to the TAKL-D and TAKL-L mRNA, TAKL-1 protein can also be expressed by two other mRNA variants, TAKL-J and TAKL-K, and TAKL-2 protein also can be expressed by TAKL-I. However, as it has been mentioned previously, the custom-TaqMan assays for TAKL-J, TAKL-K and TAKL-I were found not to be reliable (see section 3.3.2 and 3.3.3) and we therefore did not attempt to assay these variants.

The results shown in Figure 3.6 therefore suggest that the up-regulation of two specific mRNA variants, TAKL-D and TAKL-L (which encode respectively the TAKL-1 and TAKL-2 proteins) probably contribute to the changes in overall TAKL gene expression that had been detected previously with the TAKL-all assay during the THP-1 differentiation into macrophages (Figure 3.6). This suggests that the alternative promoters that control the expression of the TAKL-D and TAKL-L mRNA variant may be activated specifically during PMA-induced differentiation of THP-1 into macrophages.

3.5. Assessing the expression of genes of interest in THP-1 cells by the absolute quantitation analysis method

3.5.1. Measuring TAKL mRNAs expression levels

To ascertain if the changes in expression of TAKL-D and TAKL-L accounted quantitatively for all the of the overall increase in TAKL expression in the THP1 macrophage differentiation model, we re-produced the Fig. 14 experiments under condition suited to the analysis of the RT-qPCR data by the absolute quantification method. The main advantage of the absolute quantification method is that it analyses the data using the actual efficiency parameters previously determined for each specific assay when we produced their calibration curves using known amounts of cloned cDNA as templates (see Figure 3.3 and 3.4). These curves allow the calculation of the number of copies of template cDNA corresponding to the Ct value measured in each sample. By taking in account the number of cells used to produce the cDNA sample, the number of copies in the assay reaction mix can be converted into number of copies of mRNA per cell (see section 2.3.12 for details of these calculations).

The absolute analysis of TAKL-all mRNA levels, measured with a probe targeting a common exon junction shared by all mRNA variants, showed that in growing THP-1 cells that have not yet been exposed to PMA, the basal expression levels of the TAKL gene (all variants included) was 0.011 ± 0.005 copies per cell (Figure 3.8A). Thus, at any one time, only about 11 cells in a sample of 1,000 cells would be expressing a TAKL mRNA.

By comparison, the levels of the TAKL-D (Figure 3.8B) and TAKL-L (Figure 3.8A) mRNA variants in these cells were found to be respectively 0.015 ± 0.008 and 0.005 ± 0.002 copies / cells. The mRNA variants encoding TAKL-3 and TAKL-4 proteins (Figure 16, B) were expressed at even lower levels of 0.0011 ± 0.0009 copies / cells, a value equivalent to the expression of a single mRNA at any one time in a population of 1,000 cells. These low numbers imply that at any one time, in a population of 1,000 THP-1 cells in our standard growth culture conditions, between 7 and 23 cells would be expected to contain a single TAKL-D mRNA, 5 cells would contain a TAKL-L mRNA and only 1 cell would contain an mRNA variant encoding either TAKL-3 or TAKL-4.

Similar low expression levels equivalent to less than 1 copy per cell for have been found in other studies, for example for several up-regulated cytokine genes in monocytes (Bas et al., 2004). As will be explained in the "Discussion" section 3.8.3, these low values are thought to result from expression of certain genes in small discrete bursts of transcriptional activity that are followed by long intervals of "off" periods which can be long enough for the mRNAs produced by one burst to be degraded (Smirnov et al., 2018). The low number of copies per cells of TAKL mRNAs that we have measured are therefore consistent with the results typically obtained for genes expressed at low levels through infrequent bursts of transcription in mammalian cells.

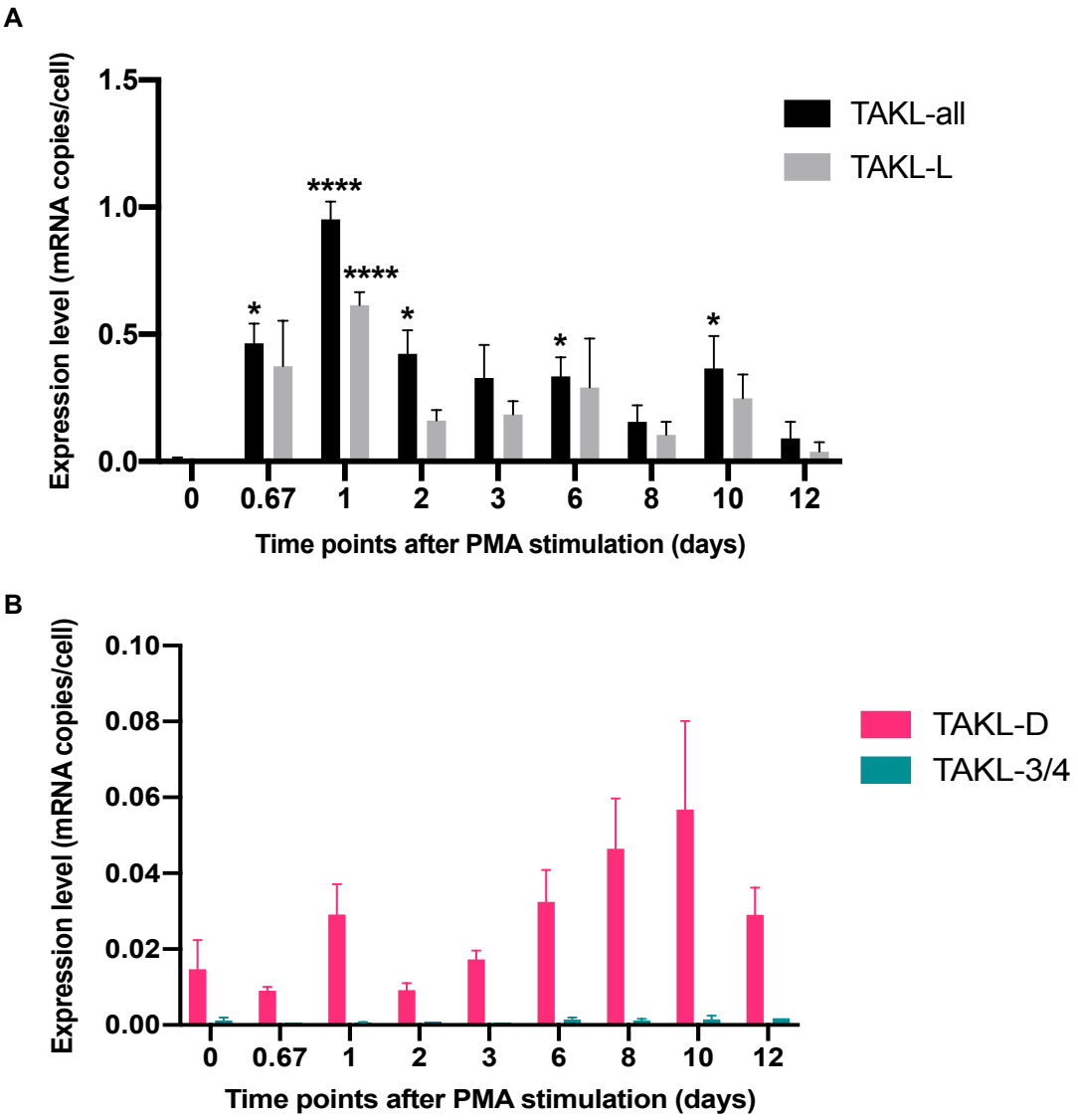

Figure 3.8 RT-qPCR assay of total TAKL mRNAs and specific variants expression during the PMA-induced macrophage differentiation of THP1 cells (Absolute quantification method)

(A) Standard curves of TAKL-all and TAKL-L were used to calculate the template copies number per cell by absolute quantification method. Data are displayed as means ± SEM of four independent experiments. Data was statistically analysed using one-way ANOVA and the stars on TAKL-all bars represent the significance levels of elevations with *P* values for mRNA expression among the time course samples comparing to PMA-untreated THP1 cells. (B) Standard curve of TAKL-D and TAKL-3/4 were used to calculate the template copies number per cell by absolute quantification method. Data are displayed as means ± SEM of four independent experiments. Data was statistically analysed using one-way ANOVA and no significant changes in TAKL-D and TAKL-3/4 expression during time points relative to time zero.

3.5.2. Expression of other genes involved in TLR4 signalling

To establish these expression levels in a functional perspective, the absolute quantification RT-qPCR approach was used to measure the expression of several genes encoding known components of the TAK1-TRAF6 signalling complex, of which TAKL proteins are hypothesised to belong. Figure 3.9 represents the expression of other genes in the signalling pathway (TRAF6, TAB2 and TAB3), and the two signalling inhibitors that have been reported to associate with TAKL-3, CIS1 and GPS2 (Rual et al., 2005, Wang et al., 2011). It was found that the expression levels of TAK1 (Figure 3.10A), TAB2, TAB3 and TRAF6 (Figure 3.9A, B and C) in growing THP-1 cells that had not been stimulated by PMA to be 0.634 ± 0.14, 1.64 ± 0.54, 0.73 ± 0.22 and 1.53 ± 0.66 respectively. The expression level of a receptor known to control this signalling pathway, TLR4 (Figure 3.9D), was also measured and found that its expression to be 0.065 ± 0.019 in PMA untreated THP-1 cells. This value was noticeably lower than those measured for the TRAF pathway components, but it is still higher than the levels of basal expression of TAKL in THP-1 cells not stimulated by PMA. CIS1 and GPS2 expression (Figure 3.9E and F) was high, at the basal level, in PMA un-stimulated THP-1 cells. These expression values (in Figure 3.9) are within the range of what would be expected for genes expressed at constant but low level, except for TAB3 that had high significant peaks of expression compared to time 0 (between 10-20 copies/cell), P= 0.0004, 0.0365 and 0.0145, at days 6, 8 and 10 of PMA treatment, respectively.

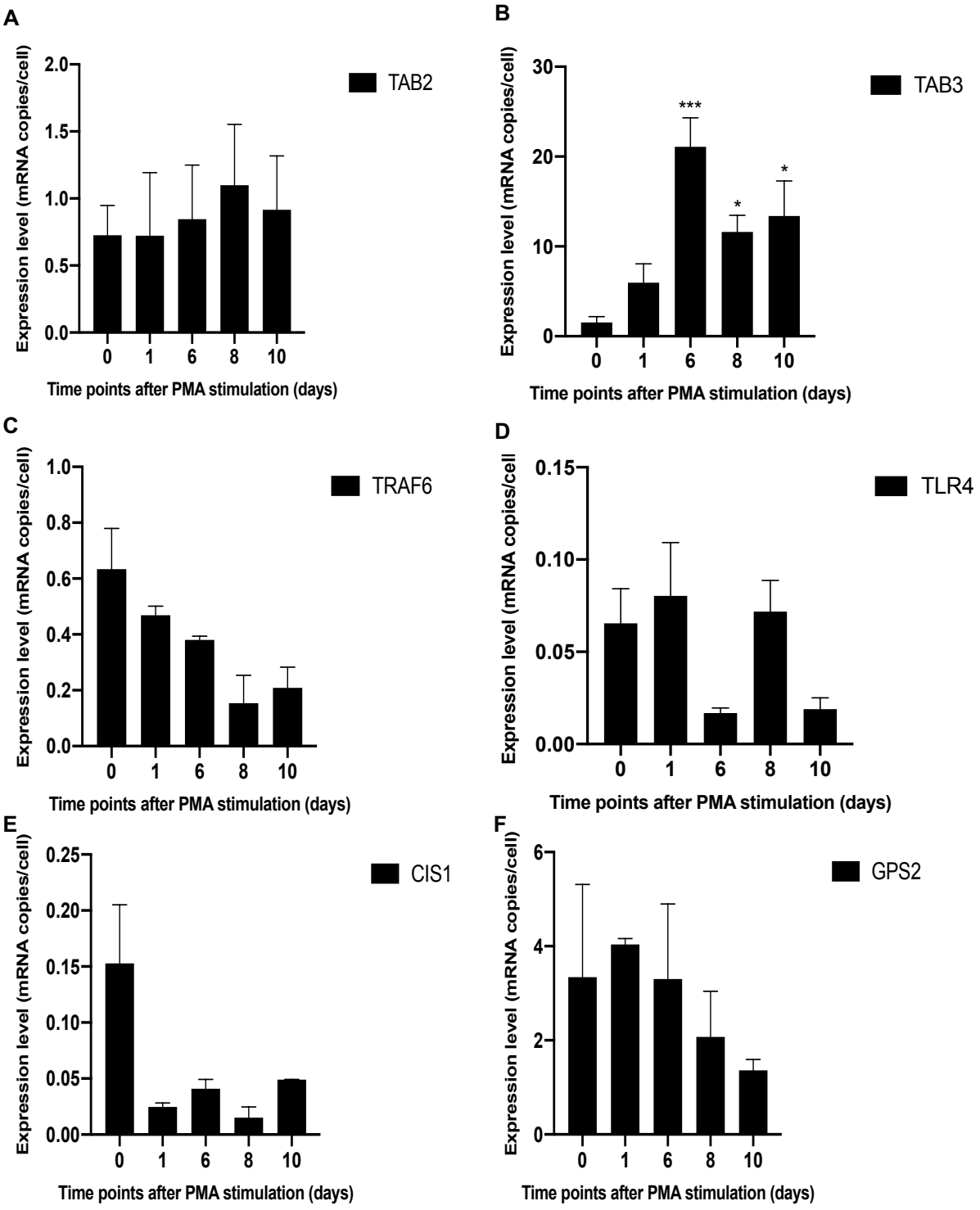

Figure 3.9 RT-qPCR assay of expression of other genes contributing in TAK1-TRAF6 signalling pathway during the PMA-induced macrophage differentiation of THP1 cells (Absolute quantification method)

Standard curves of TAB2 (A), TAB3 (B), TRAF6 (C), TLR4 (D), CIS1 (E) and GPS2 (F) were used to calculate the template copies number per cell by absolute quantification method. Data are displayed as means ± SEM of Three independent experiments. Data of all graphs was statistically analysed using one-way ANOVA and the stars on TAB3 bars represent the significance levels of elevations with *P* values for mRNA expression among the time course samples comparing to PMA-untreated THP1 cells, and when stars are absent on TAB2, TRAF6 and TLR4, it means no significant changes in their expression levels during time points relative to time zero. P values on Graph pad prism are as follow: (*) $P \leq 0.05$, (**) $P \leq 0.01$, (***) $P \leq 0.001$ and (****) $P \leq 0.0001$.

3.5.3. Analysing TAKL-L absolute expression in relation to expression of mRNAs encoding its partners in the TRAF complexes

It has been hypothesised that TAKL may function as a competitive inhibitor of the binding of the kinase TAK1 to its adapters TAB2 and TAB3. In this model of TAKL function, the activity of TAK1 is regulated by changes in the relative amounts of expression between the agonist (TAK1) and its inhibitor (TAKL) or their receptors (TAB2-TAB3-TRAF6).

The ratios of TAKL-all and TAKL-L mRNA expression to TAK1 expression (Figure 3.10B) were measured to determine if TAKL gene plays any inhibitory role in TAK1 gene expression as it has been hypothesised. Unfortunately, the ratio graph reflects the same peaks points of TAK1 mRNA expression at 1, 6 and 10 days of the PMA treatment on THP-1 cells, with un-noticeable difference in copies number of TAK1.

In conclusion therefore, the absolute quantification results on the undifferentiated growing THP-1 cells which have not been stimulated by PMA, the TAKL gene is expressed only at very low levels that are much lower than those of the RNAs that encode the major components of the TRAF signalling complexes. This suggests TAKL proteins are also likely to be expressed at levels lower than TRAF complex components such as TRAF6, TAK1, TAB2 or TAB3.

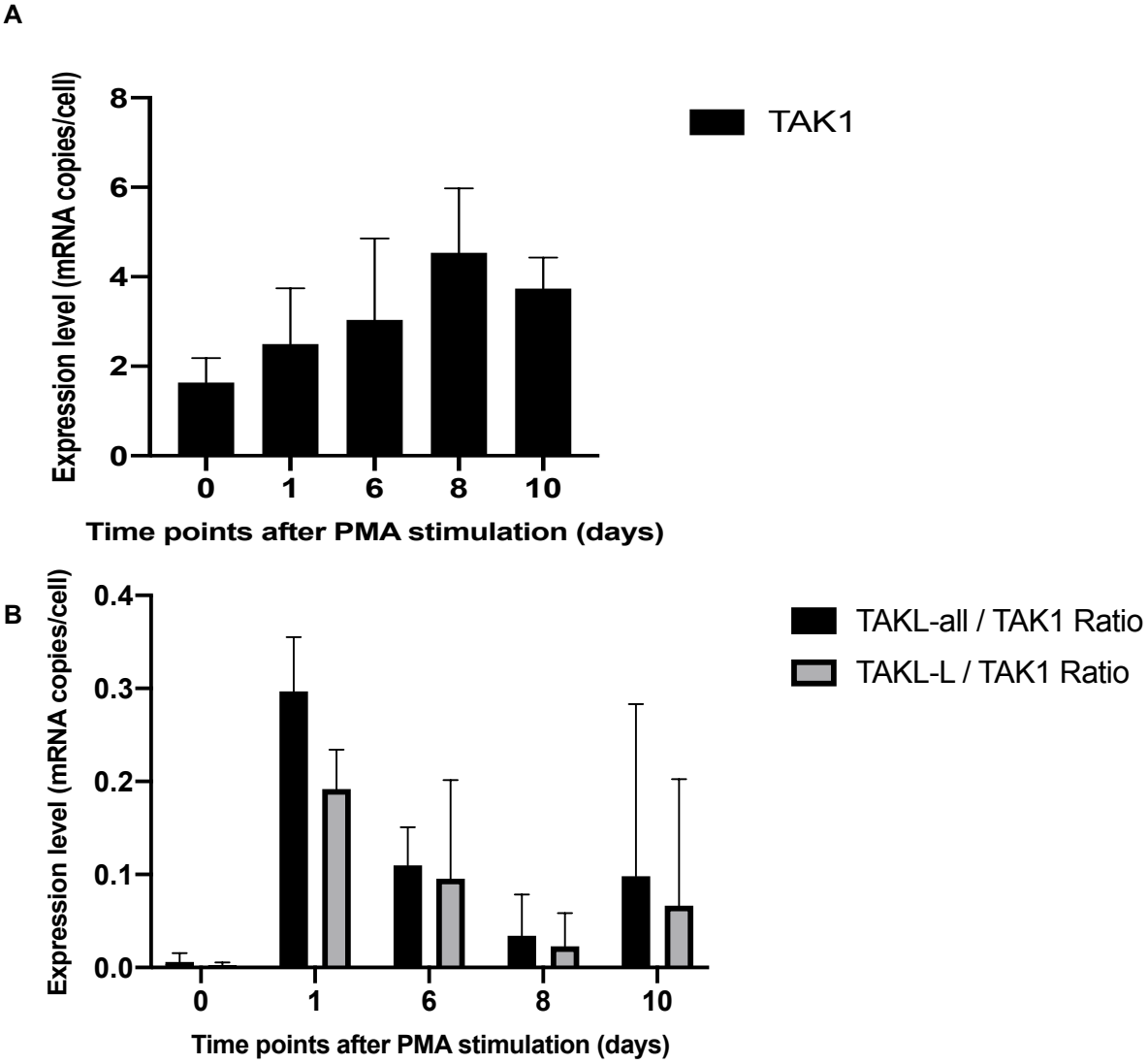

Figure 3.10 RT-qPCR assay of total TAK1 mRNAs expression and TAKLs/TAK1 ratios during the PMA-induced macrophage differentiation of THP1 cells (Absolute quantification method)
(A) Standard curve of TAK1 was used to calculate the template copies number per cell by absolute quantification method. (B) The ratios of TAKL-all/TAK1and TAKL-L/TAK1 were calculated from means of absolute expression levels. Data of both graphs are displayed as means ± SEM of four independent experiments, and statistically analysed using one-way ANOVA and no significant changes in TAKL-D and TAKL-3/4 expression during time points relative to time zero.

To conclude the absolute quantification method results, the data confirmed earlier observations, by ΔΔCt method, of increased TAKL expression during PMA-induced monocytic differentiation of THP-1 cells. Absolute data has showed that in PMA treated THP-1 cells; overall expression of TAKL mRNAs was strongly increased 0.66 at 1 day after PMA treatment (Figure 3.8A). The maximum significant increase *(P value <0.0001)* was measured 24 hours after PMA stimulation with 0.95± 0.07 TAKL mRNA copies / cell. Expression levels then decreased over the next few days to reach a post-stimulation minimum of 0.15 ± 0.07 copies / cell at day 8 and then rose again to reach a second peak of 0.37 ± 0.13 copies / cell on the 10th day after PMA stimulation (Figure 3.8A). This is the day on which the differentiation process was deemed to be complete according to earlier studies (Daigneault et al., 2010). These differences of TAKL-all expression, at day 1 with *P <0.0001*, day 2 with *P = 0.0140*, day 6 with *P = 0.0446*, and day 10 with *P = 0.0237*, are statistically significant (Figure 3.8A). Expressed as ratios relative to the basal expression level before stimulation they correspond to increased expression levels of 90 and 35-fold for the 1st (day 1) and 2nd (day 10) peaks, respectively.

Similar to the overall gene expression, the expression of the TAKL-L mRNA variant (encoding TAKL-2 protein) also showed a rapid strong significant (*P <0.0001*) increase relative to basal level that peaked at day 1 with 0.62 ± 0.05 copies / cell. This was followed by a decrease to intermediate values of about 0.10 to 0.30copies /cell between days 2 and days 10 of the differentiation process (Figure 3.8A). These values correspond to fold increases of 204 and 82-fold relative to expression of TAKL-L before stimulation. The expression then decreases gradually during the following days of the PMA-rest.

In order to compare the overall findings of absolute and ΔΔCt approaches, we noticed the values measured for overall TAKL expression (TAKL-all probe) are consistent with those measured for the two main individual variants (TAKL-L and -D). Also, the same expression peak of TAKL-all was found after 1 day of PMA stimulation, and this was a highly significant increase in both methods with *P <0.0001*. That elevation in TAKL-all mRNA expression is mainly due to TAKL-L, a lesser extent to TAKL-D, and no change in other variants encoding TAKL-3 and TAKL-4) are qualitatively identical to those obtained previously by ΔΔCt method.

In absolute results, the increase at day 1 was highly significant in both TAKL-all and –L (*P <0.0001).* On the other-hand in the relative results, the increase was highly significant in

TAKL-all expression (*P <0.0001*), and less significant in TAKL-L (*P =0.0023*). Even the SEM upper and lower limits of TAKL-all at day 1 were huge with ΔΔCt, comparing to the SEM limits of the absolute. Based on the significant tests and the SEM of both methods, the absolute increase in TAKL-all expression appears to be more reliable than ΔΔCt.

The expression of other genes in TAK1-TRAF6 signalling pathway was measured by RT-qPCR and analysed using the absolute quantification method, such as TAB2, TAB3, TRAF6, TLR4, CIS1 and GPS2 (Figure 3.9). The mRNA expression of TAB2, TRAF6 and TLR4 did not show any statistically significant difference (Figure 3.9). TAB3 mRNA increases in PMA treated THP-1 cells 1, 6, 8 and 10 days after treatment, relative to untreated cells; this increase is gradual perhaps not significant at day 1 but significant at days 6, 8 and 10 (*P*= 0.0004, 0.0365 and 0.0145, respectively).

The expression of TRAF6 mRNA decreases in PMA treated THP-1 cells on 1, 6, 8 and 10 days after treatment, relative to untreated cells this decrease seems gradual, but not significant. Additionally, the expression of CIS-1 mRNA appears to be strongly decreased in PMA treated THP-1 cells 1, 6, 8 and 10 days after treatment relative to untreated cells. The decrease seems to occur rapidly, within 1 day of PMA administration.

The change in TAKL mRNA expression affecting by monocytes differentiation is considered to be very robust results, because they were carried out in many experiments by Dr Guesdon group. Unlike the changes in mRNA expression of TAB3, TRAF6 and CIS1 during the PMA-induced differentiation of THP-1 cells were not known before. They correspond to potentially interesting new findings but because of the small number of samples (n = 3) in this preliminary study, they need to be confirmed by additional experiments.

3.6. Assessing expression of TAKL variants in human primary monocytes and macrophages

The monocytic THP-1 cell line was used in the previous sections as a model for primary monocyte/macrophage. Results findings of monocytic THP-1 cells had to be confirmed on primary cells because the in-vitro cell lines are more stable and might response to the stress differently to primary cells. We used monocyte-derived macrophage (hMDM) as human primary cells.

Many literature studies (Auwerx, 1991, Qin, 2012, Daigneault et al., 2010) have tested the reliability of THP-1 cells line as a macrophage model and they found that THP-1 cells post-PMA treatment differentiate to macrophages which is functionally similar to primary macrophages. However, both cells types are physiologically different with respect to apoptosis; PMA treated-THP-1 cells can grow, divide and adhere faster than primary monocytes which differentiate only after adding inflammatory mediators such as TNFα, IL-1β and LPS, to prevent apoptosis. In addition, these cell types are different in morphology; PMA differentiated THP-1 cell nuclei are irregular in shape and there was an increase of phagosomes in the cytoplasm (Auwerx, 1991, Daigneault et al., 2010). Furthermore, they are also different in responding to LPS stimulation: a reduction in TLR4 surface expression in THP-1 cells was shown, but not in human primary macrophages (Qin, 2012). In conclusion, the studies have proved that THP-1 cells provide a model which mimics many features of monocyte/macrophage and can be suitable to understand the molecular mechanisms regulating the responses of monocytes and their interactions with vascular smooth muscle cells, T cells and platelets, but they are not reliable for all aspects of monocyte functions, including lipid studies where there is a wide difference in gene expression relating to lipid metabolism (Qin, 2012). The advantage of the THP-1 model compared to primary monocytes is obviously the practical convenience of its continuous availability in larger amounts than primary monocytes, which allowed us to carry out exploratory studies. In this project, we have used PMA differentiated THP-1 cells line to mirror the function and mechanism of macrophage in atherosclerotic plaque formation and also to study macrophage-T cell interaction and for these purposes they are a reasonable model to be studied.

In order to measure the expression of TAKL mRNA variants during differentiation, the human primary monocytes where differentiated into un-polarised macrophages (Mun) and then polarised into two phenotypes, M1-like ($M^{IFN\gamma+LPS}$) and M2-like ($M^{IL\text{-}4}$).

The mRNA expression was measured for TAKL, TAKL-1-D and TAKL-2-L (Figure 3.11) and the samples were collected from four healthy volunteers, GAPDH was used as a housekeeping gene to normalise hMDM data.

The genes expression was varying between healthy individuals and that might be correlated with many biological features such as gender, age or the time of taking the samples during the day. However, figure 3.11A and B graphs show that the mRNA expression pattern is similar for TAKL-All and TAKL-1-D.

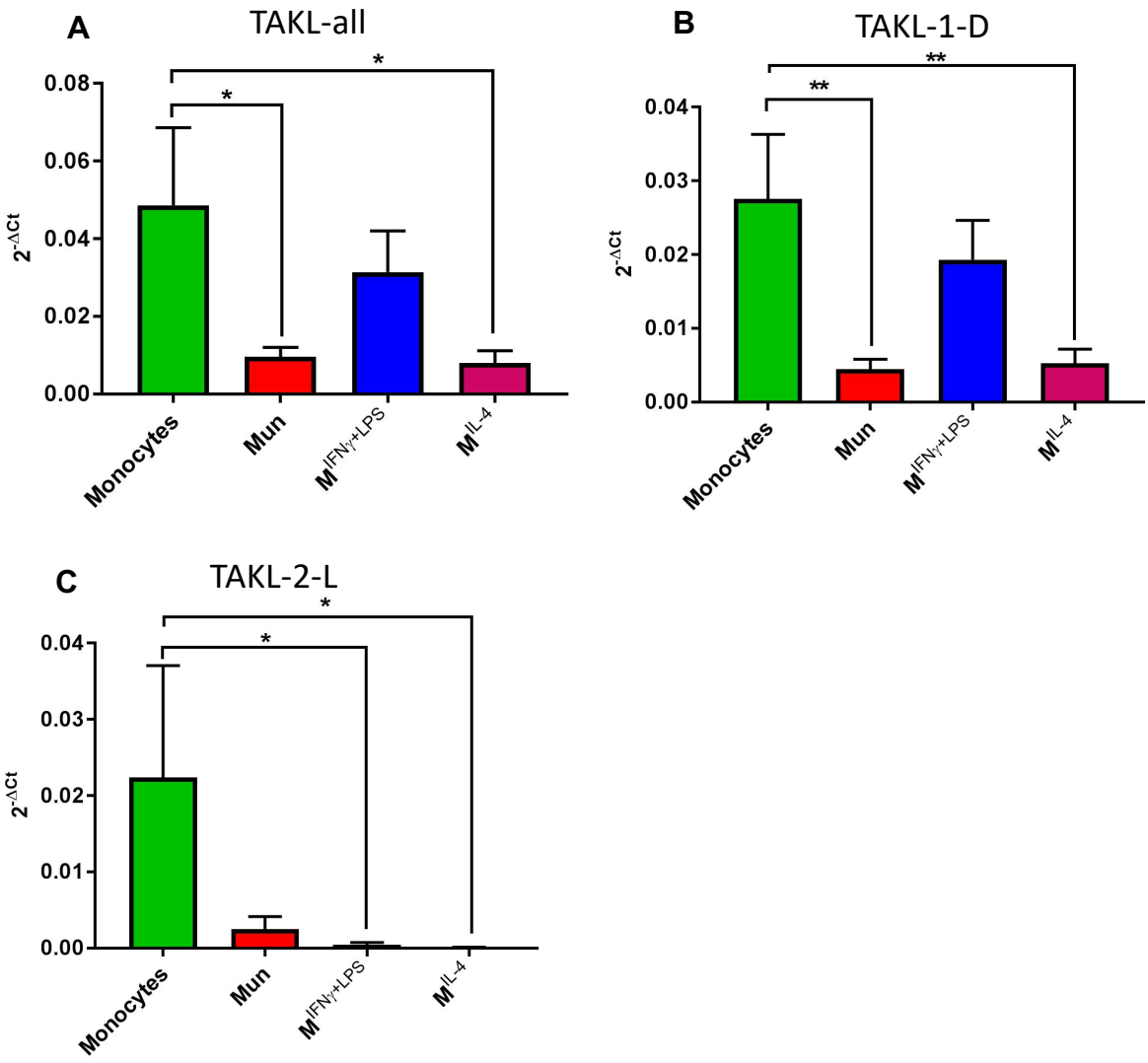

Figure 3.11 RT-qPCR assay of TAKL variants expression in human monocytes-derived macrophages

(A) Expression graph of TAKL all variants in human primary monocytes, unpolarised macrophages, Mun, and the polarised isoforms M1-like, $M^{IFN\gamma+LPS}$, and M2-like, M^{IL-4}. (B) Expression graph of TAKL-1-D variant in human primary monocytes, unpolarised macrophages, Mun, and the polarised isoforms M1-like, $M^{IFN\gamma+LPS}$, and M2-like, M^{IL-4}. (C) Expression graph of TAKL-2-L variant in human primary monocytes, unpolarised macrophages, Mun, and the polarised isoforms M1-like,$M^{IFN\gamma+LPS}$, and M2-like, M^{IL-4}. Data were normalised to GAPDH by the ΔCt method and are means ± SEM of n=4. Stars show the significant changes in expression compared to monocytes, P values on Graph pad prism are as follow: (*) *P≤0.05*, (**) *P ≤0.01*, (***) *P ≤0.001* and (****) *P ≤0.0001.* When stars are absent, it means no significant changes in their expression levels.

As in the previous section, we re-analysed the expression data on hMDMs by the absolute quantification method. The hMDMs assay was a preliminary study with limited number of donors, resulting in not many cell preparations and the small number of cells obtained in each preparation, only TAKLs (-all, -L and –D) have been looked at and the number of measurements so far is only n = 2.

The results of hMDMs when analysed by the relative method showed that the TAKL-all mRNA expression elevates on monocytes and M1-like macrophages (macrophages polarised with IFNγ and LPS) (Figure 3.11). While in absolute findings, the high expression of TAKL-all mRNA was on unpolarised and M1- like macrophages (Figure 3.12). This discrepancy in results could be due to the small number of samples. However, the investigation was not carried out further within the time of this PhD project because TAKL did not seem to be the optimal marker for the purpose of this macrophage study. However, the main purpose of this study was to establish a macrophage marker for the inflammatory macrophage phenotype M1, to be able to study the behaviour of these cells during inflammatory diseases such as atherosclerosis. We measured TAKL expression during different monocytic conditions, but unfortunately TAKL does not elevate very high in M1 cells and its mRNA expression levels are not stable under M1 treatment conditions, unlike FAM26F that has been found to be expressed consistently on M1 cells at both mRNA and protein levels.

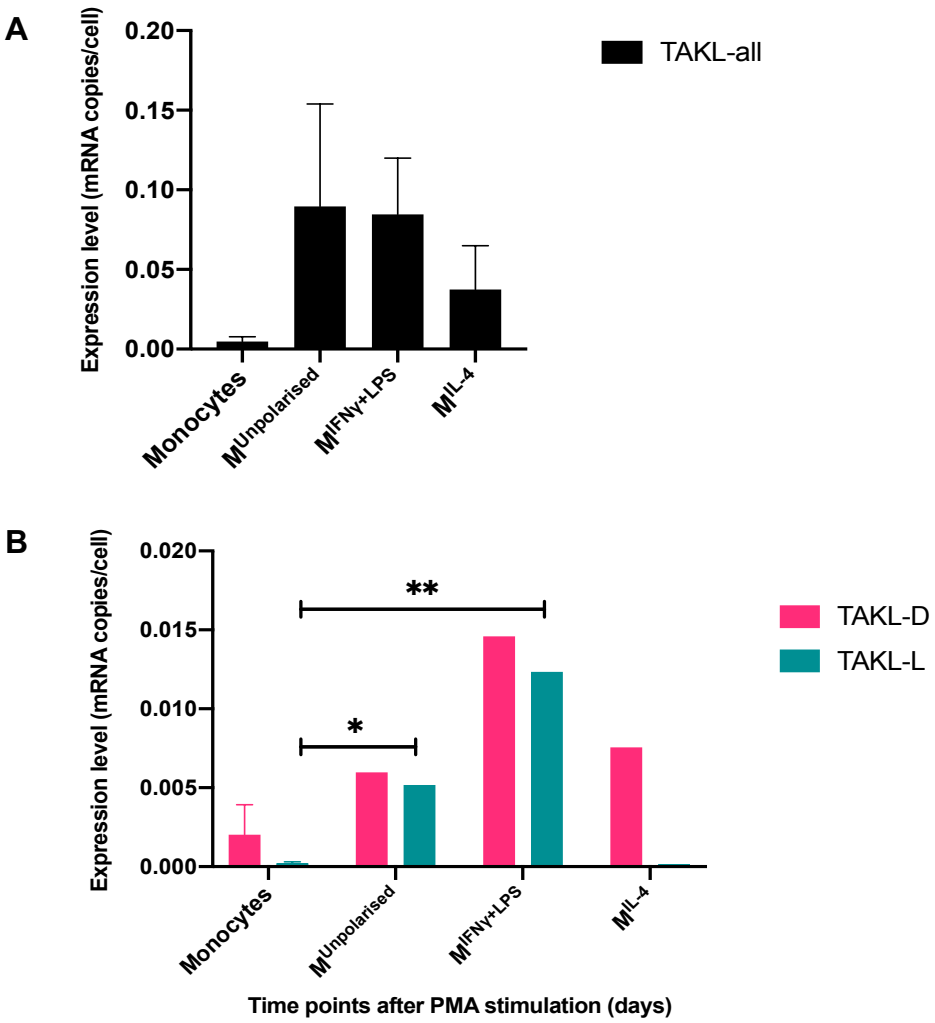

Figure 3.12 RT-qPCR assay of TAKL variant mRNAs expression in human monocytes-derived macrophages (Absolute quantification method)

(A) Standard curves of TAKL-all were used to calculate the template copies number per cell by absolute quantification method. Data are displayed as means ± SEM of four independent experiments. (B) Standard curves of TAKL variants were used to calculate the template copies number per cell by absolute quantification method. Pink bars represent the mRNA expression of TAKL-1-D and the green bars represent the mRNA expression of TAKL-2-L. Data are displayed as means ± SEM of four independent experiments. Data was statistically analysed using one-way ANOVA and the stars represents the significance levels of elevations with *P* values for mRNA expression in human macrophages: unpolarised macrophages Mun, $M^{IFN\gamma+LPS}$, and M^{IL-4} compared to monocytes. Stars show the significant changes in expression compared to monocytes, P values on Graph pad prism are as follow: (*) *P≤0.05*, (**) *P ≤0.01*, (***) *P ≤0.001* and (****) *P ≤0.0001*. When stars are absent, it means no significant changes in their expression levels.

3.7. Investigating expression of TAKL proteins in monocytic cells

Previous findings had shown that the TAKL-2 mRNA is the highly expressed variant in PMA-treated THP-1 cells, and TAKL-1 is also altered by differentiation at 5 and 10 days' time points. In order to confirm these results on proteins, THP-1 and hMDM protein samples were tested with TAKL antibody by western blotting. These experiments were done to determine the expression of TAKL-1 and TAKL-2 proteins. Samples were tested by using TAKL antiserum that recognises TAKL-1, TAKL-2 and TAKL-3 proteins but not TAKL-4.

TAKL antiserum was a rabbit polyclonal antibody to a synthetic peptide of TAKL of sequence (NH2-) CQIAEEYHEVKKEI (-CONH2) was produced by Innovagen AB (Lund, Sweden). The peptide corresponds to a fragment of the human sequence (residues 64-77 of TAKL-1) that is also present in TAKL-3 and TAKL-2 and is fully conserved in the mouse and rat homologues of TAKL-1. The synthetic peptide was made by Innovagen. They amidated the peptide at its carboxy-terminal end. This amidation is indicated by the (CONH2) extension after the peptide sequence. It was done to neutralise the negative charge of the COOH group of the terminal isoleucine, thus making the c-terminal end more similar to the CO-NH peptide bond that would be there in the full protein. For immunisation, the amidated synthetic peptide was coupled to the carrier protein KLH via the side chain of the amino-terminal cysteine. Innovagen did three injections of the KLH-coupled peptide in a rabbit over a 12-week period (details in attached documents they sent me). They took test bleeds after the first two injections and a terminal bleed after the third. The serum from all test bleeds and the final bleed were sent.

We first attempted to detect TAKL proteins in samples of THP-1 cells at different time points during their PMA-induced differentiation into monocytes (Fig. 3.13). In these experiments the antibodies were used at the standard dilution usually recommended for purified IgGs in western blotting protocols (0.1 μg/ml in blotting buffer). No bands appeared on the membrane (Figure 3.13C). Due to the negative results with TAKL antibodies, β-actin antibodies were used instead as technical controls to check that our western blot reagents and procedures were functioning correctly (Figure 3.13A and B). The bands appeared in the predicted size the housekeeping protein β-actin. This showed that the reagents used in the western blot were functioning properly. However, unspecific high sizes protein bands were detected by Coomassie blue staining (Figure

3.13D). To trouble shoot this problem, we tried the following optimisation steps: increasing the blocking exposure time, and the antibody concentration, but this still failed to reveal any candidate TAKL protein bands in THP-1 cell samples (data not shown).

We then attempted detection of TAKL proteins in primary blood monocytes and macrophages. An example is shown in Figure 3.14B. In this experiment, an antibody to the housekeeping protein GAPDH was used as technical control (Figure 3.14A). The anti-TAKL antibody detected a faint band at the position expected for TAKL-3, as well as more intense bands of higher molecular weights that presumably resulted from cross reactivity of the antibodies with non-specific proteins but no candidate TAKL-1 or TAKL-2 bands could be seen (Figure 3.14B and C).

Finally, to increase the sensitivity of the assay we increased the TAKL antiserum concentration in the immunoblotting (Figure 3.15). Bands were then detected at the expected sizes for TAKL 1,2 and 3 proteins, but their expression levels did not vary between samples in agreement with changing TAKL mRNA expression levels, which was elevated in IFNγ and LPS macrophage (Figure 3.12).

To conclude, none of the TAKL proteins could be detected by western blotting in THP-1 cells or in primary monocytes and macrophages when the anti-TAKL antibodies were used at the recommended standard concentrations. These results indicate that the TAKL proteins are either expressed only at very low levels or that the antibodies were not fully optimised for detection. This conclusion is in agreement with our earlier findings that the TAKL mRNAs were expressed at less than 1 copy per cell.

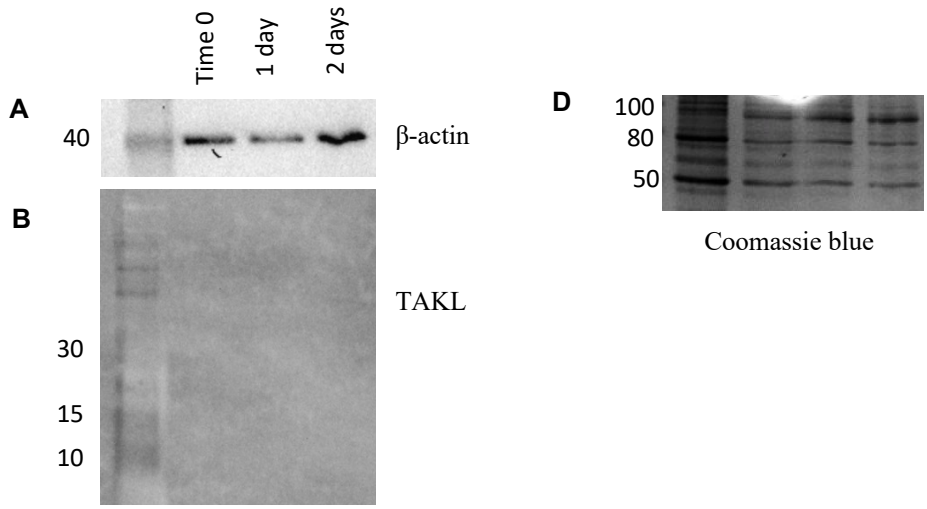

Figure 3.13 Detection of TAKL proteins on THP1 time course samples

The samples are from THP1 cells before and after PMA treatment (time 0, 1 and 2 days, respectively). (A) β-actin bands, with the size of 42 kDa, on THP1 time course samples. (B) TAKL-1, TAKL-2, TAKL-3 anti-serum was used on this membrane. TAKL proteins sizes are as follow; TAKL-1 is 30 kDa, TAKL-2 is 10.4 kDa and TAKL-3 is 26 kDa. The blue arrows show where the detected protein size should be. (C) Coomassie blue staining to detect TAKL proteins that not detected by the UV scanner due to using short exposure time. The prestained protein ladder was used on all membranes and the images were taken under hemiluminescent hi-resolution.

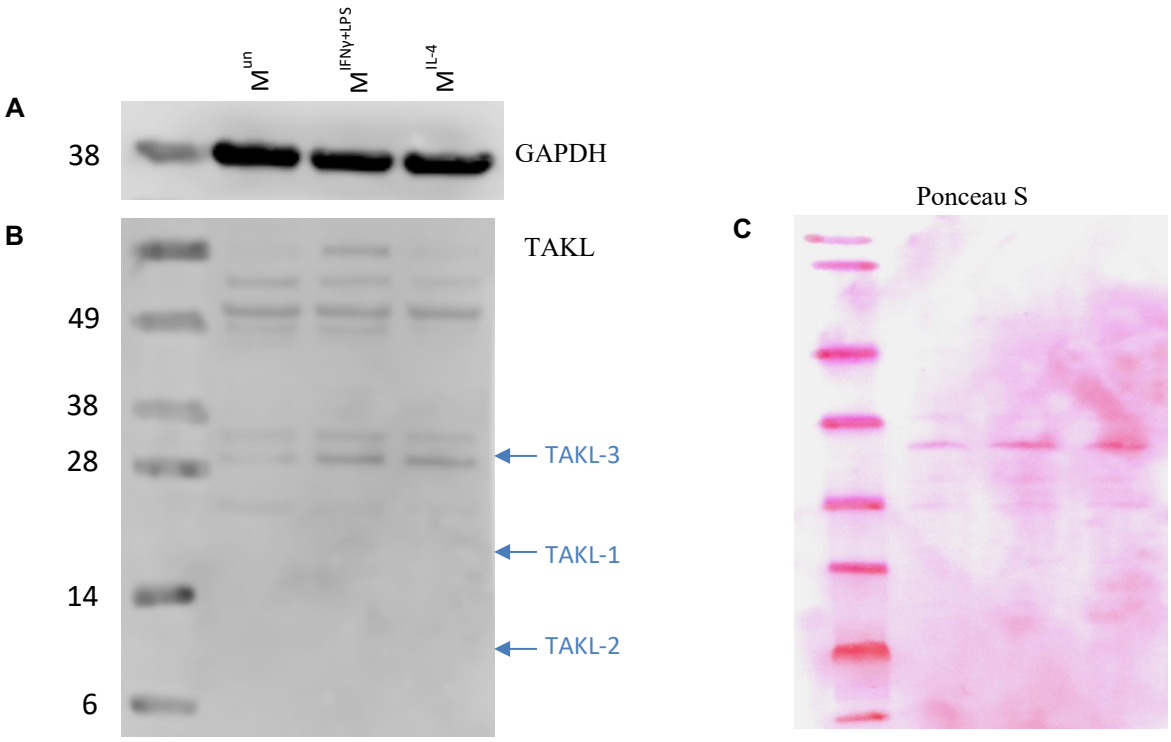

Figure 3.14 Detection of TAKL proteins on human primary macrophages by western blotting

The samples on the gels are from human primary macrophages (M^{un},$M^{IFNγ+LPS}$ and M^{IL-4}, respectively). (A) GAPDH bands, with the size of 40.2 kDa. (B) TAKL-1, TAKL-2, TAKL-3 anti-serum was used on this membrane with a concentration of 1:300. TAKL proteins sizes are as follow; TAKL-1 is 30 kDa, TAKL-2 is 10.4 kDa and TAKL-3 is 26 kDa. The blue arrows show where the detected protein size should be. (C) Ponceau S staining to detect TAKL proteins before using the LI-COR blot scanner. The prestained protein ladder was used in this WB and the images were taken under hemiluminescent hi-resolution.

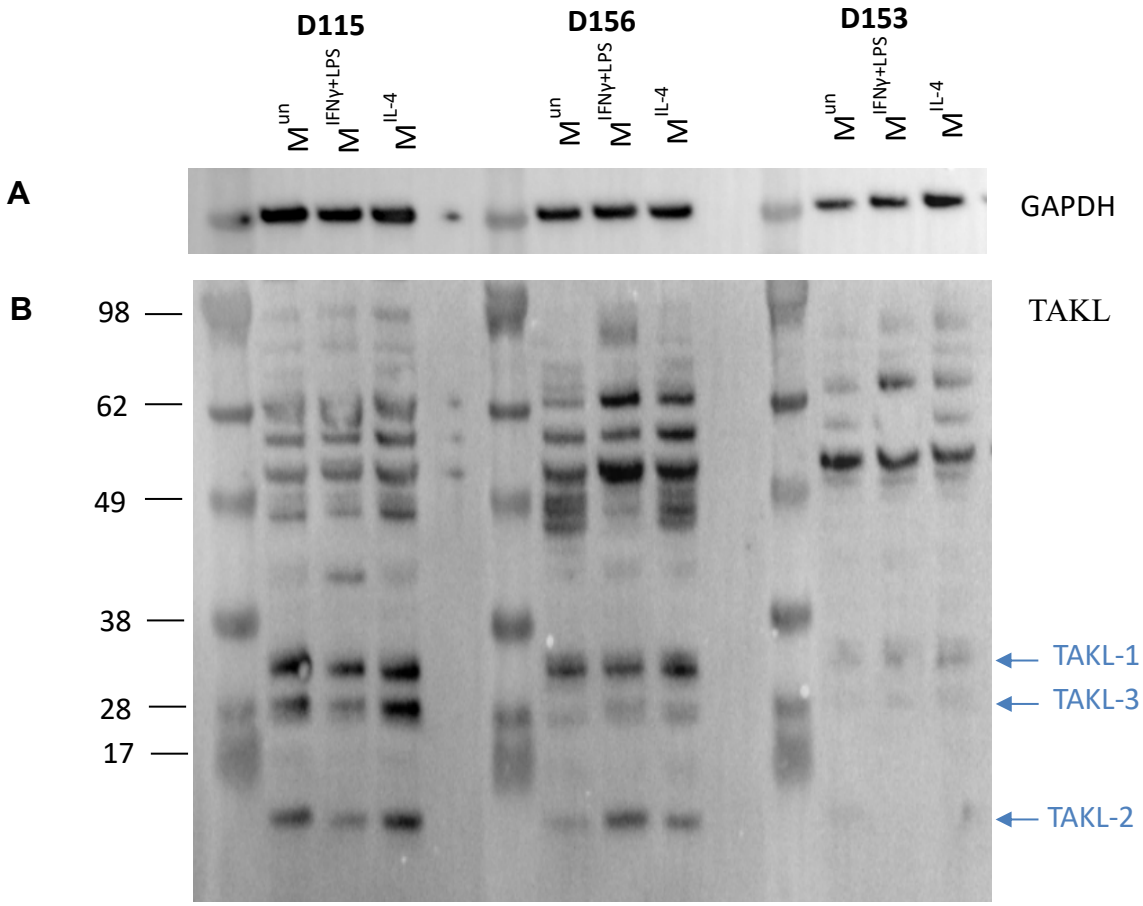

Figure 3.15 Detection of TAKL proteins on human primary macrophages by western blotting

The samples on this plot are from human primary macrophages (M^{un},$M^{IFN\gamma+LPS}$ and M^{IL-4}, respectively), and three different donors (115, 156 and 153). (A) GAPDH bands, with the size of 40.2 kDa. (B) TAKL-1, TAKL-2, TAKL-3 anti-serum was used on this membrane with a concentration of 1:300. TAKL proteins sizes are as follow; TAKL-1 is 30 kDa, TAKL-2 is 10.4 kDa and TAKL-3 is 26 kDa. The blue arrows show the bands of TAKL proteins. (C) The SeeBlue Plus2 Prestained standard ladder was used in this WB and the images were taken under hemiluminescent hi-resolution.

3.8. Discussion

3.8.1. Technical strengths and limitations of our Real-time PCR assays

Real-time PCR was used in this project to meet two major aims. First, we wanted to determine as accurately as possible the absolute levels of expression of TAKL and of several other genes involved in TLR signal transduction and any change in their expression that could occur during the THP1 monocytic differentiation process. Second, in the case of TAKL, which expresses 14 alternative transcripts encoding between them 4 alternative proteins, we wanted to determine if its increased expression during THP1 differentiation concerned all 14 mRNA variants equally of if instead the increase in expression preferentially concerned only a subset of these. Although we did not attempt to measure individually all 14 variants, our minimum requirement was to have a set of assays that would allow us to discriminate between the transcripts encoding each of the four alternative protein products, TAKL1 to TAKL-4.

The first aim was technically easy to meet because pre-designed RT-PCR assays targeting non-alternatively spliced exons were available to order for all our genes of interest. However, the second aim was more challenging because the list of pre-designed assays for TAKL was limited and did not always target the alternative exons diagnostic of certain variants. Therefore, we had to ask Applied Biosystems to design bespoke sets of primers and probes to assay some of our targets. These custom assays were designed by a proprietary algorithm of Applied Biosystems using the target exon-junction sequences that we supplied and was therefore not under our control. There was no possibility to ask the system for an alternative design in case the custom assays supplied were found to lack efficiency or specificity.

Technical reliability of each RT-qPCR assay was tested by two main approaches and each type has a different purpose. First by producing standard curves to all TaqMan assays to check their efficiency. That was assessed because any change in efficiency value can have a significant impact on the resulting gene expression quantity of each assay. The accurate 100% efficiency value corresponds to a slope of -3.32 on the standard curve. For the relative quantitation analysis method, the optimal efficiency should be within very narrow range of 95%±5, because any larger deviation would render the comparison between the normalising gene and the target gene inaccurate. By

contrast, the absolute quantitation analysis method can tolerate less optimal efficiencies because the actual measured efficiency is taken in account in the analysis method.

Four TAKL transcripts probes were custom-made to target specific exon junctions of TAKL3/4, TAKL-L, TAKL-I and TAKL-J and their efficiencies were 87.79 %, 85.90%, 101.55% and 149.07% respectively (Figure 3.3B). TAKL-I and TAKL-J efficiency values are unrealistically high and are the results of single determinations. They would certainly have needed to be determined more accurately before any reliable analysis could be done with them, however this was not necessary since neither of these probes detected any transcript in THP-1 samples.

The second parameter to assess RT-qPCR reliability was specificity by checking using gel electrophoresis that each assay produced the right size of cDNA fragment with no other product. All qPCR products were in the expected size and that means all tested assays were specific and produces one unique amplification product for each target sequence.

For the purpose of our second aim, specificity was more important than efficiency because discriminating between each TAKL variant without cross-reaction was more important than efficiency of detection, since relatively low efficiency could be taken in account and corrected by the absolute quantitation data analysis method.

3.8.2. Interpretation of our RT-PCR results

- **Comparative quantitation analysis results**

The expression of TAKL mRNA variants was measured among monocytic THP-1 cells and hMDMs. In THP-1 time course samples, TAKL-all mRNA was highly expressed between day 1 and 3 after PMA treatment. From the variants' expression, it was noticeable that TAKL-L elevated significantly at the same time points as TAKL-all.

While on hMDMs, the expression of TAKL-all, TAKL-D and TAKL-L elevated in monocytes, but after macrophage polarisation it seems that only TAKL-D expression elevated in $M^{IFNY+LPS}$.

In conclusion, the relative quantitation analysis of our data confirmed the previous results that had identified TAKL as a gene being strongly up-regulated during the PMA-induced macrophage differentiation of THP1 cells and identified TAKL-2 as a specific mRNA variant being very strongly activated. They also showed that TAKL gene expression is affected by monocytes differentiation in both the THP1 cell line model and in human primary peripheral blood monocytes. However, the results suffered from limitations of the relative quantitation analysis method. We therefore carried out further analyses by the absolute quantitation method to obtain definite measurements of the levels of expression of the mRNAs of interest in both cell types.

- **Absolute quantitation analysis results**

The absolute analysis on THP-1 data showed increase peaks on the expression level of TAKL-L, TAB2 and TRAF6 mRNA in copies / cells, and the range of elevation was between 0.5 and 1 copy / cell. Comparing all genes expression levels in un-stimulated THP-1 cells, all were slightly high except TAK1 and TAB3 which start with low expression level at time zero and then increase gradually until day 10 when they decrease again to reach the baseline level. Unlike TAKL, TRAF6, TLR4, CIS and GPS2 mRNAs, which start slightly high in the un-treated THP-1s and then their expression elevated differently along the differentiation period. Each gene has been affected by differentiation process in different time points. The maximum levels of expression of all genes, included TAKL, does not exceed 1 copy / cell except GPS2 that its maximum level of expression has reached 4 copy / cell after 1 day of PMA treatment.

In addition, if we compare changes in expression of TAKL-all, TAKL-L, TAKL-D during in vitro macrophage differentiation of human primary monocytes and PMA-rest differentiation of THP-1; we can noticed similar low levels of TAKL expression in freshly isolated monocytes and unstimulated THP-1 (less than 0.01 copies / cell). Also, an increase in TAKL expression seen when monocyte differentiate into macrophages and undergo different polarisations. TAKL-all expression appears to increase during differentiation to unpolarised macrophages, but not as high as in THP-1 during PMA-rest. It was 0.1 copies / cell in macrophages and about 0.4 copies / cell in differentiated THP-1 (days 8 and 10). The differences are not statistically significant, but this could be due to low number of assays and deserves further investigations. The differences in TAKL-all expression between unpolarised and polarised macrophages are relatively small, compared to monocytes and unpolarised macrophages. Also, these changes in TAKL-all expression levels were not statistically significant within the current small data set.

While the assays of individual variants TAKL-L and TAKL-D show that both increase significantly during in vitro differentiation of human monocytes into unpolarised macrophages, qualitatively, this is similar to what is seen in THP-1 during PMA-rest. However, quantitatively, the increase in TAKL-D and TAKL-L is smaller (maximum about 0.008 copy / cell of each variant) and together, the two variants do not account for the much higher level of expression measured with the TAKL-probe.

The same assays carried out on *in vitro* polarised macrophages suggest further increase in expression of both TAKL-L and TAKL-D variants during IFN/LPS-induced polarisation of macrophages to a maximum of 0.015 copy/cell each which was significant for TAKL-D relative to monocytes (*P=0.0006*). By contrast, in IL-4-polarised macrophages, TAKL-D remains expressed at a level similar to that of unpolarised macrophages while TAKL-L expression is supressed. Thus, in human macrophages, the total expression TAKL-L and TAKL-D is less than the overall level of TAKL-all expression. This suggests that future investigations of TAKL expression in human macrophages should investigate expression of other TAKL variants, including those expressing TAKL-3 or TAKL-4.

3.8.3. Possible reason for the low numbers of TAKL mRNA copies per cell

Investigators do not often convert mRNA expression measurements in number of copies per cell. We are aware of only one such study in monocytes, which focused on the regulation of six cytokines in PBMCs stimulated by anti-CD3 antibodies (Bass et al., 2004). This study found that for 5 of the 6 cytokines studied, basal expression levels prior to stimulation were significantly less than one mRNA copy per cell, in some cases several orders of magnitude lower (e.g. 0.006 copies per cell for IL-4) and although all 6 cytokines were strongly up-regulated by the anti-CD3 antibody, only half of them reach peak levels that exceeded one copy per cell (Bas et al., 2004). Thus, this report indicates that similar to what we found for TAKL, some genes that show very strong relative up-regulation (expressed relatively to basal levels) actually reach only low absolute expression levels even at peak expression.

Expression levels of less than one copy per cell imply that the cell population is a mixture of individual cells which contain no copy at all of the mRNA of interest and other cells that contain one or more mRNA copies. In terms of molecular mechanisms, this situation is explained by the fact that for genes expressed at low levels, transcription does not happen continuously but in discrete bursts of transcriptional activity separated by inactive periods (Smirnov et al., 2018). Measurements of burst sizes and time intervals between bursts have shown that for genes expressed at low levels, individual bursts produce between 5 and 15 mRNA copies and the “off” intervals between bursts last several hours, sometimes as long as 20 hours (Suter et al., 2011). Such long intervals exceed the typical half-lives of mRNAs (Wada and Becskei, 2017) and can therefore be long enough to allow all the mRNAs copies produced by a small burst to be degraded before the next burst occurs.

3.8.4. Comparison with previous knowledge

In order to compare our new results with previous knowledge of TAKL variants expression; a previous analysis of TAKL sequences in EST databases found that the TAKL-1 expressing clone TAKL-D was the most frequently cloned variant [Ellis et al. manuscript in appendix I], which strongly suggested it is the variant expressed in most tissue in humans as well as in other vertebrates such as shark, zebrafish, lizard and several species of birds and mammals. Relatively to the TAKL-D variant, the mRNAs expressing TAKL-2, TAKL-3 or TAKL-4 were represented much less frequently in EST databases suggesting these variants were expressed only in a small number of cell types or in response to unusual stimuli. (Ellis et al., unpublished). Additionally, prior results from Dr Guesdon's group had suggested that TAKL-2 expression was specifically induced during differentiation of THP-1 into monocytes. The new results presented here confirm that the gene is only expressed at very low levels in THP-1 cells that have not yet differentiated, and that TAKL-D is its main product at this stage.

They also show that the expression of a specific TAKL mRNA variant, TAKL-L, is up-regulated relative to its low-level basal expression in THP-1 cells during their PMA-induced differentiation into monocytes and that this variant is then expressed at much higher levels than TAKL-D.

Our results also show for the first time that TAKL-L is expressed at levels similar to those of TAKL-D in unpolarised primary human monocytes and macrophages, but that the expression of TAKL-L vary between different types of polarised macrophages. Finally, the present work provided for the first-time absolute quantitation of the expression TAKL mRNA variants. This data indicates that the basal level of expression of TAKL in suspension growing THP-1 is extremely low, so that even after the very large–fold increase in expression that happens during PMS-induced monocytic differentiation, the absolute expression levels of TAKL mRNA remain low at less than 1 copy per cell.

3.8.5. Attempts at detecting TAKL proteins by Western blotting

After detecting the high expression of TAKL-2 mRNA on PMA-treated monocytic THP-1 and human monocytes-derived macrophages hMDMs, the protein expression was assessed and it was expected to find the same high expression of TAKL-2 protein in agreement with its increased mRNA levels. Unfortunately, no bands have been detected by TAKL antiserum on THP-1 time course samples, while there were multiple bands on the stained gel. On hMDMs, bands have appeared at the position of TAKL-1, 2 and 3, but the antibody might also cross reacts with bigger proteins that cannot be TAKLs. Nevertheless, this TAKL antiserum has been tested by others on transfected cells expressing TAKL cDNA, and it has been shown that the antiserum can detect TAKL-1, 2 and 3 when these are expressed at artificially high levels in transfected cells (Ellis et al., unpublished). The most likely explanation for our failure to detect reliably any TAKL protein by western blotting is that their levels of expression remains too low compared with the sensitivity of our western-blot assay. This interpretation is in agreement with our finding that TAKL mRNA levels remain very low (less than one copy per cell) even at the time of maximum expression.

3.8.6. Conclusions

This study was the first to measure TAKL mRNA expression in primary human monocytes and their in vitro differentiation into polarised macrophages (M1 and M2a like phenotypes). The same elevation in TAKL mRNA expression was found using the absolute analysis method of RT-qPCR data of hMDMs, TAKL-L was the main variant that elevates more than TAKL-D as previously found on PMA-treated THP-1 cells. Due to the sample number limitation, TAKL-L and TAKL-D were the only variants that have been measured on the hMDM assays.

We used two cell types to study TAKLs mRNA levels in differentiating macrophages; first we used monocyte-macrophage cell model, which was a PMA-rest differentiation of THP-1 cell line. It allows limitless replication, but the model uses an artificial stimulus, PMA, on an established cell line that could have lost some of the features present in genuine stem cells so not as representative of actual monocytes and macrophages as primary cells from human blood. The second ideally preferred cell model to use was hMDMs, because it is much closer to the patient-derived cells that would be used in the future. The only difficulty was in finding donors and small number of cells collected from each donor was severely limiting the number of assays. In practice, each blood sample only produced enough cDNA for a maximum of three RT-PCR assays in duplicate from each of the four cell types of interest (monocytes, unpolarised macrophages and two types of polarised macrophages; M1 and M2a like). Due to these limitations, we decided to first use the THP-1 model to test-run each of TaqMan probes for technical checks and to narrow down the list of potentially interesting transcripts. After this phase of the project was completed and the list of potential differentiation markers was narrowed down to TAKL-D and TAKL-L, the time available was unfortunately not sufficient to obtain as many blood samples as would have been needed for a robust statistical analysis of the data.

For the genes other than TAKL in TAK1-TRAF signalling pathway (TAK1, TAB2, TAB3, TRAF6, CIS and GPS2), There was not enough time in the project to carry out enough replicates to produce accurate results, so this is still a preliminary study. Also, the hMDM assay needs more replicates and to test the other TAKL probes than TAKL-L and D, and probes of other genes such as TAB2, TAB3, TRAF6, TLR4, CIS1 and GPS2.

3.8.7. Assessing the suitability of TAK1 as clinical marker

For the purpose of this project that aims to find a reliable M1 marker. TAKL was not a practical differentiation marker for clinical diagnostic purposes; because even at its maximum expression, it was expressed at low level (always less than 1 copy / cell) and also the second reason was failure to detect protein product with custom-made antibodies. By contrast, FAM26F mRNA and protein expression levels were always high in hMDM-induced by IFNγ and LPS (Hadadi, 2015, Baidžajevas, 2019).

3.8.8. Possible directions for future research

Further studies of TAKL regulation might be a promising approach for future studies of monocyte and macrophage differentiation mechanisms; The TAKL gene is unusual in that it contains multiple promoters, and the choice of which protein variant it expresses is determined by the choice of promoter rather than by alternative splicing (Ellis et al., unpublished). Therefore, changes in the expression levels of TAKL-D and TAKL-L in differentiating THP-1 and human monocytes requires the up- or down-regulation of the two internal promoters that control these transcripts by changes to epigenetic signals and transcription factor activities near these promoters. Identifying these factors may further our understanding of the basic mechanisms involved in monocyte differentiation and macrophage polarisation.

Chapter 4

Analysis of inflammatory signalling pathways according to human macrophage phenotype

4.1. Introduction

The first part of this chapter was to confirm the TAKL chapter findings using another approach (the RNA-seq analysis). Data were, generated by Kajus Baidzajevas, from human monocyte-derived macrophages (with and without polarisation to M1 / M2) to assess the expression levels of specific genes of interest.

The second part was a bioinformatics analysis to investigate the expression, localisation, structure and function of FAM26F gene among the online available databases.

FAM26F was firstly identified by proteomics analysis of hMDMs (unpolarised and different macrophage polarised phynotypes) (Hadadi, 2015). This finding was confirmed by measuring FAM26F mRNA and protein expression levels in hMDMs, which was expressed constantly high in IFNγ and LPS-stimulated macrophages (Baidžajevas, 2019). In addition, the expression levels of FAM26F mRNA and protein confirmed the same high expression levels in M1-like macrophages in mice, this has been found by another colleague in our group (L. Campesino).

Hypothesis:

The inflammatory signalling pathways are altered and can be delineated according to macrophage polarisation state / phenotype.

Aims:

1. To analyse changes in expression of TAKL, FAM26F and of other candidate markers of macrophage differentiation and polarisation by bioinformatic analysis of an RNA-Seq experiment data set from in vitro differentiated human peripheral blood monocytes (this data set was given to us by Kajus Baidzajevas).

<u>RNA-Seq analysis was done to check the expression levels of the following:</u>

- TAKL transcripts
- TAK1-TRAF6 signalling pathway-related genes
- FAM26 gene family
- FAM26F transcripts

2. Bioinformatics databases analysis of FAM26F

4.2. Analysis of RNA-Sequencing data

Due to human monocytes-derived macrophages sample number limitation and difficulty in small number of cells that we collected from each donor was severely limiting the number of RT-qPCR assays. In practice as mentioned in the previous chapter, each blood sample only produced enough cDNA for a maximum of three RT-PCR assays in duplicate from each of the four cell types of interest (monocytes, unpolarised macrophages and two types of polarised macrophages; M1 and M2a like). We used RNA-seq data of hMDM to overcome donors availability limitation.
RNA-sequencing data from 8 healthy donors of human monocyte-derived macrophage (hMDM), unpolarised and polarised to the different macrophage phenotypes (IFNγ+LPS, IL-4, IL-10, oxPAPC and CXCL4), was isolated and polarised by Kajus Baidzajevas. The RNA-seq analysis was done by (Bernett Lee, Singapore Immunology Network) using a software with a limited access for ethical reasons (Baidžajevas, 2019). The analysed data sent to us as excel sheet with genes expressions as log2-transforming ratio of reads per kilobase of transcript per million mapped reads (log2 RPKM), while the transcripts variants data was as Transcripts Per Million (TPM) or Fragments Per Kilobase of transcript per Million (FRPM), see section 2.5.1 for full detailed protocol.
Expression data was presented as log2-transforming ratio of reads per kilobase of transcript per million mapped reads (log2 RPKM), or as Transcripts Per Million (TPM), RPKM and TPM are commonly used approaches for RNA-seq data presentation to reduce the technical and sequencing bias (Love et al., 2016). We used RPKM for genes expression (in section 4.1.2, 4.1.3 and 4.1.4), while we showed the expression levels of transcripts; TAKL isoforms (section 4.1.1) or FAM26F isoforms (section 4.1.5), the data presented as TPM, it shows reads for a transcript in 1,000,000 RNA molecules of gene in each sample (Conesa et al., 2016).

Both RPKM and TPM are commonly used normalisation methods for RNA-seq data, but the reason for not presenting genes and variants data with the same unit is due to the limited access to RNA-seq data sheet. Additionally, it was not possible to compare these data to the previous RT-qPCR expression data because they are relative to house-keeping genes unlike RNA-seq data which are not relative to a standard gene.

4.2.1. Expression of TAKL variants among hMDM phenotypes

The mRNA expression of TAKL transcripts was not statistically different compared to unpolarised or other polarised cells, but TAKL-L is the most abundant form in all conditions in fact, and it is not specifically higher in inflammatory macrophages according to Figure 4.1. This finding from human monocyte-derived macrophage RNA-seq data, that TAKL-L was the highest form found to be expressed under differentiation conditions, confirms the previous chapter finding in moncytic-THP-1 cells.

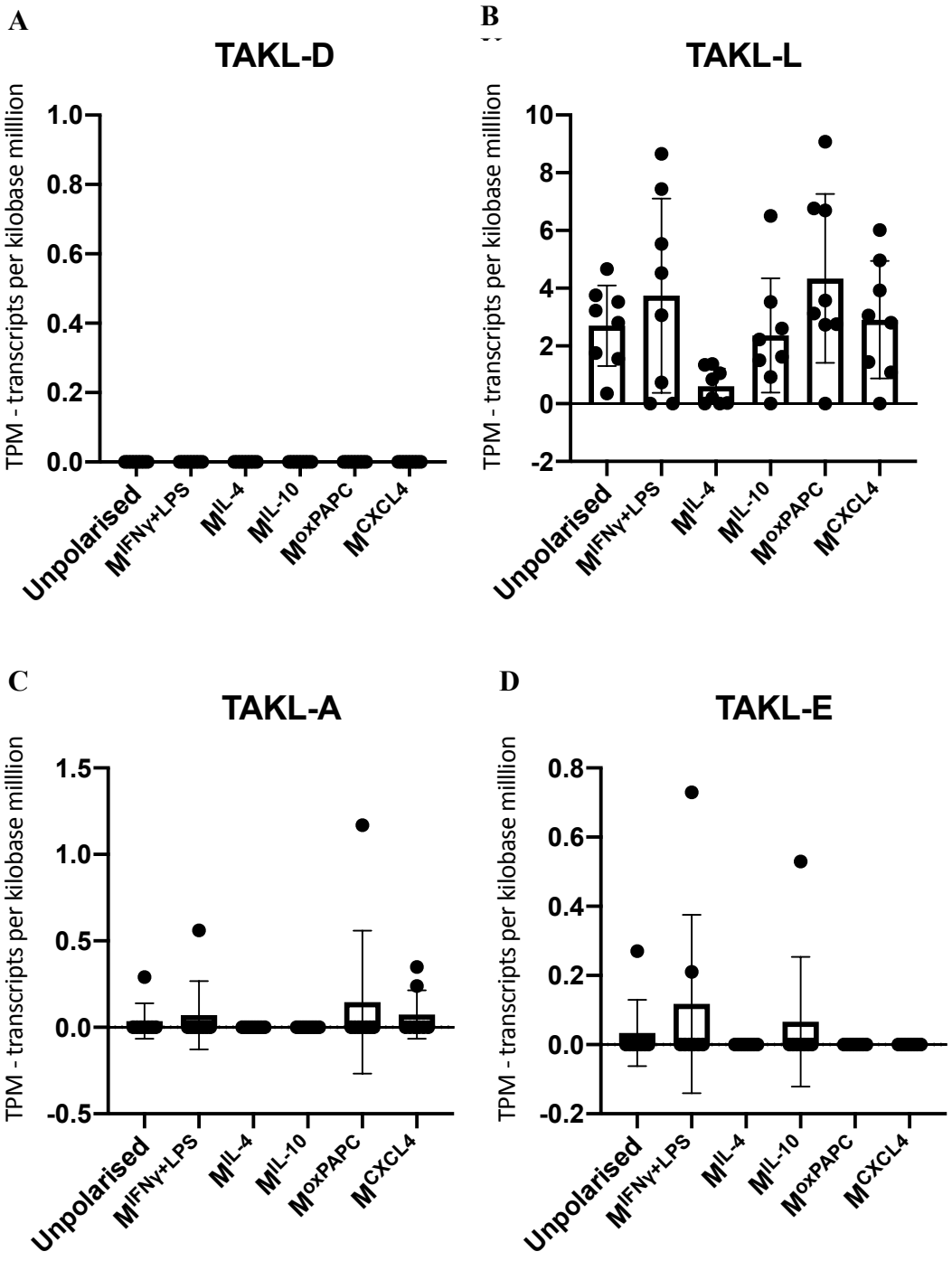

Figure 4.1 Expression of TAKL transcripts in human monocytes-derived macrophage
RNA-Sequencing data of human primary monocyte-derived macrophages that has been polarised to the different macrophage phenotypes using cytokines (n=8). The bars show the expression of TAKL variants; (A) TAKL-D, (B) TAKL-L, (C) TAKL-A and (D) TAKL-E as transcripts per kilobase million (TPM) on the Y axis. The expression was measured on human primary macrophage phenotypes on the X axis. Data were means ± SD and statistically analysed using one-way ANOVA, but the changes in expression levels of polarised macrophage was not significant compared to unpolarised macrophage.

4.2.2. Expression of other genes contributing in TAK1-TRAFs signalling pathway

We set out to explore how macrophage polarisation affects TAK1-TRAF signalling pathways including TAB2/3, TRAF2/3/6 and the adaptor inhibitory interactors CIS1 and GPS2. The RNA-seq data analysis for TABs (Figure 4.2) and TRAFs (Figure 4.3) showed that TAB2 and TRAF2/3/6 were expressed in all macrophage polarisation conditions, but the level of expression was consistent and not confined to one polarised form. Interestingly, the elevation in expression levels of TAB2/3 (Figure 4.2) and TRAF2/3 (Figure 4.3) in $M^{IFN\gamma+LPS}$ macrophage compared to unpolarised macrophage were significant, while the other expression changes was not significant with all genes. Additionally, we analysed the RNA expression of the two adaptor proteins CIS1 and GPS2 (see figure 4.4), the analysis represents the maximum expression levels of CIS1 in $M^{IL\text{-}4}$, while GPS2 expression appears to be low in all macrophage polarised forms. Comparing expression levels of TAB2, TAB3, TRAF6 and CIS1 in unpolarised macrophages with the previous expression data in THP-1 cells at time zero (see section 3.5.2 and figure 3.9), we can notice the similarity in expression profile. In unpolarised macrophages and time zero-THP-1 cells, the expression of TAB2, TRAF6 and CIS1 was high, while TAB3 which was low in both macrophage differentiation conditions (cell line and primary cells). In conclusion, expression of these genes may be altered by macrophage polarisation but more studies on primary hMDMs are needed to confirm this whether this is the case. Ideally, where suitable antibodies are available, it is informative to determine whether changes due to polarisation occur at the protein level.

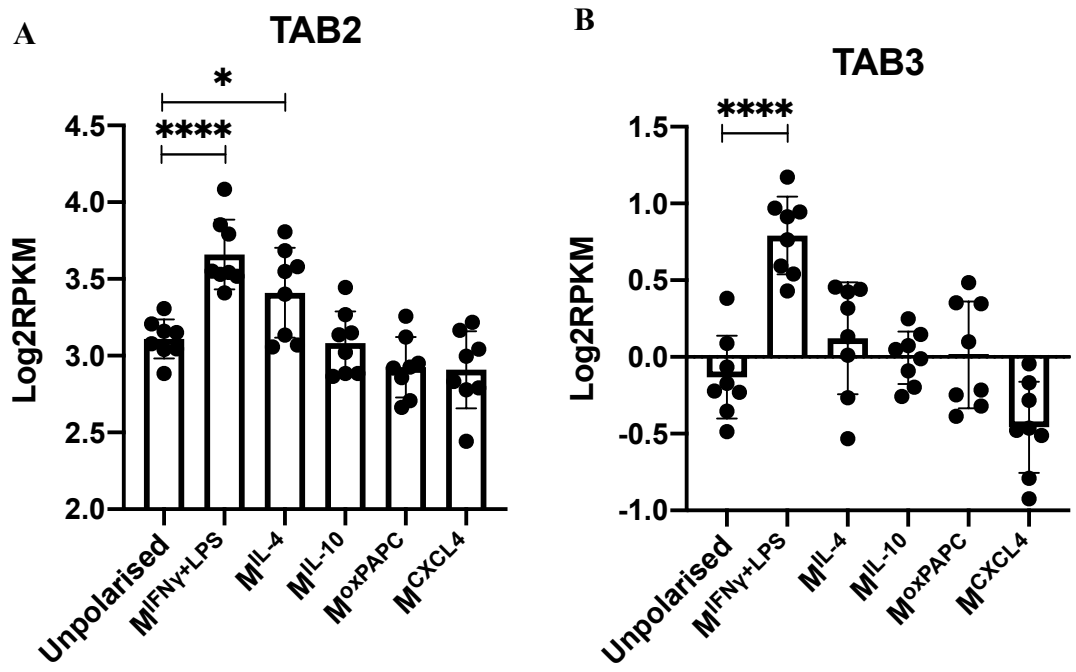

Figure 4.2 Expression of TAB genes

RNA-Sequencing data of human primary monocyte-derived macrophages that has been polarised to the different macrophage phenotypes using cytokines (n=8). The bars show the expression of (A) TAB2 and (B) TAB3 as reads per kilobase of transcript per million mapped reads (log2RPKM) on the Y axis. Data were means ± SD and statistically analysed using one-way ANOVA. When stars are on bars, it indicates the significant changes in expression level. P values on Graph pad prism are as follow: (*) *P≤0.05*, (**) *P ≤0.01*, (***) *P ≤0.001* and (****) *P ≤0.0001,* and absence of stars indicates no significant difference in expression compared to unpolarised macrophages.

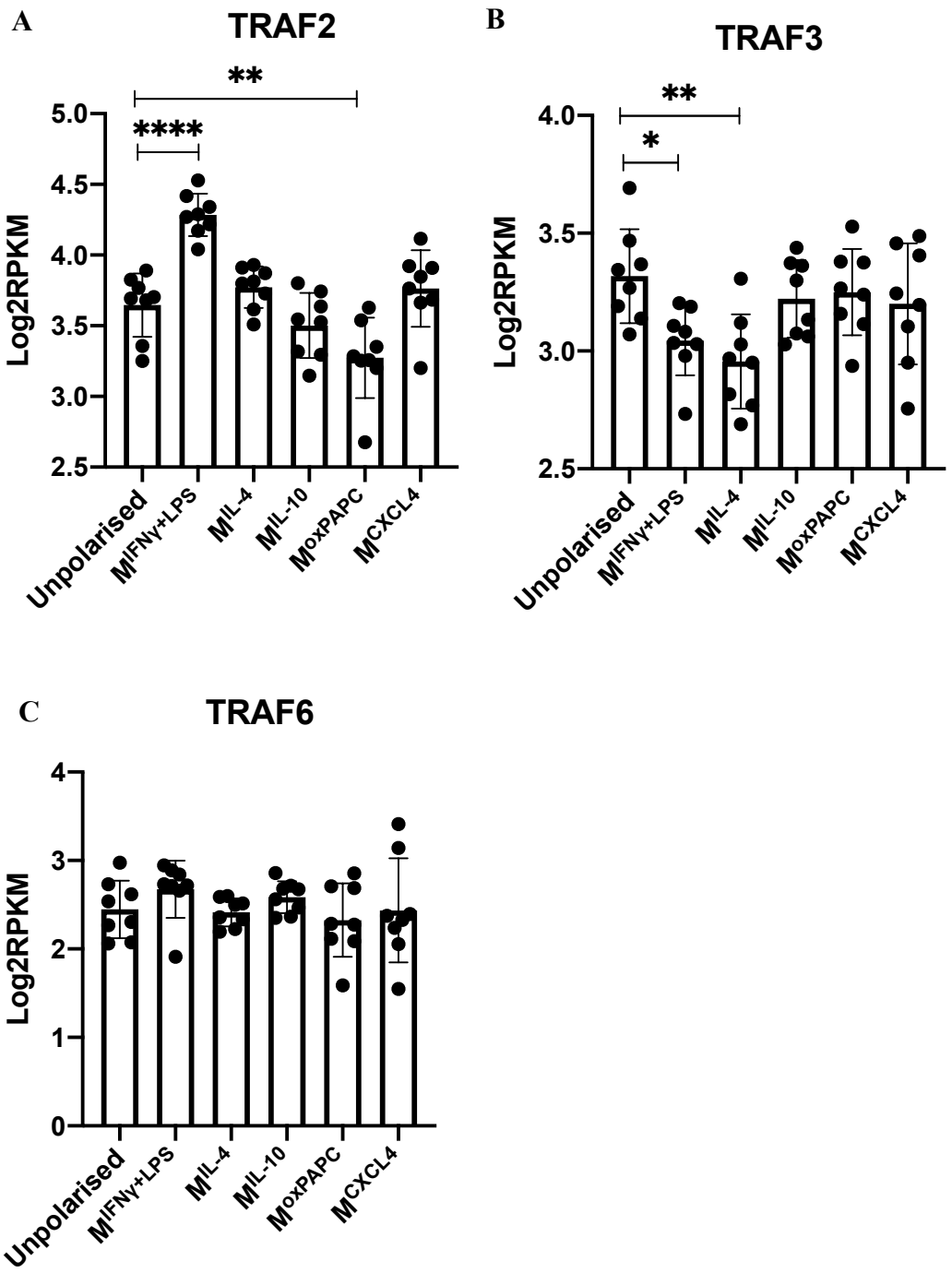

Figure 4.3 Expression of TRAF genes

RNA-Sequencing data of human primary monocyte-derived macrophages that has been polarised to the different macrophage phenotypes using cytokines (n=8). The bars show the expression of (A) TRAF2, (B) TRAF3 and (C) TRAF6 as reads per kilobase of transcript per million mapped reads (log2RPKM) on the Y axis. Data were means ± SD and statistically analysed using one-way ANOVA. When stars are on bars, it indicates the significant changes in expression level. P values on Graph pad prism are as follow: (*) *P≤0.05*, (**) *P ≤0.01*, (***) *P ≤0.001* and (****) *P ≤0.0001,* and when stars are missing, there is no significant change on expression compared to unpolarised macrophage.

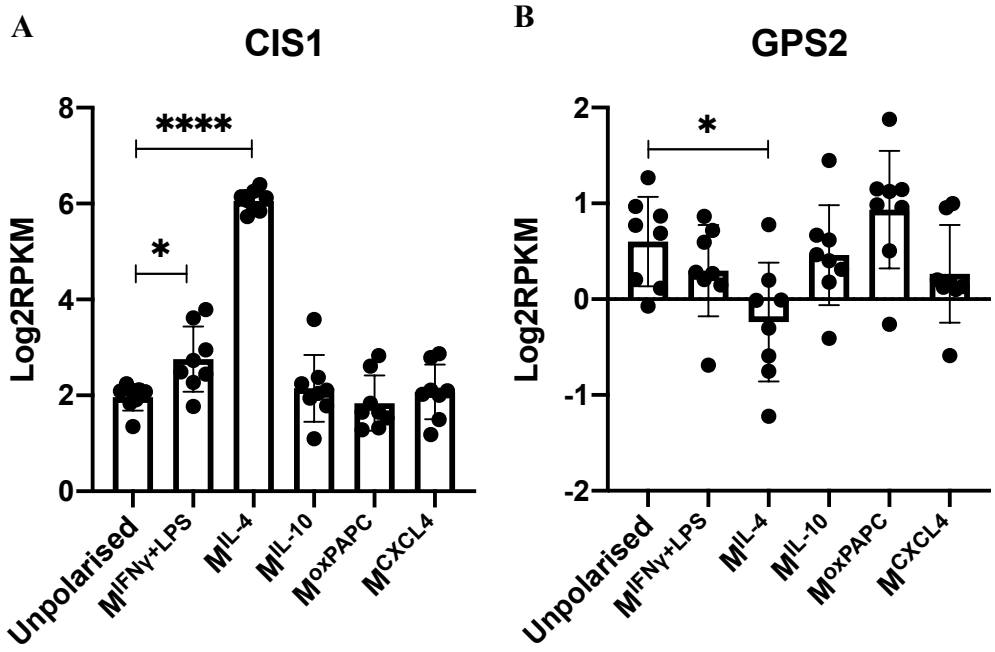

Figure 4.4 Expression of CIS1 and GPS2

RNA-Sequencing data of human primary monocyte-derived macrophages that has been polarised to the different macrophage phenotypes using cytokines (n=8). The bars show the expression of (A) CIS1 and (B) GPS2 as reads per kilobase of transcript per million mapped reads (log2RPKM) on the Y axis. Data were means ± SD and statistically analysed using one-way ANOVA. When stars are on bars, it indicates the significant changes in expression level. P values on Graph pad prism are as follow: (*) *P≤0.05*, (**) *P ≤0.01*, (***) *P ≤0.001* and (****) *P ≤0.0001,* and absence of stars indicates no significant difference in expression compared to unpolarised macrophages.

4.2.3. Expression of TAK1 and TAKL compared to FAM26F

Figure 4.5 shows the expression of TAK1, TAKL and FAM26F as log2FC. From the previous TAKL expression data on primary macrophage (see section 3.5.2), we showed that TAKL elevates in $M^{IFN\gamma+LPS}$ macrophage. We chose to compare this to the most uniquely upregulated membrane protein in $M^{IFN\gamma+LPS}$ macrophages identified previously in our group using SILAC membrane proteomics (Hadadi, 2015). In agreement, analysis here using RNA-seq showed FAM26F mRNA levels were higher in $M^{IFN\gamma+LPS}$ macrophages. This indicates that FAM26F may be suitable as an inflammatory marker to identify inflammatory macrophages and assess their function in diseases such as atherosclerosis.

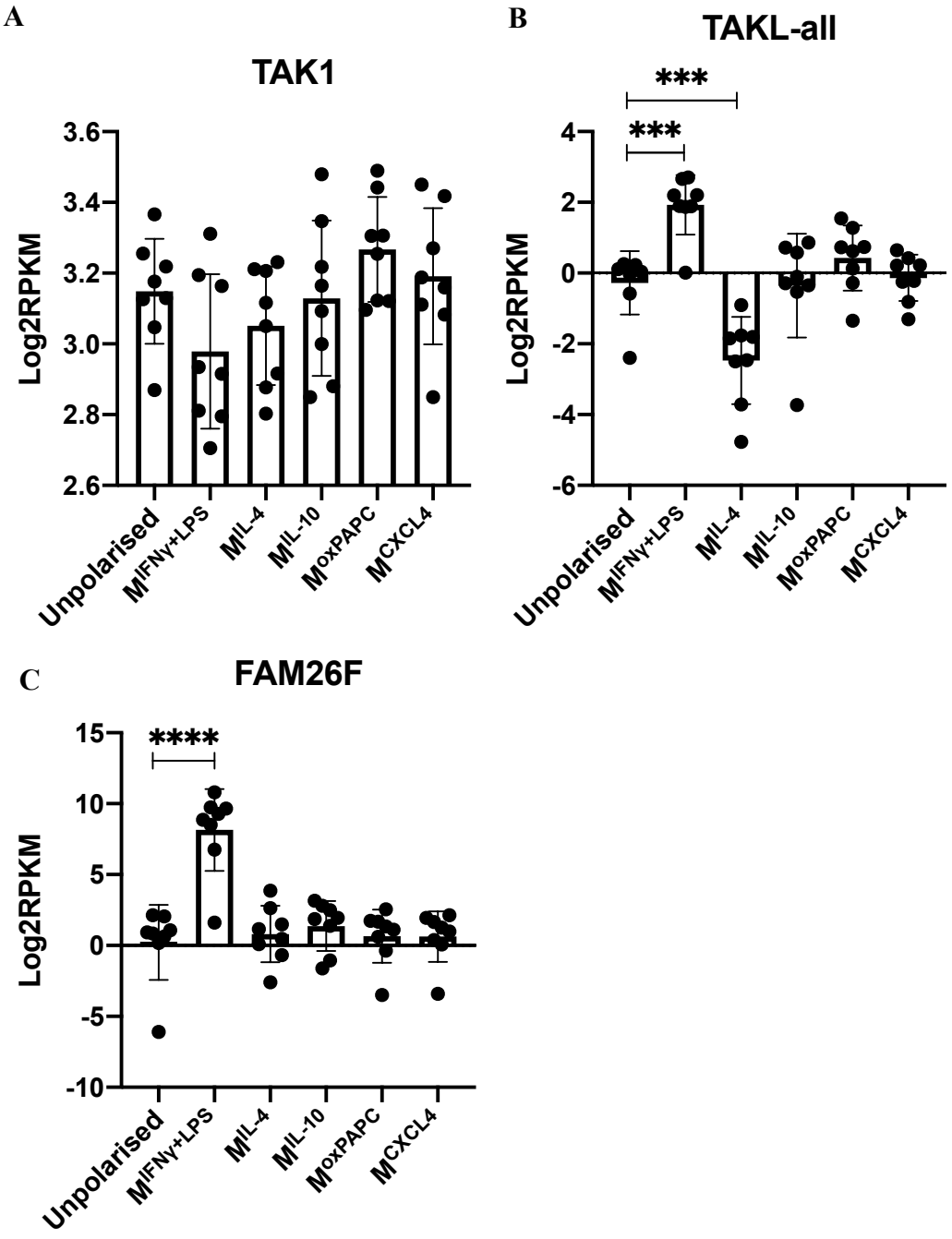

Figure 4.5 Expression of TAK1, TAKL and FAM26F in human monocytes-derived macrophages

The graph was generated using the RNA-Sequencing of 8 healthy donors. The bars show the expression of (A) TAK1, (B) TAKL and (C) FAM26F genes as reads per kilobase of transcript per million mapped reads (log2RPKM) on the Y axis. The expression was measured on human primary macrophage polarised as shown on the X axis. Data were means ± SD and statistically analysed using one-way ANOVA. When stars are on bars, it indicates the significant changes in expression level. P values on Graph pad prism are as follow: (*) *P≤0.05*, (**) *P ≤0.01*, (***) *P ≤0.001* and (****) *P ≤0.0001,* and absence of stars indicates no significant difference in expression compared to unpolarised macrophages.

4.2.4. Expression of FAM26 genes family

Since FAM26F was shown to be uniquely upregulated in $M^{IFN\gamma+LPS}$ macrophages (see above) we explored whether related proteins from this family are also altered in expression in differentially polarised human macrophages. FAM26F (family with sequence similarity member 26 F) or CALHM6 (calcium homeostasis modulator family member 6) is one member of a genes family that produce 6 proteins: FAM26 (A to F). The 6 genes were identified as a family according to homology in their sequences. FAM26 genes were found in two clusters on two chromosomes; FAM26A, FAM26B and FAM26C were clustered on chromosome 10, while FAM26D, FAM26E and FAM26F were clustered on chromosome 6 (Zhomgming et al, 2016). Studies suggested that FAM26C and FAM26F are conserved across > 20 species, including human and mouse, which suggests their biological importance. However, the physiological function of FAM26 proteins is unknown. Regarding protein structure of FAM26C and FAM26F, they contain four transmembrane (TM) spanning helices at the carboxyl terminal end (Malik et al., 2016) (see figure 4.6 for TM helices illustration for FAM26F). This adhesion region suggests a role of protein-protein interaction (Malik et al., 2016, Javed et al., 2016, Levy and Shoham, 2005).

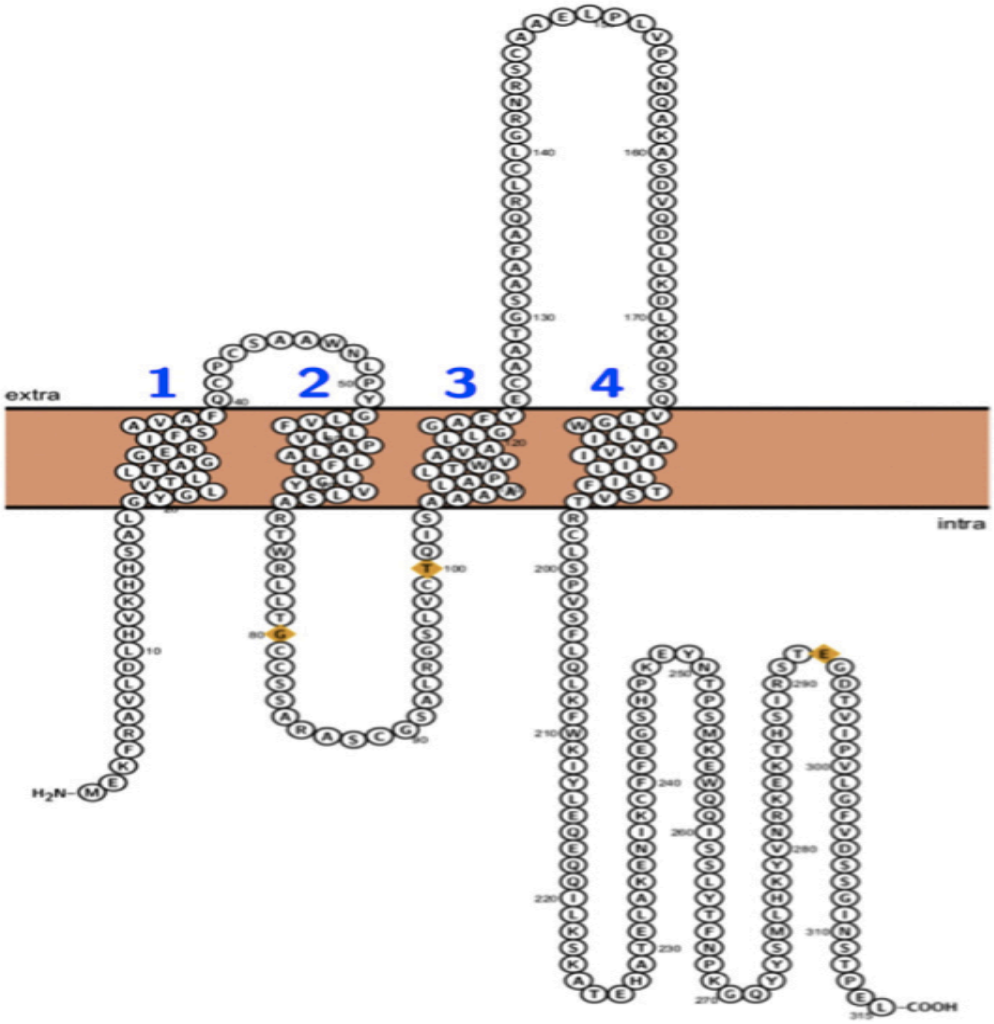

Figure 4.6 TM helices illustration in FAM26F protein structure (Malik et al., 2016)
The image represents the four consensus TM helices (numbers in blue) with the corresponding amino acids positions; 19-39, 52-72, 104-124 and 176-96, respectively.

According to the human protein atlas, accessed on 12th of November 2019, the most abundant gene in the FAM family that is expressed in human tissues is FAM26B (CALHM2), while the other FAM genes are specific to certain tissues such as placenta. Interestingly, FAM26F is the only one that has a relative expression to immune organs such as lymph node, spleen, bone marrow and appendix (see section 4.2 for more details about FAM26-B and -F tissue expression).

Our RNA-seq data analysis showed that the other FAM26 family mRNAs that been found to be expressed in hMDMs were FAM26B (CALHM2), FAM26C (CALHM10) (see figure 4.7), in addition to FAM26F (CALHM6) (see figure 4.5C). FAM26B was highly expressed in all macrophage phenotypes, but its expression was consistent in all phenotypes, while FAM26F has a specific elevation in IFNγ and LPS macrophage. Additionally, FAM26C expression levels appeared to be down regulated in the two macrophage forms induced by IFNγ +LPS and oxPAPC. The cellular stimulants, IFNγ, LPS and oxPAPC, known to be involved in inflammasome activation signalling in atherosclerosis, which contributes in the release of IL-1β in macrophage (Gibson et al, 2018). This suggests that FAM26C may has a role in atherosclerosis.

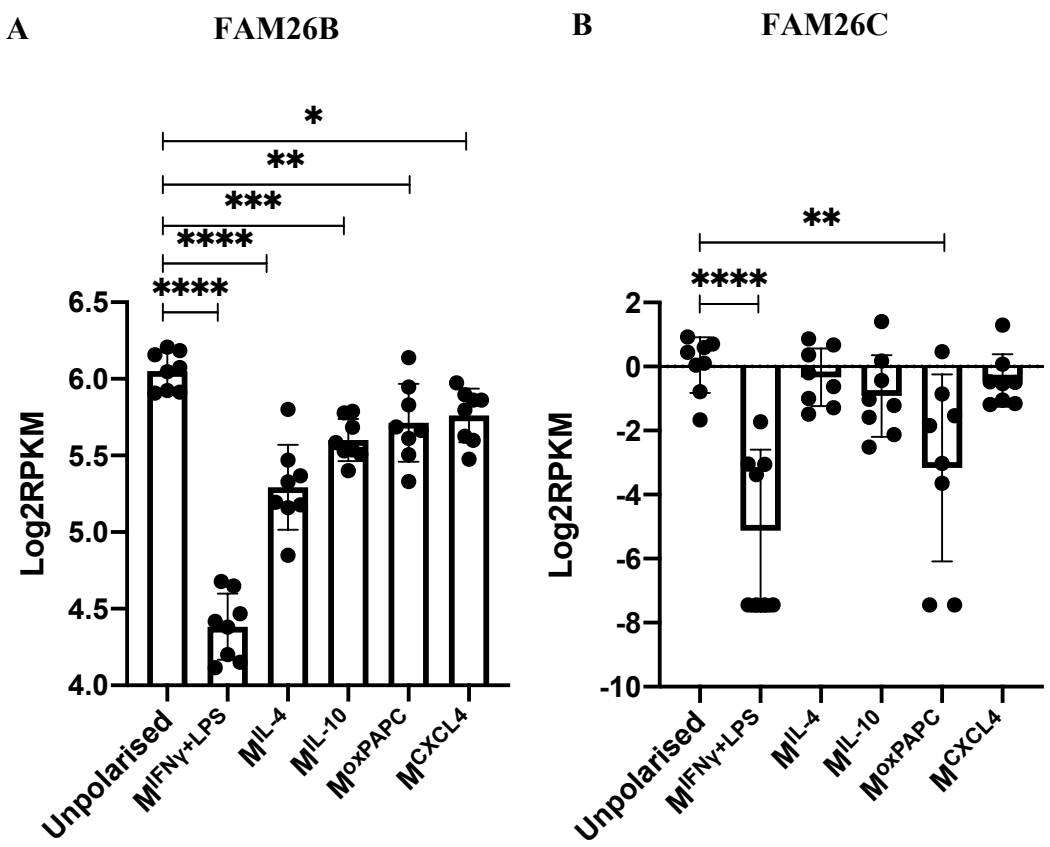

Figure 4.7 Expression of FAM26 genes in human monocytes-derived macrophages
The graph was generated using the RNA-Sequencing of 8 healthy donors. The bars show the expression of (A) FAM26B and (B) FAM26C genes as reads per kilobase of transcript per million mapped reads (log2RPKM) on the Y axis. The expression was measured on human primary macrophage phenotypes on the X axis. Data were means ± SD and statistically analysed using one-way ANOVA. When stars are on bars, it indicates the significant changes in expression level. P values on Graph pad prism are as follow: (*) *P≤0.05*, (**) *P ≤0.01*, (***) *P ≤0.001* and (****) *P ≤0.0001* and absence of stars indicates no significant difference in expression compared to unpolarised macrophages.

4.2.5. Expression of FAM26F transcripts

FAM26F has previously known as IRF-3-dependent NK-activating molecule and (INAM). FAM26F gene is located in human chromosome 6 (chromosomal location: 6q22.1), it consists of 3 exons and encoding 315 amino acid (Malik et al., 2016).

Using the database of ENSEMBL (accessed on 12th of November 2019), we identified three splice variants of FAM26F (Figure 4.8A). The most abundant isoform was the full-length transcript-2 (ENST00000368605.3), and transcript-3 that lacks the 5'-end region (ENST00000368604.2), they were specifically highly expressed in IFNγ and LPS-macrophages (Figure 4.8C and D). The last one was transcript-1, which has no exon 2 (ENST00000368606.7) was expressed less in macrophage phenotypes, but still the maximum expression found in IFNγ and LPS-macrophages (Figure 4.8B).

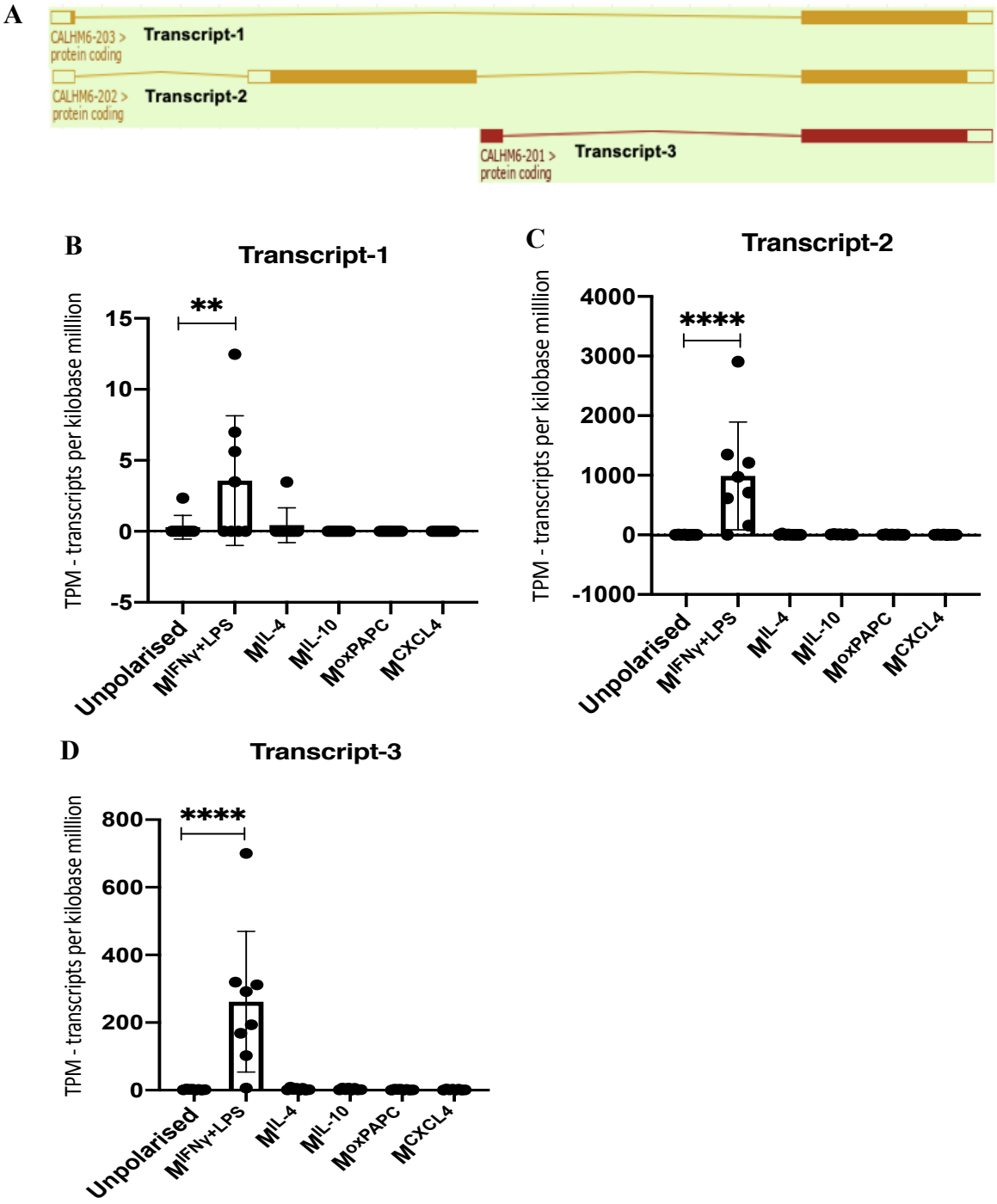

Figure 4.8 FAM26F transcripts

(A) Schematic diagram of FAM26F transcripts from ENSEMBL (accessed on 14th of November 2019). The bar graphs show RNA-Sequencing data of human primary monocyte-derived macrophages that has been polarised to the different macrophage phenotypes using cytokines (n=8). The bars show the expression of FAM26F transcripts (B, C and D) as transcripts per kilobase million (TPM) on the Y axis, the corresponding ENSEMBL number for each isoform is on the top of each graph. The expression was measured on human primary macrophage phenotypes on the X axis. Data were means ± SEM and statistically analysed using one-way ANOVA. Stars on bars indicate the significant changes in expression level compared to unpolarised macrophages. P values on Graph pad prism are as follow: (*) *P≤0.05*, (**) *P ≤0.01*, (***) *P ≤0.001* and (****) *P ≤0.0001,* and absence of stars indicates no significant difference in expression compared to unpolarised macrophages.

4.3. FAM26F and FAM26B expression in human tissues

Since we detected FAM26F and FAM26B mRNAs to be expressed at high levels in human macrophages, but not FAM26C, we wished to assess the tissue specificity of expression of these transcripts to address whether these are unique to macrophages or expressed in other cell types. Human RNA consensus tissue gene data on the human atlas were collected from three data sources (HPA, GTEx and FANTOM5) in 74 tissues for each gene. The (NX) value is the total normalised value from the three sources. FAM26F RNA expression levels appeared to be high in lymphoid and myeloid organs/cells such as spleen, lymph node, monocytes and B cells (see figure 4.9). Additionally, studies of RNA expression on primary cell types and cell lines have showed the same, that cells enhanced with FAM26F were of the lymphoid and myeloid organs. Primary cells such as monocytes, B cells and dendritic cells, and cell lines such as HEL, Karpas-707, RPMI-8226, U-937 and THP-1 (The human protein atlas, accessed on 12th of November 2019).

The RNA and protein expression of FAM26B showed a low tissue specificity compared to FAM26F. FAM26B was expressed in all the 74 tissues that has been tested in the human atlas data sources, with maximum expression levels in some tissues including brain, endocrine tissues, lung, kidney and female tissues. In terms of cellular RNA expression, interestingly, the maximum levels were found in immune cells such as monocytes, dendritic cells, T cells, NK cells.

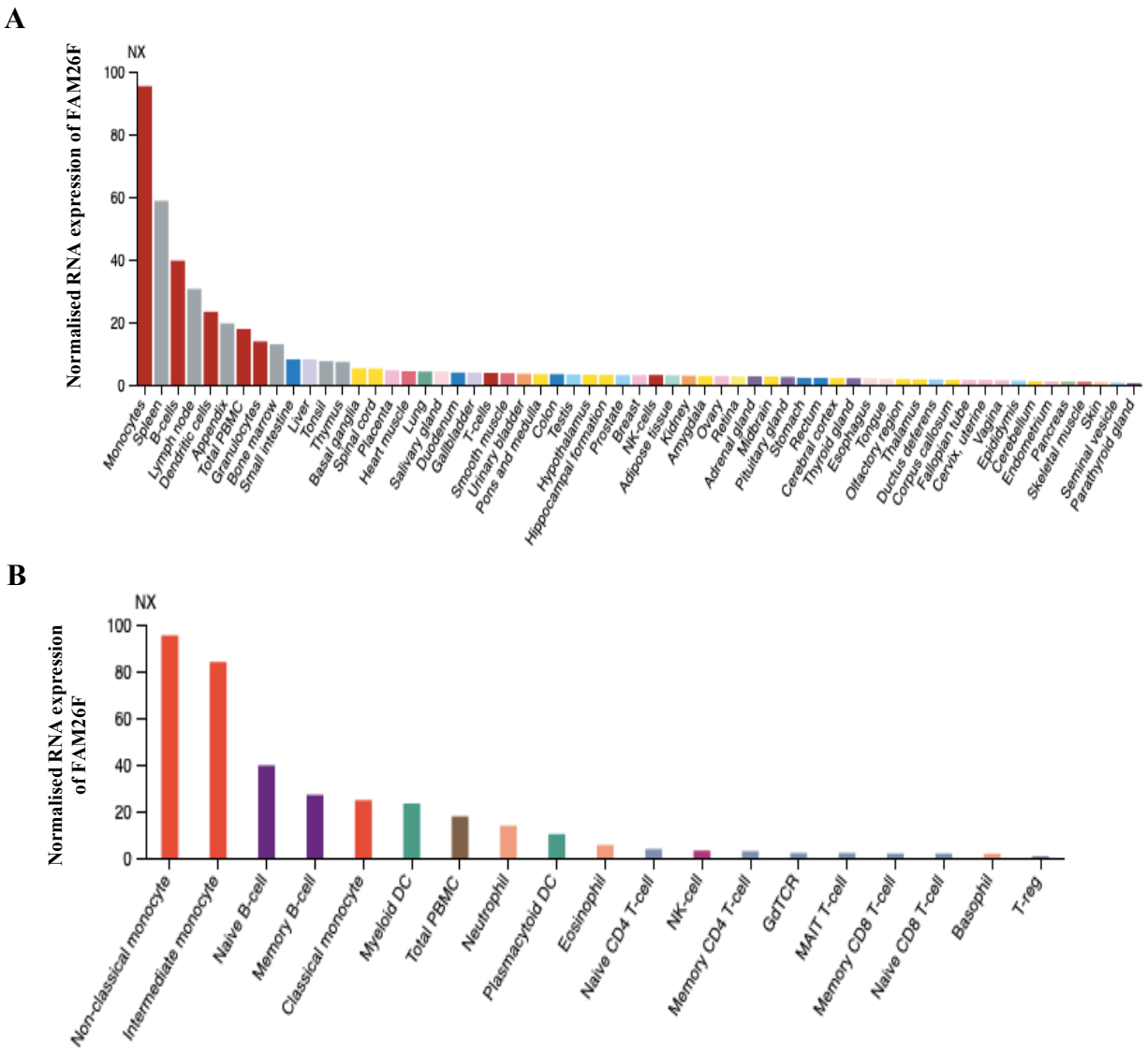

Figure 4.9 RNA expression of FAM26F in human tissues (The human protein atlas, accessed on 12th of November 2019)

The graph shows the RNA expression of FAM26F (A)in human tissues and (B) in human cell types. Data measured the expression in 74 tissues and were collected from three data sources. The bars show the expression of FAM26F RNA on the Y axis as (NX) which is the total normalised RNA value of the individual TPM values of each sample from three sources (HPA, GTEx and FANTOM5).

4.4. Pathway analysis of FAM26F and its potential protein partners

In this section, we have conducted two different in silico analysis for predicted FAM26F interacting proteins, the first analysis was using the protein association networks, STRING (Figure 4.10) and GENEMANIA (Figure 4.11), accessed on 20th of November 2019, the results show many proteins related to FAM26F regarding to structure (sharing same protein domains), co-expressed or co-localised with FAM26F.

The second analysis was carried out using a functional protein pathway analysis database (Reactome.org), but in this analysis we have added a list of 26 proteins besides FAM26F. The list was including the following proteins: ACADV, APOBR, FAM26F, CD300, CNPY3, DCD-1, PRKDC, EFTU, EMC7, ERP29, GDIR1, LAT, LMAN2, MARCS, PA2G4, PDIA4, PFD2, PRDX5, PSB2, RAB5B, RBP2, SCAM3, SETLP, SRPRA, TMX2 and USO1 (Table 4.1). This list of FAM26F potential protein partners were obtained from the mass spectrometry analysis of the immunoprecipitation samples (see next chapter, section 5.5).

As a result of Reactome analysis, most proteins of the previous list have been found to be related to 697 human cellular pathways, except ACADV, FAM26F, EMC7, GDIR1, PDIA4 and SETLP. However, the pathways were limited to 25 significant pathways according to p-value (Table 4.2). Different individual proteins to those on our list were involved in each of the 25 pathways, the data was further narrowed down to the pathways that have more than one protein involved (two or three). The resulting proteins in this list include: MARCS, PRDX5, RAB5B, CD300, PA2G4, PSB2,LMAN2 and USO1 (Table 4.3).

Two of these proteins appeared to be related to interesting functional pathways of granulation. Firstly, myristoylated alanine-rich C kinase substrate (MARCKS), which has a role in increasing the insulin granules in response to acetylcholine. The other protein is antigen-like family member A (CD300A), which contributes to the neutrophil granulation pathway. Interestingly, neutrophil granules are important in introducing the proteins to cell surface and cytokines secreting, especially in MHC II antigen presenting to T cells. For the future functional studies, it is worth testing if FAM26F is linked to MARCKS and CD300, which could contribute to the understanding of FAM26F function or its cellular pathway.

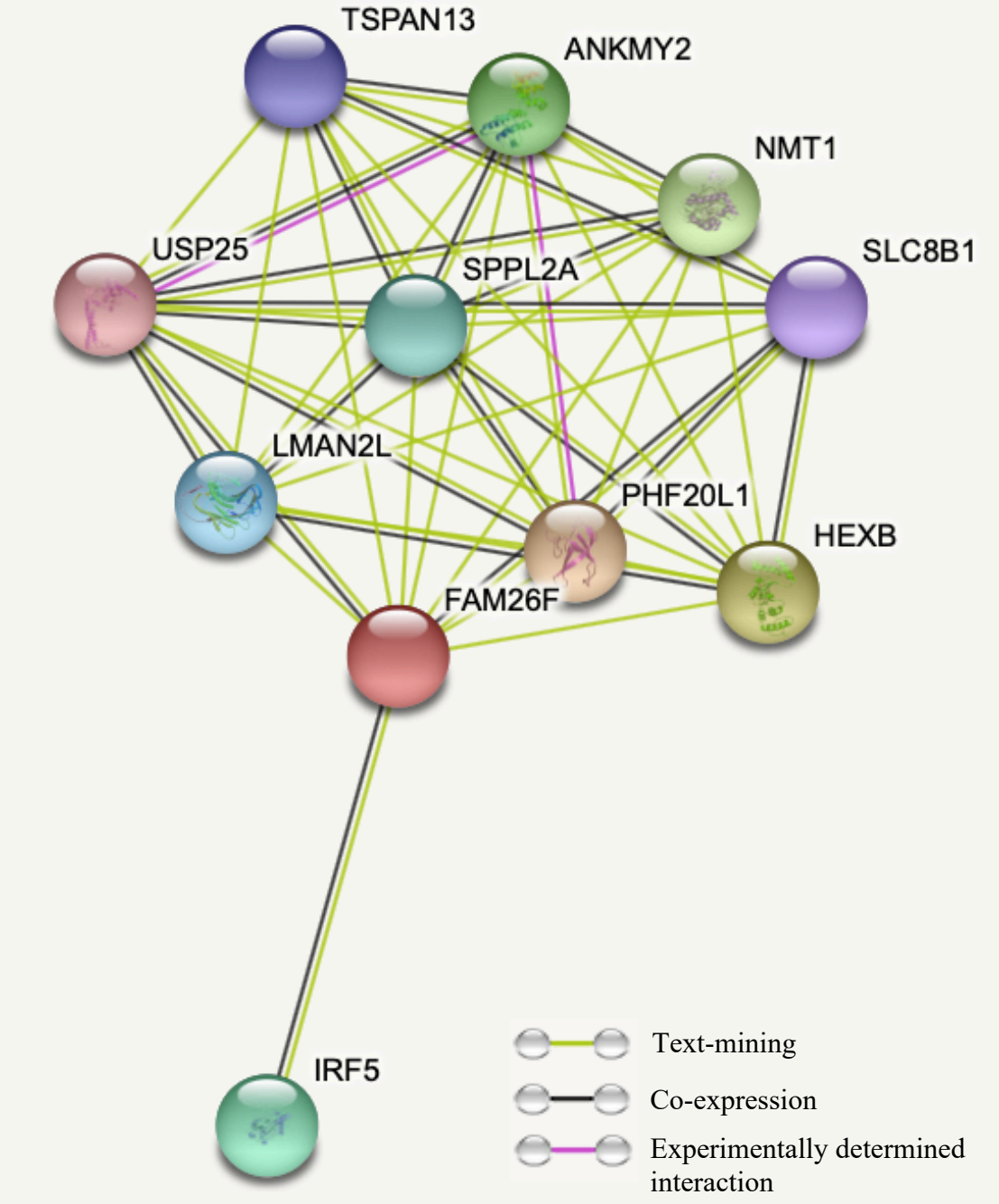

Figure 4.10 Protein association analysis (STRING, accessed on 20th of November 2019)
This image shows a network of potential interacting protein partners to FAM26F or to each other according to automated text-mining and computational predictions of literature resources (green linking lines), co-expression (black linking lines) or experimentally determined interaction (pink linking lines), see the key on right bottom corner. This network was obtained as a result of entering FAM26F only in STRING resource.

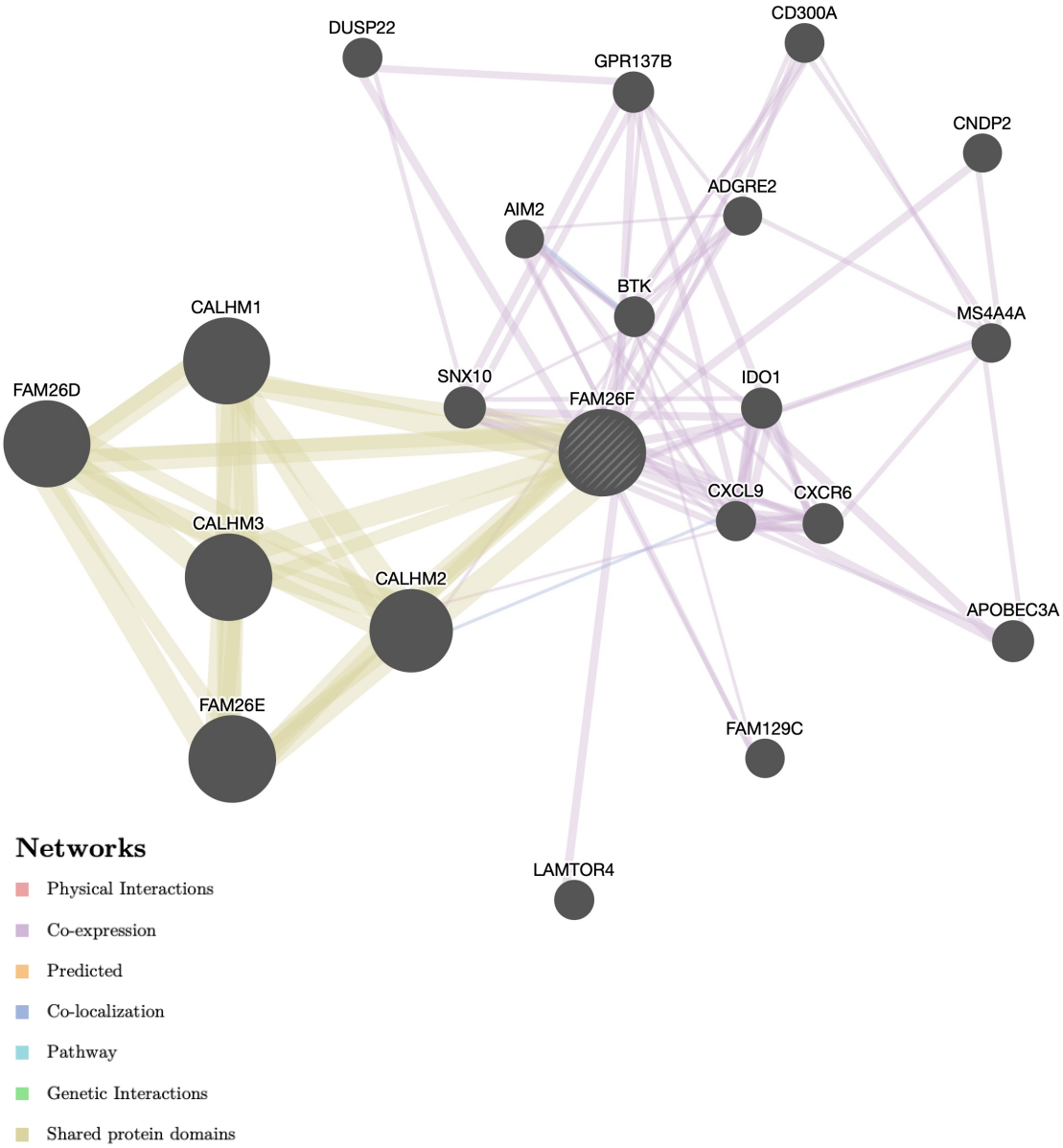

Figure 4.11 Protein association analysis (GENEMANIA, accessed on 20th of November 2019)
This image shows a network of potential interacting protein partners to FAM26F or to each other according to shared protein domains (brown linking lines) or co-expression (purple linking lines), see the key on left bottom corner. This network was obtained as a result of entering FAM26F only in STRING resource.

Table 4.1 FAM26F potential interacting protein partners from mass spectrometry analysis (see chapter 5, section 5.5)

Official symbol	Protein name
ACADV	Very long-chain specific acyl-CoA dehydrogenase
APOBR	Apolipoprotein B receptor
CAHM6 or FAM26F	Calcium homeostasis modulator protein 6
CLM-8 or CD300	CMRF35-like molecule 8 CD300 antigen-like family member A
CNPY3	Protein canopy homolog 3
DCD-1	Dermcidin
DNA-PK or PRKDC	DNA-dependent protein kinase catalytic subunit
EFTU	Elongation factor Tu
EMC7	ER membrane protein complex subunit 7
ERP29	Endoplasmic reticulum resident protein 29
GDIR1	Rho GDP-dissociation inhibitor 1
LAT	Linker for activation of T-cells family member 1
LMAN2	Lectin mannose-binding 2
MARCS	Myristoylated alanine-rich C-kinase substrate
PA2G4	Proliferation-associated protein 2G4
PDIA4	Protein disulfide-isomerase A4
PFD2	Prefoldin subunit 2
PRDX5	Peroxiredoxin-5
PSB2	Proteasome subunit beta type 2
RAB5B	Ras-related protein Rab-5B
RBP2	Ran-binding protein 2
SCAM3	Secretory carrier-associated membrane protein 3
SETLP	Protein SETSIP
SRPRA	Signal recognition particle receptor subunit alpha
TMX2	Thioredoxin-related transmembrane protein 2
USO1	General vesicular transport factor p115

Table 4.2 The most significant pathways (Reactome.org accessed on 12th of November 2019)

The following table shows the 25 most relevant pathways sorted by p-value.

Pathway name	Entities				Reactions	
	found	ratio	p-value	FDR*	found	ratio
Acetylcholine regulates insulin secretion	3 / 113	0.006	0.019	0.305	4 / 7	5.69e-04
Defective RFT1 causes RFT1-CDG (CDG-1n)	1 / 12	5.90e-04	0.022	0.305	1 / 1	8.12e-05
VLDL clearance	1 / 12	5.90e-04	0.022	0.305	1 / 3	2.44e-04
Presynaptic function of Kainate receptors	1 / 23	0.001	0.042	0.305	1 / 2	1.62e-04
Prefoldin mediated transfer of substrate to CCT/TriC	1 / 29	0.001	0.053	0.305	2 / 2	1.62e-04
FBXW7 Mutants and NOTCH1 in Cancer	1 / 31	0.002	0.056	0.305	1 / 1	8.12e-05
Loss of Function of FBXW7 in Cancer and NOTCH1 Signaling	1 / 31	0.002	0.056	0.305	1 / 1	8.12e-05
Separation of Sister Chromatids	2 / 208	0.01	0.058	0.305	3 / 8	6.50e-04
Interleukin receptor SHC signaling	1 / 32	0.002	0.058	0.305	1 / 6	4.87e-04
Neutrophil degranulation	3 / 480	0.024	0.06	0.305	4 / 10	8.12e-04
Josephin domain DUBs	1 / 34	0.002	0.062	0.305	2 / 6	4.87e-04
Signalling to p38 via RIT and RIN	1 / 34	0.002	0.062	0.305	1 / 3	2.44e-04
TP53 Regulates Transcription of Death Receptors and Ligands	1 / 34	0.002	0.062	0.305	2 / 7	5.69e-04
COPII-mediated vesicle transport	3 / 217	0.011	0.062	0.305	11 / 16	0.001
Synthesis of GDP-mannose	1 / 35	0.002	0.063	0.305	1 / 3	2.44e-04
Signaling by NOTCH1 t(7;9)(NOTCH1:M1580_K2555) Translocation Mutant	1 / 35	0.002	0.063	0.305	1 / 5	4.06e-04
Constitutive Signaling by NOTCH1 t(7;9)(NOTCH1:M1580_K2555) Translocation Mutant	1 / 35	0.002	0.063	0.305	1 / 5	4.06e-04
Defective TPR may confer susceptibility towards thyroid papillary carcinoma (TPC)	1 / 36	0.002	0.065	0.305	1 / 1	8.12e-05
SOS-mediated signalling	1 / 36	0.002	0.065	0.305	1 / 2	1.62e-04
Recycling of eIF2:GDP	1 / 36	0.002	0.065	0.305	1 / 2	1.62e-04
NTRK2 activates RAC1	1 / 36	0.002	0.065	0.305	1 / 2	1.62e-04
Mitotic Anaphase	2 / 223	0.011	0.065	0.305	3 / 11	8.94e-04
Activation of RAS in B cells	1 / 37	0.002	0.067	0.305	1 / 2	1.62e-04
Activation of kainate receptors upon glutamate binding	1 / 37	0.002	0.067	0.305	1 / 6	4.87e-04
ARMS-mediated activation	1 / 38	0.002	0.069	0.305	1 / 6	4.87e-04

Table 4.3 The narrowed list of pathways analysis of FAM26F potential partners (Reactome.org accessed on 12th of November 2019)

Pathway name	Number of proteins found	Proteins
Acetylcholine regulates insulin secretion	3/26	MARCKS, PRDX5, RAB5B
Neutrophil degranulation	3/26	CD300A, PA2G4, RAB5B
COPII-mediated vesicle transport	3/26	LMAN2, USO1, RAB5B
Separation of sister chromatids	2/26	PSMB2, RANBP2
Mitotic anaphase	2/26	PSMB2, RANBP2

4.5. Conclusions

- **RNA-Sequencing data analysis**

  From the RNA-Seq data, we found the same finding from the previous chapter, TAKL RNA expression is elevated in macrophage induced by IFNγ and LPS.
  Additionally, these data set allowed us to analyse the expression of more TAKL variants such as TAKL-A and TAKL-E, which are not been tested by RT-qPCR. The same conclusion has been found that TAKL-L is the main variant, which elevates in IFNγ and LPS-macrophage.
  Regarding FAM26 RNA expression, the most abundant gene was FAM26B, but its expression was consistent among macrophage phenotypes. While, the RNA expression of FAM26F was specifically high in IFNγ and LPS-macrophage. Additionally, FAM26C is down regulated in inflammatory macrophage which induced by chemokines related to atherosclerosis inflammasome signalling.

- **The in-silico analysis for FAM26F interacting partners**

  Comparing the early analysis of FAM26F for protein interactors, using STRING and GENEMANIA, to our mass spectrometry list (Table 4.1), we found few proteins to be presented in both in-silico analysis and our list, which were LMAN2 and CD300A, from STRING and GENEMANIA, respectively. Nevertheless, CXCL9 found to have a co-expression link to FAM26F, according to GENEMANIA analysis, this protein has an interesting function as a chemoattractant induced by IFNγ in activated T cell (Tokunaga et al., 2018).

- **Protein functional pathways study**

  FAM26F and the 26 possible interacting partner proteins from the mass spectrometry list, were further analysed using (Reactome.org), to investigate if they linked to the known cellular pathways. Two proteins, MARCKS and CD300A were found to be linked to firstly, the pathway that regulates insulin secretion by acetylcholine and secondly, neutrophil degranulation, respectively.

4.6. Discussion

- **Identifying the suitable prognostic inflammatory macrophage marker**

This project aimed to identify a prognostic marker for inflammatory macrophages that allows us to detect pro-inflammatory macrophages in inflammatory diseases such as atherosclerosis. From chapter 3 RT-qPCR studies, we found high RNA expression levels of TAKL in monocytic THP-1 model cell line and primary hMDMs, but we were unable to confirm the same elevation at the protein level because the antibody was not adequate for such an assessment.

While FAM26F was expressed in high levels specifically in IFNγ and LPS-macrophages at the mRNA and protein level in human and mouse (determined by my colleagues: E. Hadadi, K. Baidzajevas and L. Campesino). The RNA-Seq analysis confirmed the same finding when we compared the expression levels of TAKL and FAM26F. We were interested to assess whether FAM26F may be a suitable clinical marker of inflammatory macrophages. However, since little is known about FAM26F function or cellular pathway, we aimed to understand its function in addition to its use as a potential prognostic marker for inflammatory macrophages in atherosclerosis (chapter 5).

- **Findings of the in-silico analysis for FAM26 family and FAM26F interacting partners**

We identified the same two proteins (LMAN2 and CD300A) in the in-silico FAM26F partners lists (from STRING and GENEMANIA) and our co-expression analysis list from the mass spectrometry. LMAN2 is a type 1 transmembrane lectin that has a transport function between the plasma membrane, endoplasmic reticulum and Golgi apparatus (GeneCards.org), and FAM26F is an ion/cation transmembrane transport protein (Malik et al., 2016). This functional similarity suggests that there may be an interaction and/or functional relation between LMAN2 and FAM26F. Furthermore, CD300A is a glycoprotein and LMNA2 has a binding activity to glycoproteins, however more protein-protein interaction experiments are required in order to validate these suggestions.

Interestingly, CXCL9 was found from in-silico analysis as a potential partner according to FAM25F, and it has chemokine activity role in T cell, and we aimed to study the effect of FAM26F overexpression on macrophage-T cell interaction.

- **Limitations and possible future studies**

The pathway analysis for FAM26F partners was not a wide study due to the time limitations. The 26 co-IP interacting FAM26F protein partners were compared to our in silico analysis; two proteins were found to appear in both results lists, MARCS and CD300A. It will be interesting to undertake further analysis of this interaction in the future. These proteins can be linked to FAM26F by testing their mRNA and protein expression levels in macrophage phenotypes, this is can be initially tested using the RNA-seq data. Beyond this, it would be interesting to assess the protein-protein interaction using different methods such as immunoprecipitation or fluorescence resonance energy transfer (FRET).

Chapter 5

Assessing the function of FAM26F in inflammatory macrophages

5.1. Introduction

We identified a novel inflammatory marker, FAM26F in our group's recent proteomics analysis (Hadadi, 2015) and our RNA-seq analysis of human monocyte-derived macrophage, differentially polarised to M1 (inflammatory) or M2 (anti-inflammatory/repair) phenotypes (Baidžajevas, 2019) and see Chapter 4 of this thesis. FAM26F is a putative plasma membrane expressed protein, upregulated in several inflammatory diseases. Our first aim was to use FAM26F as a prognostic marker to understand the role of inflammatory macrophage in atherosclerosis. Since nothing is known about FAM26F in inflammation and the only available functional relation in the literature was suggested that FAM26F plays a role in mouse myeloid and lymphocyte cells interactions. The work of Ebihara group suggested that FAM26F is expressed from mouse dendritic (mDC) and NK cell and in overexpression conditions, it activates the mDC-NK cell interaction, but this interaction has not proven with protein partners or an interaction mechanism (Ebihara et al., 2010, Kasamatsu et al., 2014). The ability of FAM26F in cell synapse formation, because it has four transmembrane regions which is similar to tetraspanins adhesion region that could support cell-cell interaction (Levy and Shoham, 2005, Malik et al., 2016).

- **Hypotheses:**

1. FAM26F is a marker for M1 macrophages and therefore is detected in a specific inflammatory population of macrophages in diseased atherosclerotic plaques.
2. FAM26F plays a role in inflammation by interacting with proteins related to its immune function.

- **Aims:**

1. Compare the expression of FAM26F with known M1 markers such as CD86 by immunocytochemistry in human inflammation-polarised macrophages.
2. Assessing immunofluorescence staining to FAM26F (co-stained for pan-macrophage markers, CD68) in human carotid artery sections from a biobank of samples collected from vascular diseased-patients.
3. Identification of interacting protein partners of FAM26F by co-immunoprecipitation using stimulated FAM26F-THP-1-3xFLAG cells.
4. Assessing whether FAM26F overexpression in THP-1 cells alters T-cell interactions.

5.2. FAM26F as a specific human pro-inflammatory macrophage marker

FAM26F was identified using a proteomics approach for cell surface markers upregulated in M1 polarised human macrophages and was highly upregulated at the mRNA level by RNA-seq of inflammatory polarised human macrophages. We therefore set out to determine whether FAM26F is upregulated at the protein level in differently polarised human monocyte-derived macrophages using immunofluorescent staining. We used a polyclonal FAM26F antibody as well as the previously characterised macrophage antibodies; CD68 pan-macrophage marker and CD86 M1 marker (Roszer, 2015, Duluc et al., 2007).

Human monocyte-derived macrophages ($CD14^+$ macrophages) were used in this immunocytochemistry study, and they were differentiated into macrophages by M-CSF stimulation for 7 days. Then macrophages were treated for 24 hour with IFNγ and LPS (see the hMDM differentiation and polarisation procedure in section 2.1.4).

$CD14^+$ human monocyte-dervied macrophages were either untreated (unpolarised) or polarised to pro-inflammatory macrophages ($M^{IFN\gamma + LPS}$). The immunofluorescence staining (Figure 5.1) was used on unpolarised and polarised macrophages to detect CD68 (pan-macrophage marker), CD86 and FAM26F (M1 markers). Figure 5.1 shows that CD68 was highly expressed in both macrophage types, unpolarized macrophage and $M^{IFN\gamma + LPS}$, as it is expected. While, FAM26F was expressed specifically in $M^{IFN\gamma + LPS}$, but not in the unpolarised macrophages, while CD86 was expressed in both macrophages and not specific to M1. The analysis shows the fluorescence intensity levels for all markers on the two-macrophage conditions (Figure 5.2) and reflects the same conclusion that FAM26F is a specific marker for M1 macrophages. This immunocytochemistry study on hMdMs was from a single donor, while across the group we have shown this is highly reproducible. Reason to do this, because it shows the antibody appears specific for testing in immunofluorescence, in order to use it on human plaques sections.

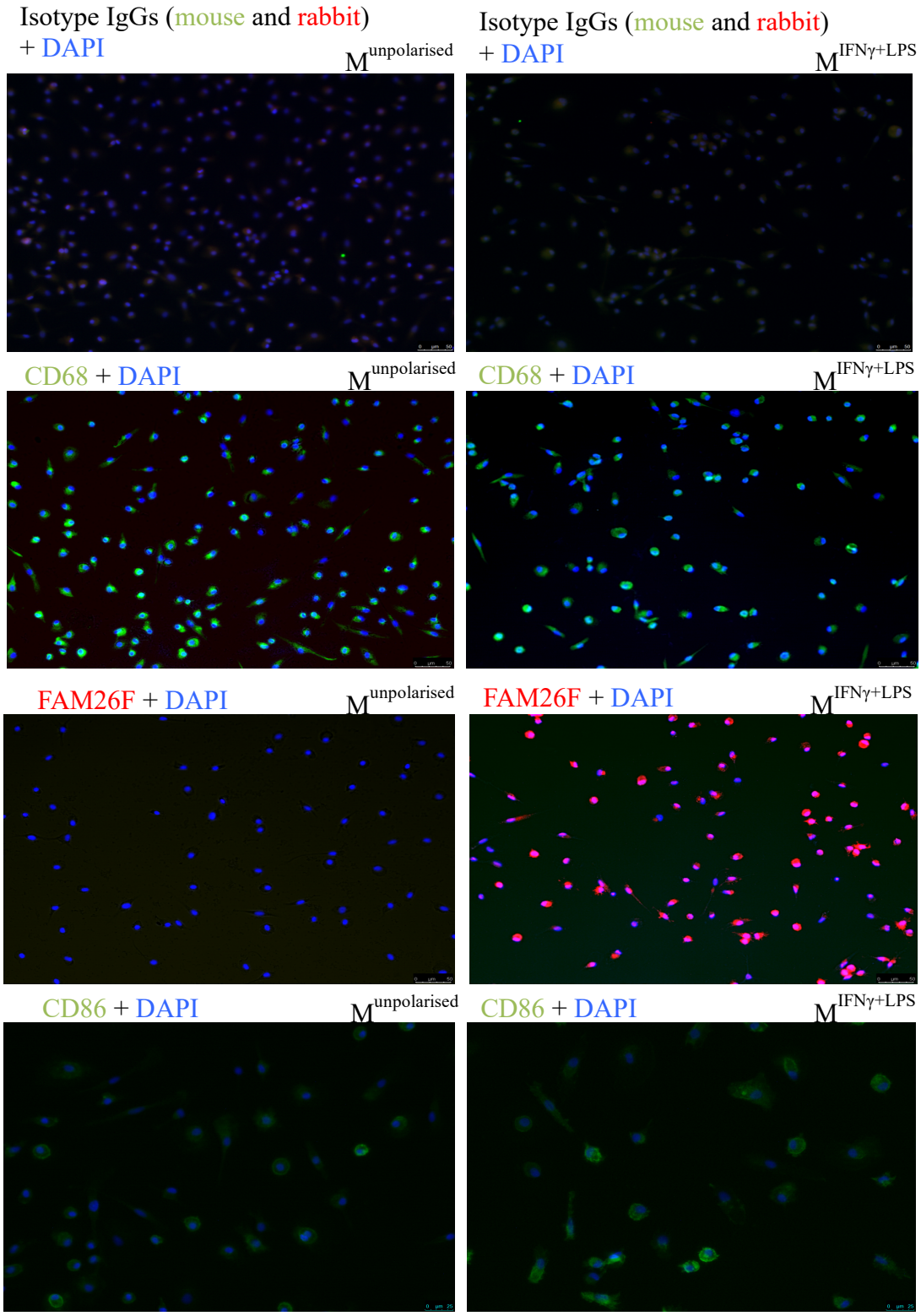

Figure 5.1 Immunofluorescence staining of hMDM with pan- and M1 macrophage markers

(A and B) Immunofluorescence staining of IgG isotype controls (anti-mouse in green and anti-rabbit in red), on unpolarised MDMs (left) and IFNγ and LPS –stimulated MDMs (right). (C) Mouse anti-CD68 in green on unpolarised MDMs. (D) Mouse anti-CD68 in green on IFNϒ and LPS –stimulated MDMs. (E) Rabbit anti-FAM26F in red on unpolarised MDMs. (F) Rabbit anti-FAM26F in red on IFNϒ and LPS –stimulated MDMs. (G) Mouse anti-CD86 in green on unpolarised MDMs. (H) Mouse anti-CD86 in GREEN on IFNϒ and LPS –stimulated MDMs.

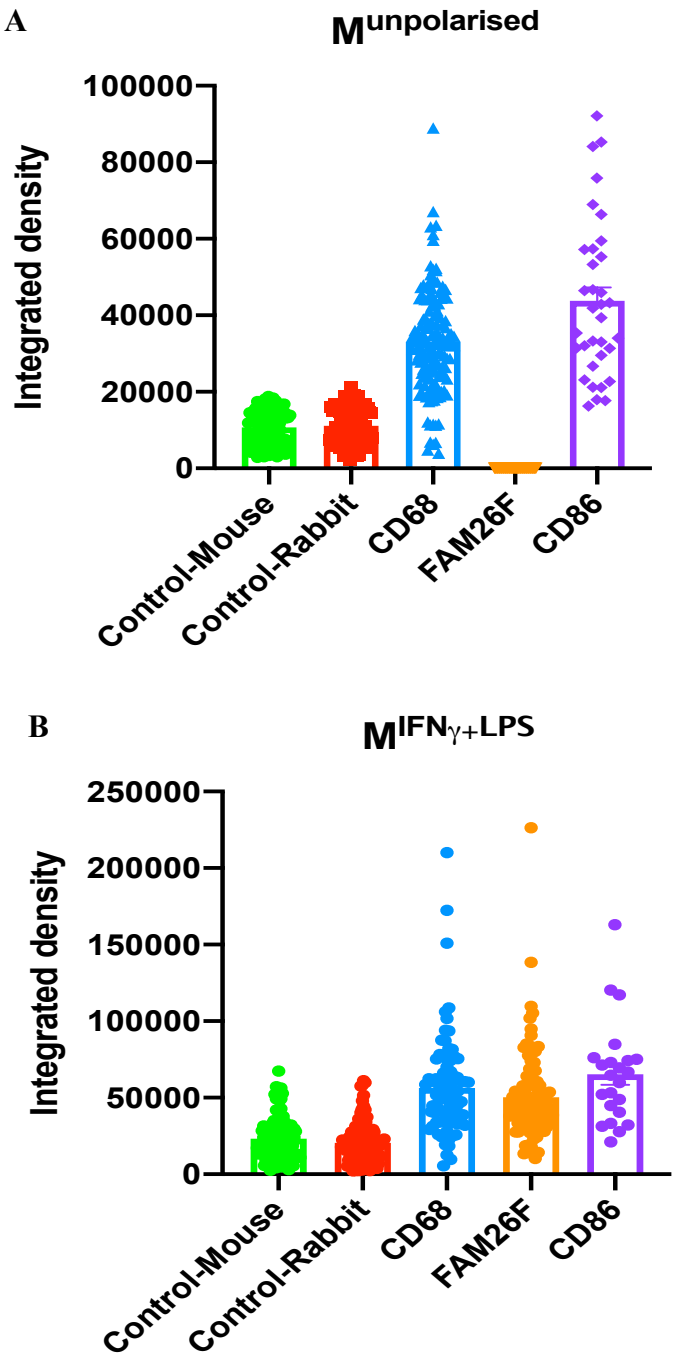

Figure 5.2 Fluorescence intensity of macrophage markers from the immuno-fluorescence staining

The immunofluorescence images (shown in figure 5.1) were analysed, and fluorescence intensity measured using ImageJ software. The bars represent the integrated density of the florescent signals of IgG isotype controls anti-mouse (green) and anti-rabbit (red), CD68 (blue) and CD86 (purple) on (A) unpolarised MDMs and (B) on IFNϒ and LPS –stimulated MDMs. This quantification of immunofluorescence was for different cells from a single donor (n=1).

5.3. FAM26F is expressed in a subpopulation of macrophages in diseased human atherosclerotic plaques

Macrophages in atherosclerotic plaque have the ability to switch between pro-inflammatory M1 and anti-inflammatory M2 phenotypes. The specific aim of the immunohistochemistry studies on carotid sections was to identify the macrophage subpopulations. Specifically, this experiment was considered to test if FAM26F is expressed from the pro-inflammatory M1 population of macrophages in atherosclerotic plaques. In order to investigate that, human carotid artery sections from a biobank of samples collected from atherosclerosis patients were stained with known macrophage markers such as; macrophage-pan marker (CD68), M1-markers (CD86), or M2-marker (mannose receptor, MR), also the carotid sections were stained with FAM26F to check if it is expressed in the inflammatory areas of atherosclerotic-plaque sections. Especially in the inflammatory plaque shoulder area, which is the region of interest in plaque-carotid sections for inflammatory cells such as M1 macrophages (see figure 5.3 for carotid section illustration).

It has been found that $CD68^{+}$and $FAM26F^{+}$ macrophages (pro-inflammatory macrophages) are localised in the inflammatory plaque shoulder area (Figure 5.4).

Macrophages in atherosclerotic plaque have the ability to switch between pro-inflammatory M1 and anti-inflammatory M2 phenotypes. The specific aim of the immunohistochemistry studies on carotid sections was to identify the macrophage subpopulations. Figure 5.5 shows the two different macrophage populations; $CD86^{+}$ macrophages (M1) and MR^{+} macrophages (M2). Comparing FAM26F and CD86 in carotid images, this finding confirms that FAM26F labels a subpopulation of macrophages, which correlate with staining in the shoulder region for CD86 inflammatory macrophages. This links with in vitro MDMs showing FAM26F is specific to M1, suggesting FAM26F labels inflammatory macrophages in human diseased atherosclerotic plaques.

However, our aim was to co-stain the sections with anti-FAM26F and other antibodies against CD68, CD86 and SMA to understand more about the macrophage population that express FAM26F. Unfortunately, we could not achieve that because FAM26F antibody staining required a permeabilization step, with Triton, to detect FAM26F epitope in the cytoplasmic region; we therefore needed to use anti-FAM26F (HPA017948, Sigma) with Triton but not for other antibodies. This anti-FAM26F could therefore not be used in co-staining of MDMs (ICC) or plaque sections (IHC). Interestingly, my colleague in the group (Klaudia Kocsy) had the chance to try a different anti-FAM26F (NBPI-86754, Novus) co-stained with anti-CD68 on human carotid plaque sections which gave successful immunohistochemistry quantitative data with a high number of replicates (n=32), see figure 1 in appendix III.

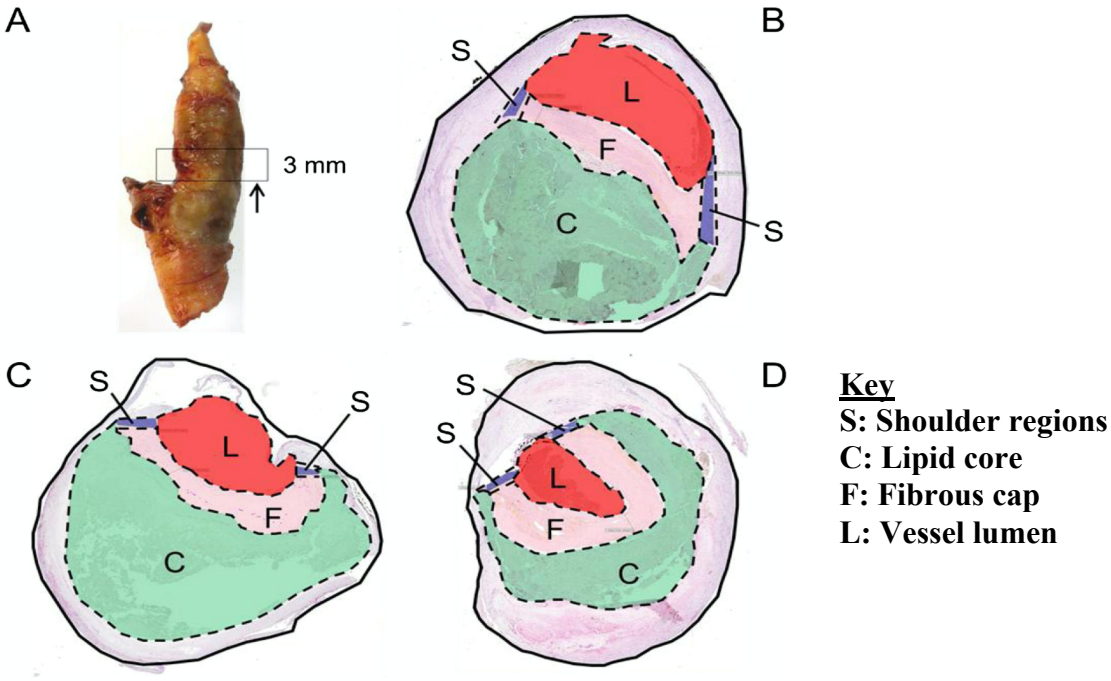

Figure 5.3 Schematic illustration of the carotid-plaque section (Olson et al., 2011)
This image represents a carotid endarterectomy sample from consented stroke patients. (A) The image shows the location of the carotid-plaque section. (B-D) Different types (in-appearance) of carotid section marked with the plaque regions. The shoulder region marked with S (see the key on the right side).

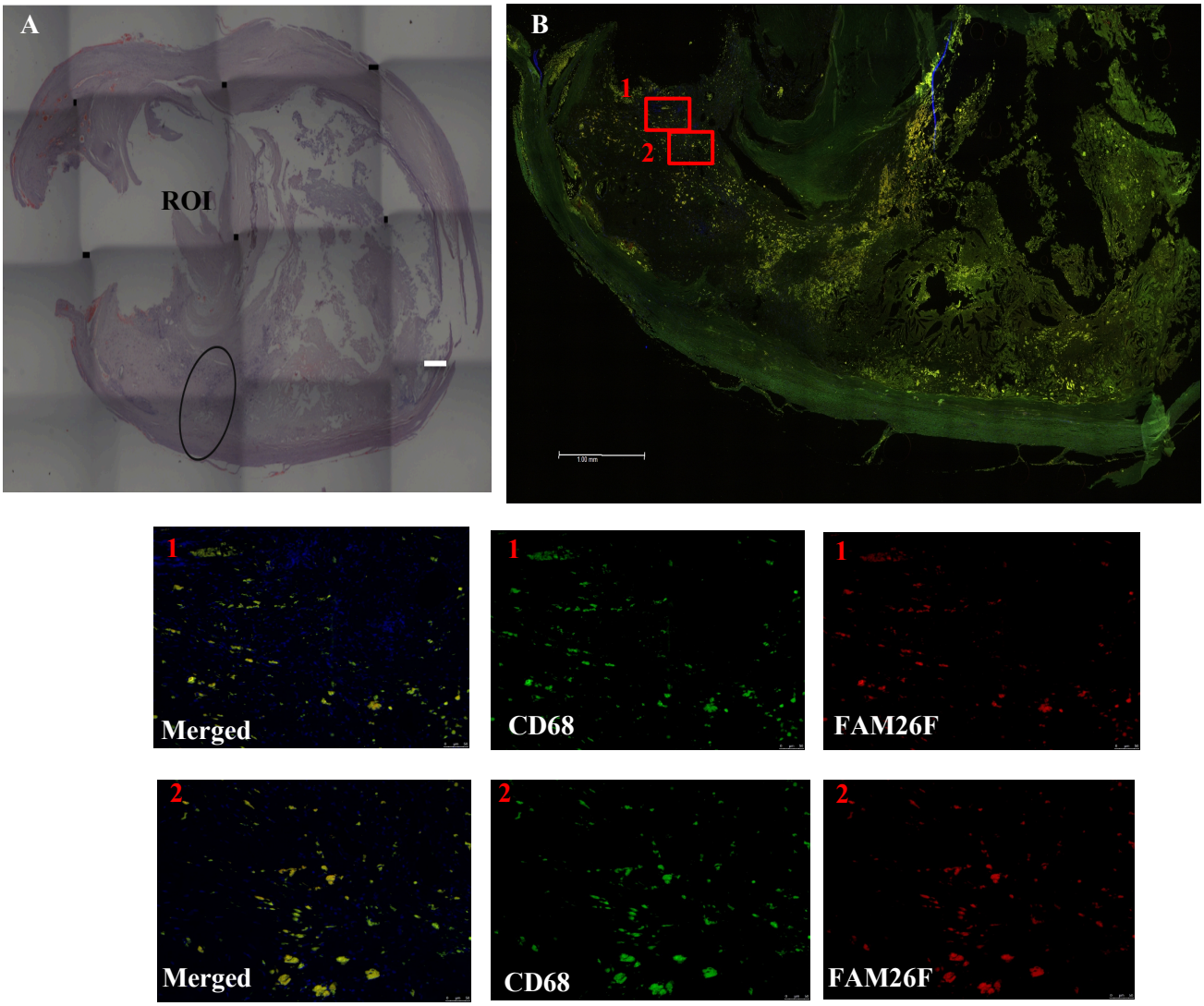

Figure 5.4 CD68^{+} macrophages express FAM26F in atherosclerosis
Representative images of human carotid artery plaque sections. (A) H&E staining of the section, and the inflammatory plaque shoulder (ROI) is indicated with a black circle. (B) Tile-scan of the section with an immunofluorescence staining for pan-macrophage marker CD68 (green), FAM26F (red) and DAPI (blue). In merged images, CD68^{+} and FAM26F^{+} co-localisation can be viewed (yellow). Two different areas in the ROI are shown (1) and (2). Scale bar represents 50 µm for all images except for the tile scan image, the scale bar shown represents 1 mm.

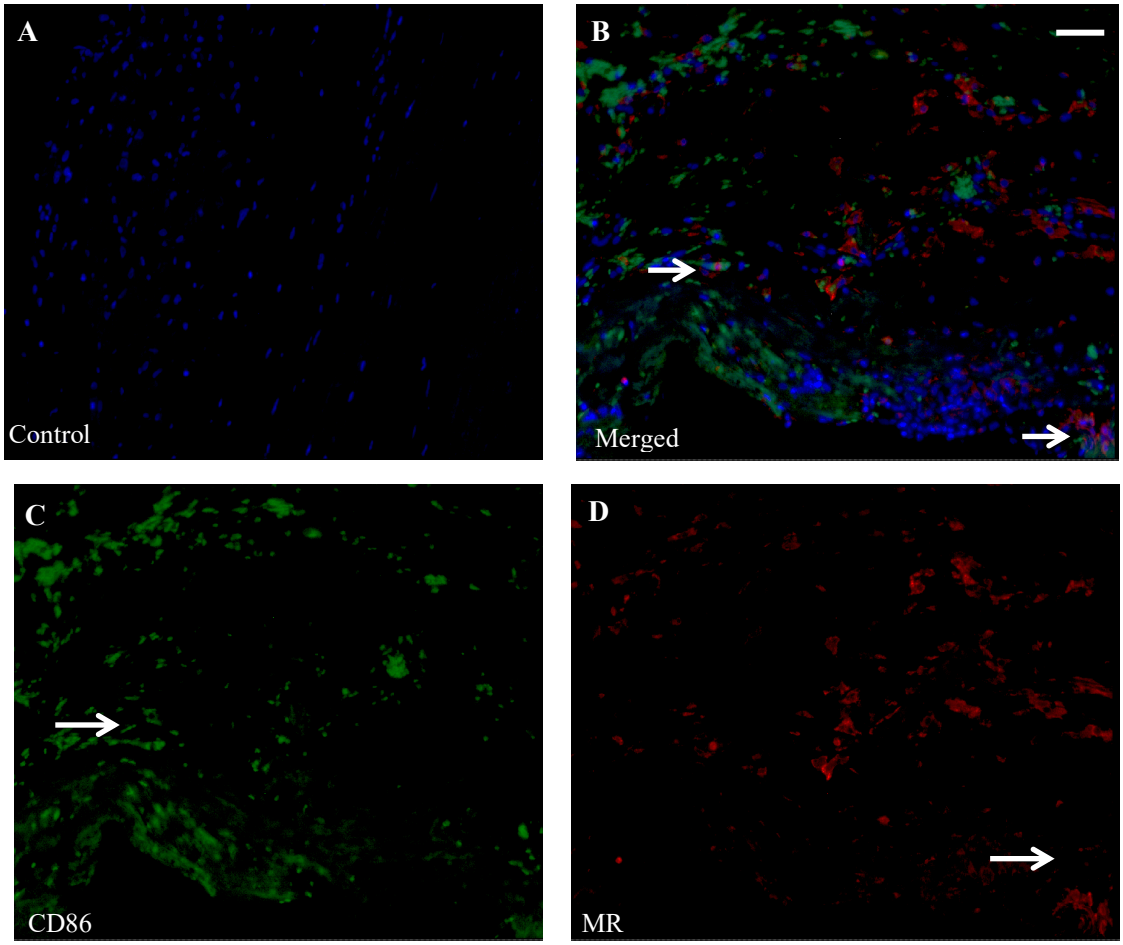

Figure 5.5 CD86 M1-macrophage and MR M2-macrophage immunofluorescence staining in human carotid endarterectomy arterial plaques

Images represent human carotid artery plaque sections. (A) IgG controls. (B) Immunofluorescence staining for CD86 (green), MR (red) and DAPI (blue). (C) CD86 single channel. (D) MR single channel. Scale bar represents 50 µm for all images.

5.4. Identification of interacting proteins to FAM26F by co-immunoprecipitation on THP-1-3xFLAG cells

Since nothing is known about FAM26F function, its signalling mechanism or interacting partners in immune cells. Therefore, identify interacting partners will improve understanding of its function. The aim of this study was to precipitate FAM26F and investigate about the protein partners that will bind to FAM26F protein using mass spectrometry.

The available FAM26F antibodies are not specific enough to be tested using immunoprecipitation assay. In order to circumvent limitations in the availability of endogenous-specific FAM26F antibody, we have developed a THP-1 cell line transfected with FAM26F plasmid tagged with a 3×FLAG epitope that can be detected with anti-FLAG antibody generated by Dilip Kumar from Singapore Immunology Network (SIgN), see figure 5.6 (for full details about the procedure, see section FAM26F-3×FLAG THP-1s in materials and methods of appendix III).
The overexpressed FLAG-FAM26F expression was tested by RT-qPCR, in pre-differentiated and post-differentiated (unpolarised macrophages, Mun) and polarised ($M^{IFN\gamma+LPS}$, M1) THP-1 cells (Figure 5.7). The beads that has been used to precipitate FAM26F were Anti-FLAG M2 gel and the antibody to detect FAM26F was monoclonal anti-FLAG as well (For the co-IP procedure see section 2.8).

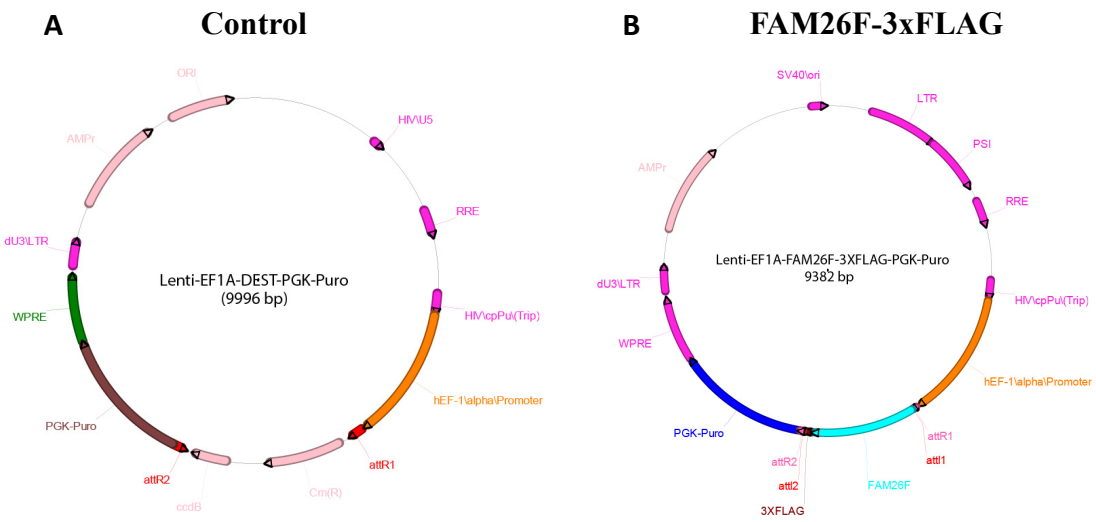

Figure 5.6 FAM26F-3×FLAG expression construct (Baidžajevas, 2019)
Maps of (A) control and (B) FAM26F-3×FLAG plasmids transfected into monocytic THP-1 cells.

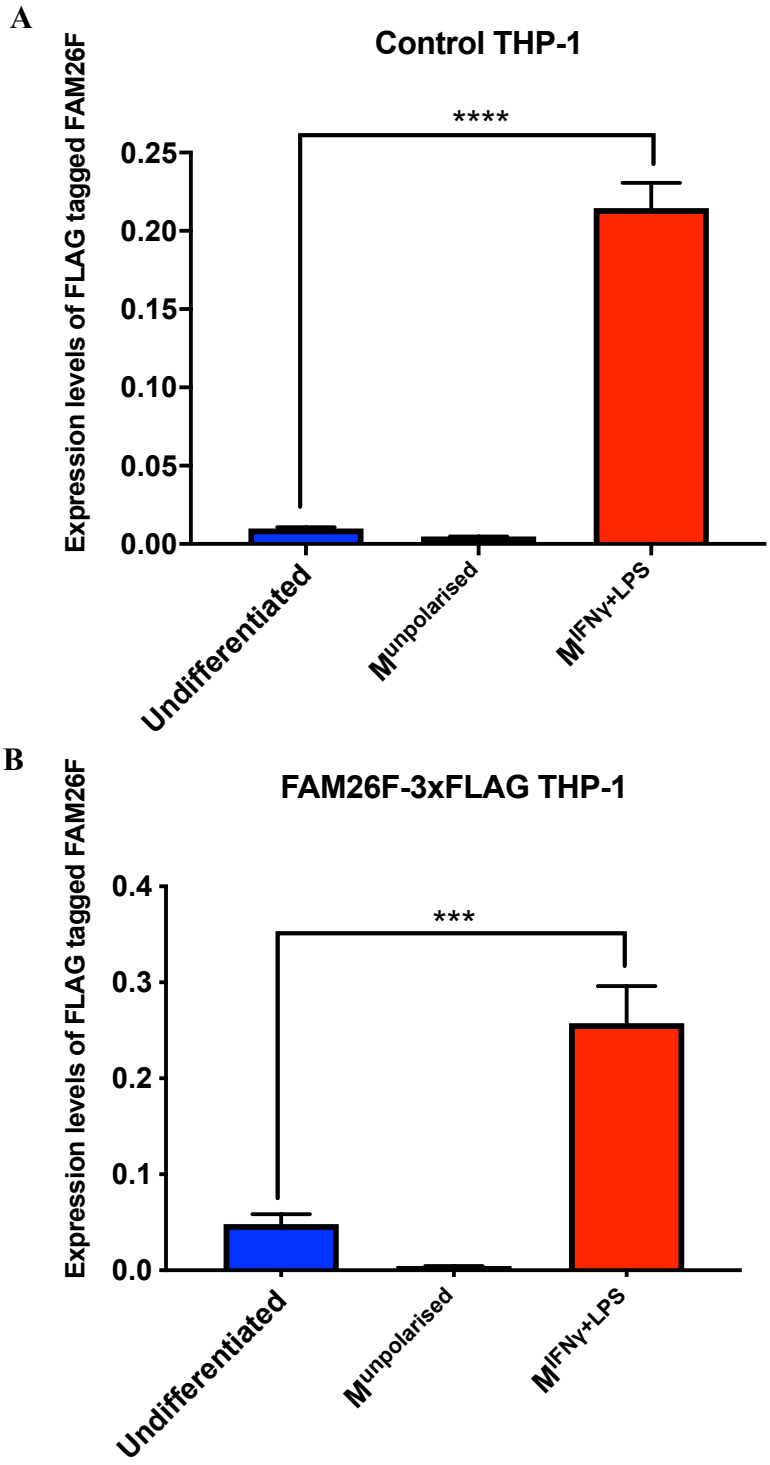

Figure 5.7 Expression levels of FLAG tagged FAM26F in control and FAM26F-3xFLAG THP-1-cells lines before and after PMA differentiation and with or without IFNγ/LPS polarisation

The graphs show FLAG tagged FAM26F mRNA expression levels relative to GAPDH house-keeping gene in (A) Control-1-3xFLAG THP-1 cells or (B) FAM26F-3xFLAG THP-1 cells: before PMA differentiation (undifferentiated), after PMA treatment but before polarisation ($M^{unpolarised}$, Mun) and $M^{IFN\gamma+LPS}$, M1). Data on graphs was statistically analysed using one-way ANOVA and the stars on bars represent the significance levels of elevations with *P* values for mRNA expression compared to undifferentiated cells, and when stars are missing, it means no significant changes in their expression levels. P values on Graph pad prism are as follow: (*) $P \leq 0.05$, (**) $P \leq 0.01$, (***) $P \leq 0.001$ and (****) $P \leq 0.0001$.

For each IP experiment, two gels were prepared: one stained with coomassie blue and the other one was for the immunoblotting. Figure 5.8A shows coomassie blue staining with FAM26F bands appearing with predicted size 37 kDa. Additionally, there were bands on control and FAM26F elutions, which were at sizes of 25 and 55 kDa, these were the light and heavy chain, respectively, of the antibody.

FAM26F-FLAG protein was detected in the immunoblotting by anti-FLAG (Figure 5.8 B). The IP immunoblots showed FAM26F-3xFLAG bands at the correct targeted size, additionally there was a smear band appeared with FAM26F-3xFLAG, which indicates the glycosylation state of FAM26F.

FAM26F was detected in elution samples of THP-1-FAM26F-3xFLAG cells but not in THP-1-control cells. This showed that FLAG-FAM26F was successfully precipitated by immunoprecipitation. We therefore went on to use the IP elution samples to run mass spectrometry assay on them. After analysing the mass spectrometry data, we obtained a list of possible protein partners to FAM26F. The protein list was subjected to a range of selections depending on the subcellular location and immune function. Finally, we were able to validate mass spectrometry results using western blotting with specific antibodies against proteins of interest as interacting partners to FAM26F.

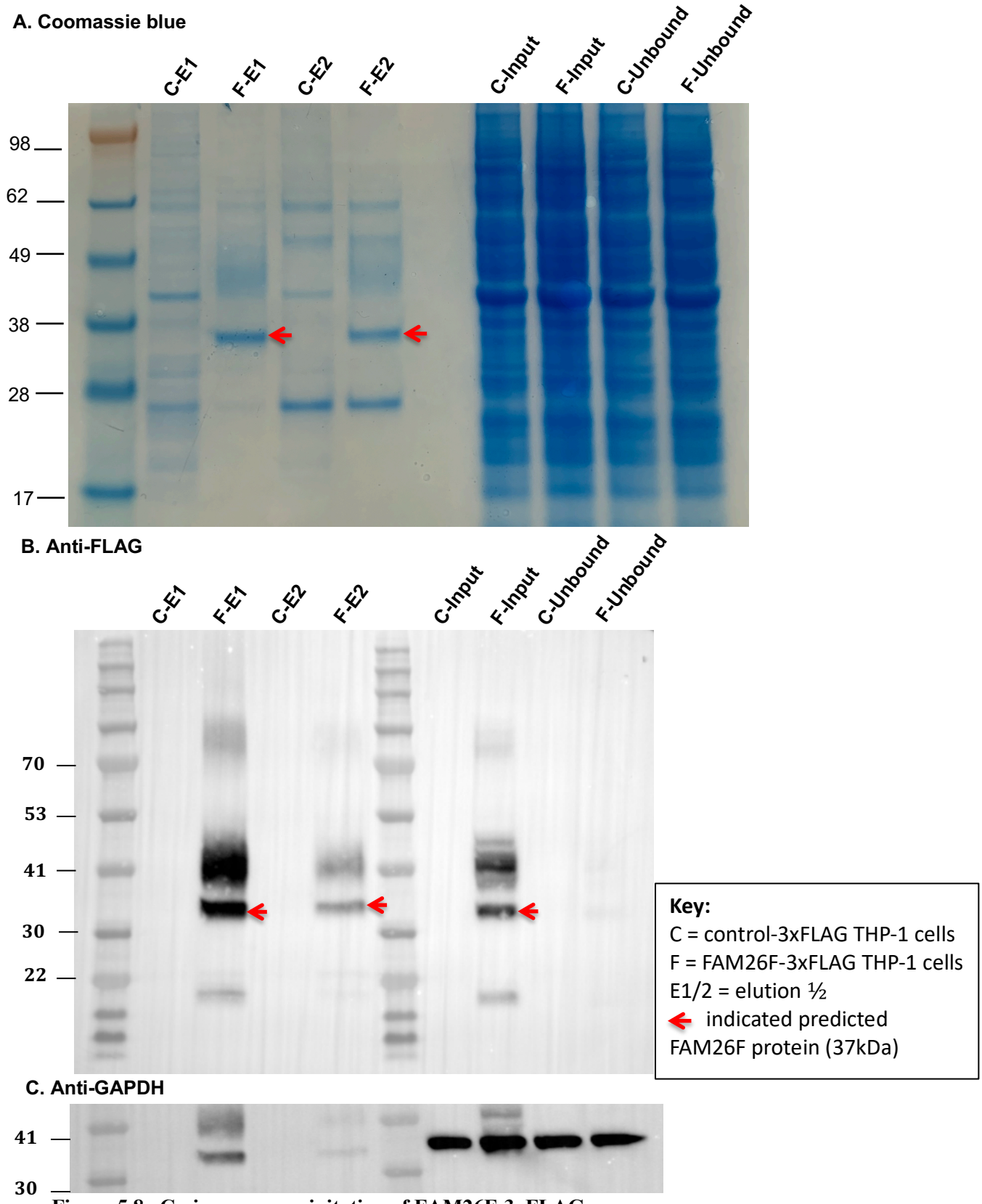

Figure 5.8 Co-immunoprecipitation of FAM26F-3xFLAG

(A) The IP samples were loaded into a 4-12% Bis-Tris gel, which stained by coomassie blue. Elution IP samples on the left of gel/blot (see the key on the right), input and unbound samples on the right of gel/blot (input samples were lysates before adding anti-FLAG beads) and (unbound samples were supernatants of beads post elution). (B) The same samples were loaded into another gel and immunobloted using ani-FLAG antibody to detect FAM26F protein. In both A and B, red arrows indicate FAM26F protein bands at size of 37.5 kDA. (C) The same blot in B was stripped and then used to detect the housekeeping protein GAPDH at size of 37 kDa, on input and unbound samples of both control and FAM26F THP-1 cells.

5.5. Mass spectrometry analysis of FAM26F immunoprecipitation samples

Elution 1 and 2 samples of immunoprecipitation, from control and FAM26F THP-1 cells, were analysed using mass spectrometry to detect FAM26F interacting partners (Done by Caroline Evans). The list of protein data from mass spectrometry was further analysed to find out 26 unique proteins have been identified in FAM26F THP-1 elution samples, but not in control THP-1 elution samples (Table 5.1). The protein list was initially identified depending on the protein subcellular localisation using the database (UniProt: a worldwide hub of protein knowledge, 2019). The localisation of interest was plasma membrane, where FAM26F is found in immune cells. From the MS list, nine proteins were found to be expressed in plasma membrane, which are: APOBR, CD300, DCD, EFTU, EMC7, LAT, MARCKS, RAB5B, SCAM3 and TMX2. To reduce the number of proteins to be tested, the list was then classified according to their function in inflammation; we reached a final list of four proteins to be further tested for the possibility of FAM26F interaction. They were as follow: CD300, DCD, LAT and MARCKS. The first logical step was to optimise the antibodies against these proteins, on IP elution samples, using western blotting. Two antibodies, anti-DCD and anti-LAT, detected the correct region of target proteins. We investigated these two proteins using co- immunoprecipitation on THP-1 cells (FAM26F-3x-FLAG and control) (see the next section 5.6).

Table 5.1 Predicted interacting proteins to FAM26F from MS

- All proteins in the list are human proteins except CO3-bovin, printed in blue.
- The intensity values from the two mass spectrometry experiments are displayed as (intensity-1 and intensity-2). FAM26F, which is expected to have the highest intensity, is printed in red colour. The next high intensity values are highlighted in yellow or blue.
- Proteins with the first high expression values are highlighted in yellow; ranges are from 6.06E+06 to 2.43E+06 in experiment-1, or from 3.31E+07 to 2.00E+07 in experiment-2. The second-high expression values are highlighted in blue; ranges are from 1.76E+06 to 1.17E+06 in experiment-1, or from 1.74E+07 to 1.10E+07 in experiment-2.
- The proteins of interest for this list, according to their role in inflammation, that we initially want to investigate further were: CD300, DCD-1, LAT and MARCKS.

NCBI accession number	Official symbol	Protein name	Intensity-1	Intensity-2
P49748	ACADV	Very long-chain specific acyl-CoA dehydrogenase	2.87E+06	3.06E+07
Q0VD83	APOBR	Apolipoprotein B receptor	2.59E+06	1.30E+07
Q5R3K3	CAHM6 or FAM26F	Calcium homeostasis modulator protein 6	5.46E+08	7.10E+09
Q9UGN4	CLM-8 or CD300	CMRF35-like molecule 8 CD300 antigen-like family member A	2.43E+06	4.14E+06
Q9BT09	CNPY3	Protein canopy homolog 3	3.55E+06	1.74E+07
Q2UVX4	CO3_BOVIN	Complement C3	4.84E+05	1.65E+07
P81605	DCD-1	Dermcidin	5.11E+05	8.99E+06
P78527	DNA-PK or PRKDC	DNA-dependent protein kinase catalytic subunit	1.31E+06	2.24E+07
P49411	EFTU	Elongation factor Tu	9.31E+05	1.53E+07
Q9NPA0	EMC7	ER membrane protein complex subunit 7	9.10E+05	5.06E+06
P30040	ERP29	Endoplasmic reticulum resident protein 29	1.18E+06	2.00E+07
P52565	GDIR1	Rho GDP-dissociation inhibitor 1	2.00E+07	7.27E+06
O43561	LAT	Linker for activation of T-cells family member 1	1.23E+06	8.20E+06
Q12907	LMAN2	Lectin mannose-binding 2	4.83E+06	3.31E+07
P29966	MARCS	Myristoylated alanine-rich C-kinase substrate	2.97E+05	6.15E+06
Q9UQ80	PA2G4	Proliferation-associated protein 2G4	3.84E+05	2.69E+06
P13667	PDIA4	Protein disulfide-isomerase A4	8.17E+05	1.27E+07
Q9UHV9	PFD2	Prefoldin subunit 2	7.40E+05	3.48E+06
P30044	PRDX5	Peroxiredoxin-5	1.68E+06	3.57E+06
P49721	PSB2	Proteasome subunit beta type-2	2.86E+05	5.69E+06
P61020	RAB5B	Ras-related protein Rab-5B	4.98E+05	1.62E+07
P49792	RBP2	Ran-binding protein 2	1.99E+05	2.94E+06
O14828	SCAM3	Secretory carrier-associated membrane protein 3	6.06E+06	3.34E+06
P0DME0	SETLP	Protein SETSIP	1.66E+06	1.10E+07
P08240	SRPRA	Signal recognition particle receptor subunit alpha	1.17E+06	1.43E+07
Q9Y320	TMX2	Thioredoxin-related transmembrane protein 2	1.76E+06	6.77E+06
O60763	USO1	General vesicular transport factor p115	1.27E+06	8.25E+06

5.6. Validating mass spectrometry detection of specific FAM26F interacting proteins

As mentioned previously in section 5.5, that we have identified two proteins, Linker for activation of T-cells family member 1 (LAT) and dermcidin (DCD-1), from the MS list to be tested for FAM26F interaction, because their antibodies were successfully optimised and detected the correct target proteins (see figure 5.10), unlike the other two proteins (CD300 and MARCKS), which need further optimisation (see figure 5.9). We hypothesised that LAT and DCD may have a relevant function in inflammatory signalling and interacting with FAM26F at the plasma membrane.

We investigated FAM26F interaction to DCD and LAT using co-immunoprecipitation studies on THP-1 cells, FAM26F-3x-FLAG and control, (n=2). LAT was an interesting interacting partner to test, because it might contribute in T cells interaction. The immunoblots were incubated with anti-LAT and anti-DCD as mentioned in Table 6. Immunoprecipitation elution samples were tested for LAT and DCD compared to control, figure 5.11 shows the detected bands of LAT on the elution samples of THP-1-control and THP-1-FAM26F cells, while there are no bands showed for DCD protein. Comparing the intensity of LAT bands between control and FAM26F-3xFLAG THP-1 cells shows a higher intensity of LAT with FAM26F overexpression cell line.

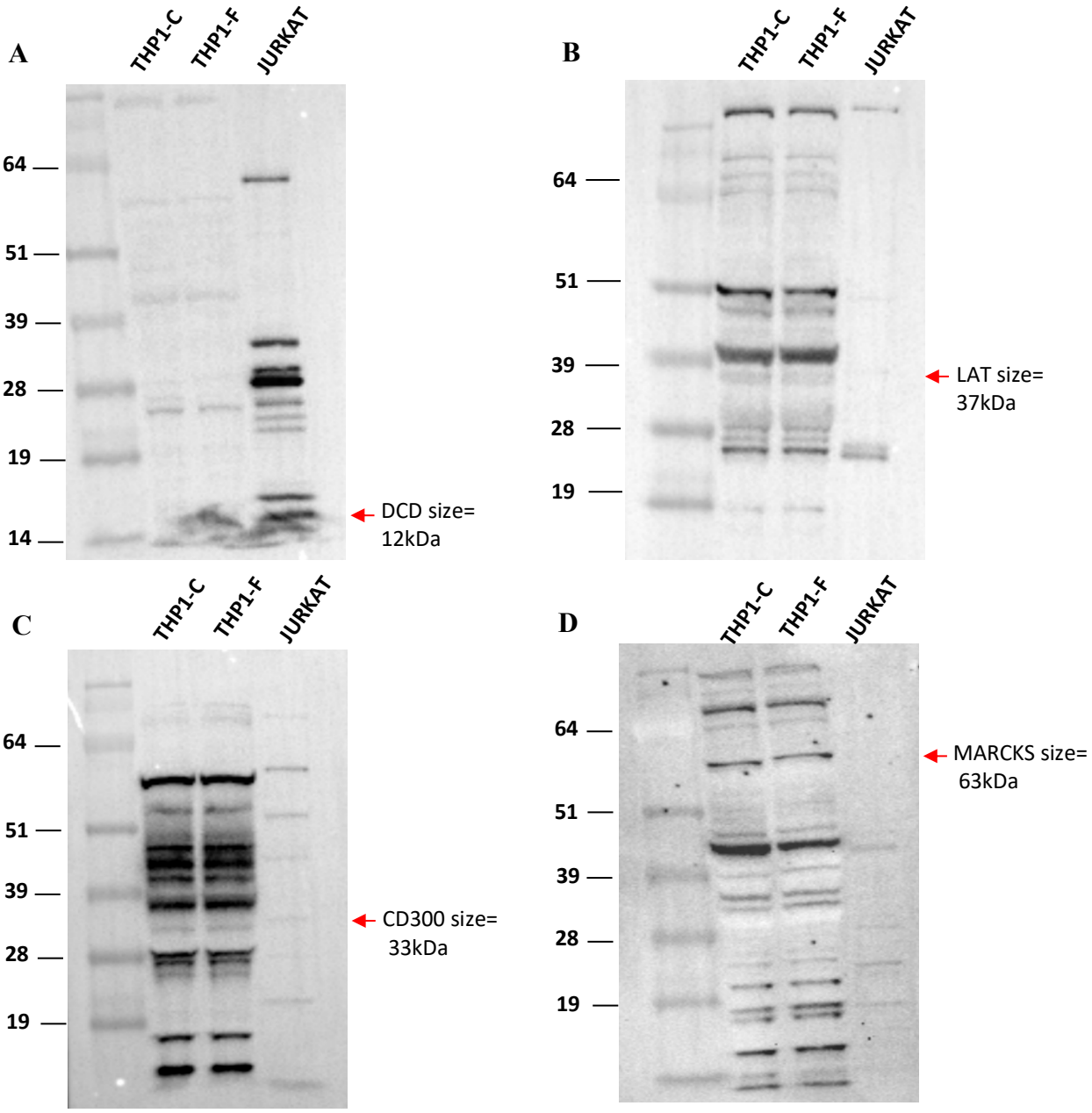

Figure 5.9 Optimisation (1st stage) of the four antibodies against proteins of interest from MS list

The samples loaded on these four blots were lysates from THP-1 cells (control and FAM26F-3xFLAG) and Jurkat cells without any stimulation. (A) The blot was to detect DCD protein at predicted size of 12 kDa. (B) The blot was to detect LAT protein at predicted size of 37 kDa. (C) The blot was to detect CD300 protein at predicted size of 33 kDa. (D) The blot was to detect DCD protein at predicted size of 63 kDa.

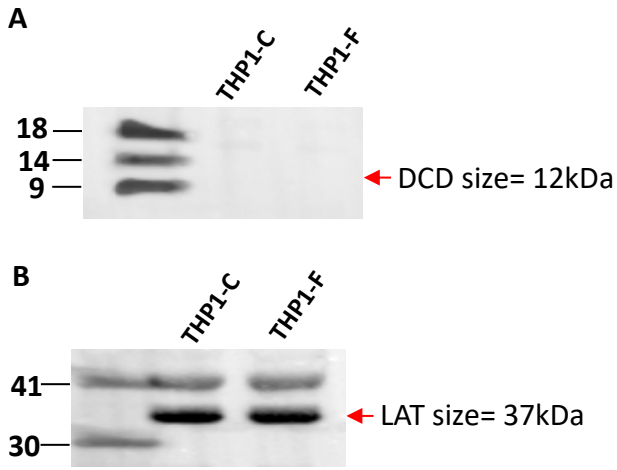

Figure 5.10 Optimisation (2nd stage) of DCD and LAT
The samples loaded on both blots were lysates from THP-1 cells (control and FAM26F-3xFLAG) without any stimulation. (A) The blot was to detect DCD protein at predicted size of 12 kDa. (B) The blot was to detect LAT protein at predicted size of 37 kDa.

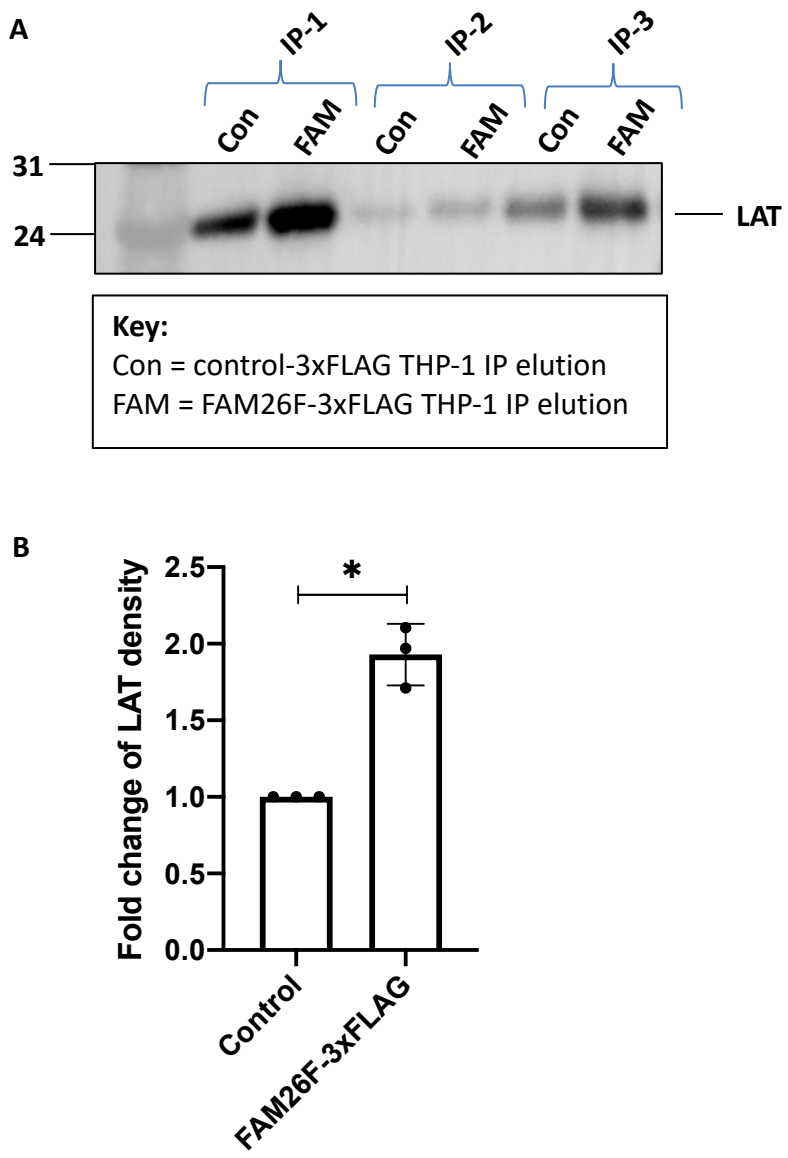

Figure 5.11 Immunoblotting of FAM26F-FLAG co-immunoprecipitation eluates for LAT protein

(A) The elution samples from IP of control and FAM26F THP-1 cells co-cultured with Jurkat cells were loaded in this blot (n=3), and anti-LAT antibody was used to detect LAT protein with predicted molecular weight ~ 24.8 – 28.6 kDa. (B) The graph shows the fold change of LAT density, data was statistically analysed using one-way ANOVA and the stars on bars represent the significance levels of LAT density expressed in FAM26F-3xFLAG THP-1 elutions compared to control THP-1 elutions. P values on Graph pad prism are as follow: (*) *P≤0.05*, (**) *P ≤0.01*, (***) *P ≤0.001* and (****) *P ≤0.0001.*

5.7. Determining if macrophage FAM26F overexpression influences T-cell interactions

Linker for Activation of T-cells (LAT) is a transmembrane adaptor protein that binds to the TCR and activate the downstream signalling that leads to T cell activation. It is essential for T cells activation and interaction to myeloid cells. Furthermore, it has a vital role in memory T cell response against pathogens (Malissen et al., 2005, Ou-Yang et al., 2013).

From the previous sections (5.5 and 5.6), we found that LAT is expressed on macrophage (THP-1) cells as FAM26F-interacting protein, so we hypothesised that FAM26F expression may influence binding to T-cells. To investigate the possible interaction between pro-inflammatory macrophages and T lymphocytes, we used Jurkat as cell line model, treated with chemical inflammatory stimulants (PMA and Ca^{2+} ionophore).

Published studies indicated that FAM26F has a role in cell-cell interactions, particularly it has been identified to facilitate mouse myeloid dendritic cells (mDCs) and NK cells interaction (Ebihara et al., 2010, Kasamatsu et al., 2014). Compared to our findings, FAM26F may contribute also in human myeloid and lymphocytes interactions similar to mouse cells.

The *in vitro* cell lines that have been co-cultured, where THP-1-control and FAM26F cells after stimulation with PMA and then IFNϒ and LPS with Jurkat cells treated with PMA and Ca^{2+} ionophore (For procedure details see section 2.10).

In order to decide the best labelling stain for cells, we tested two types of membrane dyes using flow cytometry: the proliferation dye and PKH stain (see figure 5.12), both staining dyes were labelled 100% of the cells. Next, both cell lines where labelled with membrane intercalating dye PKH stain before stimulation, PKH26 (red) for THP-1 cells and PKH67 (green) for Jurkat cells. The attached Jurkat cells were counted when they were in contact or overlapped with THP-1 cells (see Figure 5.13 as an illustration).

In Figure 5.14A, the images show the interaction between Jurkat cells and THP-1 cells (control and FAM26F-3xFLAG) during three time points (4, 6 and 24 hours). The percentage of attached Jurkat cells to FAM26F-3XFLAG THP-1 cells was ~ 80% in all time points, which is higher than the control-THP-1 cells, which does not exceed 50% (Figure 5.14B).

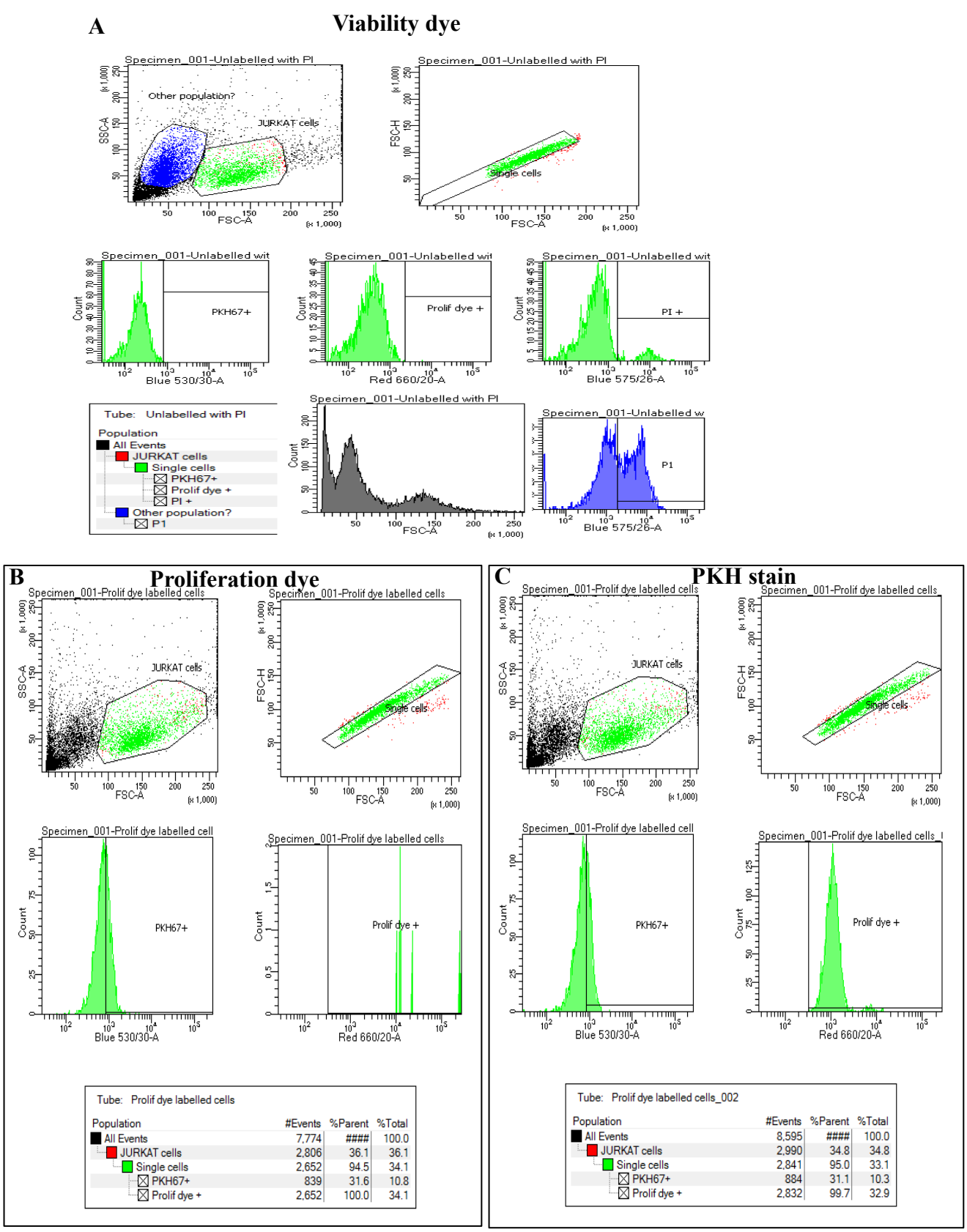

Figure 5.12 Labelling dyes on Jurkat cells
(A) Viability dye (Propidium Iodide, PI) to define the live/dead populations of Jurkat cells. (B) Jurkat cells were labeled with the proliferation dye. (C) Jurkat cells were labeled with the PKH stain.

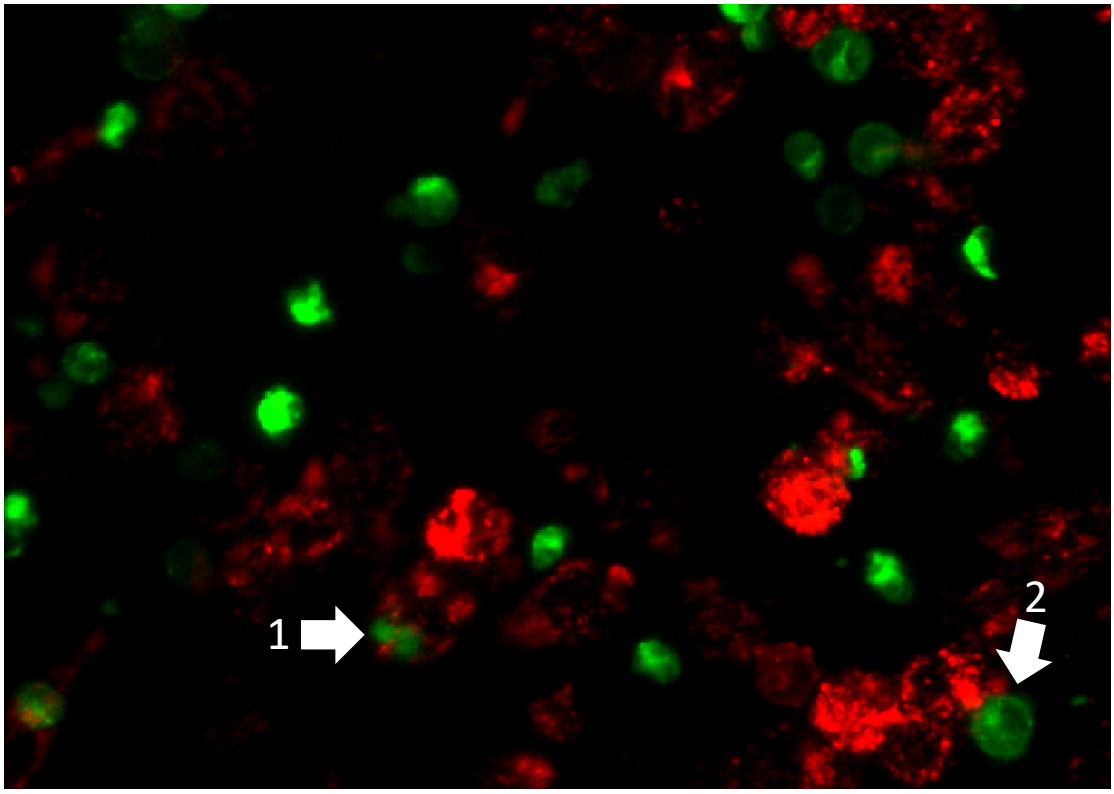

Figure 5.13 Interaction of Jurkat cells to FAM26F-3xFLAG THP-1 cells
The image shows Jurkat cells (in green) co-cultured with FAM26F-3xFLAG THP-1 cells (in red). High magnification images were used to count the cells. The arrows represent attached Jurkat cells by overlapping (1) or being in contact (2) to THP-1 cells.

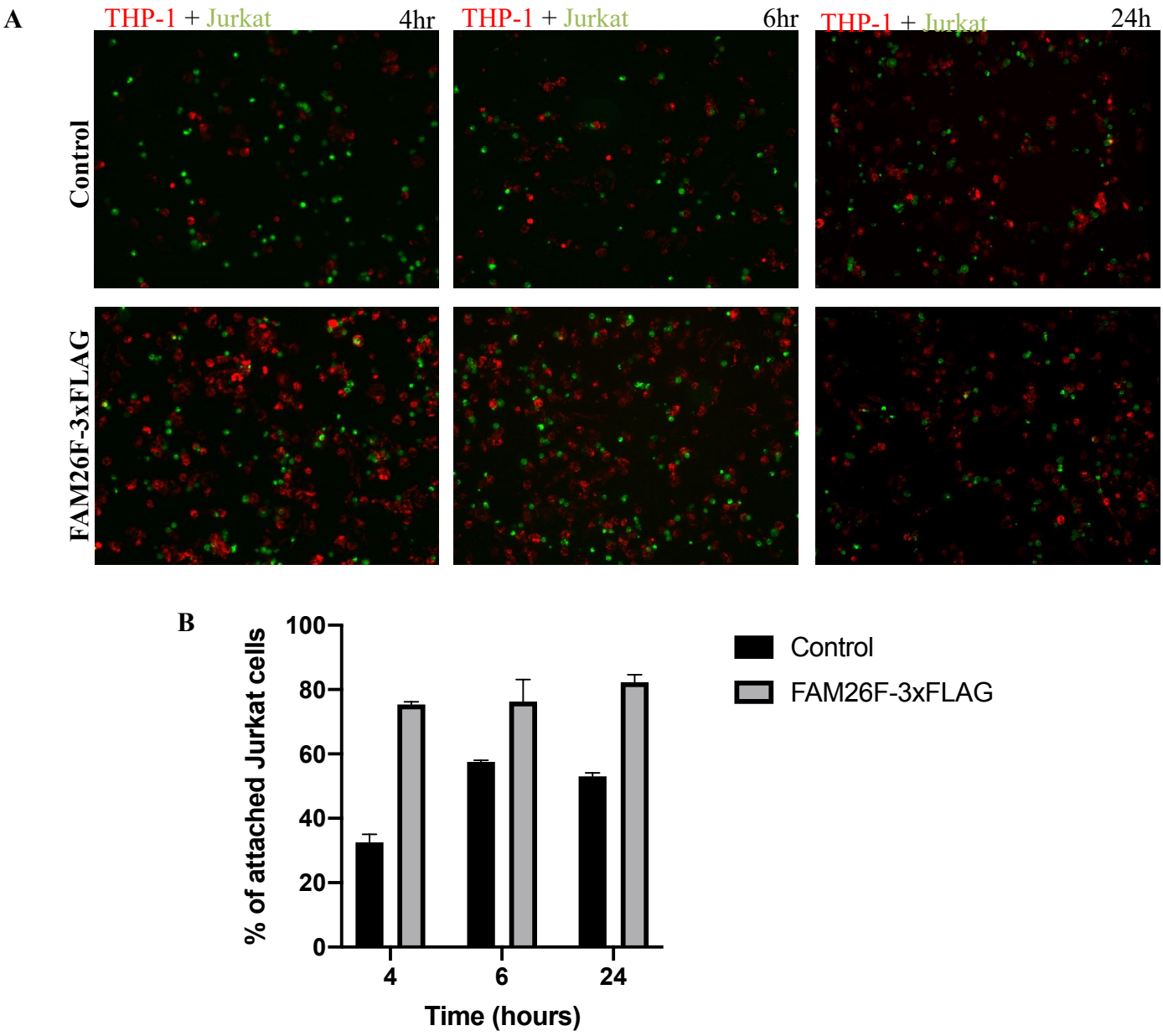

Figure 5.14 THP-1 and Jurkat cells co-culture
(A) The images show examples of interaction of THP-1 and Jurkat cells at different time points. THP-1 cells (control in the first row and FAM26F-3xFLAG in the second row) were labelled with PKH26 (in red), and Jurkat cells were labelled with PKH67 (in green). Both cells were co-culture for different time points; 4 hours (1st column), 6 hours (2nd column) and 24 hours (3rd column). (B) The bars represent the percentage of attached Jurkat cells to control THP-1 cells (black bars) or to FAM26F-3xFLAG THP-1 cells (grey bars). Data are displayed as means ± SEM of 3 or 4 technical replicates (different microscopic fields), (n=1).

5.8. Conclusions

- We identified FAM26F as a novel inflammatory marker in human and mouse.
- FAM26F has been found to be expressed in $CD68^{+}$ macrophage subpopulation in atherosclerotic plaque.
- 26 possible interacting protein partners to FAM26F from mass spectrometry list of co-IP, the only protein that has been validated to interact to FAM26F was LAT, which has been found to be expressed in higher levels in co-IP elutions of FAM26F-FLAG compared to control cells.
- LAT interaction led us to test macrophage-T cell interactions, preliminary data showed much higher number of Jurkat cells (T-cell model) to be attached to FAM26F-FLAG THP-1 cells induced by IFNγ and LPS (inflammatory macrophage model), compared to Jurkat cells attached to control THP-1 cells.

5.9. Discussion

Macrophages in atherosclerotic plaques are able to switch between pro-inflammatory and anti-inflammatory phenotypes. In order to study the functional role of inflammatory macrophages in atherosclerotic plaques, we focused our studies to identify a prognostic M1 marker (in human and mouse). We tested one of the current M1 markers CD86, which worked in immunohistochemistry studies, but it was not ideal to carry out the immune assays (immunoblotting and immunoprecipitation). That was because its RNA and protein expression levels were inconsistent across species such as mouse and human.

5.9.1. Previously Known findings in the group about FAM26F as an M1 marker

Our group has identified FAM26F as a novel M1 marker, since we identified, using RNA-seq and SILAC membrane proteomics, that its mRNA and protein levels, respectively, were highly and specifically up-regulated in IFNγ and LPS-stimulated macrophages compared to all other proteins. The differentiation and polarisation protocols of THP-1 and hMDMs were well established in our group and all the required tests for monocyte and macrophage markers measurements were already confirmed. Therefore, in more recent months since its discovery, we have routinely used FAM26F as both a human and mouse M1 marker for other projects in the group.

Additionally, it has been found in hMDMs that STAT1 and TICAM1 in IFNγ and LPS pathways, respectively, are involved in FAM26F induction (Baidžajevas, 2019).

5.9.2. New preliminary findings for this project

We found a subpopulation of $CD68^{+}$ macrophage, which express FAM26F in atherosclerotic plaques, particularly in the shoulder region, which is known to be the vulnerable area containing inflammatory cells. Therefore, FAM26F may prove useful for identifying vulnerable and unstable plaques. This immunohistochemistry studies were limited to only a few sections at present. It is our intention to expand this to several patients and different regions of the carotid plaques, but we have been limited by antibody availability at the present time, since the antibody that is effective in this application has been discontinued by the manufacturer.

We wished to carry out co-IP experiments to identify interacting protein partners to FAM26F in order to understand more about its function. Since there is no commercially available monoclonal antibody against FAM26F, we used FAM26F-3xFLAG THP-1 cells to pull down

FAM26F protein partners, which will provide us with an insight into its immune function. We purified FAM26F and interacting proteins, using co-immunoprecipitation and detected interacting proteins by mass spectrometry. The group of proteins that we identified were then classified due to subcellular localisation and their immune function. We chose four proteins of interest to be further tested: CD300, DCD, LAT and MARCKS. The antibodies against these proteins were optimised; due to the time limitation the only antibodies that could be used were anti-DCD and anti-LAT. While the other two antibodies need further optimisation. Next we validated the mass spectrometry results for DCD and LAT using western blotting on control and FAM26F-3xFLAG THP-1 cells treated with IFNγ and LPS. No bands were detected for DCD, while we detected that LAT is expressed in much higher levels in the co-IP elutions for FAM26F-FLAG compared to control cells, confirming its interaction with FAM26F, but the mechanism and functional role is not known. Published work suggests FAM26F as an activator molecule which facilities myeloid and lymphocyte cells interactions (Ebihara et al., 2010, Kasamatsu et al., 2014). Therefore, the logical step next was to test if LAT and FAM26F interaction will activate macrophages and T cells interactions.

Jurkat cells have been used as a cell line model of T cells, which is a human acute T lymphocyte cell line, and it is widely used in the *in-vitro* studies since 1980s in screening purposes of T cell signal transduction, cytokines and protein receptors in various infectious diseases (Chen Jing-Lun, 2018). We carried out co-culture assays of Jurkat cells with control or FAM26F-3xFLAG THP-1 cells, to study the cell-cell interaction. The data analysis shows that the percentage of attached Jurkat cells to FAM26F-overexpressed THP-1 cells was two times higher compared to control THP-1 cells. This suggests that FAM26F may activate the interaction between Jurkats and M1-like THP-1 cells. We had no chance to confirm if LAT has a role in this interaction with FAM26F.

5.9.3. Limitations of this work

- In order to improve the immunohistochemistry staining, we can co-stain with M1 marker (CD86) with FAM26F on the same section and / or sequential sections of same carotid artery sections. In order to carry out this experiment ideally, we need more sections from several atherosclerotic patients. Additionally, there was limited polyclonal antibody available to complete this work.
- There is no commercially available monoclonal specific antibody against FAM26F, suitable for use in co-IP or immunoblotting applications. In order to overcome this limitation, we used anti-FLAG to co-IP FAM26F-FLAG from our THP-1 stable cell line.
- We would wish to validate co-IP FAM26F interactions using an endogenous antibody to FAM26F in future experiments on primary human macrophages, therefore we are in the process of generating our own FAM26F monoclonal antibodies.
- As mentioned previously in section 5.8.2 that the antibodies against CD300 and MARCKS need more optimisation on western blotting, which could not be done due to time limitation.
- Co-culture experiment and PKH labelling was limited to one test due to time, but more experiments are ongoing.
- We have attempted the co-culture assay using FAM26F siRNA knockdown in human MDMs and Jurkat cell. However, the PKH labelling protocol requires further optimisation in these primary cells since it was not effective when we attempted labelling post-differentiation.

5.9.4. Future planned experiments

- Replicating co-culture experiment of FAM26F overexpression THP-1 cell line and Jurkat cells.
- Replicating the western blotting on the predicted FAM26F protein partners: CD300, DCD, LAT and MARCKS.
- Co-immunoprecipitation on FAM26F-3xFLAG THP-1 and Jurkat cell lysates, then testing IP elution samples for LAT, to compare that to data on figure 34.
- Co-culture assay using FAM26F siRNA knockdown hMDMs and Jurkat cells.
- Co-culture assay using FAM26F siRNA knockdown hMDMs and primary human T cells.

- Co-culture assay using FAM26F siRNA knockdown hMDMs and primary human T cells with LAT siRNA knockdown.
- Co-culture assay using FAM26F siRNA knockdown hMDMs and primary human T cells with anti-LAT antibody blocking.
- One of the predicted FAM26F partners that has been excluded because it found to be expressed in the endoplasmic reticulum but not in the plasma membrane, which is protein canopy homolog 3 (CNPY3). Interestingly, the function of this protein is associated with activation of TLR4 (LPS) signalling pathway. FAM26F could facilitate the TLR4 activation in contribution with this protein.

Chapter 6
General Discussion

6.1. Summary of the aims of this thesis

We aimed for understanding the role of inflammatory macrophage in chronic inflammatory diseases such as atherosclerosis. In order to investigate macrophage immune responses, we required a reliable inflammatory macrophage marker. Depending of previous work, we hypothesised that TAKL expression altered during monocyte/macrophage differentiation. Our first aim was to measure the expression TAKL and its variants in monocytic THP-1 cells under differentiation conditions (PMA treatment). Secondly, we focused on FAM26F as a M1 marker to understand the role of inflammatory macrophage in atherosclerosis. Interestingly, FAM26F was detected specifically in an inflammatory population of macrophages in diseased atherosclerotic plaques (Nagenborg et al., 2017, Chmielewski et al., 2014, Baidžajevas, 2019). However, since there is no enough evidence about FAM26F immune function or signalling, we investigated FAM26F protein interacting partners to understand its functional role in proinflammatory macrophage ($M^{IFN\gamma \text{ and } LPS}$).

We used THP-1 and Jurkat cell lines as macrophage and T cell models, respectively. We treated them with inflammatory stimuli to be polarised to M1-like macrophages and Th1-like T cells, to test them under the same inflammatory environment. These human cell lines are leukemic cells and different from primary human cells, but they allowed us to investigate our experimental approach. Our aim was to use cell lines as an initial experimental tool followed by primary cells experiments.

We used THP-1 cells to generate a stable cell line tagged with FAM26F, because the antibodies were limited, and we could not use antibody to endogenous FAM26F followed by IP to identify interacting proteins. Our future aim is to test FAM26F endogenous antibody on hMDMs, and human T cells to carry out macrophage-T cell interaction assays.

In this research, we focused on inflammatory macrophage but there are many other cell types that contribute in plaque vulnerability such as anti-inflammatory macrophage, T cells, B cells, NK cells and mast cells (as previously mentioned in section 1.3.2), it would be interesting to understand the signalling of cells bridging in atherosclerotic plaque.

6.2. Summary of our findings

- **TAKL findings**

Our interest in this project was to find a reliable macrophage differentiation marker, specifically under the inflammatory polarisation conditions. We first investigated TAKL because of the studies (Dr Guesdon's group), see appendix I and II, that found TAKL mRNA expression to be altered by differentiation in monocytic THP-1-time course samples. We measured the mRNA expression level of TAKL, its transcripts and other related genes in TAK1-TRAF pathway using RT-qPCR. Our data confirmed the previous knowledge that TAKL-all expression is up-regulated at day 1 and 3 of PMA treatment, and the only TAKL variant elevated significantly in this initial 3-day period was TAKL-L, with a peak expression level of 200-fold its basal expression level before PM treatment. However, its absolute levels of expression remained low and even at peak value were slightly less than one mRNA copy per cell. After that, we wanted to validate these findings on primary human monocyte-derived macrophage (hMDM), we found high expression levels of TAKL and its two variants TAKL-L and TAKL-D in monocyte and IFNγ and LPS macrophage.

To ensure the accuracy of our findings, we further analysed the RT-qPCR data using the absolute quantitation method. The data of THP-1 cells showed high expression peaks of TAKL-all, TAKL-L and for other genes in TAK1-TRAF pathway including TAB2 and TRAF6.

TRAF molecules have been linked to inflammation and inflammatory diseases since 1990s, which lead to NF-κB activation through MAP kinases and IRFs (Inoue et al., 2000, Wajant et al., 2001). Many evidences showed that TRAFs (TRAF2/3/6) high expression regulates the inflammatory responses and contributes in the pathogenesis of inflammatory diseases (Lalani et al., 2018). Deletion of TRAF2 and TRAF3 contributes in developing inflammatory diseases such as (skin inflammation, atherosclerotic plaque, Crohn's disease, ulcerative colitis, liver inflammation, Alzheimer's disease and Parkinson's disease) (Zirlik et al., 2007, Huang et al., 2014, Qiao et al., 2013), and autoimmune inflammatory diseases such as (lupus, arthritis and multiple sclerosis) (Myles et al., 2012, Baranzini et al., 2013). In addition, TRAF6 deficiency plays a pivotal role in LPS-induced septic shock (Lv et al., 2016), and TRAF6 also enhances lung airway inflammation through TLR4-IRAK signalling by stimulating K63-linked ubiquitination and activating the downstream MAPK and NF-κB signalling in alveolar macrophage (Karimi et al., 2006). Additionally, TAB2 found to activate TAK1/TAB1 complex

via TNF-α and LPS signalling pathways (Takaesu et al., 2000, Liu et al., 2009). TAB2 is a critical regulatory component of TAK1 activation and it can bind to TAKL (see figure 5 in appendix I). Depending on these evidences, we can assume that TAK1 or TAKL high expression may correspond to TAB2 expression elevation.

We could not measure the expression of all genes of interest that we tested in THP-1 cells, using primary macrophage (hMDMs), because of the limited amounts of RNA samples from donors. However, TAKL-all expression in hMDMs seems to be activated after macrophage differentiation, the high levels were in unpolarised macrophage and in IFNγ and LPS macrophage. However, TAKL maximum induction findings of THP-1 cells and hMDMs, using RT-qPCR absolute analysis, were not significant compared to unstimulated (in THP-1 cells) or undifferentiated cells (in hMDMs). Additionally, RNA-seq data analysis of the different macrophage polarised forms, provided us with the same conclusion of expression induction of TAKL-all and TAKL-L in IFNγ and LPS macrophages.

Recent data has reported the presence of TAKL in gene fusion in patients with dermatofibrosarcoma protuberans (Maloney et al., 2019), also another in-silico data analysis has identified TAKL gene to be expressed in relation to an osteoarthritis SNP (Parker et al., 2019). However, TAKL gene function and signalling remain poorly understood because there is not enough published data. Our novel data confirmed that TAKL isoforms bind to TAB2 and TAB3 but not TRAFs (appendix I), which suggests that TAKL may bind to TABs and block TRAFs binding and their downstream signalling. Unfortunately, we could not test the interaction of other potential protein partners of TAK1 pathway. Interesting future experiments can be done to confirm TAKL/TABs interaction to TRAFs and check if TAKL deactivates TAK1 signalling pathway, and then test the effect of this binding on the inflammatory response and apoptosis in macrophage.

- **FAM26F findings**

To investigate the purpose of this research, we identified a novel pro-inflammatory macrophage marker, FAM26F, because it found to be expressed specifically at high levels in IFNγ and LPS macrophages at both mRNA and protein levels, and in human and mouse.
Firstly, we confirmed the validity of FAM26F as an inflammatory marker using immunocytochemistry staining, we found that it is expressed highly in IFNγ and LPS macrophages, but not in unpolarised macrophages.

Secondly, we used FAM26F as an M1 marker to understand the role of inflammatory macrophage in atherosclerosis. We found FAM26F to be expressed in $CD68^{+}$ macrophage subpopulation in atherosclerotic plaque, but we could not do any further co-stain on carotid artery sections, using anti-FAM26F combined with other antibodies against CD86, smooth muscle actin (SMA) or mannose receptor (MR). The polyclonal anti-FAM26F that we had used for these preliminary studies was discontinued and is no longer commercially available to conduct further immunohistochemistry staining. Since there is no commercially available monoclonal anti-FAM26F, our group is in the process of producing our own monoclonal antibody (Rabbit anti-FAM26F) to continue experiments and fully understand the upregulation of FAM26F in inflammatory macrophages, particularly with respect to atherosclerotic plaque development.

In order to improve our understanding of FAM26F function, we used an overexpression cell line (FAM26F-3xFLAG THP-1 cells) in co-immunoprecipitation to identify FAM26F protein partners. From the mass spectrometry analysis on elution samples of co-IP, we identified 26 potential protein partners that were specific for the FAM26F-3xFLAG THP-1 elutions, but not in the control elutions list. By comparing the two MS lists control and FAM26F-3xFLAG, we eliminated the non-specific binding and confirmed the specificity of anti-FLAG pulldown.
The list for follow-up analysis was prioritised according to their subcellular localisation and immune function and was narrowed down to four proteins of interest: CD300, DCD, LAT and MARCS. The proteins were tested for FAM26F interaction by co-IP using FAM26F-3xFLAG THP-1 cells. Additionally, the in-silico analysis for FAM26F interacting partners showed CD300A and MARCS as potential partners to FAM26F in two online databases; Reactome and GENEMANIA.
The validation co-IP and immunoblotting data showed that LAT is co-immunoprecipitated at higher levels in FAM26F-3xFLAG elutions compared to control. Since studies in the literature

found that FAM26F may contribute in facilitating cellular interactions between myeloid and lymphocyte cells (Ebihara et al., 2010, Kasamatsu et al., 2014), we aimed to determine whether LAT is co-precipitated with FAM26F, as LAT is known to be involved in T cell activation (Malissen et al., 2005). Therefore, we tested whether interaction between THP-1 cells and Jurkat cells (T cell line) was altered due to FAM26F-3xFLAG overexpression. Our preliminary findings indicate that FAM26F overexpression enhances Jurkat cell binding to THP-1 cells, since the percentage of attached Jurkat cells to FAM26F-3xFLAG THP-1 cells was higher than control. Our finding suggest a similar conclusion to the published data that showed FAM26F to be involved in regulating myeloid and lymphoid mouse cells (Ebihara et al., 2010, Kasamatsu et al., 2014). It will be interesting to test this further to assess whether FAM26F knockdown has an opposite effect in reducing T-cell binding, or LAT disruption by LAT antibody attachment or LAT knockdown attenuates macrophage-T-cell interactions.

6.3. Summary of current knowledge about FAM26F

The available studies suggested that FAM26F may has a role in cell-cell interaction, because it has an adhesion region on the carboxyl end (see section 4.2.4 and figure 4.6). However, the adhesive mechanism or the interaction is not known and there is no clear signalling pathway for FAM26F. The prediction of FAM26F function in immune cells (dendritic cells and macrophages) is that it is can be activated through several receptors including IFN receptors (IFNAR), TLR3, TLR4 and dectin-1, then the down-stream signalling will trigger the signal transducer and activator of transcription 1 (STAT1) (Ebihara et al., 2010, Kasamatsu et al., 2014, Chiba et al., 2014, Javed et al., 2016). Additionally, it has been shown that FAM26F expression can produce an induction in IFNγ expression in NK cells (Kasamatsu et al., 2014). The increase in IFNγ expression in immune cells such as NK cells, T cells, B cells and macrophages may facilitate the cell-cell interaction, but there is no enough evidence to confirm this hypothesis (Javed et al., 2016). See Figure 6.1 for a schematic illustration of the current knowledge about FAM26F role in immune response.

In addition, my colleague has proved a similar published data on mouse about FAM26F signalling (Chmielewski et al., 2014), Baidžajevas has found that STAT1 and TICAM1 are involved in regulation FAM26F expression in human macrophage after stimulation with IFNγ and LPS (Baidžajevas, 2019), see appendix III.

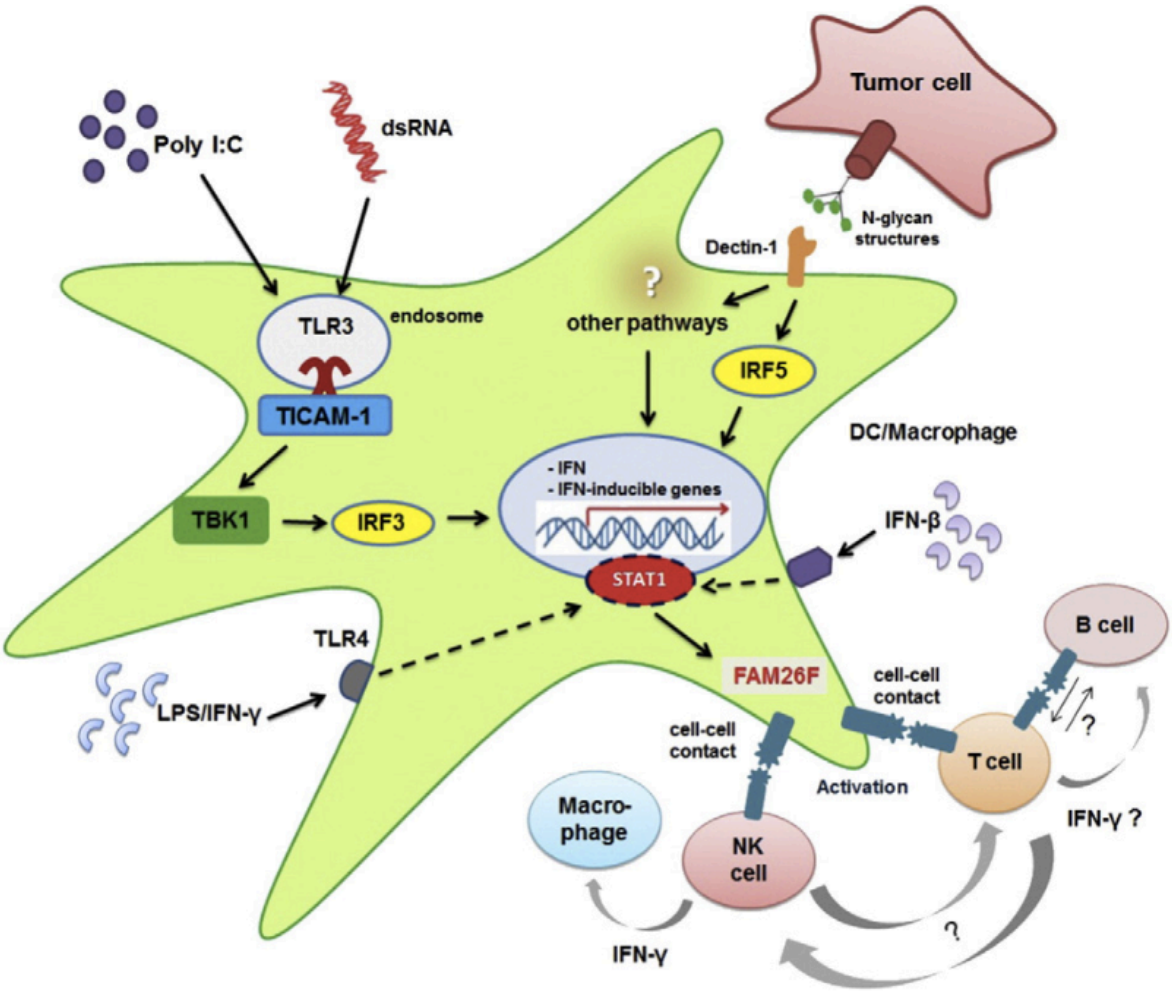

Figure 6.1 FAM26F role in immune response (Malik et al., 2016)

This image represents a schematic illustration of FAM26F role in the immune signalling pathway that have been studied in mouse dendritic cells and macrophages. FAM26F can be activated by different receptors such as TLR3, dectin-1, which can trigger STAT1 signalling. FAM26F may have the ability to facilitate cell-cell interaction by increasing the expression of IFNγ.

6.4. Limitations of this work

The first limitation was the antibodies availability (anti-TAKL or anti-FAM26F), which limited the conducted experiments. Secondly, human MDMs assays size number was low due to the limited number of donors. Additionally, the number of carotid artery blocks from atherosclerotic patients was restricted and we require more carotid sections to carry out more immunohistochemistry studies. Finally, time limits for this thesis, which was not long enough to conduct more optimisations on antibodies for FAM26F interacting partners including CD300A and MARCKS, or to increase the size number of the co-culture interaction experiments.

6.5. Possible future studies

Literature studies has confirmed that FAM26F can initiate homophilic interactions, which can establish synapses between immune cells (Ebihara et al., 2010). However, there is poor knowledge about the interaction mechanisms, so more studies in cell-cell interaction are needed. We started to study the FAM26F role in the interaction between FAM26F-3xFLAG THP-1 cells (M1 cell line) and Jurkat cells (T cell line). More studies can be done on primary macrophages and T cells. Additionally, FAM26F interaction role can be further studies using other immune cells including NK cells and B cells. Studying the potential protein partners such as CD300A, LAT and MARCS may improve our understanding of the innate and adaptive cell adhesion mechanism and FAM26F signalling in the immune response. The interaction between the innate and the adaptive immune cells in the atherosclerotic plaque is thought to underlie critical changes in the plaque that alter its vulnerability to rupture. Understanding these mechanisms may offer us the opportunity to therapeutically reduce plaque vulnerability to rupture thereby reducing the incidence of MI and stroke, particularly following infection.

References

AUWERX, J. 1991. The human leukemia cell line, THP-1: A multifacetted model for the study of monocyte-macrophage differentiation. *Experientia,* 47**,** 22-31.

BAIDŽAJEVAS, K. 2019. *Investigation into human macrophage phenotype transcriptome and importance of FAM26F.* PhD, The University of Sheffield.

BALKWILL, F. & MANTOVANI, A. 2001. Inflammation and cancer: back to Virchow? *The Lancet,* 357**,** 539-545.

BARANZINI, SERGIO E., KHANKHANIAN, P., PATSOPOULOS, NIKOLAOS A., LI, M., STANKOVICH, J., COTSAPAS, C., SØNDERGAARD, HELLE B., BAN, M., BARIZZONE, N., BERGAMASCHI, L., BOOTH, D., BUCK, D., CAVALLA, P., CELIUS, ELISABETH G., COMABELLA, M., COMI, G., COMPSTON, A., COURNU-REBEIX, I., D'ALFONSO, S., DAMOTTE, V., DIN, L., DUBOIS, B., ELOVAARA, I., ESPOSITO, F., FONTAINE, B., FRANKE, A., GORIS, A., GOURRAUD, P.-A., GRAETZ, C., GUERINI, FRANCA R., GUILLOT-NOEL, L., HAFLER, D., HAKONARSON, H., HALL, P., HAMSTEN, A., HARBO, HANNE F., HEMMER, B., HILLERT, J., KEMPPINEN, A., KOCKUM, I., KOIVISTO, K., LARSSON, M., LATHROP, M., LEONE, M., LILL, CHRISTINA M., MACCIARDI, F., MARTIN, R., MARTINELLI, V., MARTINELLI-BONESCHI, F., MCCAULEY, JACOB L., MYHR, K.-M., NALDI, P., OLSSON, T., OTURAI, A., PERICAK-VANCE, MARGARET A., PERLA, F., REUNANEN, M., SAARELA, J., SAKER-DELYE, S., SALVETTI, M., SELLEBJERG, F., SØRENSEN, PER S., SPURKLAND, A., STEWART, G., TAYLOR, B., TIENARI, P., WINKELMANN, J., ZIPP, F., IVINSON, ADRIAN J., HAINES, JONATHAN L., SAWCER, S., DEJAGER, P., HAUSER, STEPHEN L. & OKSENBERG, JORGE R. 2013. Network-Based Multiple Sclerosis Pathway Analysis with GWAS Data from 15,000 Cases and 30,000 Controls. *The American Journal of Human Genetics,* 92**,** 854-865.

BAS, A., FORSBERG, G., HAMMARSTRÖM, S. & HAMMARSTRÖM, M. L. 2004. Utility of the housekeeping genes 18S rRNA, beta-actin and glyceraldehyde-3-phosphate-dehydrogenase for normalization in real-time quantitative reverse transcriptase-polymerase chain reaction analysis of gene expression in human T lymphocytes. *Scand J Immunol,* 59**,** 566-73.

BENJAMINI, Y. & HOCHBERG, Y. 1995. Controlling the False Discovery Rate: A Practical and Powerful Approach to Multiple Testing. *Journal of the Royal Statistical Society: Series B (Methodological),* 57**,** 289-300.

BI, Y., CHEN, J., HU, F., LIU, J., LI, M. & ZHAO, L. 2019. M2 Macrophages as a Potential Target for Antiatherosclerosis Treatment. *Neural Plasticity,* 2019**,** 21.

CAMARÉ, C., PUCELLE, M., NÈGRE-SALVAYRE, A. & SALVAYRE, R. 2017. Angiogenesis in the atherosclerotic plaque. *Redox biology,* 12**,** 18-34.

CARDAMONE, M. D., KRONES, A., TANASA, B., TAYLOR, H., RICCI, L., OHGI, K. A., GLASS, C. K., ROSENFELD, M. G. & PERISSI, V. 2012. A protective strategy against hyperinflammatory responses requiring the nontranscriptional actions of GPS2. *Molecular cell,* 46**,** 91-104.

CHEN JING-LUN, N. G.-M. 2018. Advances in application of Jurkat cell model in research on infectious diseases. *CJCP,* 20**,** 236-242.

CHEN, Y.-H., HSIEH, S.-C., CHEN, W.-Y., LI, K.-J., WU, C.-H., WU, P.-C., TSAI, C.-Y. & YU, C.-L. 2011. Spontaneous resolution of acute gouty arthritis is associated with rapid induction of the anti-inflammatory factors TGFβ1, IL-10 and soluble TNF receptors

and the intracellular cytokine negative regulators CIS and SOCS3. *Annals of the rheumatic diseases,* 70**,** 1655-1663.

CHIBA, S., IKUSHIMA, H., UEKI, H., YANAI, H., KIMURA, Y., HANGAI, S., NISHIO, J., NEGISHI, H., TAMURA, T., SAIJO, S., IWAKURA, Y. & TANIGUCHI, T. 2014. Recognition of tumor cells by Dectin-1 orchestrates innate immune cells for anti-tumor responses. *eLife,* 3**,** e04177-e04177.

CHINETTI-GBAGUIDI, G., COLIN, S. & STAELS, B. 2015. Macrophage subsets in atherosclerosis. *Nature Reviews Cardiology,* 12**,** 10-17.

CHMIELEWSKI, S., OLEJNIK, A., SIKORSKI, K., PELISEK, J., BŁASZCZYK, K., AOQUI, C., NOWICKA, H., ZERNECKE, A., HEEMANN, U., WESOLY, J., BAUMANN, M. & BLUYSSEN, H. A. R. 2014. STAT1-Dependent Signal Integration between IFNγ and TLR4 in Vascular Cells Reflect Pro-Atherogenic Responses in Human Atherosclerosis. *PLOS ONE,* 9**,** e113318.

CHO, K. Y., MIYOSHI, H., KURODA, S., YASUDA, H., KAMIYAMA, K., NAKAGAWARA, J., TAKIGAMI, M., KONDO, T. & ATSUMI, T. 2013. The Phenotype of Infiltrating Macrophages Influences Arteriosclerotic Plaque Vulnerability in the Carotid Artery. *Journal of Stroke and Cerebrovascular Diseases,* 22**,** 910-918.

CHUANG, Y., HUNG, M. E., CANGELOSE, B. K. & LEONARD, J. N. 2016. Regulation of the IL-10-driven macrophage phenotype under incoherent stimuli. *Innate immunity,* 22**,** 647-657.

CHUNG, J. Y., PARK, Y. C., YE, H. & WU, H. 2002. All TRAFs are not created equal: common and distinct molecular mechanisms of TRAF-mediated signal transduction. *Journal of Cell Science,* 115**,** 679-688.

CONESA, A., MADRIGAL, P., TARAZONA, S., GOMEZ-CABRERO, D., CERVERA, A., MCPHERSON, A., SZCZEŚNIAK, M. W., GAFFNEY, D. J., ELO, L. L., ZHANG, X. & MORTAZAVI, A. 2016. A survey of best practices for RNA-seq data analysis. *Genome biology,* 17**,** 13-13.

COUSSENS, L. M. & WERB, Z. 2002. Inflammation and cancer. *Nature,* 420**,** 860-867.

DAIGNEAULT, M., PRESTON, J. A., MARRIOTT, H. M., WHYTE, M. K. B. & DOCKRELL, D. H. 2010. The identification of markers of macrophage differentiation in PMA-stimulated THP-1 cells and monocyte-derived macrophages. *PloS one,* 5**,** e8668.

DE GAETANO, M., CREAN, D., BARRY, M. & BELTON, O. 2016. M1- and M2-Type Macrophage Responses Are Predictive of Adverse Outcomes in Human Atherosclerosis. *Frontiers in immunology,* 7**,** 275-275.

DE JONGE, H. J. M., FEHRMANN, R. S. N., DE BONT, E. S. J. M., HOFSTRA, R. M. W., GERBENS, F., KAMPS, W. A., DE VRIES, E. G. E., VAN DER ZEE, A. G. J., TE MEERMAN, G. J. & TER ELST, A. 2007. Evidence based selection of housekeeping genes. *PloS one,* 2**,** e898-e898.

DE TORRE-MINGUELA, C., BARBERÀ-CREMADES, M., GÓMEZ, A. I., MARTÍN-SÁNCHEZ, F. & PELEGRÍN, P. 2016. Macrophage activation and polarization modify P2X7 receptor secretome influencing the inflammatory process. *Scientific Reports,* 6**,** 22586.

DEMPSEY, C. E., SAKURAI, H., SUGITA, T. & GUESDON, F. 2000. Alternative splicing and gene structure of the transforming growth factor β-activated kinase 1. *Biochimica et Biophysica Acta (BBA) - Gene Structure and Expression,* 1517**,** 46-52.

DHEDA, K., HUGGETT, J. F., BUSTIN, S. A., JOHNSON, M. A., ROOK, G. & ZUMLA, A. 2004. Validation of housekeeping genes for normalizing RNA expression in real-time PCR. *BioTechniques,* 37**,** 112-119.

DOBIN, A., DAVIS, C. A., SCHLESINGER, F., DRENKOW, J., ZALESKI, C., JHA, S., BATUT, P., CHAISSON, M. & GINGERAS, T. R. 2012. STAR: ultrafast universal RNA-seq aligner. *Bioinformatics,* 29**,** 15-21.

DULUC, D., DELNESTE, Y., TAN, F., MOLES, M.-P., GRIMAUD, L., LENOIR, J., PREISSER, L., ANEGON, I., CATALA, L., IFRAH, N., DESCAMPS, P., GAMELIN, E., GASCAN, H., HEBBAR, M. & JEANNIN, P. 2007. Tumor-associated leukemia inhibitory factor and IL-6 skew monocyte differentiation into tumor-associated macrophage-like cells. *Blood,* 110**,** 4319-4330.

EBIHARA, T., AZUMA, M., OSHIUMI, H., KASAMATSU, J., IWABUCHI, K., MATSUMOTO, K., SAITO, H., TANIGUCHI, T., MATSUMOTO, M. & SEYA, T. 2010. Identification of a polyI:C-inducible membrane protein that participates in dendritic cell–mediated natural killer cell activation. *The Journal of Experimental Medicine,* 207**,** 2675.

ELLIS, C. D., ROSS, K., DOWER, S. K. & GUESDON, F. unpublished. Regulation of TRAF6-mediated signalling by TAK-like (TAKL) proteins encoded by the human C21orf7 gene. Manuscript submitted to *Biochem. J.* .

FAN, Y., CHENG, J., VASUDEVAN, S. A., PATEL, R. H., LIANG, L., XU, X., ZHAO, Y., JIA, W., LU, F. & ZHANG, H. 2013. TAK1 inhibitor 5Z-7-oxozeaenol sensitizes neuroblastoma to chemotherapy. *Apoptosis,* 18**,** 1224-1234.

FROBØSE, H., GROTH RØNN, S., HEDING, P. E., MENDOZA, H., COHEN, P., MANDRUP-POULSEN, T. & BILLESTRUP, N. 2006. Suppressor of cytokine signaling-3 inhibits interleukin-1 signaling by targeting the TRAF-6/TAK1 complex. *Molecular endocrinology,* 20**,** 1587-1596.

FUJIWARA, N. & KOBAYASHI, K. 2005. Macrophages in Inflammation. *Current Drug Targets - Inflammation & Allergy,* 4**,** 281-286.

GARAY-MALPARTIDA, H. M., MOURÃO, R. F., MANTOVANI, M., SANTOS, I. A., SOGAYAR, M. C. & GOLDBERG, A. C. 2011. Toll-like receptor 4 (TLR4) expression in human and murine pancreatic beta-cells affects cell viability and insulin homeostasis. *BMC Immunology,* 12**,** 18.

GUO, L., AKAHORI, H., HARARI, E., SMITH, S. L., POLAVARAPU, R., KARMALI, V., OTSUKA, F., GANNON, R. L., BRAUMANN, R. E., DICKINSON, M. H., GUPTA, A., JENKINS, A. L., LIPINSKI, M. J., KIM, J., CHHOUR, P., DE VRIES, P. S., JINNOUCHI, H., KUTYS, R., MORI, H., KUTYNA, M. D., TORII, S., SAKAMOTO, A., CHOI, C. U., CHENG, Q., GROVE, M. L., SAWAN, M. A., ZHANG, Y., CAO, Y., KOLODGIE, F. D., CORMODE, D. P., ARKING, D. E., BOERWINKLE, E., MORRISON, A. C., ERDMANN, J., SOTOODEHNIA, N., VIRMANI, R. & FINN, A. V. 2018. CD163+ macrophages promote angiogenesis and vascular permeability accompanied by inflammation in atherosclerosis. *The Journal of clinical investigation,* 128**,** 1106-1124.

HADADI, E. 2015. *Contribution of macrophage phenotypes and their precursors in inflammatory function and the development of cardiovascular disease.* PhD, The University of Sheffield.

HARTMAN, J. & FRISHMAN, W. H. 2014. Inflammation and Atherosclerosis: A Review of the Role of Interleukin-6 in the Development of Atherosclerosis and the Potential for Targeted Drug Therapy. *Cardiology in Review,* 22.

HEPPNER, F., RANSOHOFF, R. & BECHER, B. 2015. Immune attack: The role of inflammation in Alzheimer disease. *Nature reviews. Neuroscience,* 16**,** 358-72.

HUANG, Y., WU, D., ZHANG, X., JIANG, M., HU, C., LIN, J., TANG, J. & WU, L. 2014. Cardiac-specific Traf2 overexpression enhances cardiac hypertrophy through activating AKT/GSK3β signaling. *Gene,* 536**,** 225-231.

INOUE, J.-I., ISHIDA, T., TSUKAMOTO, N., KOBAYASHI, N., NAITO, A., AZUMA, S. & YAMAMOTO, T. 2000. Tumor Necrosis Factor Receptor-Associated Factor (TRAF) Family: Adapter Proteins That Mediate Cytokine Signaling. *Experimental Cell Research,* 254**,** 14-24.

JAIPERSAD, A. S., LIP, G. Y. H., SILVERMAN, S. & SHANTSILA, E. 2014. The Role of Monocytes in Angiogenesis and Atherosclerosis. *Journal of the American College of Cardiology,* 63**,** 1.

JAVED, A., LEUCHTE, N., SALINAS-RIESTER, G., OPITZ, L., HENNIG, C., SOPPER, S. & SAUERMANN, U. 2016. Pre-Infection Transcript Levels of FAM26F in PBMCS Inform about Overall Plasma Viral Load in Acute and Postacute Phase after SIV-Infection. *The Journal of general virology,* 97.

JONASSON, L., HOLM, J., SKALLI, O., BONDJERS, G. & HANSSON, G. K. 1986. Regional accumulations of T cells, macrophages, and smooth muscle cells in the human atherosclerotic plaque. *Arteriosclerosis: An Official Journal of the American Heart Association, Inc.,* 6**,** 131-138.

KARIMI, K., SARIR, H., MORTAZ, E., SMIT, J. J., HOSSEINI, H., DE KIMPE, S. J., NIJKAMP, F. P. & FOLKERTS, G. 2006. Toll-like receptor-4 mediates cigarette smoke-induced cytokine production by human macrophages. *Respiratory Research,* 7**,** 66.

KASAMATSU, J., AZUMA, M., OSHIUMI, H., MORIOKA, Y., OKABE, M., EBIHARA, T., MATSUMOTO, M. & SEYA, T. 2014. INAM Plays a Critical Role in IFN-γ Production by NK Cells Interacting with Polyinosinic-Polycytidylic Acid–Stimulated Accessory Cells. *The Journal of Immunology,* 193**,** 5199.

KILPINEN, S., OJALA, K. & KALLIONIEMI, O. 2010. Analysis of kinase gene expression patterns across 5681 human tissue samples reveals functional genomic taxonomy of the kinome. *PLoS One,* 5**,** e15068.

KLUTH, M., HESSE, J., HEINL, A., KROHN, A., STEURER, S., SIRMA, H., SIMON, R., MAYER, P.-S., SCHUMACHER, U. & GRUPP, K. 2013. Genomic deletion of MAP3K7 at 6q12-22 is associated with early PSA recurrence in prostate cancer and absence of TMPRSS2: ERG fusions. *Modern pathology,* 26**,** 975-983.

LALANI, A. I., ZHU, S., GOKHALE, S., JIN, J. & XIE, P. 2018. TRAF molecules in inflammation and inflammatory diseases. *Current pharmacology reports,* 4**,** 64-90.

LEVY, S. & SHOHAM, T. 2005. Levy, S. & Shoham, T. The tetraspanin web modulates immune-signalling complexes. Nat. Rev. Immunol. 5, 136-148. *Nature reviews. Immunology,* 5**,** 136-48.

LI, J. X., JI, C. N., YANG, Q. S., CHEN, J. Z., GU, S. H., YING, K., XIE, Y. & MAO, Y. M. 2004. Cloning and characterization of a novel human TGF-beta activated kinase-like gene. *Biochemical Genetics,* 42**,** 129-137.

LIAO, Y., SMYTH, G. K. & SHI, W. 2013. featureCounts: an efficient general purpose program for assigning sequence reads to genomic features. *Bioinformatics,* 30**,** 923-930.

LIBBY, P., RIDKER PAUL, M. & MASERI, A. 2002. Inflammation and Atherosclerosis. *Circulation,* 105**,** 1135-1143.

LIU, Q., BUSBY, J. C. & MOLKENTIN, J. D. 2009. Interaction between TAK1–TAB1–TAB2 and RCAN1–calcineurin defines a signalling nodal control point. *Nature Cell Biology,* 11**,** 154-161.

LIU, Y.-C., ZOU, X.-B., CHAI, Y.-F. & YAO, Y.-M. 2014. Macrophage polarization in inflammatory diseases. *International journal of biological sciences,* 10**,** 520-529.

LOVE, M. I., HOGENESCH, J. B. & IRIZARRY, R. A. 2016. Modeling of RNA-seq fragment sequence bias reduces systematic errors in transcript abundance estimation. *Nature biotechnology,* 34**,** 1287-1291.

LV, S., QIU, X., LI, J., LI, W., ZHANG, C., ZHANG, Z.-N. & LUAN, B. 2016. Suppression of CRTC2-mediated hepatic gluconeogenesis by TRAF6 contributes to hypoglycemia in septic shock. *Cell Discovery,* 2**,** 16046.

MALIK, U., JAVED, A., ALI, A. & ASGHAR, D. K. 2016. Structural and functional annotation of human FAM26F: A multifaceted protein having a critical role in the immune system. *Gene,* 597.

MALISSEN, B., AGUADO, E. & MALISSEN, M. 2005. Role of the LAT Adaptor in T-Cell Development and Th2 Differentiation. *Advances in immunology,* 87**,** 1-25.

MALONEY, N., BRIDGE, J. A., DE ABREU, F., KORKOLOPOULOU, P., SAKELLARIOU, S. & LINOS, K. 2019. A novel MAP3K7CL-ERG fusion in a molecularly confirmed case of dermatofibrosarcoma protuberans with fibrosarcomatous transformation. *Journal of Cutaneous Pathology,* 46**,** 532-537.

MARTIN, S. E., WU, Z. H., GEHLHAUS, K., JONES, T. L., ZHANG, Y. W., GUHA, R., MIYAMOTO, S., POMMIER, Y. & CAPLEN, N. J. 2011. RNAi screening identifies TAK1 as a potential target for the enhanced efficacy of topoisomerase inhibitors. *Current cancer drug targets,* 11**,** 976.

MARTINEZ, F. O. & GORDON, S. 2014. The M1 and M2 paradigm of macrophage activation: time for reassessment. *F1000prime reports,* 6**,** 13-13.

MCKENZIE, ANDREW N. J., SPITS, H. & EBERL, G. 2014. Innate Lymphoid Cells in Inflammation and Immunity. *Immunity,* 41**,** 366-374.

MELISI, D., XIA, Q., PARADISO, G., LING, J., MOCCIA, T., CARBONE, C., BUDILLON, A., ABBRUZZESE, J. L. & CHIAO, P. J. 2011. Modulation of pancreatic cancer chemoresistance by inhibition of TAK1. *Journal of the National Cancer Institute,* 103**,** 1190-1204.

MILLS, E. L. & O'NEILL, L. A. 2016. Reprogramming mitochondrial metabolism in macrophages as an anti-inflammatory signal. *European Journal of Immunology,* 46**,** 13-21.

MOORE, K. J., SHEEDY, F. J. & FISHER, E. A. 2013. Macrophages in atherosclerosis: a dynamic balance. *Nature reviews. Immunology,* 13**,** 709-721.

MORONI, F., AMMIRATI, E., NORATA, G. D., MAGNONI, M. & CAMICI, P. G. 2019. The Role of Monocytes and Macrophages in Human Atherosclerosis, Plaque Neoangiogenesis, and Atherothrombosis. *Mediators of inflammation,* 2019**,** 7434376-7434376.

MOSMANN, T. R., CHERWINSKI, H., BOND, M. W., GIEDLIN, M. A. & COFFMAN, R. L. 1986. Two types of murine helper T cell clone. I. Definition according to profiles of lymphokine activities and secreted proteins. *The Journal of Immunology,* 136**,** 2348.

MURRAY, P. J., ALLEN, J. E., BISWAS, S. K., FISHER, E. A., GILROY, D. W., GOERDT, S., GORDON, S., HAMILTON, J. A., IVASHKIV, L. B., LAWRENCE, T., LOCATI, M., MANTOVANI, A., MARTINEZ, F. O., MEGE, J.-L., MOSSER, D. M., NATOLI, G., SAEIJ, J. P., SCHULTZE, J. L., SHIREY, K. A., SICA, A., SUTTLES, J., UDALOVA, I., VAN GINDERACHTER, J. A., VOGEL, S. N. & WYNN, T. A. 2014. Macrophage activation and polarization: nomenclature and experimental guidelines. *Immunity,* 41**,** 14-20.

MYLES, A., RAHMAN, M. T. & AGGARWAL, A. 2012. Membrane-Bound Toll-Like Receptors are Overexpressed in Peripheral Blood and Synovial Fluid Mononuclear Cells of Enthesitis-Related Arthritis Category of Juvenile Idiopathic Arthritis (JIA–

ERA) Patients and Lead to Secretion of Inflammatory Mediators. *Journal of Clinical Immunology,* 32**,** 488-496.
NAGENBORG, J., GOOSSENS, P., BIESSEN, E. A. L. & DONNERS, M. M. P. C. 2017. Heterogeneity of atherosclerotic plaque macrophage origin, phenotype and functions: Implications for treatment. *European Journal of Pharmacology,* 816**,** 14-24.
NEWBY ANDREW, C. 2008. Metalloproteinase Expression in Monocytes and Macrophages and its Relationship to Atherosclerotic Plaque Instability. *Arteriosclerosis, Thrombosis, and Vascular Biology,* 28**,** 2108-2114.
OU-YANG, C.-W., ZHU, M., SULLIVAN, S. A., FULLER, D. M. & ZHANG, W. 2013. The Requirement of Linker for Activation of T Cells in the Primary and Memory Responses of CD8 T Cells. *The Journal of Immunology,* 190**,** 2938.
PARKER, E., ANJUM, S., TSELEPI, M., RICE, S. J., DEEHAN, D., REYNARD, L. N. & LOUGHLIN, J. 2019. Gene expression and DNA methylation analysis at the OA susceptibility locus marked by rs6516886 prioritizes specific gene and regulatory sequences as functional targets of the association signal. *Osteoarthritis and Cartilage,* 27**,** S284.
PICELLI, S., FARIDANI, O. R., BJÖRKLUND, Å. K., WINBERG, G., SAGASSER, S. & SANDBERG, R. 2014. Full-length RNA-seq from single cells using Smart-seq2. *Nature Protocols,* 9**,** 171-181.
PRAME KUMAR, K., NICHOLLS, A. J. & WONG, C. H. Y. 2018. Partners in crime: neutrophils and monocytes/macrophages in inflammation and disease. *Cell and tissue research,* 371**,** 551-565.
QIAO, Y. Q., SHEN, J., GU, Y., TONG, J. L., XU, X. T., HUANG, M. L. & RAN, Z. H. 2013. Gene expression of tumor necrosis factor receptor associated-factor (TRAF)-1 and TRAF-2 in inflammatory bowel disease. *Journal of Digestive Diseases,* 14**,** 244-250.
QIN, Z. 2012. The use of THP-1 cells as a model for mimicking the function and regulation of monocytes and macrophages in the vasculature. *Atherosclerosis,* 221**,** 2-11.
REKHTER, M. D. & GORDON, D. 1995. Active proliferation of different cell types, including lymphocytes, in human atherosclerotic plaques. *The American journal of pathology,* 147**,** 668-677.
REYMOND, A., FRIEDLI, M., HENRICHSEN, C. N., CHAPOT, F., DEUTSCH, S., UCLA, C., ROSSIER, C., LYLE, R., GUIPPONI, M. & ANTONARAKIS, S. E. 2001. From PREDs and open reading frames to cDNA isolation: revisiting the human chromosome 21 transcription map. *Genomics,* 78**,** 46-54.
RIDKER, P. M., EVERETT, B. M., THUREN, T., MACFADYEN, J. G., CHANG, W. H., BALLANTYNE, C., FONSECA, F., NICOLAU, J., KOENIG, W., ANKER, S. D., KASTELEIN, J. J. P., CORNEL, J. H., PAIS, P., PELLA, D., GENEST, J., CIFKOVA, R., LORENZATTI, A., FORSTER, T., KOBALAVA, Z., VIDA-SIMITI, L., FLATHER, M., SHIMOKAWA, H., OGAWA, H., DELLBORG, M., ROSSI, P. R. F., TROQUAY, R. P. T., LIBBY, P. & GLYNN, R. J. 2017. Antiinflammatory Therapy with Canakinumab for Atherosclerotic Disease. *New England Journal of Medicine,* 377**,** 1119-1131.
ROBINSON, M. D., MCCARTHY, D. J. & SMYTH, G. K. 2009. edgeR: a Bioconductor package for differential expression analysis of digital gene expression data. *Bioinformatics,* 26**,** 139-140.
ROSZER, T. 2015. Understanding the mysterious M2 macrophage through activation markers and effector mechanisms. *Mediators of Inflammation*.
RUAL, J.-F., VENKATESAN, K., HAO, T., HIROZANE-KISHIKAWA, T., DRICOT, A., LI, N., BERRIZ, G. F., GIBBONS, F. D., DREZE, M. & AYIVI-GUEDEHOUSSOU,

N. 2005. Towards a proteome-scale map of the human protein–protein interaction network. *Nature,* 437**,** 1173-1178.
SCHOBER, A., NAZARI-JAHANTIGH, M. & WEBER, C. 2015. MicroRNA-mediated mechanisms of the cellular stress response in atherosclerosis. *Nature Reviews Cardiology,* 12**,** 361.
SCHRODER, K. & TSCHOPP, J. 2010. The Inflammasomes. *Cell,* 140**,** 821-832.
SHALAPOUR, S. & KARIN, M. 2015. Immunity, inflammation, and cancer: an eternal fight between good and evil. *The Journal of Clinical Investigation,* 125**,** 3347-3355.
SINDER, B. P., PETTIT, A. R. & MCCAULEY, L. K. 2015. Macrophages: Their Emerging Roles in Bone. *Journal of Bone and Mineral Research,* 30**,** 2140-2149.
SINGH, A., SWEENEY, M. F., YU, M., BURGER, A., GRENINGER, P., BENES, C., HABER, D. A. & SETTLEMAN, J. 2012. TAK1 inhibition promotes apoptosis in KRAS-dependent colon cancers. *Cell,* 148**,** 639-650.
SMIRNOV, E., HORNÁČEK, M., VACÍK, T., CMARKO, D. & RAŠKA, I. 2018. Discontinuous transcription. *Nucleus,* 9**,** 149-160.
STÖGER, J. L., GIJBELS, M. J. J., VAN DER VELDEN, S., MANCA, M., VAN DER LOOS, C. M., BIESSEN, E. A. L., DAEMEN, M. J. A. P., LUTGENS, E. & DE WINTHER, M. P. J. 2012. Distribution of macrophage polarization markers in human atherosclerosis. *Atherosclerosis,* 225**,** 461-468.
SUTER, D. M., MOLINA, N., GATFIELD, D., SCHNEIDER, K., SCHIBLER, U. & NAEF, F. 2011. Mammalian Genes Are Transcribed with Widely Different Bursting Kinetics. *Science,* 332**,** 472.
TABAS, I. & LICHTMAN, A. H. 2017. Monocyte-Macrophages and T Cells in Atherosclerosis. *Immunity,* 47**,** 621-634.
TAIRA, M., CHOSA, N., SASAKI, K., SAITOH, S., NEZU, T., SATO, N. & ARAKI, Y. 2005. DNA microarray analyses of gene expression in human mesenchymal stem cells cultured in osteogenic differentiation medium for 14 days. *Journal of Oral Tissue Engineering,* 3**,** 25-53.
TAKAESU, G., KISHIDA, S., HIYAMA, A., YAMAGUCHI, K., SHIBUYA, H., IRIE, K., NINOMIYA-TSUJI, J. & MATSUMOTO, K. 2000. TAB2, a Novel Adaptor Protein, Mediates Activation of TAK1 MAPKKK by Linking TAK1 to TRAF6 in the IL-1 Signal Transduction Pathway. *Molecular Cell,* 5**,** 649-658.
TALL, A. R., COSTET, P. & WANG, N. 2002. Regulation and mechanisms of macrophage cholesterol efflux. *The Journal of clinical investigation,* 110**,** 899-904.
TANAKA, T., NARAZAKI, M. & KISHIMOTO, T. 2014. IL-6 in Inflammation, Immunity, and Disease. *Cold Spring Harbor Perspectives in Biology,* 6.
TOKUNAGA, R., ZHANG, W., NASEEM, M., PUCCINI, A., BERGER, M. D., SONI, S., MCSKANE, M., BABA, H. & LENZ, H.-J. 2018. CXCL9, CXCL10, CXCL11/CXCR3 axis for immune activation – A target for novel cancer therapy. *Cancer Treatment Reviews,* 63**,** 40-47.
VERGADI, E., IERONYMAKI, E., LYRONI, K., VAPORIDI, K. & TSATSANIS, C. 2017. Akt Signaling Pathway in Macrophage Activation and M1/M2 Polarization. *The Journal of Immunology,* 198**,** 1006.
WADA, T. & BECSKEI, A. 2017. Impact of Methods on the Measurement of mRNA Turnover. *Int J Mol Sci,* 18.
WAJANT, H., HENKLER, F. & SCHEURICH, P. 2001. The TNF-receptor-associated factor family: Scaffold molecules for cytokine receptors, kinases and their regulators. *Cellular Signalling,* 13**,** 389-400.

WANG, J., HUO, K., MA, L., TANG, L., LI, D., HUANG, X., YUAN, Y., LI, C., WANG, W. & GUAN, W. 2011. Toward an understanding of the protein interaction network of the human liver. *Molecular systems biology,* 7**,** 536, 1744-4292.

XIE, P. 2013. TRAF molecules in cell signaling and in human diseases. *Journal of molecular signaling,* 8**,** 7-7.

ZIRLIK, A., BAVENDIEK, U., LIBBY, P., MACFARLANE, L., GERDES, N., JAGIELSKA, J., ERNST, S., AIKAWA, M., NAKANO, H., TSITSIKOV, E. & SCHÖNBECK, U. 2007. TRAF-1, -2, -3, -5, and -6 Are Induced in Atherosclerotic Plaques and Differentially Mediate Proinflammatory Functions of CD40L in Endothelial Cells. *Arteriosclerosis, Thrombosis, and Vascular Biology,* 27**,** 1101-1107.

Appendix I

Unpublished research manuscript by Ellis *et al. (2015):*

Regulation of TRAF6-mediated signalling by TAK1-like (TAKL) proteins encoded by the human C21orf7 gene

REGULATION OF THE TGF-β-ACTIVATED KINASE FUNCTION BY TAK1-LIKE PROTEINS*

Charles D. Ellis[1], Victoria Tomlinson[2], Kehinde Ross[3] and François Guesdon

From the Department of Infection and Immunity, University of Sheffield, Medical School, Beech Hill Road, Sheffield, S10 2RX, UK, United Kingdom

Running title: Evolution and function of TAKL / C21orf7

Address correspondence to: François Guesdon, School of Medicine and Biomedical Sciences, Beech Hill Road, Sheffield, S10 2RX, United Kingdom. E-mail: f.a.guesdon@sheffield.ac.uk

We have investigated the evolution and function of the TGF-β-activated kinase-like (TAKL) gene, also known as C21orf7 in humans. We sequenced four new C21orf7 mRNA variants and determined the intron/exon structure of the gene. Phylogenetic analysis shows that TAKL arose from a duplication of the TAK1 gene early in vertebrate evolution. TAKL does not encode a kinase domain. In most vertebrates, its unique product is a 142-residue protein called TAKL-1 that is homologous to the TAB2/3-binding domain of TAK1. Mammalian TAKL genes encode an additional shorter predicted product, TAKL-2. In primates, TAKL also acquired an upstream alternative transcription start site and additional exons that enable C21orf7 to encode two additional proteins, TAKL-3 and TAKL-4. An anti-TAKL antibody detected antigens corresponding to TAKL-1 and TAKL-3 in several human cell lines. Recombinant TAKL-1 and TAKL-3 bind TAB2 and TAB3 directly and associate with TRAF6 in a TAB2-dependent manner. TAKL-1 and TAKL-3 also prevent phosphorylation of TAB2 or TAB3 and activation of the c-Jun-N-terminal kinase (JNK), but not of the p38 and p44/42 mitogen-activated protein (MAP) kinase or NF-κB. TAKL-1 also partially inhibits activation of the interleukin-8 gene promoter by pro-inflammatory stimuli. Two possible mechanisms by which TAKL may inhibit pro-inflammatory responses are discussed.

The Transforming Growth Factor (TGF[4]) β-activated kinase (TAK1) plays crucial roles in the development and immune responses of organisms as diverse as *Drosophila* or humans. In mammals, the kinase is implicated in the signaling mechanisms of the TGF-β family of cytokines (1, 2), interleukins (IL) 2, 7 and 15 (3), the B and T cell receptors (3-5) and Wnt (6). TAK1 also plays critical roles in the signaling pathways of most Toll-like-receptors (TLRs), the IL-1 receptor (IL-1R1) and several members of the tumor necrosis factor receptor (TNF-R) family (1, 4, 7-9); in these pathways, TAK1 controls the c-Jun-N-terminal kinase (JNK) and the IκB kinases (IKK), and is also involved in the activation of the p38 kinase (1, 4, 7, 8).

Four isoforms of TAK1 are produced by alternative splicing (10) but except for two studies (11, 12), functional investigations have focused exclusively on the TAK1-a isoform. The activation of TAK1-a generally involves its recruitment and that of its co-factor, the TAK1-binding protein 1 (TAB1), to protein complexes whose key components are the TNF-R-associated factors (TRAF) 2 or 6. TRAF2 is a component of the TNF-R-1 signaling complex (13-15) whereas TRAF6 is involved in the signaling pathways of the type I TGF-β receptor (2), the T cell receptor (5), most TLRs (15-17), IL-1R1 (18), RANK (8, 9, 17, 18), CD40 (17, 18) and Edaradd (9). TAK1-a cannot bind TRAF2 or TRAF6 directly, however, and its recruitment to TRAF complexes is dependent upon two adaptors, TAB2 and TAB3 (13, 19-21).

TRAF2 and TRAF6 possess E3-ubiquitin ligase activities that play essential roles in the dynamics of formation and activation of TRAF complexes. Upon activation, TRAF2 and TRAF6 catalyse their own K-63-linked poly-ubiquitination (5, 22, 23) as well as those of other complex components (13, 15). TAB2 and TAB3 have multiple

roles in these complexes. They first associate with the non-ubiquitinated TRAF2 or TRAF6 (13, 19) and, in the case of TAB2, facilitate the ubiquitin-ligase activity of TRAF6 (24). They also recruit to the complexes additional components such as TAK1-a (21) or IKK-α (24). Finally, TAB2 and TAB3 function as K63-polyubiquitin-binding proteins and it is their binding to K63-polyubiquitin chains that triggers the activation of TAK1-a (24, 25).

We have recently shown that the TAK1-b isoform can also associate with TAB2 or TAB3, but that TAK1-c and TAK1-d cannot, which suggests that only the TAK1-a/b isoforms are competent for activation by TRAF complexes[5]. This is in agreement with the observation that the binding of TAK1 to TAB2 or TAB3 requires a 97-residue carboxy-terminal domain of the kinase that is present in TAK1-a/b, but absent from TAK1-c/d (21) (Fig. 1).

Interestingly, a sequence very similar to this domain is encoded by a human gene located at 21q22.1, in the Down syndrome critical region of chromosome 21. The gene, called TAK1-like (TAKL) or C21orf7, does not encode a kinase domain and its function is unknown (26, 27). The strong sequence similarity between TAKL and the TAB2/3-binding domain of TAK1-a/b (supplemental Fig. SF1) suggests that TAKL gene products may be capable of associating with TAB2 or TAB3 and participate in TRAF6- and TRAF2-mediated signaling pathways.

We have now investigated the structure of the TAKL gene, the expression of its products and their involvement in pro-inflammatory signaling pathways. Our results show that the TAKL gene is a regulator of TRAF6-mediated signaling whose structure has been strongly conserved in most classes of vertebrates but has evolved dramatically in primates.

EXPERIMENTAL PROCEDURES

Analysis of genomic, cDNA and protein sequences

The cDNA sequences encoding new C21orf7 and TAKL variants were identified using the BLAST server at the NCBI web site. Human, chimpanzee, mouse, dog and chicken genomic sequences matching the TAKL cDNAs were identified in the GenBank database using the advanced BLAST algorithm. Macaque and Xenopus genomic sequences were retrieved from the BLAT server at the UCSC Genome Bioinformatics site (*http://genome.ucsc.edu/*). The cDNA sequences that appeared to result from unique incomplete or non-canonical splicing events were identified at this stage and were excluded from further analyses. Repeated sequence elements and CpG islands were identified using the RepeatMasker (Institute for Systems Biology, *http://www.repeatmasker.org/*) and CpGplot (European Bioinformatics Institute, http://www.ebi.ac.uk/emboss/cpgplot/) programs. Genomic sequences fragments conserved across species were identified with PipMaker (http://pipmaker.bx.psu.edu/pipmaker/). Multiple sequence alignments were generated with ClustalW, accessed at European Bioinformatics Institute (*http://www.ebi.ac.uk/clustalw/*) and the Boxshade server at http://www.ch.embnet.org/.

Construction of pD-C1, pD-G1 and pD-Y1 *destination vectors for expression of fluorescent fusion proteins*

The open reading frames of the enhanced Cyan (ECFP), Green (EGFP) and yellow (EYFP) fluorescent proteins were excised from the pECFP-C1, pEGFP-C1 and pEYFP-C1 vectors (Clontech) using *Nhe I* and *Bgl II* and ligated into the *Nhe I* and *Bam H I* sites of pcDNA 3.1 + (Invitrogen). The Gateway conversion cassette (Invitrogen, reading frame A) was then ligated into the unique *Eco R V* sites of the three constructs. The resulting Gateway destination vectors, designated pD-C1, pD-G1 and pD-Y1, allow fusions of Gateway entry clones inserts to the 3' ends of the ECFP, EGFP and EYFP ORFs, respectively. The vectors were linearized with *Bsm B1* prior to using them in the LR reactions.

Other reagents and plasmids

Recombinant human IL-1β and TNF-α were from R&D system (Abingdon, UK) and *E. coli* lipopolysaccharide (LPS), serotype R515, from Alexis (Nottingham, UK). Restriction enzymes, T4 ligase and Taq DNA polymerase were from Promega. Unless otherwise stated, all amplifications were carried out with Pfu polymerase (Stratagene). Synthetic oligonucleotides were from Life Technologies (Paisley, UK). The pDNOR201-GUS construct, containing the ß-glucoronidase (GUS) cDNA, was from Invitrogen. All IMAGE cDNA

clones were obtained from the HGMP (Hinxton, Cambridge). The pIL-8-Luc promoter-reporter construct and the expression constructs encoding FLAG-TRAF6 and the IL-1R1-activated kinase (IRAK) have been described previously (28, 29). The pCMVT7-TAB2 and FLAG-K63W constructs were generous gifts from professor. K. Matsumoto (Nagoya University, Japan and Professor L. A. J. O'Neill (Trinity College, Dublin, Ireland). The pRL-TK construct, containing the *Renilla reniformis* luciferase reporter under control of the herpes simplex virus thymidine kinase promoter, was from Promega.

The p44/42 and p38 mitogen-activated protein (MAP) kinases and IκBα were detected with antibodies from Cell Signaling Technology, New England Biolabs, Hitchin, UK (Cat. # 9102, 9212, and 9242). The antibody to the JNK MAP kinase (Cat. # sc-571) was from Santa Cruz Biotechnology (Santa-Cruz, CA, USA). The active forms of the p44/42, JNK and p38 kinases were detected with phospho-specific antibodies from Cell Signaling Technology (Cat. # 9101S and 9251S) and Promega (Cat. # V121A). Tagged proteins were precipitated and detected with antibodies to FLAG, GST, HA (all from Sigma), EGFP (Roche) and T7 (Novagen). Horseradish peroxidase (HRP)-conjugated antibodies against rabbit or mouse immunoglobulin G (IgG) were from Cell Signaling Technology.

Cells

Murine macrophage-derived RAW264.7 cells, green African monkey COS-7 cells, human HeLa and HEK293T cells were obtained from the European Collection of Cell Cultures (ECACC) and maintained in Dulbecco's modified Eagle's medium supplemented with 10 % de-complemented fetal calf serum, penicillin G (100 µg/ml) and streptomycin (100 µg/ml) (all from Life Technologies). Human monocytes and polymorphonuclear cells were prepared from peripheral blood obtained with informed consent from volunteers, in accordance with a protocol approved by the South Sheffield Research Ethics Committee. The cells were using Dextran sedimentation, centrifugation over Histopaque 1077 and negative magnetic separation as described before (30, 31).

TAKL antibody

A rabbit polyclonal antibody to a synthetic peptide of TAKL (residues 64-77 of TAKL-1, sequence CQIAEEYHEVKKEI) was produced by Innovagen AB (Lund, Sweden). The peptide corresponds to a fragment of the human sequence that is also present in TAKL-3 and TAKL-2 (supplemental Fig. SF1) and is fully conserved in the mouse and rat homologues of TAKL-1. The peptide was amidated at its carboxy-terminal end. For immunization, it was coupled to the carrier protein KLH via the side chain of the amino-terminal cysteine. The antibody was purified from the serum by ammonium sulfate precipitation and affinity purification against the antigenic peptide, which had been covalently linked to agarose beads using the AminoLink Plus immobilization kit (PIERCE).

Entry clones for the Gateway recombination cloning system

The cDNAs encoding a442 and c284 were produced by PCR using AttB1-containing forward primers of sequences GGGGACAAGTTTG TACAAAAAAGCAGGCTCCTCAGACCAACCT CAGAAAAGCCAACTCG and GGGGACAAGTT TGTACAAAAAAGCAGGCTTGAAAATAATGC TCACTTGATGCGGTATTTCC and an AttB2-containing reverse primer of sequence GGG GACCACTTTGTACAAGAAAGCTGGGTCTCAT GAAGTGCCTTGTCGTTTCTGC. The TAB2 open reading frame was amplified from the T7-TAB2 construct using the AttB-containing primers GGGGACAAGTTTGTACAAAAAAGCAGGCTG CGAAATCATGGCCCAAGGAAGCCACC and GGGGACCACTTTGTACAAGAAAGCTGGGTG CTCAGAAATGCCTTGGCATCTC. The a442, c284 and TAB2 amplimers were inserted into pDONR201 by in vitro recombination between the attB sites and the attP sites of the vector using the BP reaction mix (Invitrogen). The coding sequences of TAB3, TAKL-1 and the amino-terminal domain (ATD) of TAKL-3 were amplified from IMAGE clones 5502039, 4244723 and 4857774, respectively, and the products were inserted directionally between the *attL1* and *attL2* sites of the pENTR/D-TOPO vector (Invitrogen). The TAKL-3 open reading frame was generated by a modified version of the splicing by overlap extension procedure (32). First, two PCR products corresponding to the 5' and 3' ends of the

TAKL-3 ORF, called T3-5 and T3-3, were amplified from the IMAGE clones 4857774 and 4244723, respectively, using primers of sequence CACCATGGTTCAGCTGATTGCAC (T3-5 forward), GTCTTCAGGGGGTGTATCA TCCAGAGGGGAGCTGGG (T3-5 reverse), ATGATACACCCCCTGAAGACTCCATTCTT TGGTCT (T3-3 forward) and TTAGGACGAG CCCTGCCTCTTC (T3-3 reverse). The products were purified with the QIAquick PCR purification kit (Qiagen) and the + strand of T3-5 and the - strand of T3-3 were then further amplified to a 10-fold excess relative to their complementary strands in reactions that contained 200 ng of double-stranded template (T3-5 or T3-3), DNA polymerase and either the T3-5 forward primer or T3-3 reverse primer, respectively. The amplifications were done using 10 cycles of 95 °C for 30 sec, 65 °C and 72 °C for 1 min and the single-stranded products were purified using the QIA quick PCR purification kit. In the final step, the T3-5 + strand and the T3-3 - strand were annealed through their 20-nucleotides complementary ends and were elongated by AccuTaq DNA polymerase (Sigma) to generate a double-stranded TAKL-3 cDNA. The product was cloned in pENTR/D-TOPO. Except for pDNOR201-gus, all entry clones inserts were fully sequenced to ensure that they did not contain mutations.

Mammalian expression constructs

The pCMVT7-TAB3 construct was generated by substituting the TAB2 coding sequence of pCMVT7-TAB2 by that of TAB3a (21), which we amplified from IMAGE clone 5502039 with primers of sequences CCCGAATTCATGGCGCAAAGCAGCCCA and CGCGTCGACTCAGGTGTACCGTGGCA TC, containing *EcoRI* and *SalI* sites, respectively. All other mammalian expression constructs were generated by *in vitro* recombination of the *attL* sites of the pDONR201 or pENTR constructs with the *attR* sites of the destination vectors using the LR reaction (Gateway cloning system, Invitrogen). The destination vectors used were pcDNA3.2-DEST for expression of untagged products, pDEST27 for GST-tagged products (both from Invitrogen), and pD-C1, pD-G1 or pD-Y1 for expression of fluorescent fusion proteins

Promoter-reporter assays

These assays were carried out as described previously (33).

GST pull-down, immunoprecipitation and western blotting

For detection of associations between tagged constructs, HeLa and 293T cells were seeded at 1.6 x 10^6 cells / 10-cm dish and transfected the following day. At 24 hours post-transfection, cells were lysed in 400 µl lysis buffer (20 mM HEPES, pH 7.9, 0.5% Triton X-100, 150 mM NaCl, 2 mM DTT, 2 mM EDTA, 12.5 mM β-glycerophosphate, 10 mM sodium fluoride, 1 mM sodium orthovanadate) supplemented with protease inhibitor cocktail no. 3 (Calbiochem). The cell lysates were then centrifuged (16,000 g for 15 mins) to remove cellular debris and pre-cleared by addition of Sepharose 4B beads (Sigma) to remove proteins that were bound non-specifically to the beads. For affinity precipitation of GST-tagged proteins, the cleared lysates were incubated with glutathione agarose beads (Sigma) for 2 hours at 4 °C. For immunoprecipitations, antibodies were added to the lysates at concentrations recommended by the manufacturers and the reactions were incubated for 2 hours at 4 °C. Protein A or G sepharose (Sigma) was then added and incubations were carried on for a further hour. The GST pull-down and immunoprecipitation procedures were both ended by washing the beads three times in lysis buffer. For western blotting, the samples (cell lysates, GST pull-downs or immunoprecipitates) were heated at 100 °C for 5 minutes in 40 µl SDS-PAGE sample buffer, then separated on 10 % SDS-PAGE gels and transferred to Hybond P polyvinylidene difluoride membranes (GE Healthcare, Little Chalfont, UK). The membranes were probed with appropriate antibodies, after which the HRP-conjugated antibodies were detected using chemoluminescence detection reagents and Hyperfilm ECL from GE Healthcare. The chemoluminescence was quantified by densitometric scanning of the films using the ImageJ image processing software, available at http://rsbweb.nih.gov/ij/. The densitometric measurements of the phosphorylated forms of JNK and p38 MAP kinases were normalized to total JNK and p38 antigens, measured from the same samples as loading controls.

Fluorescence microscopy

Cells were seeded at 5 x 10^4 per well in four-well chambered coverglass slides (NalgeNunc) and transfected the following day with 1 µg of plasmid. Images of ECFP and EYFP fluorescence were recorded 24 hours later with a Nikon Diaphot 300 microscope equipped with the XF114 (excitation 440nm, emission 480nm) and XF104 (excitation 500nm, emission 545nm) filter sets, respectively (Omega Optical, Brattleboro, VT).

RESULTS

Identification of new C21orf7 mRNA variants and structure of the C21orf7 gene

Five C21orf7 mRNA variants, called C21orf7-A to C21orf7-D and TAKL (designated here C21orf7-E) have been described before[6] (26, 27). We systematically searched GenBank for partial cDNA and expressed sequence tag (EST) data containing human TAKL exons. This identified sequences from 38 independent cDNA clones generated from a variety of cell and tissue types (Supplemental Table ST1). To complete this cDNA sequence data set, we obtained four EST clones of interest and fully sequenced their inserts. Analysis of the EST and cDNA sequences available in GenBank and of our additional sequence data eventually revealed nine new C21orf7 mRNA variants[7], which we designated by the letters F to N.

Structure of the C21orf7 gene

Alignment of the 14 C21orf7 mRNA sequences with the human chromosome 21 genomic sequence identified 17 exons, which are distributed over 98.4 kb of genomic DNA (Fig. 2A). All intervening sequences are GT-AG or, in one case, GC-AG introns (Supplemental Table ST2).

The first exon overlaps a long terminal repeat (LTR) and a CpG island while exons 5 and 6 overlap an Alu element and exon 9, another LTR (Supplemental Table ST2). The protein-coding regions of exons 13, 15, 16 and 17 are the only parts of C21orf7 that show significant homology to the TAK1 gene (Supplemental Fig. SF1). The fact that the two genes appear to have the same number of exons thus seems to be purely coincidental.

Alternative transcription start and polyadenylation sites

A surprising result was that only six of the 38 human C21orf7 cDNA sequences retrieved from GenBank contain exon 1: they correspond to variants A, B, C, F, G and M (Fig. 2B, Supplemental Table ST1). The other 29 other cDNAs appear to originate from alternative transcription start sites located downstream of exon 1. The majority of these cDNAs (26 out of 29) can be categorized into four groups based on their 5' exons. The largest group consists of 14 C21orf7-D clones, whose 5' ends correspond to exon 10, and the second largest group of seven C21orf7-L clones having exon 14 at their 5' ends (Fig. 2B, Supplemental Table ST1). This strongly indicates the existence of two alternative transcription start (TS) sites located at the 5' ends of exons 10 and 14. The other two groups consist of three independent TAKL-K cDNA clones whose sequences begin at exon 12 and the two clones representing the TAKL-K and TAKL-N variants, whose 5' ends match exon 7 (Fig. 2B).

Each of the four groups of cDNAs starting at exons 7, 10, 12 and 14 include clones produced by the oligo-cap method (Supplemental Table ST1), designed to identify transcription start sites (34). This indicates the existence of four alternative transcription start (TS) sites, designated here TS II to TS V in order of increasing distance from exon 1 and which are located at the 5' ends of exons 7, 10, 12 and 14, respectively (Fig. 2A and B).

GenBank also contains the sequences of three cDNA clones whose 5' ends cannot be assigned to any of the five TS sites. They are variants E, I and J, whose 5' ends correspond to exons 2, 9 and 11, respectively (Fig. 2B). They could correspond either to cDNAs with incomplete 5' ends or to the products of very rarely used alternative TS sites. The existence of a macaque TAKL-J cDNA clone (Supplemental Table ST3) suggests that this latter interpretation is the most likely in the case of exon 11.

.

Alternative polyadenylation and splicing

The six transcripts that originate from TS I differ as a result of alternative splicing involving exons 2, 3, 8, 10 or 13 and the two transcripts that originate from TS II (variants H and N) differ by alternative splicing of exons 7 and 8 (Figure 2B). It is interesting to note that although exon 10 appears to function primarily as a first exon for the C21orf7-D

mRNA, it also contains an alternative internal acceptor splice site that allows it to serve as an internal cryptic exon in variants B and H (Fig. 2B).

Almost all variants terminate with exon 17. The only exceptions are variants F and, possibly, G. Variant F terminates with a cryptic exon, exon 8, and a polyA tail, indicating that the exon can function as an alternative transcription terminator. However, as mentioned above, Exon 8 is also used as internal exon in C21orf7 mRNA variants H and N (Fig. 2B). This indicates that exon 8 contains an alternative internal donor splice site. Variant G is represented by a single partial sequence in GenBank and its last exon is therefore undetermined.

Predicted protein products of C21orf7

Five C21orf7 mRNA variants (B, C, H, M and N) contain open reading frames that terminate in an internal exon and are thus predicted to be destined for nonsense-mediated decay (34). Because their sequences may not be complete, the open reading frames of variants G, and I cannot be accurately predicted. The remaining C21orf7 variants are predicted to encode four proteins, which we have designated TAKL-1 to TAKL-4 (Fig. 2B).

TAKL-1 is encoded by the variants originating from TS III or TS IV (variants D, J and K). It is a 142-residue protein whose sequence is closely related to the last 143 residues of TAK1-a and TAK1-b, the region that contains the TAB2/3 -binding domain of the two isoforms (21, Supplemental Fig. SF1).

TAKL-2 is the predicted product of the TS V-originating mRNA variant, TAKL-L. It is a truncated version of TAKL-1 that consists of the last 87 residues of the latter (Fig. 2B and C).

The TAKL-3 and TAKL-4 proteins are encoded by some of the alternatively spliced variants that originate from TS I. TAKL-3 is the predicted product of variants A and E (Fig. 2B). It is a 242-residue protein whose last 119 residues are 51 % identical to the last 119 residues of TAK1-a and TAK1-b, but which also contains an amino-terminal domain (ATD) of 123 residues which does not have any significant homology to any other protein (26, 27). TAKL-4, which is encoded by variant F, consists primarily of the 123-residue ATD, followed by a carboxy-terminal glycine residue encoded by exon 8. It is the only predicted protein of C21orf7 that does not have any homology to TAK1 (Fig. 2B).

Evolution of the C21orf7 gene

We retrieved from GenBank genomic and cDNA TAKL sequences from most classes of vertebrates but could not identify any invertebrate orthologue. Comparison of TAKL genes from several species shows major differences in their exon composition (Fig. 3). The four exons that contain the TAKL-1 coding sequence, numbered 13, 15, 16 and 17, are the only exons that are conserved in all the vertebrate genes that we examined (Fig. 3). The other exons appeared at different stages in the evolution of vertebrates, starting with exon 10 in tetrapods and exons 11 and 14 in mammals. Exons 1-9 and 12 have a much more recent origin as they appeared in primates. Among the genes that we compared, the chimpanzee TAKL is the only orthologue of C21orf7 whose structure and predicted products closely resemble those of the human gene (Fig. 3). In the macaque TAKL gene, the regions homologous to C21orf7 exons 3, 4, 6 and 12 lack the donor or acceptor splice sites of the human exons and the regions homologous to the C21orf7 coding exons 4-7 do not form a continuous open reading frame (Supplemental Fig. SF2). Although it contains a structurally complete homologue of exon 1, the macaque TAKL gene therefore cannot produce TAKL-3 or TAKL-4.

These findings show that exons 13, 15, 16 and 17 correspond to the coding sequence of the primitive TAKL gene, which encoded TAKL-1. This indicates that TAKL probably originated as a duplicate of the TAK1 gene. Phylogenetic analysis of the TAKL-1 and TAK1 sequences suggests that this happened after the vertebrates differentiated from protochordates, but before the divergence of cartilaginous and bony fish (Supplemental Fig. SF3). The TAKL-1 protein has been highly conserved throughout the evolution of jawed vertebrates: the human and chicken TAKL-1 sequences are 71 and 75 % identical to that of *Xenopus tropicalis*, respectively, and are both 54 % identical to that of the dogfish shark, *Squalus acanthias* (Supplemental Fig. SF3).

In most classes of vertebrates, the evolution of the intron/exon structure of TAKL only involved the addition of untranslated exons, either upstream of exon 13 or, in the case of exon 14, potentially

allowing the expression of the shorter predicted protein, TAKL-2 (Fig. 3). The lack of non-human cDNA sequences homologous to C21orf7-L in GenBank suggests, however, that exon 14 does not function as an alternative transcription start site in most non-human mammals (Supplemental Table ST3). The extensive structural changes undergone by TAKL in primates involved the insertion of the LTR corresponding to exon 1 of C21orf7 and the gradual exonization of intronic elements. The final steps in the evolution of C21orf7 were the formation of exons 3, 4, 6 and 12, which occurred after the divergence of anthropoids from old world monkeys and enabled C21orf7 and its chimpanzee homologue to encode TAKL-3 and TAKL-4 (Fig. 3).

Detection of endogenous TAKL proteins

Two earlier reports indicate that C21orf7 mRNAs are preferentially expressed in peripheral blood leukocytes, relative to other tissues (26, 27). Because of the high heterogeneity of C21orf7 transcripts, we decided to monitor the expression of the gene at the protein level. A polyclonal antibody to a synthetic peptide of TAKL-1 was produced in rabbit and anti-TAKL immunoglobulins were then purified by affinity to the peptide. The sequence of the peptide was chosen to allow detection of human and murine TAKL proteins while minimizing the risk of cross-reaction with TAK1. Specificity tests carried out by immunoblotting lysates of transfected cells expressing TAKL-1, TAKL-3 or TAK1-a showed that the antibody could detect TAKL and did not cross-react with TAK1-a (Fig. 4A). These tests also showed that TAKL-1 and TAKL-3 migrated at positions corresponding to apparent molecular masses of 24 and 34 kDa, respectively, which are values well in excess of the molecular weights deduced from the sequences (16.4 and 27.2 kDa). The tagged versions of TAKL-1 (Fig. 4A) and TAKL-3 (not shown) also had apparent molecular masses that were in excess of the predicted values by about 8 kDa. When used to immunoblot cell lysates, the anti-TAKL antibody occasionally cross-reacted with unidentified cellular proteins of about 40 and 48 kDa (Fig. 4A and C). The antibody was unable to immunoprecipitate the recombinant TAKL proteins (data not shown) and our searches for endogenous TAKL proteins thus relied entirely on western blotting.

The anti-TAKL antibody identified an antigen of same apparent molecular weight as recombinant TAKL-3 (34 kDa) in human cell lines such as Hela (data not shown), PC-3 or Jurkat (Fig. 4B). The detection of the 34-kDa band was blocked by incubating the antibody with excess immunizing peptide (Fig. 4B). This identifies the 34-kDa antigen as TAKL-3. Interestingly, TAKL-3 was not detected in murine 3T3 cells (Fig. 4B) or monkey COS-7 cells (data not shown). Its absence from the 3T3 and COS-7 samples is consistent with it being a product of anthropoid-specific exons.

Association of TAKL with TAB2 and TAB3

The ability of TAKL-1 and TAKl-3 to associate with TAB2 or TAB3 was then investigated. In transfected mammalian cells, the T7-TAB2 protein co-precipitated with GST-tagged versions of TAKL-3 or TAKL-1, but did not co-precipitate with the GST-GUS control construct or with a GST-tagged construct corresponding to the amino-terminal domain (ATD) of TAKL-3 (Fig. 5A). These results thus show that TAKL-1 and the carboxy-terminal domain of TAKL-3 correspond to functional TAB2- and TAB3-binding domain.

T7-TAB2 and T7-TAB3 both migrated as doublets in control immunoblots of the lysates (Fig. 5A). These doublets have already been described: the lower bands correspond to the native forms of the proteins and the upper bands, to phosphorylated forms (13, 20). The phosphorylated forms of adapters were predominant relative to the non-phosphorylated forms in the control co-transfections with GST-GUS, but the adapters were predominantly unphosphorylated when they were co-expressed with GST-TAKL-1 or GST-TAKL-3 (Fig. 5A, middle panels). This indicates that their association with GST-TAKL-1 or GST-TAKL-3 prevented the adapters from interacting with an endogenous protein kinase. This interpretation is also supported by the observation that only the faster-migrating non-phosphorylated forms of TAB2 and TAB3 were observed in the GST-TAKL-1 and GST-TAKL-3 precipitates (Fig. 5A, top panels).

Fluorescent microscopy of transfected cells expressing EYFP-TAKL-1 showed that the protein distributed evenly in both cytoplasmic and nuclear compartments, whereas the EYFP-TAKL-3 protein distributed evenly in the cytoplasm but was excluded

from the nucleus (Fig. 5B). Unlike the TAKL constructs, ECFP-TAB2 and ECFP-TAB3 adopted a punctate distribution in the cytoplasm of transfected cells (Fig. 5B). This indicated that the fluorescent TAB2 and TAB3 associated in complexes, which is consistent with the reported ability of TAB2 to self-associate (19). In cells that co-expressed ECFP-TAB3 and either YFP-TAKL-1 or EYFP-TAKL-3, the pools of YFP-TAKL split into two fractions: one fraction consisted of evenly distributed yellow fluorescent proteins while the second fraction accumulated in punctate patterns that indicated the recruitment of EYFP-TAKL molecules to complexes (Fig. 5C). Merging images of the cyan and yellow fluorescent constructs confirmed that the punctate YFP-TAKL co-localized with ECFP-TAB3 (Fig. 5C). Similar results were obtained when CFP-TAB2 was used instead of CFP-TAB3 (data not shown). This indicated that the association of TAKL with either TAB2 or TAB3 involved quantitatively significant fractions of the cellular pools of each protein.

To test whether or not the TAKL-TAB2 complexes were capable of associating with TRAF6, we carried out co-immunoprecipitation experiments from cells co-transfected with FLAG-TRAF6, T7-TAB2 and either GST-TAKL-1 or GST-TAKL-3. The TAKL proteins co-precipitated with FLAG-TRAF6 in the transfections that also included T7-TAB2, but did not do so in control transfections carried out without the adaptor (Fig. 5C). These results show that TAKL-1 and TAKL-3 are not capable of interacting directly with TRAF6 but that they can form ternary complexes with TRAF6 and TAB2 via their interactions with the latter protein. They also indicate that TAKL-3 and TAKL-1 do not interfere with the binding of TAB2 to TRAF6 and that they are therefore potential components of TRAF6 and TRAF2 signaling complexes.

We also investigated whether or not TAKL proteins might be capable of associating with themselves and with several components of the canonical IL-1/TLR signaling pathway. We found that GST-tagged TAKL-3 and TAKL-1 both failed to associate with co-expressed EYFP-tagged TAKLs, EGFP-TAB1, EGFP-TAK1, EGFP-IRAK, FLAG-Pellino1, Flag-Pellino2, HA-tagged IKK-α, HA-IKK-β or IKK-γ in mammalian cells (data not shown). The TAKL proteins thus appear to be unable to form homodimers or to associate with any of the pathway components that we tested other than TAB2 and TAB3.

Inhibition of pro-inflammatory signaling by TAKL-1

We then investigated the effects of over-expressed TAKL-1 on the expression of a luciferase reporter construct containing a fragment of the IL-8 promoter, pIL-8-Luc. Expression of the construct is strongly activated by IL-1 or TNF in COS-7 and HeLa cells, and is also activated by LPS stimulation in RAW264.7 cells (Fig. 6). We found that transfection of these cells with 50 ng of TAKL-1 expression construct prior to the stimulations partially inhibited all these responses (Fig. 6). In some experiments, we compared the effects of TAKL-1 to those of the a442 construct, which contains the TAB2/TAB3-binding domain of TAK1-a and is 50% identical to the TAKL-1 sequence (Fig. 1 and Supplemental Fig. SF1). The results showed that the inhibitory effects of TAKL-1 and a442 were quantitatively very similar (Fig. 6A). In contrast to TAKL-1 and a442, experiments carried out with TAKL-3 expression constructs showed no significant inhibitory effect on reporter activity in most cases, although a weak inhibitory effect was observed occasionally (data not shown).

Interference of TAKL-1 3 with IL-1R1 and TLR signaling pathway components

To further characterize the roles of TAKL-1 and TAKL-3 on the functioning of TRAF6 complexes, we then carried out experiments in which the pIL-8-Luc reporter was activated by co-transfected expression constructs encoding IRAK, FLAG-TRAF6, TAK1 or HA-IKK-β. The results showed that TAKL-1 could inhibit both IRAK- and TRAF6- induced activation of the reporter (Fig. 7A and B), but only had a comparatively very weak inhibitory effect on TAK1-induced reporter activation (Fig. 7C), and did not impinge at all on IKK-β-induced reporter expression (Fig. 7D). These results indicate that TAKL-1 probably inhibits activation of the IL-8 promoter by interfering with one or several specific pathway components acting between TRAF6 and IKK-β.

In experiments where the a442 construct was used, it was found to have an inhibitory effect that was quantitatively very similar to that of TAKL-1 (Fig. 7A). Altogether, these results were thus consistent with the hypothesis that TAKL-1 and the

a442 construct acted through similar mechanisms, which presumably involved their association with endogenous TAB2 or TAB3 proteins, thereby possibly preventing recruitment of TAK1 to TRAF6 complexes.

In marked contrast to TAKL-1, the TAKL-3 expression construct did not significantly affect the expression of the IL-8 promoter construct in these experiments (Fig. 7B and C). This result was consistent with the lack of effects of TAKL-3 on cytokine- or LPS-induced reporter expression mentioned in the previous section and suggests that functional differences exist between TAKL-1 and TAKL-3.

Interference of TAKL-1 and TAKL-3 with JNK activation

We also monitored the effects of TAKL-1 and TAKL-3 on the activation of downstream kinase cascades by IL-1-β. The results showed that the IL-1-induced activation of JNK/SAPK1 was inhibited in cells expressing either GST-tagged TAKL-1 or GST-TAKL-3 (Fig. 8A and Supplemental Fig. SF4). By contrast, the activation of the p38 and p44/42 subtypes of MAP kinases and the degradation of IκB were not significantly affected by either construct (Fig. 8B and C; Supplemental Fig. SF4). Both the dominant-negative mutant of TAK1-a, K63W, and the a442 deletion mutant inhibited JNK activation in a similar manner as TAKL-1 and TAKL-3 (Fig. 8A, Supplemental Fig. SF4). The specificity of inhibition of the JNK kinase pathway by TAKL-1 and TAKL-3 thus closely resembled the specific effects caused by the kinase-inactive TAK1 mutant or the TAB2/3-binding domain of TAK1 alone in our experimental system.

In contrast to K63W and a442, a construct encoding the carboxy-terminal half of the TAK1-c sequence, c284 (Fig. 1), had no inhibitory activity on JNK (Fig. 8A). This suggests that the inhibitory effects of K63W and a442 on JNK depended on their ability to bind TAB2 or TAB3, which c284 lacks.

DISCUSSION

The TAKL gene attracted our attention because of its strong homology to the TAB2/TAB3-binding domain of TAK1-a and TAK1-b. The human TAKL gene, C21orf7, was already known to produce five mRNA variants (26, 27). We identified several new mRNA variants and characterized the intron/exon structure of the gene. We found that C21orf7 contains seventeen exons and can produce alternative mRNA variants through a combination of alternative transcription starts and alternative splicing mechanisms. This allows it to produce 14 known alternative mRNAs and potentially produce four predicted proteins, which we named TAKL-1 to TAKL-4.

Comparisons between C21orf7 and the TAKL genes of other species then showed that in most vertebrates, TAKL possesses a much simpler structure than C21orf7 and encodes a single protein, TAKL-1, whose entire sequence is a closely related to the last 143 residues of TAK1-a/b. The TAKL gene probably originated from a duplication of a genomic segment containing exons 14 to 17 of TAK1, or from a duplication of the entire TAK1 gene followed by the selective loss of exons 1 to 13. Our analysis indicates that this occurred after the vertebrates differentiated from protochordates, but before the divergence of cartilaginous and bony fish. Two genome duplications probably occurred in this interval (36), which further supports the hypothesis that TAKL is the remnant of a full duplicated TAK1 gene. Duplicate genes that do not differentiate functionally from their paralogues tend to get silenced or deleted whithin about 4 million years (37). The conservation of a functional TAKL-1-coding gene in most classes of jawed vertebrates thus strongly suggests that the protein has a significant physiological role.

The identification of exons 1 and 9 of C21orf7 as LTR fragments and of two ATD-coding exons as parts of an Alu element (Supplemental Table S1) indicates that the colonization of the genomic region upstream of TAKL by transposable elements and their subsequent exonization played a significant part in the evolution of TAKL in primates. This hypothesis is also consistent the structure of the macaque TAKL gene, which contains non-functional precursors of some of the C21orf7 exons. Alu motifs expanded in the primate evolutionary lineage and have been linked to the evolution of other genes, for example the TNF receptor 2 gene (38, 39).

We then showed that TAKL-1 and TAKl-3 can associate with TAB2 or TAB3 and that the association with TAB2 allows the TAKL proteins to be recruited to TRAF6 complexes. This identified

TAKL-1 and TAKL-3 as potential components of TRAF2- and TRAF6-mediated signaling pathways.

Expression of TAKL-1 cDNA in transfected cells inhibited IL-1-, TNF- or LPS-induced expression of the pIL-8-Luc promoter/reporter in a dose-dependent manner. Experiments in which expression of pIL-8-Luc was induced by co-transfected signaling pathway components indicated that the action of TAKL-1 was epistatic to IRAK and TRAF6 but hypostatic to IKK-β. We also found that TAKL-1 expression specifically inhibited the activation by IL-1 of the JNK subtype of MAP kinase but, had no significantly effect on the activation of p38 and p44/42 or the degradation of IκB.

The simplest interpretation of our results is that TAKL-1 competes with TAK1 for binding to TAB2- or TAB3, thereby preventing recruitment and activation of the kinase by TRAF complexes (Fig. 9A). This model is supported by the inhibitory effect of TAKL-1 on TAK1-induced expression of pIL-8-Luc (Fig. 7C). Also in agreement with this model are the observations that the selective effect of TAKL-1 on JNK is identical to that of the dominant-negative mutant of TAK1, K63W, and that the a442 construct, which corresponds to the TAB2/3-binding domain of TAK1-a/b, also inhibits JNK activation, whereas the c284 construct, which corresponds to the remainder of non-catalytic region of TAK1, does not (Fig. 8).

The lack of effect of K63W or TAKL-1 on p38 activation and IκB degradation was unexpected, since expression of K63W or blockade of TAK1 expression have often been reported to prevent activation of p38 (4, 13, 21, 40, 42) or NF-κB (1, 4, 8, 9, 19-21, 40) in addition to JNK (1, 4, 8, 19, 40). In a few other experimental systems, however, JNK appears to be the primary downstream target of the TRAF6/TAB2/TAK1 module (4, 23, 41). It is possible that in these experimental systems and in ours, the activation of p38 and the degradation of IκB are mediated by TAK1-independent mechanisms, perhaps involving the interactions of TAB1 with TRAF6 and p38 (42) or the direct recruitment of the IKKs to TRAF complexes by TAB2 and TAB3 (Fig. 9). The latter hypothesis is supported by observations that TAB2 associates with IKK-α (24) and that over-expression of TAB2 or TAB3 induces NF-κB activation in a TAK1-independent manner (20, 25).

Alternatively, the specific inhibition of JNK that we observed could be explained by the recruitment of inhibitors of JNK to TRAF complexes via their association with TAKL-1. This is suggested by the identification of G-protein pathway suppressor 2 (GPS2), which inhibits the JNK pathway through unknown mechanisms (43), as a partner of TAKL-1 (44). Further studies will be needed to determine whether TAKL-1 functions as a competitive inhibitor of TAK1 recruitment or by recruiting GPS2, or other inhibitors of signaling.

Unlike TAKL-1, TAKL-3 did not inhibit expression of pIL-8-Luc. This was unexpected considering that like TAKL-1, TAKL-3 associates with TRAF6-TAB2 complexes and inhibits both the phosphorylation of over-expressed TAB2 or TAB3 and the IL-1-induced activation of JNK. This suggests that TAKL-1, but not TAKL-3, may inhibit a component of the IL-1-signaling pathway other than JNK, which remains to be identified. Two earlier reports identified peripheral blood leukocytes as a cell type where the expression of C21orf7 mRNAs was particularly high (26, 27). This suggest that TAKL-1 and TAKL-3 might be preferentially expressed in cells involved in immune reactions, where they may function to regulate or inhibit TRAF signalling based responses.

The human TAKL gene, C21orf7 is a resident of the critical region of chromosome 21, which contains the genes whose over-expression may contribute to Down syndrome. A recent study of the Ts65Dn mouse model of the syndrome suggested that in certain tissues, expression of murine TAKL (also known as ORF63) was compensated for the presence of an extra copy of the gene (45). Although several primate-specific genes have been identified in the critical region, the structural differences between C21orf7 and ORF63 do not appear to have been noticed before. The ability of C21orf7 to produce many alternative transcripts could lead to significant differences in the regulation of expression of TAKL-1 between mouse and humans (35). It is also possible that the recently evolved TAKL-3 and TAKL-4 proteins have added new functions to C21orf7. Further investigations will be needed to fully assess the roles that the TAKL/C21orf7 gene may play in TRAF-mediated signaling or Down syndrome.

REFERENCES

1. Shim, J. H., Xiao, C., Paschal, A. E., Bailey, S. T., Rao, P., Hayden, M. S., Lee, K. Y., Bussey, C., Steckel, M., Tanaka, N., Yamada, G., Akira, S., Matsumoto, K., and Ghosh, S. (2005) *Genes Dev.* **19,** 2668-2681
2. Sorrentino, A., Thakur, N., Grimsby, S., Marcusson, A., von Bulow, V., Schuster, N., Zhang, S., Heldin, C. H., and Landström, M (2008) *Nature Cell Biol.* **10,** 1199-1207
3. Wan, Y. Y., Chi, H., Xie, M., Schneider, M. D., and Flavell, R. A. (2006) *Nature Immunol.* **7**, 851-858
4. Sato, S., Sanjo, H., Takeda, K., Ninomiya-Tsuji, J., Yamamoto, M., Kawai, T., Matsumoto, K., Takeuchi, O., and Akira, S. (2005) *Nature Immunol*. **6,** 1087-1095
5. Sun, L., Deng, L., Ea, C. K., Xia, Z. P., and Chen, Z. J. (2004) *Mol. Cell* **14,** 289-301
6. Winkel, A., Stricker, S., Tylzanowski, P., Seiffart, V., Mundlos, S., Gross, G., and Hoffmann, A. (2008) *Cell Signal.* **20,** 213421-44
7. Takaesu, G., Surabhi, R.M., Park, K. J., Ninomiya-Tsuji, J., Matsumoto, K., and Gaynor, R. B. (2003) *J. Mol. Biol.* **326**, 105-115
8. Mizukami, J., Takaesu, G., Akatsuka, H., Sakurai, H., Ninomiya-Tsuji, J., Matsumoto, K., and Sakurai, N. (2002) *Mol. Cell. Biol.* **22**, 992–1000
9. Morlon, A., Munnich, A., and Smahi, A. (2005) *Human Mol. Genet.* **14,** 3751-3757
10. Dempsey, C. E., Sakurai, H., Sugita, T., and Guesdon, F. (2000) *Biochim. Biophys. Acta* **1517**, 46-52
11. Watkins, S. J., Jonker, L., and Arthur, H. M. (2006). *Cardiovasc. Res.* **69**, 432-439
12. Kodym, R., Kodym, E., and Story, M. D. (2008) *RNA* **14,** 535-542.
13. Ishitani, T., Takaesu, G., Ninomiya-Tsuji, J., Shibuya, H., Gaynor, R.B., and Matsumoto, K. (2003) *EMBO J.* **22**, 6277-6288
14. Blonska, M., Shambharkar, P. B., Kobayashi, M., Zhang, D., Sakurai, H., Su, B., and Lin, X. (2005) J. *Biol. Chem.* **280,** 43056-43063
15. Cusson-Hermance, N., Khurana, S., Lee, T. H., Fitzgerald, K. A., and Kelliher, M. A. (2005) *J. Biol. Chem.* **280**, 36560-36566
16. Kawai, T., Sato, S., Ishii, K. J., Coban, C., Hemmi, H., Yamamoto, M., Terai, K., Matsuda, M., Inoue, J., Uematsu, S., Takeuchi, O., and Akira, S. (2004) *Nature Immunol.* **5**, 1061-1068
17. Lomaga, M. A., Yeh, W.-C., Sarosi, I., Duncan, G. S., Furlonger, C., Ho, A., Morony, S., Capparelli, C., Van, G., Kaufman, S., van der Heiden, A., Itie, A., Wakeham, A., Khoo, W., Sasaki, T., Cao, Z., Penninger, J. M., Paige, C. J., Lacey, D. L., Dunstan, C. R., Boyle, W. J., Goeddel, D. V., and Mak, T. W. (1999) *Genes Dev.* **13**, 1015–1024
18. Naito, A., Azuma, S., Tanaka, S., Miyazaki, T., Takaki, S., Takatsu, K., Nakao, K., Nakamura, K., Katsuki, M., Yamamoto, T., and Inoue, J. (1999) *Genes Cells* **4**, 353–362
19. Takaesu, G., Kishida, S., Hiyama, A., Yamaguchi, K., Shibuya, H., Irie, K., Ninomiya-Tsuji, J., and Matsumoto, K. (2000) *Mol. Cell* **5**, 649-658
20. Jin, G., Klika, A., Callahan, M., Faga, B., Danzig, J., Jiang, Z., Li, X., Stark, G. R., Harrington, J., and Sherf, B. (2004) *Proc. Natl. Acad. Sci.* USA **101,** 2028-2033
21. Besse, A., Lamothe, B., Campos, A. D., Webster, W. K., Maddineni, U., Lin, S.-C., Wu, H., and Darnay, B. G. (2007) *J. Biol. Chem.* **282**, 3918-3928
22. Wang, C., Deng, L., Hong, M., Akkaraju, G. R., Inoue, J.-I., and Chen, Z. J. (2001) *Nature* **412**, 346-351
23. Habelhah, H., Takahashi S., Cho, S. G., Kadoya, T., Watanabe, T., and Ronai, Z. (2004) *EMBO J.* **23**, 322-332
24. Kishida, S., Sanjo, H., Akira, S., Matsumoto, K., and Ninomiya-Tsuji, J. (2005) *Genes Cells* **10,** 447-454
25. Kanayama, A., Seth, R. B., Sun, L., Ea, C. K., Hong ,M., Shaito, A., Chiu, Y. H., Deng, L., and Chen, Z. J. (2004) *Mol. Cell* **15,** 535-348
26. Reymond, A., Friedli, M., Henrichsen, C. N., Chapot, F., Deutsch, S., Ucla, C., Rossier, C.,

Lyle, R., Guipponi, M., and Antonarakis, S. E. (2001) *Genomics* **78**, 46-54

27. Li, J., Ji, C., Yang, Q., Chen, J. Gu, S. Ying, K., Xie, Y., and Mao, Y. (2004) *Biochemical Genetics* **42,** 129-137
28. Kiss-Toth, E., Wyllie, D. H., Holland, K., Marsden, L., Jozsa, V., Oxley, K. M., Polgar, T., Qwarnström, E. E., and Dower, S. K. (2006) *Cellular Signaling* **18**, 202-214
29. Ross, K., Yang, L., Dower, S., Volpe, F., and Guesdon, F (2002) *J. Biol. Chem.* **277**, 37414-37421
30. Parker, L. C., Whyte, M. K. B., Vogel, S. N., Dower, S. K., and Sabroe, I. (2004) *J. Immunol.* **172**, 4977-4986
31. Parker, L. C., Jones, E. C., Prince, L. R., Dower, S. K., Whyte, M. K., and Sabroe, I. (2005) *J. Leukoc. Biol.* 7**8,** 1301-1305
32. Horton, R. M. (1995) *Mol. Biotechnol.* **3**, 93-99
33. Greetham, D., Ellis, C. D., Mewar, D., Fearon, U., Nic an Ultaigh, S., Veale, D. J., Guesdon, F., and Wilson, A. G. (2007). *Human. Mol. Genet.* **16**, 3027–3036
34. Suzuki, Y., Yamashita, R., Shirota, M., Sakakibara, Y., Chiba, J., Mizushima-Sugano, J., Nakai, K., and Sugano, S. (2004) *Genome Res.* **14**, 1711-1718
35. Hillman, R. T., Green, R. E., and Brenner, S. (2004) *Genome Biol.* **5,** R8
36. Dehal, P., and Boore, J. L. (2005) *PLoSi Biol.* **3**, 1700-1708
37. Lynch, M., and Conery, J. S. (2000) *Science* **290**, 1151-1155
38. Krull, M., Brosius, J., and Schmitz, J. (2005) *Mol. Biol. Evol.* **22**, 1702-1711
39. Singer, S. S., Mannel, D. N., Hehlgans, T., Brosius, J., and Schmitz, J. (2004) *J. Mol. Biol.* **341**, 883-886
40. Thiefes, A., Wolter, S., Mushinski, J. F., Hoffmann, E., Dittrich-Breiholz, O., Graue, N., Dorrie, A., Schneider, H., Wirth, D., Luckow, B., Resch, K., and Kracht, M. (2005) *J. Biol. Chem.* **280**, 27728-27741
41. Uemura, N., Kajino, T., Sanjo, H., Sato, S., Akira, S., Matsumoto, K., and Ninomiya-Tsuji, J. (2006) *J. Biol. Chem.* **281**, 7863-7872
42. Ge, B., Gram, H., Di Padova, F., Huang, B., New, L., Ulevitch, R. J., Luo, Y., and Han, J. (2002) *Science* **295**, 1291-1294
43. Zhang, J., Kalkum, M., Chait, B. T., and Roeder, R. G. (2002) *Mol. Cell* **9**, 611-623
44. Rual, J. F., Venkatesan, K., Hao, T., Hirozane-Kishikawa, T., Dricot, A., Li, N., Berriz, G. F., Gibbons, F. D., Dreze, M., Ayivi-Guedehoussou, N., Klitgord, N., Simon, C., Boxem, M., Milstein, S., Rosenberg, J., Goldberg, D. S., Zhang, L. V., Wong, S. L., Franklin, G., Li, S., Albala, J. S., Lim, J., Fraughton, C., Llamosas, E., Cevik, S., Bex, C., Lamesch, P., Sikorski, R. S., Vandenhaute, J., Zoghbi, H. Y., Smolyar, A., Bosak, S., Sequerra, R., Doucette-Stamm, L., Cusick, M. E., Hill, D. E., Roth, F. P., and Vidal, M. (2005) *Nature* **437**, 1173-1178
45. Kahlem, P., Sultan, M., Herwig, R., Steinfath, M., Balzereit, D., Eppens, B., Saran, N. G., Pletcher, M. T., South, S. T., Stetten, G., Lehrach, H., Reeves, R. H., and Yaspo, M. L. (2004) *Genome Res.* **14**, 1258-1267

FOOTNOTES

*We would like to thank professor Kunihiro Matsumoto (Nagoya University, Japan), Professor L. A. J. O'Neill (Trinity College, Dublin, Ireland) and Dr. Endre Kiss-Toth (University of Sheffield) for kindly providing us with the T7-TAB2, FLAG-K63W and pIL-8-Luc constructs. This work was funded by the Arthritis Research Campaign (Project Grant 14366), the Sheffield Hospital Charitable Trust (Research Grant No 7815) and the Wellcome Trust (Vacation Scholarship VS/01/SHE/10/CH/TH/JJ to V.T.).

[1]Present address: Section of Immunology and Infection, Division of Cell and Molecular Biology, Faculty of Life Sciences, Imperial College, London, SW7 2AZ, UK

[2]Present address: Cell Survival Signalling Laboratory, Centre for Molecular Oncology, Institute of Cancer, Charterhouse Square, London, EC1 6BQ, UK

[3]Present address: School of Pharmacy and Biomolecular Sciences, Liverpool John Moores University, Byrom Street, Liverpool, L3 3AF, UK

[4]The abbreviations used are: ATD, amino-terminal domain; ECFP, Enhanced cyan fluorescent protein; EGFP, Enhanced green fluorescent protein; EYFP, Enhanced yellow fluorescent protein; GPS2, G-protein pathway suppressor 2; Glutathione S transferase; GUS, β-glucuronidase; HRP, horseradish peroxidase; IκB, inhibitor of NF-κB; IKK, IκB kinase; IL, interleukin; IL-1R1, IL-1 Receptor 1; IRAK, IL-1R1-activated kinase; JNK, c-Jun-N-terminal kinase; LPS, lipopolysaccharide; MAP kinase, Mitogen-activated protein kinase; NF, Nuclear factor; RANK, receptor activator of NF-κB; TAB, TAK1-binding protein; TAK1, TGF-β-activated kinase; TAKL, TAK1-like; TGF, Transforming Growth Factor; TLR, Toll-like receptor; TNF, Tumor necrosis factor; TRAF, TNF receptor-associated factor; TS, transcription start.

[5]Ellis, C. D. and Guesdon, F., unpublished observations.

[6]The GenBank accession numbers of C21orf7-A to C21orf7-D are AF269161 to AF269164 and that of TAKL (aka C21orf7-E) is AY171599.

[7]The sequences of the IMAGE clone inserts representative of C21orf7 mRNA variants F, I, J and L have been deposited in GenBank under accession numbers EF219157 to EF219160. Third-party annotations of C21orf7 mRNA variants E (AY171599), G (DA815639) and K (DA021298) have been deposited under accession numbers BK0006116, BK006114 and BK006115, respectively.

FIGURES

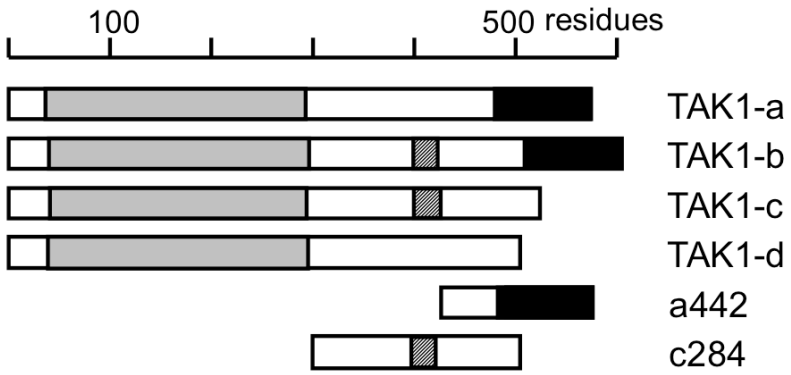

Figure 1. TAK1 isoforms and deletion mutants used in this study. The *light grey* and *hatched boxes* represent respectively the kinase domain and the region encoded by alternative exon 12 (10). The *black box* represents the region encoded by alternative exon 16 and exon 17, which contains the TAB2/TAB3-binding domain[5] (10, 21). The a442 and c284 deletion mutants used in this study correspond to residues 442 to 579 of TAK1-a and residues 284 to 518 of TAK1-c respectively.

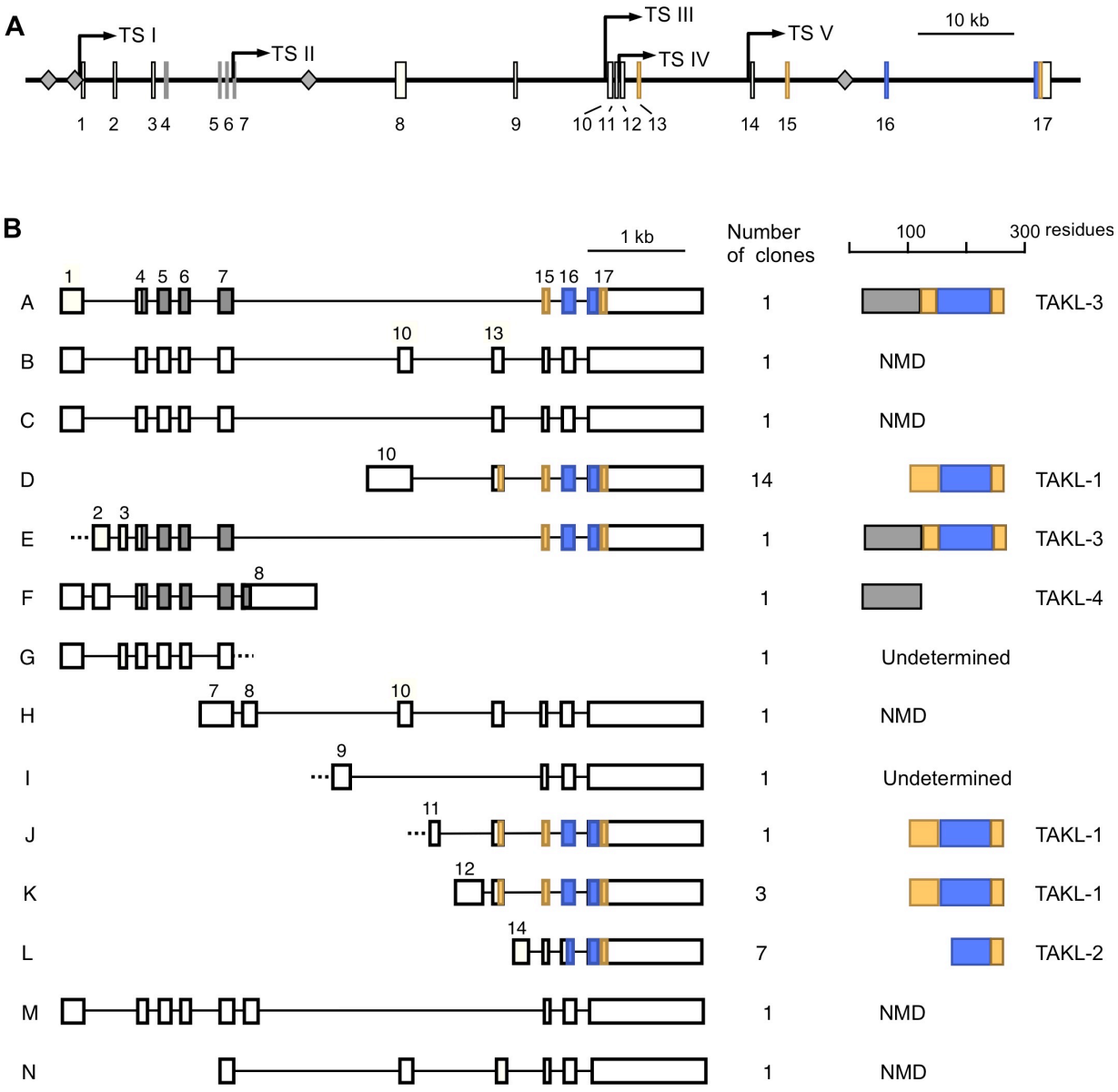

Figure 2. Structures of C21orf7 and its products. ***A***, Structure of the C21orf7 gene. Exons are shown as *white vertical bars* except for the regions containing fragments of open reading frames which are coloured in *blue* for the coding regions homologous to the TAB2/3 binding domain of TAK1, *yellow* for those homologous to other regions of TAK1 and *grey* for the coding regions with no significant homology to other proteins., CpG islands are shown as *diamonds* and transcription start sites (TS) as *arrows*. *Exon numbers* are indicated. ***B***, Exon composition and protein products of C21orf7 mRNA variants. The mRNA variants A to N are represented on the left-hand side. Their open reading frames are shaded in *grey*, *yellow* or *blue* as in panel A. Incomplete or unconfirmed sequence ends are indicated by *dotted lines*. The numbers of independent cDNA clones of each variant found in GenBank are indicated. The predicted protein encoded by each variant is shown on the right hand side, except in the case of variants destined for nonsense-mediated decay (NMD) or for which open reading frames were not securely identified. The regions of the proteins homologous to the TAB2/3-inding domain of TAK1 are shown in blue and those homologous to other regions of TAK1 are in yellow.

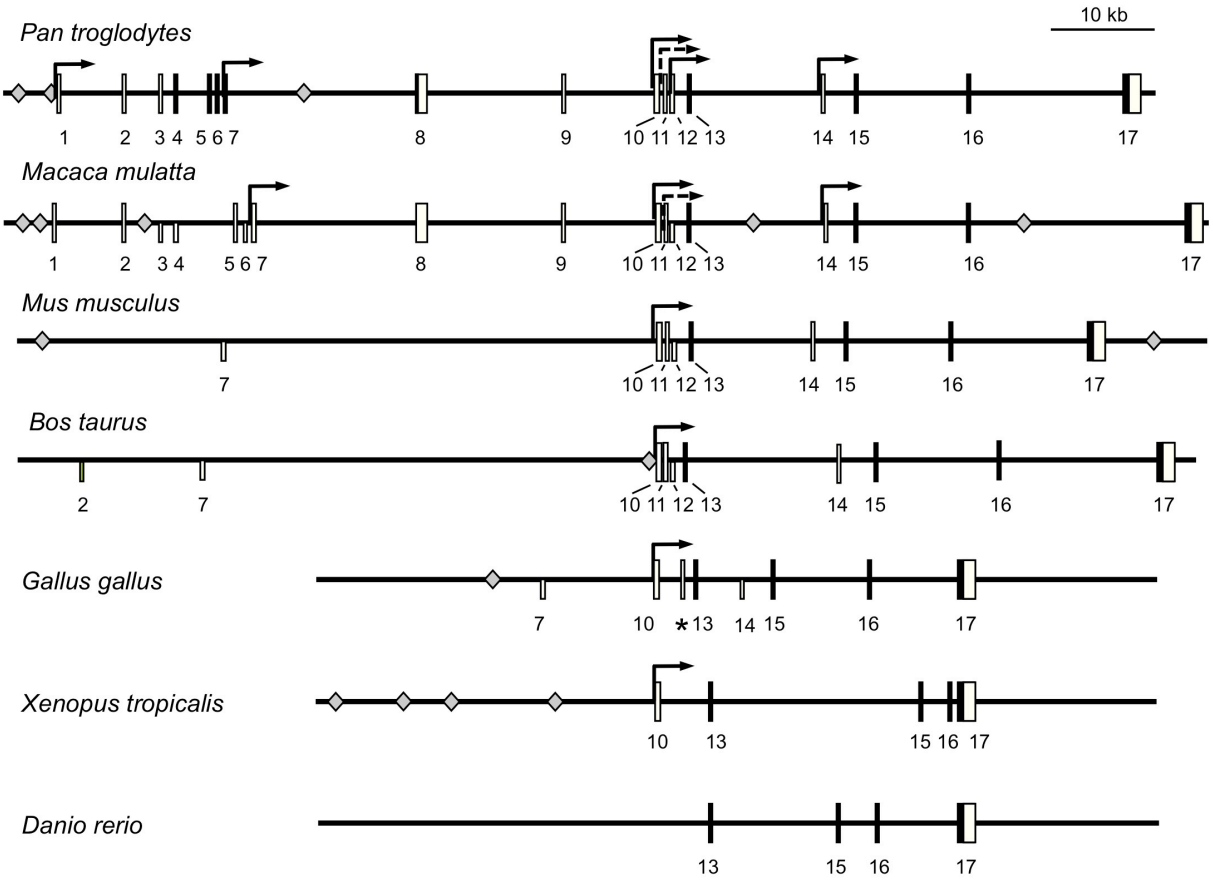

Figure 3. Intron/exon structures of vertebrate TAKL genes. The TAKL genes of chimpanzee (*P. troglodytes*), macaque (*M. mulatta*), mouse (*M. musculus*), *Bos Taurus*, chicken (*G. gallus*), *Xenopus tropicalis* and *Danio rerio* are shown. Regions of the genomic sequences that are homologous to C21orf7 exons are represented by *vertical bars* and designated by the same number as their C21orf7 homologues (see Fig. 2*A*). The *full-size vertical bars* represent exons which we deem to be functional, as determined either from experimental evidence (EST sequences) or by the conservation of donor and acceptor splice sites in genomic sequences. Coding and non-coding exons are colored *black* and *white*, respectively. The *half-size vertical bars* represent regions homologous to C21orf7 exons but which lack the donor or acceptor splice sites of their human counterparts. CpG islands are represented as *diamonds.* The a*sterisk* identifies an untranslated chicken exon identified by analysis of EST data but has no homologues in other TAKL genes. Actual transcription start sites (identified from by alignments of genomic and EST sequences) and predicted transcription start sites (based on conservation of 5' ends of exons and nearby upstream sequences) are both represented by *arrows*. The actual TSs are those of *X tropicalis*, *G. gallus*, *B. Taurus*, *M. musculus* and the site located upstream of exon 11 in *M. mulatta* (represented by a *dashed arrow*),

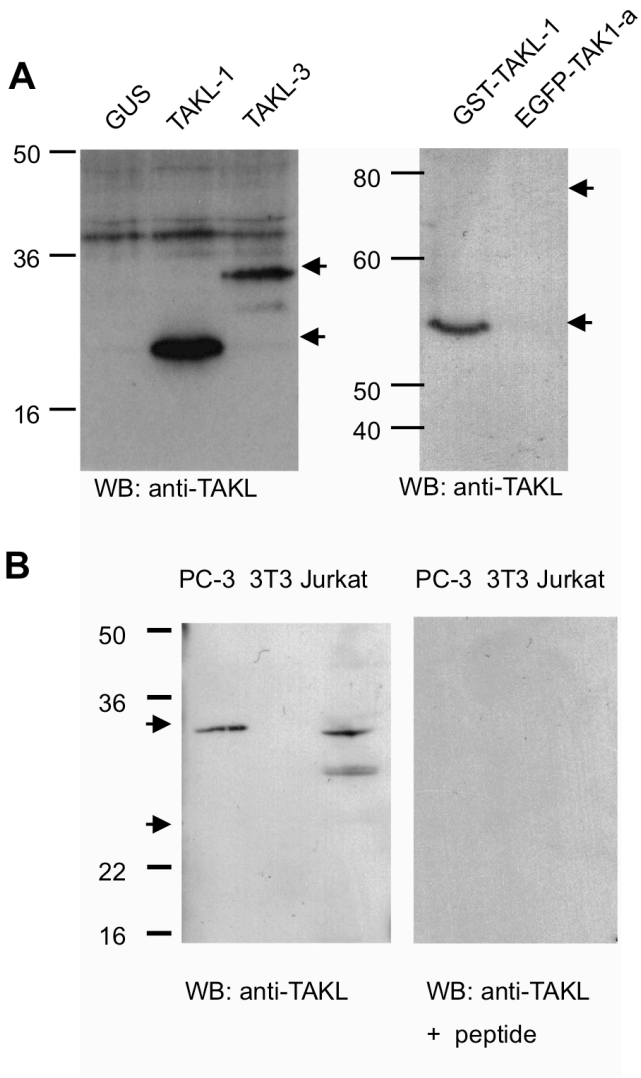

Figure 4. Detection of endogenous TAKL proteins. ***A***, Test of the affinity purified anti-TAKL antibody. Immunoblots of lysates of HeLa cells that had been transfected 24 hours earlier with expression constructs encoding GUS (negative control), TAKL-1, TAKL-3, GST-TAKL-1 and EGFP-TAK1-a are shown. The positions of the recombinant proteins are indicated by *arrowheads*. ***B***, Immunoblots of lysates of PC-3, 3T3 and Jurkat cell lines. Each lane was loaded with 40 µg of protein. The left-hand blot was obtained with the anti-TAKL antibody and the right-hand blot, with the same antibody in the presence of a 1000-fold excess (30 µM) of immunizing peptide. The *arrowheads* show the migration positions of recombinant TAKL-3 (*top*) and TAKL-1 (*bottom*) used as molecular mass standards.

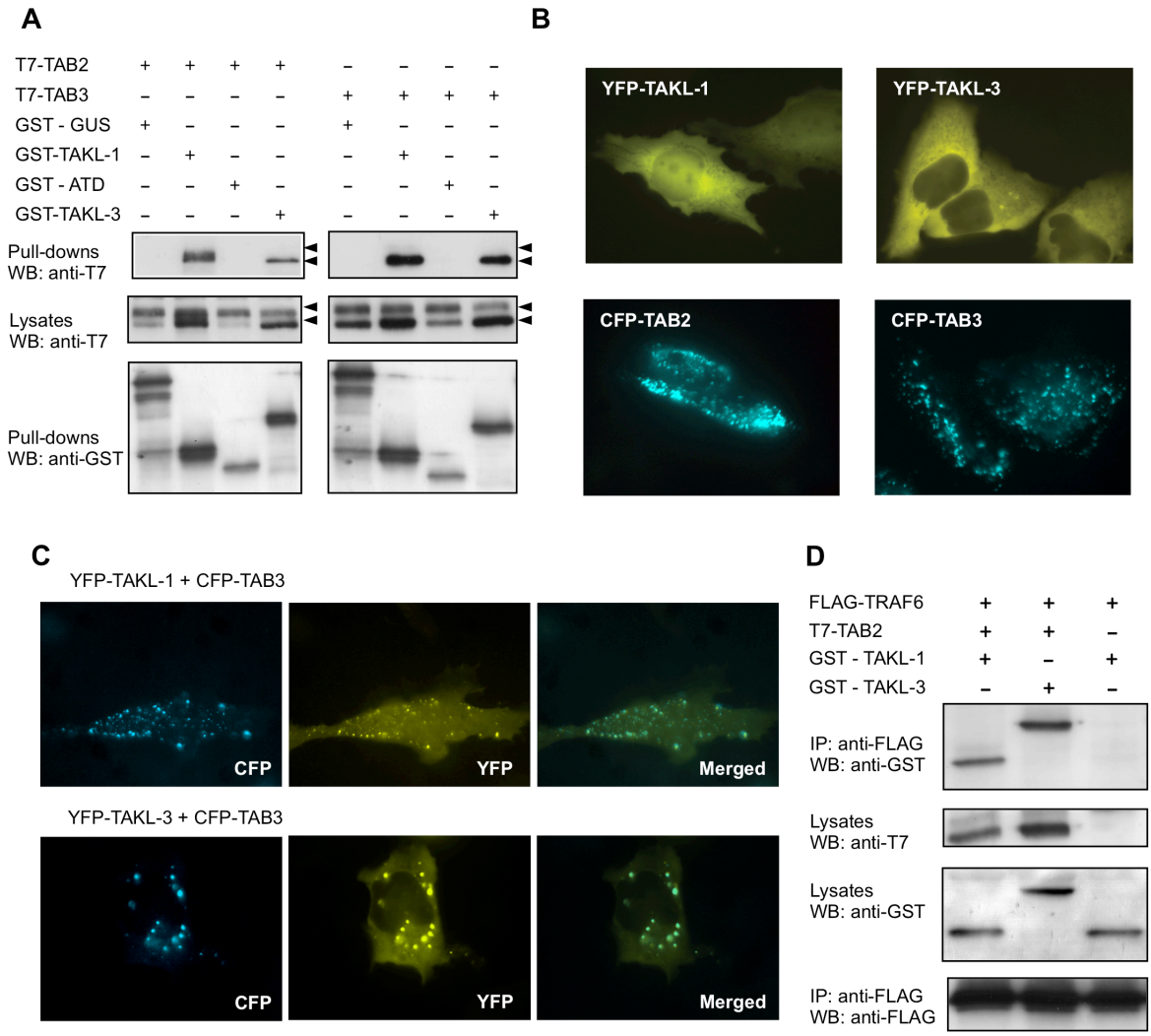

Figure 5. Association of TAKL-1 and TAKL-3 with signaling pathway components. ***A***, Interactions of TAKL proteins with TAB2 and TAB3. HeLa cells were co-transfected with constructs encoding either T7-TAB2 or T7-TAB3 and GST-TAKL-1, GST-ATD or GST-TAKL-3. The cells were lysed 24 hours later and the GST-tagged proteins were then precipitated with glutathione beads. The pulled-down materials (*top panel*) and samples of the lysates (*middle and bottom panels*) were then immunoblotted with anti-T7 (*top and middle panels*) and anti-GST (*bottom panels*) antibodies. The *arrowheads* indicate the migration positions of the two components of the TAB2 and TAB3 doublets. ***B***, Intracellular distributions of fluorescent tagged TAKL-1, TAKL-3 and TAB3. HeLa cells were transfected with constructs encoding EYFP-TAKL-1, EYFP-TAKL-3 or ECFP-TAB3. Images were recorded using a 60x oil immersion lens and the fluorescent filter set appropriate to each construct. ***C****, R*ecruitment of YFP-tagged TAKL-1 and TAKL-3 to TAB3 complexes. HeLa cells were co-transfected with constructs encoding ECFP-TAB3 and either EYFP-TAKL-1 (*top row*) or EYFP-TAKL-3 (*bottom row*). Images were recorded 24 hours later using a 60x oil immersion lens with both yellow and cyan fluorescence filter sets. ***D****, T*AB2-mediated association of TAKL-1 and TAKL-3 with TRAF6. HEK293T cells were co-transfected with constructs encoding FLAG-TRAF6, and either GST - TAKL-1 or GST - TAKL-3, in the presence or absence of T7-TAB2 construct as indicated. Immunoprecipitations were carried with the anti-FLAG antibody 24 hours after transfection. The immunoprecipitates (*top and bottom panels*) and samples of the lysates (*middle two panels*) were then analyzed by western blotting with anti-TAKL (*top two panels*), anti-T7 (*lower middle panel*) and anti-FLAG (*bottom panel*) antibodies.

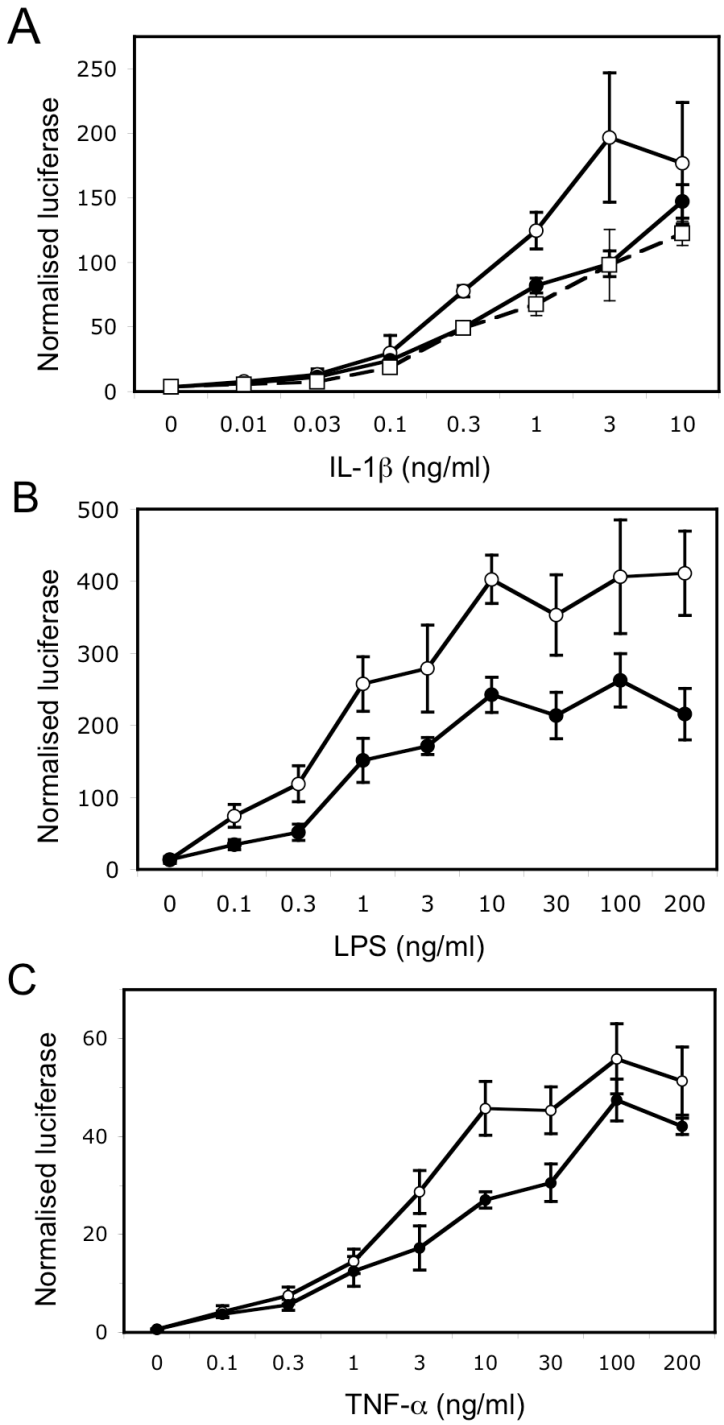

Figure 6. Inhibition of IL-1-, LPS- and TNF-induced reporter expression by TAKL-1. ***A***, Inhibition of IL-1 signaling. COS-7 cells were co-transfected with the pIL8-Luc and pTK-Luc reporters and 50 ng of construct encoding either GUS (*open circles*), TAKL-1 (*black circles*) or a442 (*squares*). The cells were challenged with IL-1-β at the indicated doses eighteen hours after transfection and were lysed 6 hours later. Means and standard deviations of three independent normalized luciferase determinations are shown. ***B***, Inhibition of LPS-mediated signaling. Same as *A* except that RAW264.7 cells and LPS were used instead of COS-7 cells and IL-1-β. ***C***, Inhibition of TNF signaling. Same as *A* and *B* but the cells used were HeLa and the stimulus, TNF-α.

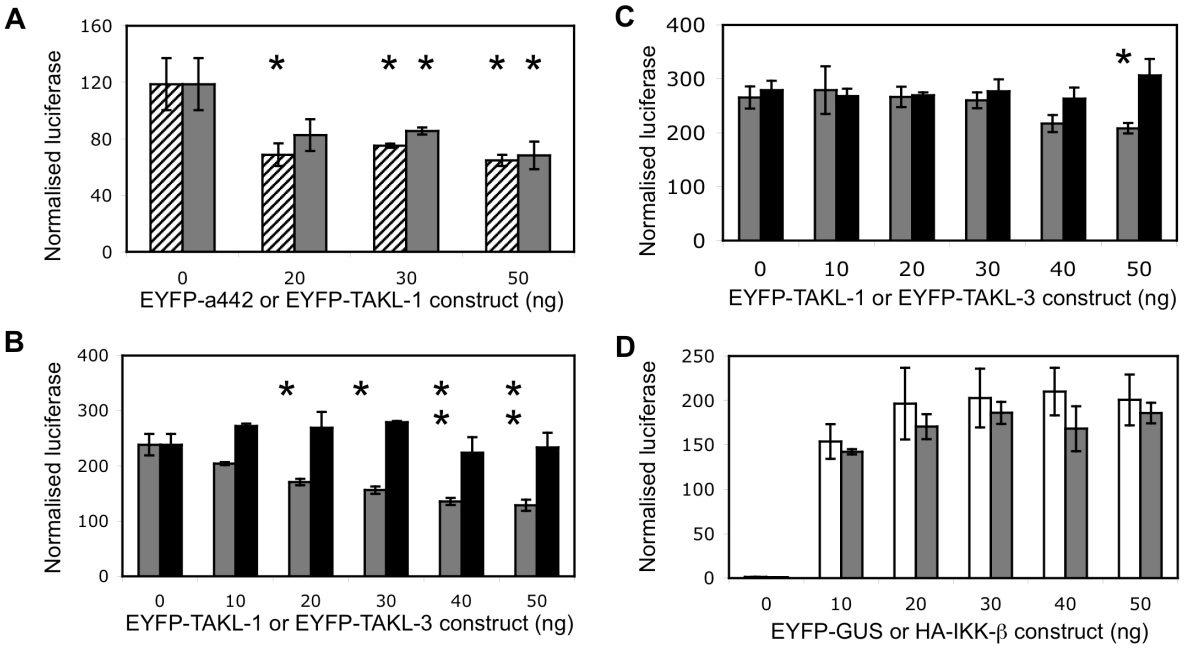

Figure 7. Effects of TAKL-1 on the activities of IL-1R1 and TRAF6 complex components. ***A***, Effects of the a442 and TAKL-1 expression constructs on IRAK-induced reporter expression. HeLa cells were co-transfected with the pIL8-Luc and pTK-Luc reporters, 10 ng of IRAK expression construct and different amounts of constructs encoding EYFP-a442 (*hatched bars*) or EYFP-TAKL-1 (*grey bars*). The cells were lysed 24 hours after transfection. Means and standard deviations of three independent normalized luciferase determinations are shown, except for the 0 ng controls (6 determinations). Values differing significantly from the control according to paired t-tests are indicated by one ($P<0.05$) or two ($P<0.01$) *asterisks*. ***B***, Effects of TAKL-1 and TAKL-3 constructs on TRAF6-induced reporter expression. The cells were co-transfected with the pIL8-Luc and pTK-Luc reporters, 10 ng of FLAG-TRAF6 expression construct and the indicated amounts of EYFP-TAKL-1 (*grey bars*) or EYFP-TAKL-3 (*black bars*) expression construct. Transfections, luciferase assays and statistical tests were carried out as described for *panel A*. ***C***, Effects of TAKL-1 and TAKL-3 constructs on TAK1-induced reporter expression. Same as *B* except that the FLAG-TRAF6 construct was replaced by 25 ng each of TAK1 and TAB1 expression constructs. ***D***, Effects of TAKL-1 on IKK-β-induced reporter expression. The cells were transfected with the pIL8-Luc and pTK-Luc reporters, 50 ng of EYFP-GUS (*white bars*) or EYFP-TAKL-1 (*grey bars*) construct and the indicated amounts of HA-IKK-β construct.

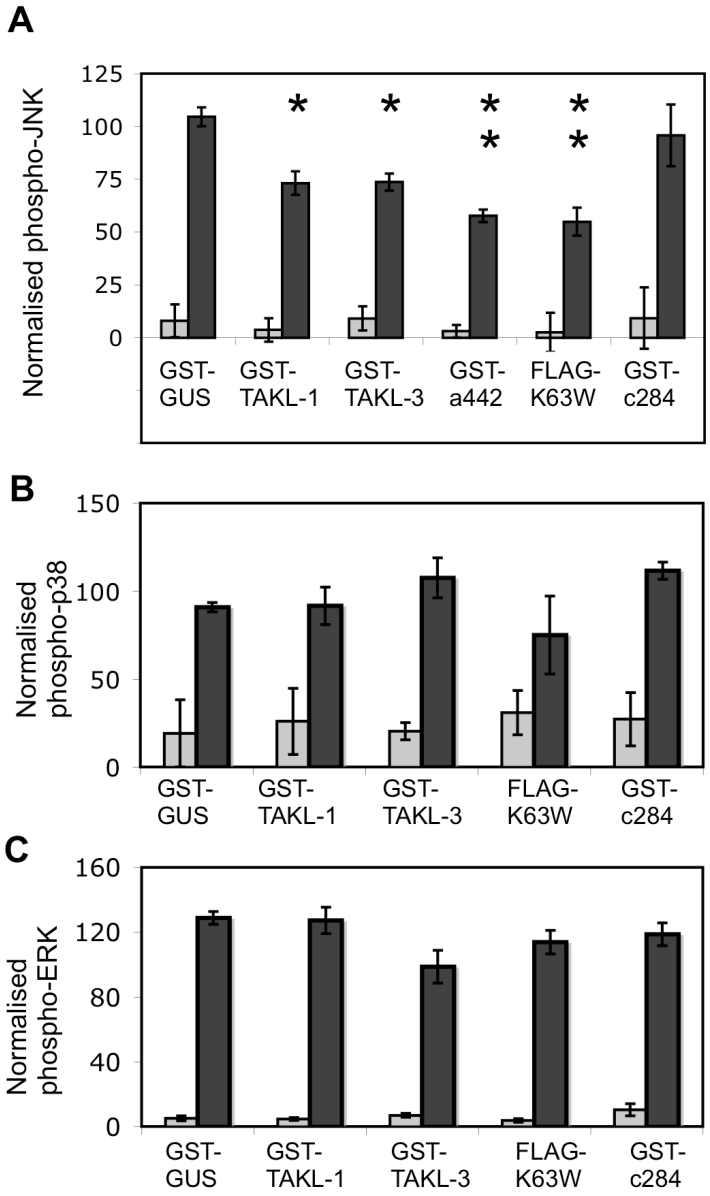

Figure 8. Effects of TAKL-1, TAKL-3 and TAK1 mutants on the activation of MAP kinases by IL-1. ***A***, Effects on JNK activation. HeLa cells transfected with the indicated expression constructs were challenged with IL-1β (*dark grey bars*) or vehicle (*light grey bars*) 24 hours after transfection and lysed 16 minutes later. The phosphorylated forms of p46 and p54 JNK were detected by immunoblotting and quantified by densitometry of the blots. The results are expressed as percentage of the amount measured in lysates of GST-GUS-expressing and IL-1- stimulated cells, used as controls. Means and s.e.m. of 4 determinations are shown. Values from IL-1 stimulated cells that differ significantly from the control are indicated by one ($P<0.05$) or two ($P<0.01$) *asterisks*. ***B***, Effects on p38 activation. Same as *A* except that the phosphorylated form of p38 was measured. ***C***, Effects on p44/42 activation. Same as *A* and *B* except that the phosphorylated forms of p44/erk1 and p42/erk2 were measured.

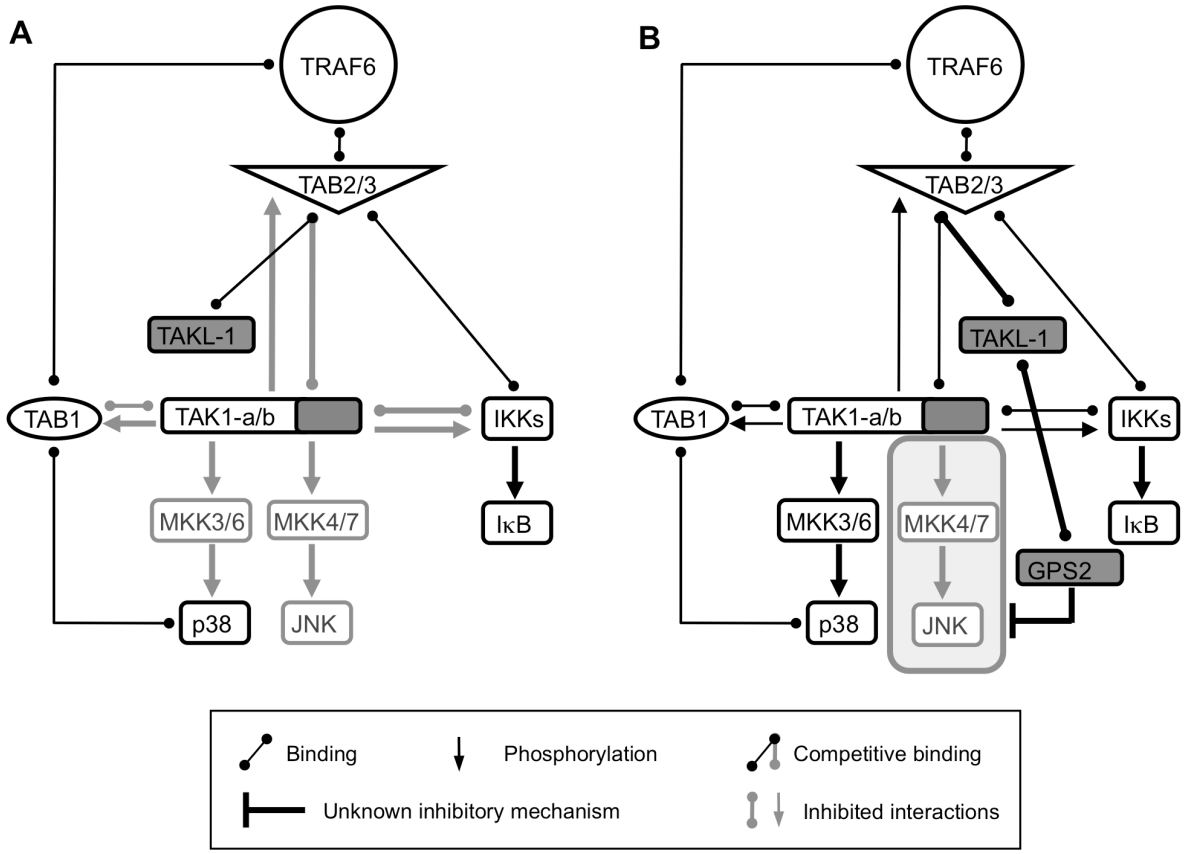

Figure 9. Possible mechanims of inhibition of JNK activation by TAKL-1. ***A***, Inhibition of TAK1 recruitment to TRAF6 complexes. The interactions between that directly regulate the recruitment of TAK1-a/b and downstream protein kinases are shown (see *Discussion* for details and references). The physical associations between proteins are represented by *dumbbell–shaped connectors* and the phosphorylations, by *arrows*. The interactions that would be inhibited as a result of competitive binding of TAKL-1 and TAK1-a/b to TAB2 or TAB3 are shown in *grey*. Interactions that should not be directly affected by TAKL-1 are shown in *black*. *B,* Recruitment of GPS2 to TRAF6 complexes. The interactions are represented as in *A*, except that here TAKL-1 is not shown as inhibiting recruitment of TAK1-a/b, but as mediating the recruitment of GPS2 to the complex. As its molecular mechanism of action is unknown GPS2 is represented as inhibiting the entire MKK4/7 / JNK cascade rather than a specific component.

Supplemental Tables and Figures

Supplemental figure SF1 - Alignment of the TAKL proteins and the carboxy-terminal end of the TAK1-a sequence.

The sequences of TAKL-1, TAKL-2, TAKL-3, TAKL-4 and residues 437 to 579 of the TAK1-a sequence are shown. The TAK1-a sequence fragment is shown in *red* and the TAK1 exon numbers are in the same colour above the sequence. The TAB2/3-binding domain of TAK1 (Besse *et al.,* J. Biol. Chem. **282**:3918-3928) is *underlined* and the amino-terminal residue of the a442 cDNA expression construct is highlighted *in white on black background*. The regions of the TAKL proteins encoded by exons 13, 15, 16 and 17 are in *blue* and the C21orf7 exon numbers are shown below the TAKL-1 or TAKL-4 sequences. The fragments of TAKL protein sequences highlighted with a *yellow background* correspond to the synthetic peptide used to generate the anti-TAKL antibody. The line in *dark red* between the TAK1-a and TAKL-1 sequences highlights the positions with identical residues or conservative substitutions (+) in TAK1 and TAKL proteins. The residues produced by codons located at exon boundaries are shown in *white* on *red*, *grey*, or *blue* boxes. The *numbers* to the right of each sequence line indicates the positions of the last residue in the protein sequence and the *asterisk*s indicate the carboxy-terminal ends of the proteins.

Supplemental Table ST1 - C21orf7 cDNA clones used in the structural analysis of the C21orf7 gene and its products

5' exon	Cloning method	Variant	Accession numbers	cDNA clone identification	Protein product	Origin
1	Not oligo-cap	A	AF269161	n.a	TAKL-3	N.A.
1	Not oligo-cap	B	AF269162	n.a	NMD	N.A.
1	Not oligo-cap	C	AF269163	n.a	NMD	N.A.
1	Not oligo-cap	F	EF219157, BQ072655	IMAGE 5756119	TAKL-4	Leukocytes from non-activated adult donors
1	Oligo-cap cDNA	G	DA815639	PEBLM2003186	Undetermined	Peripheral blood mononuclear cells
1	Oligo-cap cDNA	M	AK294287 , DA162775	BRAMY2023259	NMD	Amygdalia
1	Oligo-cap cDNA	Undetermined (A, B, C or M)	DA969821	STOMA2008863	Undetermined	Stomach
1	Not oligo-cap	Undetermined (A, B, C or M)	DR006232	TC113197	Undetermined	Prostate
2	Not oligo-cap	E	AY171599, NM_20152	n.a.	TAKL-3	Fetal Brain (Li et al., Biochemical Genetics 42:129-137, 2004)
7	Oligo-cap cDNA	H	AK122780, DA981365	SYNOV2013365	NMD	Synovial membrane tissue from rheumathoid arthritis
7	Oligo-cap cDNA	N	DA368170	BRSTN2016579	NMD	Subthalamic nucleus
9	Not oligo-cap	I	EF219158, AA465380, AA465454	IMAGE 814105	TAKL-2	Tonsillar cells enriched for germinal center B cells by flow sorting (CD20+, IgD-)
10	Not oligo-cap	D	BC008567, BF525565	IMAGE 4212641	TAKL-1	Brain, glioblastoma with EGFR amplification
10	Oligo-cap cDNA	D	AK056341, DA704787	NT2RI2008204	TAKL-1	NT2 neuronal cells treated with RA and mitotic inhibitor
10	Not oligo-cap	D	AL713701	DKFZp564A247	TAKL-1	Fetal brain
10	Oligo-cap cDNA	D	DA895510	SKMUS2003078	TAKL-1	Skeletal muscle
10	Not oligo-cap	D	BI765575	IMAGE 5185447	TAKL-1	Pooled colon, kidney, stomach
10	Oligo-cap cDNA	D	DA686717	NT2NE2005021	TAKL-1	NT2 neuronal cells
10	Not oligo-cap	D	AF269164	n.a.	TAKL-1	N.A.
10	Not oligo-cap	D	BP332267	REC04005	TAKL-1	Renal proximal tubule primary epithelial cell
10	Not oligo-cap	D	BI757072	IMAGE 5200950	TAKL-1	Brain
10	Not oligo-cap	D	BG537453	IMAGE 4688486	TAKL-1	Lung
10	Not oligo-cap	D	BF525516	IMAGE 4212579	TAKL-1	Glioblastoma with EGFR amplification
10	Oligo-cap cDNA	D	DA685306	NT2NE2003172	TAKL-1	Teratocarcinoma / in vitro differentiated neurons from NT2 cells
10	Not oligo-cap	D	BY796868	HE1927	TAKL-1	Eye
10	Not oligo-cap	D	CB963708	IMAGE 30319653	TAKL-1	Blood vessels - aorta, basilar and artery
10	Not oligo-cap	Undetermined (B, D, H or N)	H54948	n.a.	Undetermined	N.A.
11	Not oligo-cap	J	EF219159, BF692912	IMAGE 4244723	TAKL-1	Muscle (skeletal)
12	Oligo-cap cDNA	K	DA021298	ASTRO2002923	TAKL-1	Normal astrocytes
12	Not oligo-cap	K	BP290461	LNF05135	TAKL-1	Lung fibroblast
12	Oligo-cap cDNA	K	BP367403	TMS04212	TAKL-1	Thymus
14	Not oligo-cap	L	BI911525	IMAGE 5213077	TAKL-2	Leukocytes from non-activated adult donors
14	Oligo-cap cDNA	L	AK309998, DA894723	SKMUS2002091	TAKL-3	Skeletal muscle
14	Not oligo-cap	L	BU571183	IMAGE 6623270	TAKL-2	Glioblastoma (brain)
14	Not oligo-cap	L	CD641963	IMAGE 30418439	TAKL-2	Peripheral Blood Mononuclear Cells after 3/6 hour stimulation with PMA adn Ionomycin
14	Not oligo-cap	L	CK002630	IMAGE 30716818	TAKL-2	Bulk tissue from Human Spinal cord
14	Not oligo-cap	L	EF219160, BF695179	IMAGE 4247492	TAKL-2	Muscle (skeletal)
14	Not oligo-cap	L	CD641912	IMAGE 30415282	TAKL-2	Peripheral Blood Mononuclear Cells after 3/6 hour stimulation with PMA and ionomycin

Human TAKL cDNA sequences were identified by BLAST searches of nr and EST sections of GenBank on the basis of their homology to already known TAKL variants. To ascertain the origin of the sequences, we retrieved from the annotationof each sequence file thus identified the tissue or cell type of origin, the clone-identifying code (if any) and whether the cDNA was prepared by standard reverse transcription appraoches or by the oligo-cap method, specifically designed to identify transcription start sites. We then generated contigs of the clones for which several fragment sequences were available under different accession numbers. We also purchased and fully sequenced the IMAGE clones 814105, 4244723, 4247492 and 5756119, for which the complete sequences could not be retrieved from GenBank. The full sequences of these cDNA were then submitted to GenBank under the accession numbers EF219158, EF219159, EF219160 and EF219157, respectively.

For each clone, the table shows the Genbank accession numbers of all the sequences we analysed, the annotation information used to trace the origin of these sequences and the identity of the 5' exon. The mRNA variant of each clone and their predicted translation product is indicated, except in cases where an incomplete sequence did not allow their unambiguous identification. NMD: nonsense-mediated decay; N.A.: Not available.

Supplemental Table ST2 - Genomic positions and noticeable features of C21orf7 exons

Exon No	Acceptor	5' exon sequence	Position of 5' end	Position of 3' end	3' exon sequence	Donor	Noticeable feature
1	N/A	GCACCTCTCCCTCCACACCTCCCC---	30,449,812	30,450,034	---CCCAAACAGATTAAGACATGGGAG	gtatggtctctattct	Transcription start site I LTR, CpG island
2	ctctccgtgcttacag	ATGTACAAGGGCAGCCGTGGGGCT---	30,452,873	30,453,029	---ATCATTCGTAGTGTAGCCCCCAAG	gtgagtcattctgtta	
3	ttttctctcatttgag	GTGTGGAATAACCCTTAAGCCCTT---	30,457,393	30,457,464	---TTGTTGTAAAGTAATACTGCTCAG	gttcgtaagttttata	
4	tctctatatcccccag	GTGAAAGACAACTTGAGTGGTTAA---	30,458,134	30,458,238	---TGGAACGAGGCAGCAGATCTTAAG	gtatgtccgccttccc	Contains Start codon of TAKL-3 and TAKL-4 ORFs
5	tatttttttcaatacag	CCCCTTGCTCTGTCACGCAGGCTG---	30,463,822	30,463,897	---ACAGCCCTGACCTCCTGGGCCCAG	gtaattgtcccacctc	Part of an Alu Jo element
6	tcttttttttttcatag	AGATGGAGTCTCGCTATTTTGCCC---	30,463,989	30,464,082	---CTTCTTGAAGTGCTTGGATTACAG	gtatgaactactgcac	Part of same Alu Jo element as exon 5
7	N/A	GTCCAAGCCCAGTGCTCTTTCCCC---	30,464,575	30,464,902	---TGGAAATCCCCAGCTCCCCTCTGG	gtgagtattccgtcca	Transcription start site II
7b	cttgatctttatttag	TATTTCAGTTTTATGCTCTGCAAC---	30,464,760	30,464,902	---GTGGAAATCCCCAGCTCCCCTCTG	gtgagtattccgtcca	
8	ttctacttcctactag	GTTGACATTCGTAACCTTCCTGGA---	30,481,361	30,481,504	---CCTTTCCACCAGTGCGGACTGCAG	gtatggacatagggaa	Cryptics alternative internal exon in variants H and M
8 b (as alternative last exon, variant F)	ttctacttcctactag	GTTGACATTCGTAACCTTCCTGGA---	30,481,361	30,482,112	---CTAATAAAGTGTCTTTTACTTATA	N/A polyadenylation	Cryptic polyadenylation site. Last exon of mRNA variant F contains 3' end of TAKL-4 ORF
9	Undetermined	Undetermined	< 30,494,375	30,494,534	---CCTTACGGGATGGGGAACATGCAG	gtaagtgggtgcgggg	Overlaps an ERV1 LTR
10	N/A	GACAACATCCTGGCTGTTAGAGAG---	30,502,965	30,503,244	---AGTGCAGACACTCAACTAAGTGAG	gtaagccaacaggtgt	Transcription start III
10 b	tgtctccgctcctcag	ATTGTCAGTGGCTGCTATGCAGCA---	30,503,116	30,503,244	---AGTGCAGACACTCAACTAAGTGAG	gtaagccaacaggtgt	5' end is a cryptic internal splicing acceptor site used in variants B, H and N
11	Undetermined	Undetermined	< 30503282	30,503,371	---TTCCCCAGACGGTGTGATGAAAAG	gcaagttggtgtaggg	
12	N/A	ATACCAGAGGACTATTTACAAAAT---	30,503,535	30,503,812	---AACAAAATGCTTGATTCTGAGCAG	gtaagactggacagaa	Transcription start site IV
13	tctcttgctgtcacag	CTGGAAGACCCAGGAGAAGGCGGA---	30,505,627	30,505,735	---CCTTTAGCCTCAATGACGCCTCAG	gtatactctgctctgg	Contains Start codon of TAKL-1 ORF
14	N/A	ACACACCACACATCAACTTGGGGC---	30,517,901	30,518,028	---ATACAGGCCTGGCTTTCAGACTTG	gtaggcttcatacatc	Transcription start V
15	tatttccttgttttag	ATGATACACCCCCTGAAGACTCCA---	30,521,510	30,521,571	---CCAGAATTAGACCAGCAGCTACAG	gtaaggatttttctaa	Contains Start codon of TAKL-2 ORF
16	cttgttgtttgtgaag	CCCCTGCCGCCTTGTCATGACTCC---	30,532,262	30,532,377	---AATCACCCTGCTTGAGCAAAGGAA	gtaagtacctaccccc	
17	taccccgaatcttcag	GAAGGAGCTCATTGCCAAGTTAGA---	30,547,033	30,548,208	---TCATTAAACATGGATCAAAACTGA	N/A polyadenylation	Default polyadenylation site Last exon of most mRNA variants, contains 3' end of TAKL-1, TAKL-2 and TAKL-3 ORFs

Exon/intron boundaries were determined by alignment of cDNA and genomic sequences as explained in the article. *Bordered cells* in the "Exon No" and "Noticeable feature" columns highlight the 5 exons that function as transcription start sites (TS). *Grey-shaded* cells in the "Exon No" column highlights exons that contain parts of the TAKL proteins ORFs. The *drak grey*-shaded cells highlights exons homologous to the TAK1 gene.
The positions of transcriptions start sites I to V are taken as the 5' ends of the sequences of clones generated by the oligo-cap method (Kimura *et al.*, *Genome Res.* **16**:55-65, 2005), of accession numbers DA162775, DA981365, AK056341, DA021298 and AK309998, respectively. Position numbers of exon ends are from the GRCh37.p13 genome build. The 5' ends of exons 9 and 11 are considered undetermined as the available cDNA sequence data does not include an oligo-Cap clone or a junction with an upstream exon; an upstream exon; the positions of the 5' end of these incompletely sequenced exons is preceded by the < symbol.

Supplemental Table ST3 - Non-human TAKL cDNA clones

Species	Variant / exon composition	Protein	Accession numbers	Origin
Macaca mulata	J	TAKL-1	CB230365	
Rattus norvegicus	D	TAKL-1	NM_001013979, XM_221713, BC076389, CK482674	Kidney
Rattus norvegicus	D	TAKL-1	CK483806	Kidney
Mus musculus	D	TAKL-1	AY033899, NM_144854	
Mus musculus	D	TAKL-1	BX519631	Barstead stromal cell line MPL-RB5
Mus musculus	D	TAKL-1	CF586662	Pancreas
Mus musculus	D	TAKL-1	BB638361	3 days neonate thymus
Mus musculus	D	TAKL-1	AK041664	3 days neonate thymus
Mus musculus	D	TAKL-1	AA667395	Barstead mouse myotubes MPLRB5
Mus musculus	Exons 13, 15, 16 and 17	TAKL-1	BG793603	Diaphragm/Hind limb skeletal muscles
Sus scrofa	Exons 13, 15, 16 and 17	TAKL-1	DN133031	Early developmental stage pig embryos
Bos taurus	D	TAKL-1	DV927981	Muscle, 6 months old fetus
Bos taurus	D	TAKL-1	DY099098	Bovine Foetal Muscle
Gallus gallus	Chicken-specific variant	TAKL-1	BX932098, BU126220	Liver
Gallus gallus	Chicken-specific variant		BU247569	
Ictalurus punctatus	Exons 13, 15, 16 and 17	TAKL-1	CK419227	
Danio rerio	Exons 13, 15, 16 and 17	TAKL-1	EB941446	
Astatotilapia burtoni	Exons 13, 15, 16 and 17	TAKL-1	DY625923, DY655923	
Gasterosteus aculeatus	Exons 13, 15, 16 and 17	TAKL-1	DW031040, DW031041	
Squalus acanthias	Exons 13, 15, 16 and 17	TAKL-1	DV202898	

The cDNA clones were identified by BLAST searches of nr and EST sections of GenBank on the basis of their homology to human TAKL.
Clones whose protein product could be identified are shown.

Supplemental Figure SF2 - Alignment of ATD-encoding exons of C21orf7 with their chimpanzee and macaque homologues

The sequences of the amino-terminal domain of human (*Hs*) TAKL-3 and of the exons which encode it are shown in the first and second lines of the alignments, respectively. The TAKL-3 residue numbers are indicated. The homologous regions of the chimpanzee (*Pt*) and macaque (*Mm*) TAKL genes and the predicted *Macaca* translation products are shown in grey ink in lines 3, 4 and 5 respectively, with differences from the human sequences highlighted in red. Intronic donor and acceptor splice sites are shown in lowercase.

Supplemental Figure SF3 - Phylogenetic analysis of TAKL-1 and TAB2/3-binding domain of TAK1

A

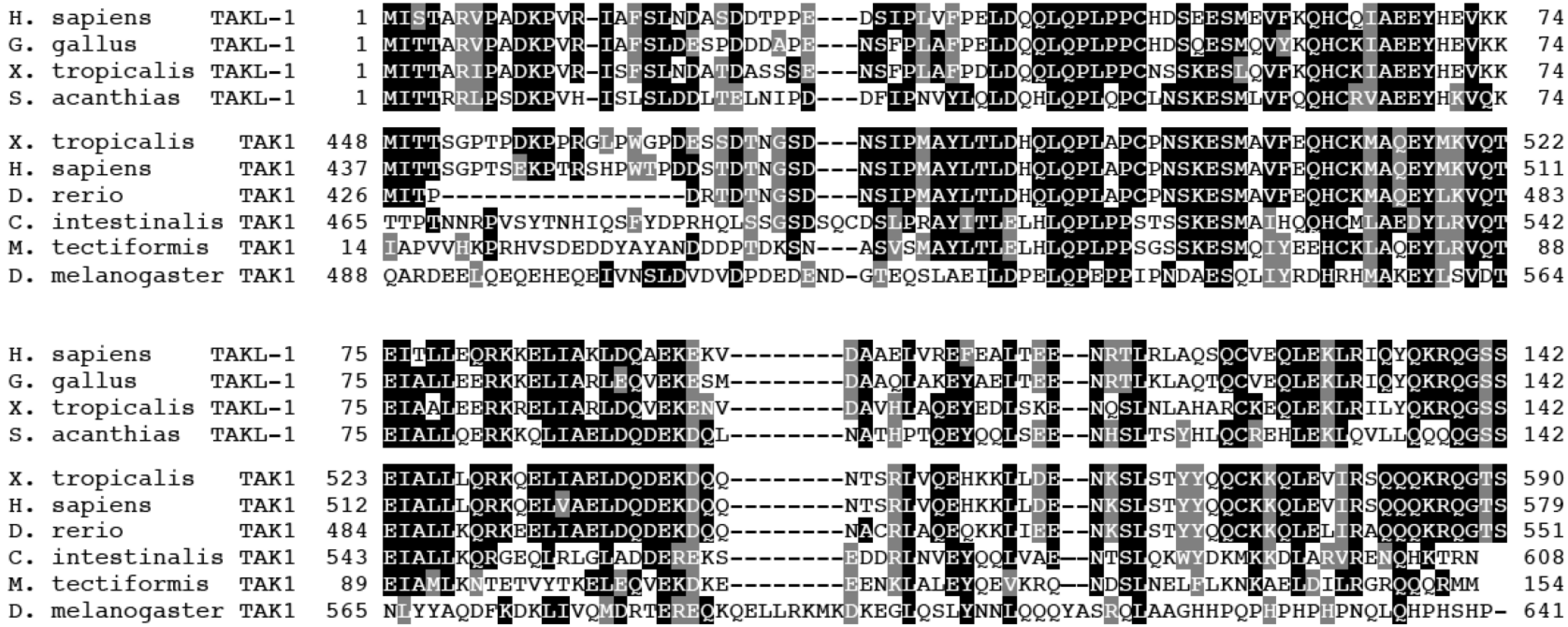

A: Alignment of the sequences of TAKL-1 and TAB2/3-binding domains of TAK1

The sequences were generated by translation of TAKL cDNA sequences from *H. sapiens*, *G. gallus*, *X, tropicalis* and *S. acanthias* (Accession numbers in Supplemental Table 3) and TAK1 cDNA sequences from *X. tropicalis* (CX877417, CR563066) *H. sapiens* (AB009356), *Danio rerio* (BC095335), *Ciona intestinalis* (AB210715), *Molgula tectiformis* (CJ399690, partial sequence) and *Drosophila melanogaster* (AF199466). The alignment was generated by CLUSTALW.

B

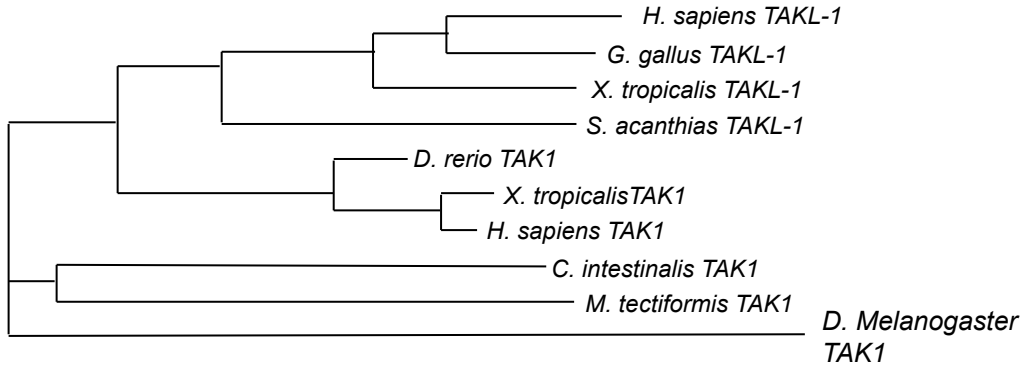

B: Phylogram generated by CLUSTALW

Supplemental Figure SF4 - Effects of TAKL-1 and TAKL-3 on IL-1-activated cytosolic signaling pathways.

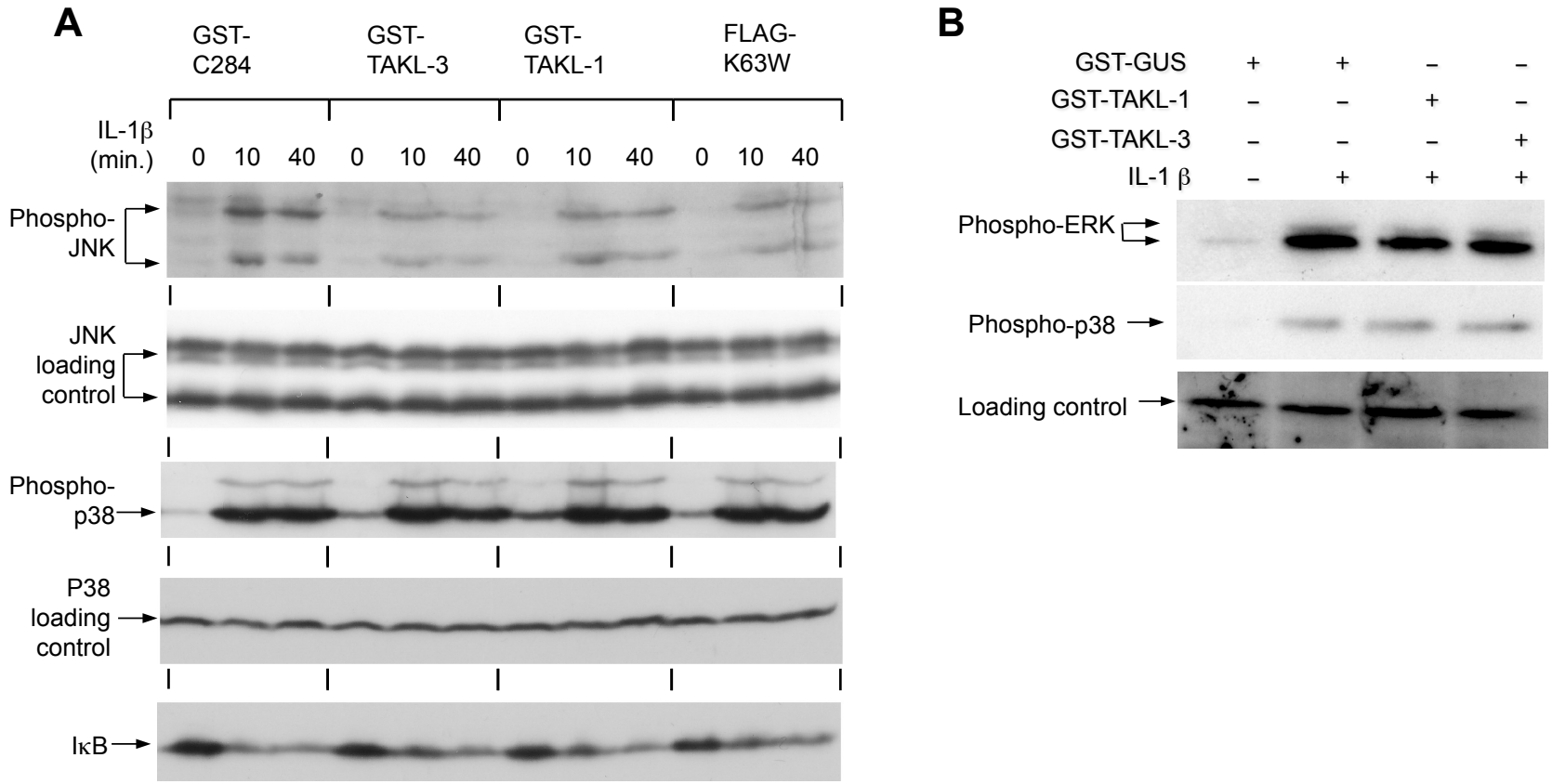

A: Effects of over-expressed TAKLs on activation of JNK and p38 and degradation of IκB.
HeLa cells were transfected with tagged constructs encoding residues 284 to 518 of TAK1-c (GST-C284, negative control), GST-TAKL-3, GST-TAKL-1 or FLAG-K63W (positive control). Twenty-four hours after transfection, the cells were challenged with 10 ng/ml IL-1β for the indicated times, then lysed. Samples of the lysates were immunoblotted with antibodies to the active forms of the JNK and p38 MAP kinases and to IκB. Loading controls obtained with antibodies to the full-length JNK and p38 kinases are also shown.

B: Effects of over-expressed TAKLs on activation of ERK and p38.
Same as panel A except that cells were transfected with tagged constructs GST-GUS (negative control), GST-TAKL-3 or GST-TAKL-1 and that stimulation by 10 ng/ml IL-1β was for 16 minutes. Samples of the lysates were immunoblotted with antibodies to the active forms of the p42 and p44 ERK kinases (top panel), the phosphorylated form of p38 (middle panel) and to the small heat shock protein, hsp27 (loading control, bottom panel).

Appendix II

Expression of TAKL mRNAs in various cell types: Up-regulation during in vitro macrophage differentiation of THP1 cells

Unpublished data by Shweta Kumar and Ioanna Tzani (2011)

This appendix contains the results of a preliminary investigation of TAKL expression in various cell types and tissues that was carried out in Dr. Guesdon's group in 2011.

Appendix II Figure 1

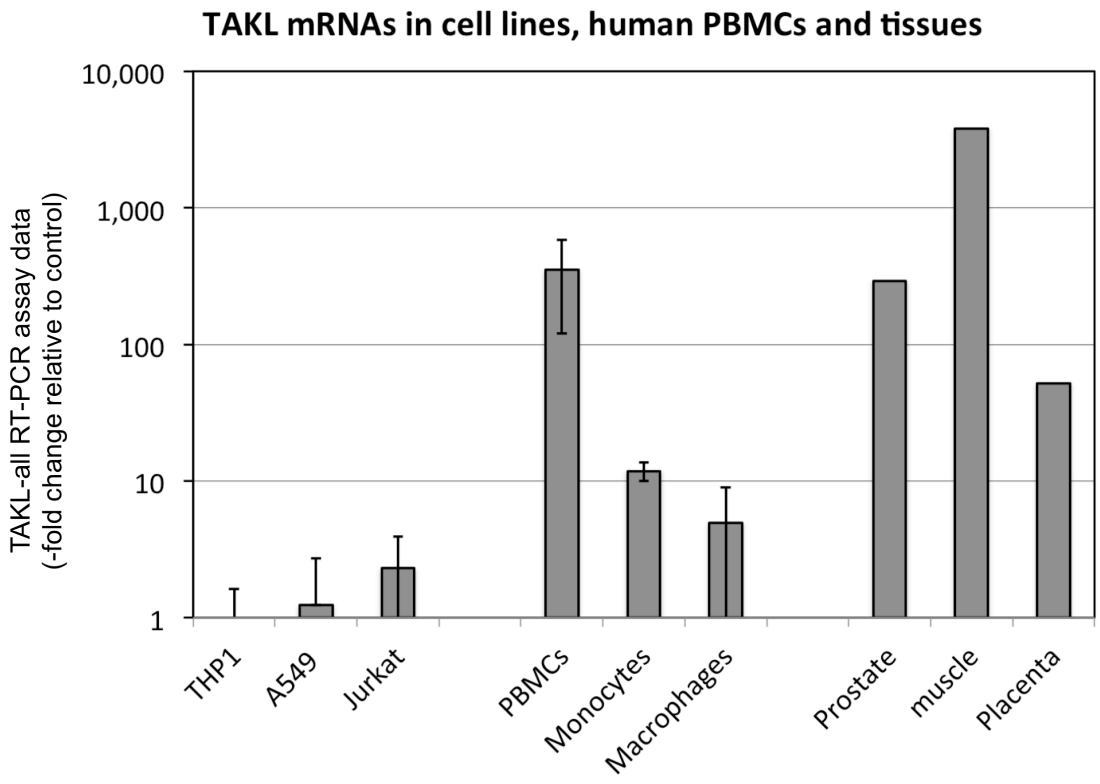

TAKL mRNAs were assayed by real-time PCR using the TAKL-all assay on first strand cDNA preparation from the cell lines THP1, A549 and Jurkat, from freshly isolated human peripheral blood monocytes (PBMCs), from monocytes and macrophages differentiated from PBMCs in vitro and from commercially available preparations of cDNAs from human differentiated tissues. Cell culture and PBMC isolations were carried out by standard operating procedures. TAKL expression was assayed with the TAK-all assay (Thermofisher TaqMan assay Hs00963407_m1). The data were analysed by the comparative method (ΔΔCt) using β-actin mRNA as normaliser and the first strand cDNA preparation from THP1 cells as reference. The data shown are the means ± s.e.m of triplicate assays except for the samples from differentiated tissues, which could only be assayed once due to their limited availability.

Appendix II Figure 2

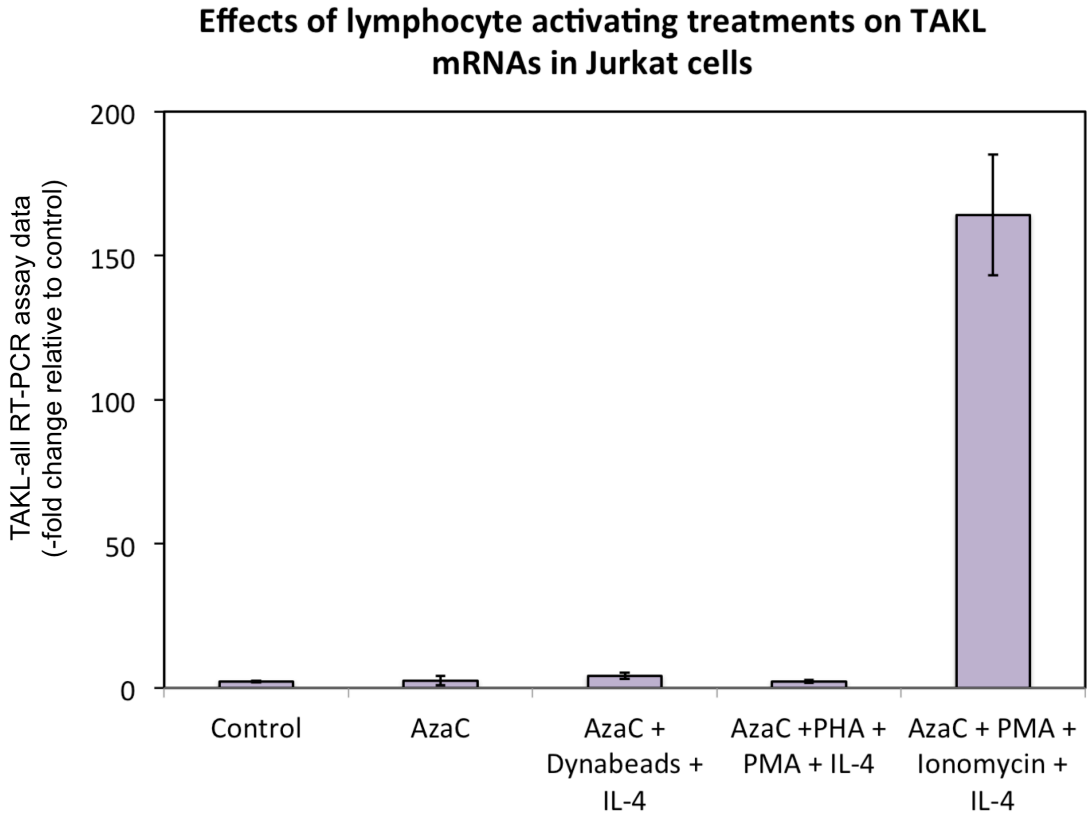

To test the effect of lymphocyte activators on TAKL expression in a lymphocytic cell line, Jurkat cells were cultured for two passages (8 days, approximately 6 doublings) in the presence of the DNA methylase inhibitor, 5-azacytidine (AzaC, 1 μM). The AzaC-treated culture was then divided into aliquots that were either left unstimulated or exposed for 16 hours to either:

- Dynabeads (T cell receptor oligomerising ligand, 20 μl of packed beads per million cells) and IL-4 (10 ng/ml)
- Phytohemaglutinin (PHA,1μg/ml), phorbol 12-myristate 13-acetate (PMA, 100 ng/ml) and IL-4 (10 ng/ml)
- PMA (100 ng/ml), ionomycin (1 μM) and IL-4 (10 ng/ml)

After 16 hours of stimulation, the samples were taken in Trizol for RNA isolation. A Control sample from Jurkat cells that had been maintained in standard culture conditions was also taken. First strand cDNA synthesis were then carried out and TAKL expression was assayed with the TAK-all assay (Thermofisher TaqMan assay Hs00963407_m1). The data were analysed by the comparative method (ΔΔCt) using β-actin mRNA as normaliser and the first strand cDNA preparation from THP1 cells as reference. The data shown are the means ± s.e.m. of triplicate assays.

Appendix II Figure 3

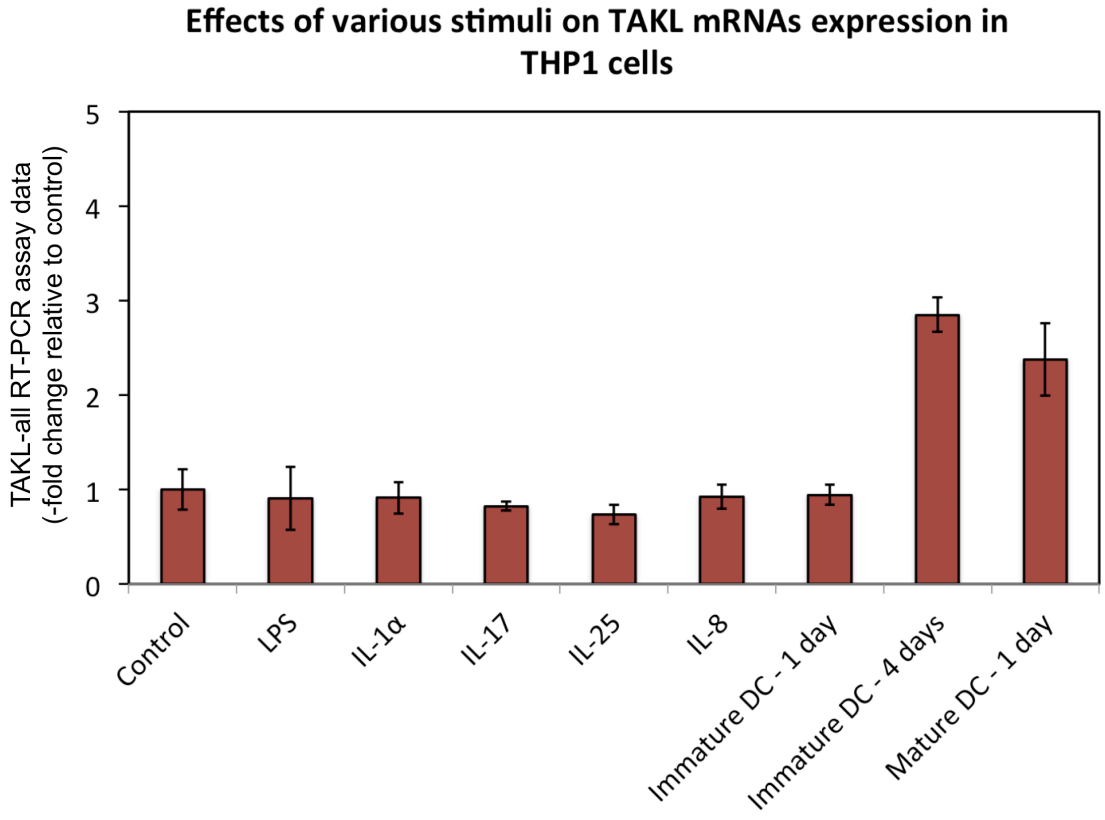

Supspension-growing THP1 cells were left unstimulated (Control) or exposed for 8 hours to LPS (100 ng/ml), IL-1α (20 ng/ml), IL-17 (100 ng/ml), IL-25 (100 ng /ml) or IL-8 (200 ng/µl). Other samples were induced to differentiate into either immature dendritic cells (DC) by exposure GM-CSF (100 ng/ml) and IL-4 (100 ng/ml) for 1 and 4 days or into mature DCs by exposure to TNF- α (20 ng/ml), IL-4 (200 ng/ml), GM-CSF (100 ng/ml) and ionomycin (200 ng/ml) for 1 day (Berges *et al.*, Biochem. Biophys. Res. Comm. 333:896, 2005).

The cells were taken in Trizol at the end of the stimulation periods and RNA isolation and first strand cDNA synthesis were carried out as before. TAKL expression was assayed with the TAK-all assay (Thermofisher TaqMan assay Hs00963407_m1). The data were analysed by the comparative method (ΔΔCt) using β-actin mRNA as normaliser and the first strand cDNA preparation from unstimulated THP1 cells (day 0 sample) as reference. The data shown are the means ± s.e.m. of triplicate assays.

Appendix II Figure 4

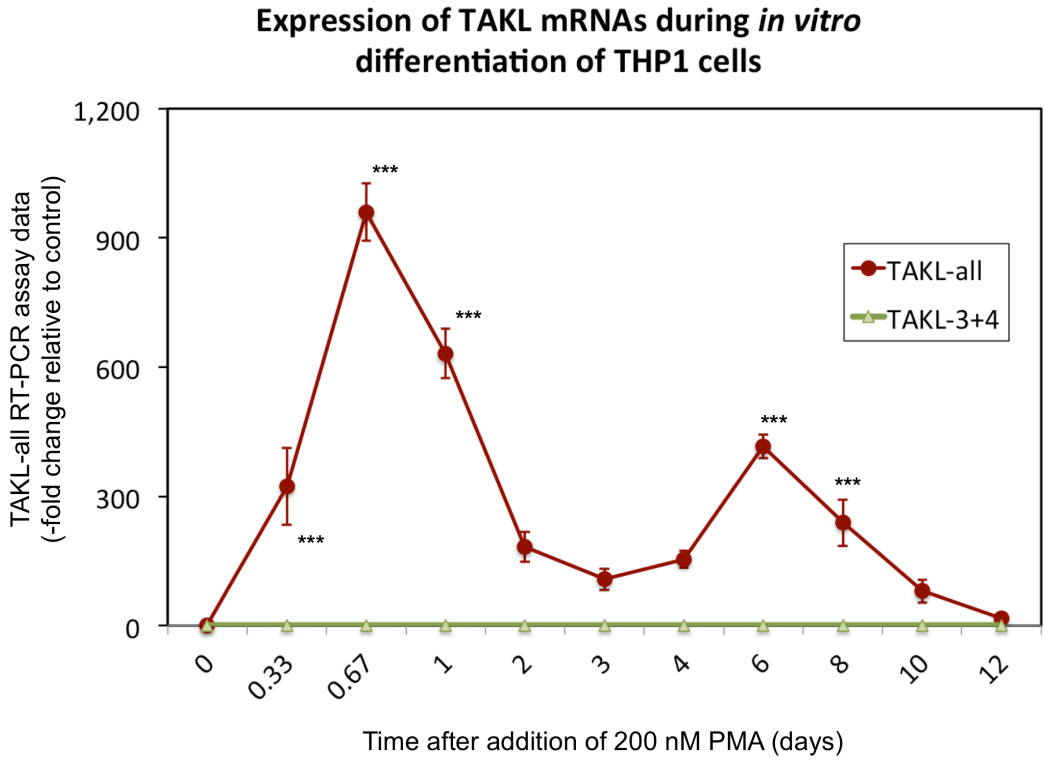

THP1 cells were induced to differentiate into macrophages by a 3-day exposure to phorbol 12-myristate 13-acetate (PMA, 200 ng/ml) followed by a rest period of at least 5 days in culture medium without PMA, as described by Daigneault *et al.* (PLOS One 5:8668, 2010). The cell suspension was aliquoted immediately after addition of PMA into samples that were then incunated for times varying from 8 hours (0.33 day) to 12 days. Samples taken prior to PMA addition (shown at 0 day on the graph) were also taken as reference.

The samples were taken in Trizol at the indicated times. RNA isolation and first strand cDNA synthesis were carried out as before and TAKL expression was assayed with the TAK-all assay (Thermofisher TaqMan assay Hs00963407_m1). The data were analysed by the comparative method (ΔΔCt) using β-actin mRNA as normaliser and the first strand cDNA preparation from unstimulated THP1 cells (day 0 sample) as reference. The data shown are the means ± s.e.m. of triplicate assays.

APPENDIX III

Human pro-inflammatory macrophage FAM26F regulates chemokine expression and macrophage–lymphocyte interaction

Kajus Baidžajevas[a, b], Rehab Alqurashi[a], Klaudia Kocsy[a], Éva Hadadi[a, b, c], Radoslaw M Sobota[d], Dilip Kumar[b], Laura Martínez Campesino[a], Bernett Lee[b], Michael Poidinger[b], Caroline Evans[d], Jessica N Redgrave[e], S Kim Suvarna[a], Mark J Dickman[d], Arshad Majid[e], Sheila E Francis[a], Siew Cheng Wong[b], Endre Kiss–Tóth[a], Heather L Wilson[a, *].

a Department of Infection, Immunity & Cardiovascular Disease, University of Sheffield, Beech Hill Road, Sheffield, S10 2RX, UK

b Singapore Immunology Network (SIgN), Agency for Science, Technology and Research (A*STAR), Singapore

c Current address: INSERM U935, Villejuif, France

d Department of Chemical and Biological Engineering, The University of Sheffield, Mappin Street, Sheffield, S1 3JD, UK

e Sheffield Institute for Translational Neuroscience, University of Sheffield, 385a Glossop Road, Sheffield, S10 2HQ, UK

* Corresponding author: Heather L Wilson: Department of Infection, Immunity & Cardiovascular Disease, University of Sheffield, Beech Hill Road, Sheffield, S10 2RX, UK. Tel. + 44 114 215 9560. Email: H.L.Wilson@sheffield.ac.uk

Key words: atherosclerosis, inflammation, macrophages, FAM26F, CALHM6, INAM

Abstract

Background

Increased abundance of pro-inflammatory macrophages in atherosclerotic plaques is a risk factor for plaque rupture. The currently used markers to identify these cells have not been extensively tested for specificity, are not always up–regulated as transcripts and cell–surface protein and also cannot always be used in model organisms and humans. We sought to identify genes up–regulated in inflammatory macrophages to identify potential markers and functional changes in plaque inflammation.

Methods

Human monocyte–derived macrophages and mouse bone marrow–derived macrophages were polarised with interferon gamma, lipopolysaccharide, interleukin 4 and 10, oxidised phospholipid and chemokine C-X-C motif ligand 4 for 24 h. Gene expression was quantified by qRT–PCR, while protein expression was measured by membrane protein SILAC proteomics, immunocytochemistry, immunohistochemistry and western blotting. siRNA was used to knockdown selected genes. THP–1s were transfected to overexpress a 3×FLAG fusion protein for co-immunoprecipitation and cell interaction experiments.

Results

Family with sequence similarity 26 member F (FAM26F) was the most highly uniquely up–regulated *in vitro* in both human and mouse primary macrophages activated with IFNγ(+LPS). FAM26F expressing macrophages were also identified in human carotid artery atherosclerosis. siRNA knockdowns of *TICAM1* and *STAT1* resulted in lower induction of *FAM26F* upon activation with LPS or IFNγ respectively. siRNA knockdown of *FAM26F* reduced STAT1 phosphorylation and expression of *CCL5*, *CXCL8* and *CXCL11*. FAM26F–3×FLAG co-immunoprecipitated with linker for activation of T cells and overexpression of this construct resulted in a higher percentage of Jurkat cells attaching to THP–1s upon stimulation with IFNγ+LPS.

Conclusions

FAM26F is a novel pro-inflammatory macrophage marker expressed in a subset of human atherosclerotic plaque macrophages involved in regulating leukocyte recruitment and activation. This finding provides us with a new understanding of immune cell activation in atherosclerotic plaques and mechanisms of inflammatory activation underlying plaque vulnerability.

Introduction

Patients with late–stage atherosclerosis are at increased risk of life–threatening ischaemia due to plaque rupture and resultant thrombosis (Yahagi et al., 2016). Leukocytes, such as pro-inflammatory macrophages, secrete matrix metalloproteinases (MMPs), which breakdown collagen and other connective proteins, thin and weaken the protective cap of the atheroma (Huang et al., 2012, Newby, 2015, Orbe et al., 2003). Plaques with caps < 65 μm in thickness, notable macrophage and lymphocyte presence, rare or no smooth muscle cells (SMCs) and a necrotic core > 10% of plaque area, are classified as rupture–prone thin–cap fibroatheromas (Yahagi et al., 2016). In advanced plaques, macrophages positive for common pro-inflammatory markers tend to localise to specific regions of the plaque, such as the cap shoulders, which are particularly prone to mechanical stresses and therefore rupture (Stoger et al., 2012).

Identification and characterisation of plaque macrophages has been a major challenge in atherosclerosis research. Early reports broadly classified macrophages into M1 and M2 pro- and anti-inflammatory phenotypes respectively, however, advancements in the field greatly expanded our understanding of macrophage heterogeneity (Murray et al., 2014). Also, recent reports on mouse atherosclerosis model single cell RNA–seq have challenged the concept of the *in vitro*–like M2 anti-inflammatory macrophage presence in plaques (Cochain et al., 2018, Kim et al., 2018). However, the use of phenotype or activation–specific markers is still common practice due to the speed, cost and convenience, especially in diagnostics and research involving patient samples. Characterisation of marker protein function may also aid in drug discovery and choice of treatment.

The current macrophage markers in use are constrained by a number of issues: (1) lack of thorough testing for specificity even in *in vitro* culture models, (2) limited choice of cell surface–expressed proteins as markers, (3) inconsistency across species, (4) expression increased only at the RNA or protein level. Therefore, it is difficult to precisely and confidently determine differentially activated macrophage presence in, and impact on, atherosclerotic plaque growth and rupture in human patients. We have therefore used a membrane proteomics approach to identify potential new macrophage phenotype markers.

We identified a new pro-inflammatory macrophage marker Family with sequence similarity 26 member F (FAM26F, also known as CAHM6 or INAM), which is a tetraspanin–like protein predicted to function as a membrane pore for signalling molecules such as ATP and calcium ions (Malik et al., 2017). Expression of the *FAM26F* gene is up–regulated in several inflammatory disease contexts. It has been shown to be induced by poly(I:C) via TLR3/TICAM-1/IRF3 in mouse bone marrow–derived dendritic (DC) and natural killer (NK) cells for cell–to–cell contact

activation of the latter cells to produce interferon (IFN) γ and induce tumour cell killing (Ebihara et al., 2010). The same group later showed that mouse $CD8\alpha^+$ DCs and macrophages can up–regulate expression of FAM26F upon poly(I:C) activation. Using a melanoma lung metastasis model they confirmed that FAM26F is important in controlling tumour metastases (Kasamatsu et al., 2014). However, it has not been entirely confirmed that up–regulated FAM26F gene and protein expression is specific to human pro-inflammatory macrophages as well as the signalling pathways involved in inducing expression. Also, further details of how FAM26F may function to bridge innate and adaptive immunities have not been tested in human cells.

Here we show that FAM26F is up–regulated specifically upon pro-inflammatory activation of human and mouse macrophages, and is expressed in human carotid atherosclerotic plaque macrophages. We have also demonstrated involvement of TICAM1 and STAT1 signalling axes in FAM26F induction as well as expanded upon its importance on macrophage activation of lymphocytes via chemokine expression regulation, co-immunoprecipitation with linker for activation of T–cells (LAT) and increased THP–1/Jurkat cell interaction upon FAM26F overexpression. These observations suggest that human FAM26F is involved in linking innate to adaptive immunity and its upregulation in human plaques undergoing inflammation provides us with a new insight into mechanisms underlying increased plaque vulnerability and disease progression.

Materials and methods

Primary human macrophages

Peripheral blood mononuclear cells (PBMCs) were isolated by Ficoll–Hypaque (GE Healthcare) density centrifugation from apheresis cones, buffy coats or whole blood donated by healthy adult donors. Apheresis cones and buffy coats were provided by the Blood Donation Centre, Health Sciences Authority and National University Hospital Transfusion Centre, Singapore respectively. Ethical approvals for all blood sources and processes used in this study have been given by either the National University of Singapore Institutional Review Board (NUS-IRB 08-352E, NUS-IRB 09-256, NUS-IRB 10-250) or the University of Sheffield Research Ethics Committee (SMBRER310). All donors gave written informed consent in accordance to the Declaration of Helsinki. Monocyte ($CD14^+$ PBMC) isolation was carried out by positive magnetic selection using CD14 microbeads (Miltenyi Biotec).

Monocytes were cultured in complete media: RPMI-1640 (Gibco), 10% (v/v) low–endotoxin heat–inactivated FBS (Biowest), 2 mM L–glutamine (Gibco/Lonza), 100 U/ml penicillin and 100 µg/ml streptomycin (Gibco/Sigma). 100 ng/ml recombinant human (rh) M–CSF (Peprotech/Immunotools) were added to differentiate the monocytes into monocyte–derived macrophages (MDMs) over 7 days. On day 7 the media was replaced with fresh complete media containing the polarising agents for 24 h: 20 ng/ml rhIFNγ (Peprotech/Immunotools), 100 ng/ml TLR grade *E. coli* LPS (Enzo Life Sciences), 20 ng/ml rhIL–4 (Peprotech/Immunotools/Miltenyi), 20 ng/ml rhIL–10 (Peprotech/Immunotools), 25 µg/ml oxPAPC (Invivogen) and 1 µM (7.8 µg/ml) rhCXCL4 (Peprotech/Immunotools/BioLegend). Unpolarised macrophages (M^{un}) were used as internal baseline controls in each experiment.

SILAC membrane proteomics

MDMs were washed twice with PBS before 24 h polarisation in media based on lysine and arginine–deprived RPMI (Sigma) with 10% dialysed FCS (v/v) (Thermo Fischer) and 100 U/ml penicillin and 100 µg/ml streptomycin (Gibco), containing 30 µg/ml Lys+8 Da (15N213C6 lysine, light) and 50 µg/ml Arg+10 Da (15N413C6 arginine, heavy) or 30 µg/ml Lys+4 Da (2H4 lysine, light) and 50 µg/ml Arg+6 Da (13C6 arginine, medium) purchased from Cambridge Isotopes. Each polarisation condition was coupled with a control condition (unpolarised). Polarisation efficiency was confirmed by AlexaFluor 488–acLDL uptake (Molecular Probes) one day before isotopic labelling.

Membrane extracts were prepared following a previously published report (Parker et al., 2011). Equal numbers of cells from all polarisations were lysed in 100 mM sodium carbonate pH 11.0 for 20 min followed by sonication and centrifugation at 100,000 g for 2 h. In–solution digestion with

Lys-C (Wako) / trypsin (Promega) was performed before isoelectric focusing technique using OFFgel equipment (Agilent) separation following a modified manufacturer's protocol (Hubner et al., 2008).

Following desalting on STAGEtips (Rappsilber et al., 2003) peptides were separated and analysed by reverse phase liquid chromatography (RP-LC) on Dionex 3000 HPLC system (Thermo) coupled with a Q-Exactive mass spectrometer (Thermo, Germany) in a 140 min gradient of solvent A (0.5% [v/v] CH_3COOH in water) and solvent B (80% [v/v] MeCN and 0.5% [v/v] CH_3COOH in water).

Raw MS/MS spectra were processed using MaxQuant (v 1.4.1.2). Peak lists were searched against Uniprot database version (73000 entries); contaminants were searched using the Andromeda search engine. Parameters used: *Fixed modification, Carbamidomethyl cysteine, Variable modifications: Oxidation on methionine; Acetylated N-terminal protein, phospho STY, deamidation (NQ), SILAC amino acids (Arg+6 Da, Arg+10 Da, Lys+4 Da, Lys+8 Da), 2 missed cleavages, MS accuracy 7 ppm, MS/MS accuracy 20 ppm*. The cut-off rate for identification was set to a False Discovery Rate of 1%. Unique and common peptides were used for protein ratio quantification with a minimum ratio count of 1.

Samples were generated from 2 different healthy donors. The majority of proteins were identified with at least 2 unique peptides. Raw XIC intensities were Quantile normalized (R software) followed by heavy/light and medium/light ratio estimation. Estimated ratios were used to calculate newly synthesized proteins by taking into account the incorporation of labelled amino acids (threshold: 10%). Proteins were enriched for membrane fraction using gene-ontology (GO-terms). For those missing annotation, manual verification was performed. Statistical analyses were performed on incorporation data to identify proteins with differential/unique expression. All missing values were given a numerical value of 0. First, Wilcoxon signed-rank tests were performed to identify uniquely expressed proteins for each macrophage phenotype by comparing the phenotype of interest to all the others. Then Kruskal-Wallis tests were used to compare incorporation levels between phenotypes and validate the results of Wilcoxon test. The level of protein induction was calculated by incorporation in polarised macrophage / median of incorporation in all controls.

Immunohistochemistry

Atherosclerotic plaques were removed from consented patients (study ethics approval STH18222) undergoing carotid artery endarterectomy surgery. The tissue was placed in 10% (v/v) neutral buffered formalin, decalcified in 0.5M EDTA pH 8 for 7 days, divided into 3 mm regions and embedded in paraffin.

For immunofluorescence staining sections were dewaxed and rehydrated for treatment with with 3% (v/v) hydrogen peroxide in methanol before antigen retrieval was performed for 10 min in 10 mM heated trisodium citrate pH 6.0 buffer. The sections were then treated with 0.1% (v/v) Triton X–100 (Sigma) in PBS for 15 min, followed by blocking in 5% (v/v) donkey serum (Sigma) in PBS for 30 min. Mouse anti-human CD68 (Abcam ab125157, 4 µg/ml), rabbit anti-human FAM26F (Novus NBP1-86754, 2.5 µg/ml), mouse (Vector Laboratories I-2000, 4 µg/ml) and rabbit (Vector Laboratories I-1000, 2.5 µg/ml) control IgGs were diluted in PBS for a 1 h incubation at room temperature. Donkey anti-mouse NL-493 (R&D Systems NL009, 2.5 µg/ml) and anti-rabbit NL-557 (R&D Systems NL004, 5 µg/ml) secondary antibodies were then incubated with the sections the same way. Coverslips were mounted with ProLong Gold Antifade Mountant with DAPI (Invitrogen) and dried overnight at room temperature before imaging using a Nikon Ti Eclipse microscope. Fluorescence intensities were adjusted in Fiji/ImageJ (v 1.52p) equally across all images according to the isotype antibody staining.

For assessment of atherosclerosis stage and plaque stability sections were cut from each region and counting from the bifurcation as the centre the same number section from each region was stained with haematoxylin and eosin, Elastic Stain Kit (Verhoeff Van Gieson / EVG Stain) (Abcam ab150667), anti-CD3 and CD68 antibodies. For antibody staining the sections were processed the same as for immunofluorescence staining except for the following: Triton treatment was omitted and blocking was performed using the ImmPRESS Horse Anti-Rabbit /Anti-Mouse IgG Plus Polymer Kit (Vector) for 20 min at room temperature. Sections were incubated with anti-CD3 (Dako A0452, 2 µg/ml) or anti-CD68 (Dako M0814, 1.85 µg/ml) primary antibodies and secondary antibodies from the ImmPRESS Horse Anti-Rabbit /Anti-Mouse IgG Plus Polymer Kit (Vector, 30 min incubation at room temperature). SignalStain® DAB Substrate Kit (Cell Signalling Technologies) was used to visualise the antibody staining before counterstaining with haematoxylin, dehydrating and coverslip mounting.

Mouse bone marrow derived macrophage culture

Mice were handled in accordance with UK legislation (1986) Animals (Scientific Procedures) Act. Mouse experiments were approved by the University of Sheffield Project Review Committee and carried out under a UK Home Office Project Licence (70/7992). All mice used were congenic on a C57BL/6J background (N17) and were housed in a controlled environment with a 12–hour light/dark cycle, at 22°C in Optimice individually ventilated cages (Animal Care Systems) and given free access to a standard chow diet (#2918; Harlan Teklad) and water. Bone marrow was isolated and bone marrow–derived macrophages (BMDMs) were cultured for 5 days in DMEM (Gibco), 10% (v/v) low–endotoxin heat–inactivated FBS (Biowest), 100 U/ml penicillin and 100

μg/ml streptomycin (Gibco) and 10% v/v L929 medium. The non-adherent cells were then washed off, while the adherent cells were scraped and plated in fresh media at 2×10^5 cells/ml. The following day the cells were polarised for 24 h with 20 ng/ml recombinant mouse IFNγ (Peprotech) and 100 ng/ml TLR grade *E. coli* LPS (Enzo), 20 ng/ml recombinant mouse IL–4 (Peprotech), 20 ng/ml recombinant mouse IL–10 (Peprotech). Unpolarised cells were used as a baseline control.

qRT–PCR

Human macrophage RNA was isolated using the Qiagen RNeasy Micro and UCP Micro kits following the manufacturer's protocol (statin pre-treatment experiments) or a modified procedure (all other experiments). Briefly, for the modified procedure 1 ml of macrophage TRIzol/TRI Reagent (Thermo Scientific/Sigma) lysates were mixed with 230 μl of chloroform, shaken for 15 s, allowed to separate for 3 min and centrifuged at 13,400 g, 4 °C for 15 min. The upper phase was collected and mixed with an equal volume of 70% ethanol before following the manufacturer's instructions, except 8,500 and 12,000 g centrifugations were used and the RNA was eluted twice using the same water first applied to each sample. The mouse BMDM RNA was isolated using the ReliaPrep™ RNA Miniprep Systems kit (Promega, following the manufacturer's instructions). RNA concentration and purity were measured using the NanoDrop 1000 spectrophotometer (Thermo Scientific). Human cDNA was prepared using the iScript™ cDNA Synthesis Kit (Bio–Rad) while the mouse cDNA was prepared using the Precision nanoScript2™ Reverse Transcription kit (PrimerDesign) following the manufacturers protocol.

cDNA was loaded with specific SYBR primer pairs (Sigma/IDT, **supplementary table 1**) and KAPA Biosystems SYBR FAST qPCR Master Mix (ABI PrismPrecision) at a total volume of 10 μl/well or Plus SYBR Green master mix (PrimerDesign) at a total volume of 10.6 μl/well in triplicate wells on a 384–well plate (STARLAB). Measurements were taken using the ABI 7900 or the Bio–Rad CFX384 system. Gene expression was calculated relative to *GAPDH* and where appropriate to the control condition and expressed as $\log_2$FC ($-\Delta$Ct and $-\Delta\Delta$Ct respectively).

Immunocytochemistry

MDMs were fixed with 4% (w/v) paraformaldehyde–PBS (Sigma) for 30 min, permeabilised with 0.1% (v/v) Triton X–100–PBS (Sigma) for 15 min and blocked with 2% (w/v) BSA–PBS for 45 min. 1:50 dilution (1 or 4 μg/ml, batch dependant) of anti-human FAM26F rabbit polyclonal (Novus NBP1–86754 or Sigma–Aldrich HPA017948) or the same concentration of IgG isotype control (Invitrogen 10500C or Vector I–1000) in 1% BSA–PBS were added and incubated overnight at 4 °C. All wells were then incubated with 2 μg/ml goat anti–rabbit AlexaFluor–647 (Abcam ab150079) in 1% BSA–PBS in the dark for 1 h. Coverslips were mounted using the ProLong Gold Antifade Mountant with DAPI (Life Technologies). Images were taken using the

Leica AF6000 microscope. Fluorescence signal intensities were adjusted using LAS AF Lite (v 2.6.3, Leica). Integrated densities of regions of interest (cells) were measured in Fiji/ImageJ (v 1.50f).

siRNA knockdown

Day 7 MDMs were treated in fresh media for 24 h with 28 nM of siRNA (Dharmacon) in Viromer Green (Lipocalyx) following the manufacturer's protocol. The media was then changed again to polarise the cells for another 24 h.

FAM26F–3×FLAG THP–1s

Codon–optimised human FAM26F isoform 1 coding sequence (from NM_001010919.3) with a CACC at the 5' end and without the STOP codon at the 3' end was purchased from IDT gBlocks and inserted into a pENTR/D vector (Thermo Fisher) following the manufacturer's protocol using high–competency *E. coli* (NEB). The plasmid was purified using a Miniprep kit (Sigma) and insert size and sequence were confirmed by EcoRV + NotI restriction digest and Sanger sequencing. A 3×FLAG tag was cloned into the vector by PCR amplifying the tag from a previously validated plasmid, recombined using the In-Fusion HD Cloning kit (Clonetech) and validated by Sanger sequencing. The control plasmid did not contain the FAM26–3×FLAG construct.

The construct was sub-cloned in into the PE1A plasmid followed by gateway transfer into the lentiviral vector. In brief, HEK293 cells were transfected using Xfect (Clontech) with the viral packaging construct (pMDLg/pRRE, pRSV/REV, pMD2.G/V-SVG). Supernatants containing lentiviral particles were collected every 48 to 72 h after transfection, concentrated by LentiX concentrator (Clontech), tittered by qPCR (determination of number of transducing or infectious units/ml) on HeLa cells. Titres for control and FAM26–3×FLAG viruses were 6×10^7 TU/ml.

THP–1 cells (ATCC) were adjusted to a concentration of 1×10^6 cells/ml, for gene transduction, duplicate wells of a flat bottom 96-well plate were seeded with 0.1 ml/well of the cell suspension (1×10^6 cells/ml) and virus was added in the presence of 6 μg/ml polybrene (Sigma); multiplicity of infection of 25 was routinely used in most experiments. Cells were then incubated overnight with the virus and the media was replaced with fresh complete media. 3 days post viral infection, cells were selected for in 2 μg/ml puromycin (Gibco)–containing complete media. The transfected cells were maintained for 3–4 weeks between 0.1 and 1×10^6 cells/ml with minimal passaging before testing for FLAG by flow cytometry (passage 6). The cells were then maintained at the same density interval or grown for co-immunoprecipitation experiments by splitting to 0.25 – 0.3×10^6 cells/ml once the density reached or exceeded 1×10^6 cells/ml.

For differentiation into macrophage–like cells, monocytic THP–1s were centrifuged at 1,000 g for 5 min and treated with 0.5 μM phorbol myristate acetate (PMA, Sigma) in fresh culture media for

3 hours at 8×10^6 cells per 75 cm^2 flask. The PMA–containing media was then discarded and replaced with fresh culture media for 21 hours. The cells were then polarised with 20 ng/ml rhIFNγ (Peprotech/Immunotools), 100 ng/ml TLR grade *E. coli* LPS (Enzo Life Sciences) for 24 hours.

Jurkat cell culture

Jurkat cells were obtained from ATCC and cultured at the same density as THP–1s, in the same media as THP–1s, but without puromycin. The cells were activated with 100 nM PMA for 20 h followed by centrifugation at 1,200 rpm for 5 min and treatment with 2 μM Ca^{2+} ionophore A23187 (Sigma C7522) for 4 hours, followed by a 20 h resting period in fresh media.

Flow cytometry

THP–1s were pelleted and then washed in PBS by centrifugation at 500 g for 5 min. Dead cells were stained with LIVE/DEAD Fixable Aqua Dead Cell stain (Invitrogen) and washed in FACS buffer (2 mM EDTA, 5% FCS, 5% HS, 0.1% NaN_3 in PBS) by centrifugation at 500 g for 5 min. CytoFix/CytoPerm (BD) was used to permeabilise and wash the cells prior to and during staining with 0.17 μg/ml anti-FLAG (rat IgG2a λ, Biolegend 637307) or isotype control (Rat IgG2a κ, BD Pharmingen 553932) APC–conjugated antibodies. Compensation was performed using Arc (Molecular Probes A10346) and UltraComp eBeads (eBioscience 01-2222-42). Measurements were taken using the LSR II cytometer (BD) and analysed in FlowJo (v 10).

Co-immunoprecipitation

Macrophage–like IFNγ+LPS control and FAM26F–3×FLAG THP–1s were collected and washed in PBS before lysis in 50 mM Hepes–NaOH (pH7.5), 100 mM NaCl, 1 mM EDTA (pH8), 0.5% Triton–X100, 10% glycerol (wash buffer) supplemented with 1% (v/v) Nonidet™ P40 (NP40, Roche), 1 mM dithiothreitol, protease inhibitors (Sigma, 1:100 dilution), 10 μg/ml RNase A. Cells were sheared using a needle and syringe before centrifugation at maximum speed for 5 min to separate the supernatants. Bradford assays (Bio–Rad) were performed following the manufacturer's protocol to quantify total protein content in the supernatants.

50 μl of FLAG–agarose beads were washed in wash buffer before blocking in wash buffer supplemented with 1% (w/v) BSA (Sigma) for 2 h at 4 °C with agitation before removal of supernatant by centrifugation at 2,500 g for 1 min and washing. Equal amounts of control and FAM26F–3×FLAG protein were loaded onto the beads and the volumes were adjusted with wash buffer, followed by incubation for 2 h at 4 °C with agitation. The unbound fraction was then removed before washing the samples in wash buffer lacking detergent or glycerol. Bound proteins were eluted in 1 M arginine (Sigma) at pH 3.5 followed by neutralisation with 1.5 M Tris–HCl at pH 8.8. Coomassie blue staining, western blotting and mass spectrometry were used to test the samples for presence of specific proteins.

Co-immunoprecipitation mass spectrometry

LC MS/MS was performed and analysed by nano-flow liquid chromatography (U3000 RSLCnano, Thermo Scientific) coupled to a hybrid quadrupole–orbitrap mass spectrometer (Q Exactive HF, Thermo Scientific). Peptides were separated on an Easy–Spray C18 column (75 µm x 50 cm) using a 2–step gradient from 97% solvent A (0.1% formic acid in water) to 10% solvent B (0.1% formic acid in 80% acetronitrile) over 5 min then 10% to 50% B over 75 min at 300 nL/min. The mass spectrometer was programmed for data dependent acquisition with 10 product ion scans (resolution 30,000, automatic gain control 1×10^5, maximum injection time 60 ms, isolation window 1.2 Th, normalised collision energy 27, intensity threshold 3.3×10^4) per full MS scan (resolution 120,000, automatic gain control 106, maximum injection time 60ms) with a 20 second exclusion time.

MaxQuant (version 1.5.2.8) software was used for database searching with the *.raw MS data file using standard settings. The data for searched against the Homo sapiens Uniprot proteome database (taxa id: 9606, downloaded 25 November 2018, 73101 entries), using the following settings: Digestion type: trypsin; Variable modifications: Acetyl (Protein N–term); Oxidation (M); fixed modifications: carbamidomethyl (C); MS scan type: MS2; PSM FDR 0.01; Protein FDR 0.01; Site FDR 0.01; MS tolerance 0.2 Da; MS/MS tolerance 0.2 Da; min peptide length 7; max peptide length 4600; max mis–cleavages 2; min number of peptides 1.

Western blotting

Human macrophages were washed with cold PBS and lysed by scraping on ice in RIPA buffer (Sigma) supplemented with protease inhibitor cocktail (Sigma) and PhosSTOP (Roche). The lysates were sonicated with a probe sonicator while on ice for 15 s and centrifuged at 10,000 g, 4 °C for 10 min. Total protein content was determined using the Pierce BCA Protein Assay Kit (Thermo Scientific). Equal amount of protein of each MDM or THP–1 co-immunoprecipitation lysate were run on a 4 – 12% Bis–Tris gel (Invitrogen) before transferring to an Immobilon–P PVDF membrane (Millipore) and blocking for 60 min in 5% (w/v) BSA– or milk–TBST (0.1% v/v) solution.

For STAT1 detection the membrane was incubated with Y701 phosphorylated (Invitrogen 33-3400, 1 µg/ml) and total STAT1 (Cell Signalling Technology 9172, 125 ng/ml) antibodies or a GAPDH antibody (Santa Cruz sc-47724, 40 ng/ml) overnight at 4 °C. Secondary antibodies (LiCor 925-32210 and 925-68071, 83.3 ng/ml) were incubated with the membranes for 60 min at room temperature before imaging on the Odyssey CLx system.

For protein detection THP–1 co-immunoprecipitation samples the membrane was incubated with one of the following primary antibodies: 60 min at room temperature anti-FLAG (Sigma F1804,

66.7 ng/ml), overnight at 4°C anti-LAT (Invitrogen, 14-9967-82, 5 µg/ml), overnight at 4°C anti-DCD (Invitrogen PA5-13677, 2 µg/ml). Secondary goat anti-mouse–HRP (Dako P0447, 500 ng/ml) or goat anti-rabbit–HRP (Dako P0448, 125 ng/ml) antibodies were incubated with the membrane for 60 min at room temperature before detection using ECL (GE Healthcare) and the Gel Doc™ XR+ imager (Bio–Rad).

Cell interaction assay

THP–1s and Jurkat cells were stained with PKH26 (Sigma) and PKH67 (Sigma) respectively before treatment with PMA. Both cell types were then differentiated and activated or polarised as described in their culture methods. Macrophage–like IFNγ+LPS control and FAM26F–3×FLAG THP–1s were co-cultured 1:1 with activated Jurkats in culture media without puromycin and imaged using the Leica AF6000 microscope. Fluorescence signal intensities were adjusted using LAS AF Lite (v 2.6.3, Leica). Overlapping or touching cells were considered as attached.

Statistical analyses

Unless otherwise stated, statistical tests were performed in GraphPad Prism (v 7.01). Paired two–tailed t test (for comparing two groups) or repeated measures/matched one–way ANOVA (for comparing more than one group) assuming Gaussian distributions and sphericity (for ANOVA) were used due to the measurements being performed on full sets of samples generated from cells of the same passage or donor in each experiment. Post tests were then carried out on addition to ANOVA to check for statistical significance. $\alpha = 0.05$ for both t test and ANOVA, the n number in each experiment represents the number of individual donors.

Results

FAM26F expressing macrophages are present in human atherosclerosis

In order to identify improved macrophage phenotype markers, we performed membrane SILAC proteomics on human *in vitro* polarised monocyte–derived macrophages (MDMs). The data showed that among proteins uniquely up–regulated in $M^{IFN\gamma+LPS}$ a tetraspanin–like protein FAM26F had the highest fold change (**table 1**). Interestingly, the expression of *FAM26F* was elevated in atherosclerotic tissue compared to adjacent macroscopically intact tissue in a previously published microarray dataset (Ayari and Bricca, 2013) (**figure 1A**). We were also able to identify $CD68^+$ macrophages that expressed FAM26F in a section of an unstable region of human carotid plaque (n = 1), particularly the vulnerable shoulder region (**figure 1B–D**). Furthermore, Kim et al. observed that in their mouse atheroma single–cell RNA–seq (Kim et al., 2018) macrophages in the interferon response cluster up–regulated expression of *Fam26f*. These data suggest that FAM26F may be a potential marker for pro-inflammatory activation of macrophages in human and mouse atherosclerosis.

FAM26F is up–regulated in IFNγ (and LPS) activated macrophages

The identification of $FAM26F^+$ macrophages in human plaques and its specific up–regulation in human primary pro-inflammatory macrophages was further investigated *in vitro*. RNA–seq results from our previous study (Baidžajevas et al., in submission 2019, see **Results chapter I**) showed unique up–regulation of *FAM26F* expression in $M^{IFN\gamma+LPS}$ inflammatory macrophages, compared to all other macrophage phenotypes (**figure 2A**). In addition, human macrophage *in vitro* exposure to statins before and during polarisation with IFNγ+LPS did not have a significant effect on *FAM26F* expression (**supplementary figure 1**). Xue et al. in their transcriptomic study observed that both IFNγ and LPS separately induced *FAM26F* expression (Xue et al., 2014). We tested the level of FAM26F upregulation by IFNγ and LPS treatment alone in our *in vitro* human macrophage model where we found that both IFNγ and LPS were capable of significantly inducing *FAM26F* expression (**figure 2B**).

Immunocytochemistry microscopy of macrophage phenotypes indicated that up–regulation of FAM26F protein was unique to $M^{IFN\gamma+LPS}$ among our polarisation conditions (**figure 2C** and **supplementary figure 2**). Interestingly, following separate treatment with IFNγ or LPS, only IFNγ significantly induced FAM26F protein expression (**figure 2D** and **supplementary figure 3**).

In order to assess whether FAM26F is specifically upregulated in inflammatory macrophages in other mammalian species, mouse bone marrow derived macrophages were activated with IFNγ+LPS. This treatment significantly and uniquely up–regulated mouse macrophage *Fam26f* expression compared to other polarisation conditions (**figure 2E**). We concluded that FAM26F

was an in vitro human pro-inflammatory macrophage maker at both transcript and protein level that could potentially be used to assess human patient and mouse model atherosclerosis samples.

FAM26F is an IFNγ and non-canonical LPS response gene

Since identifying specific up–regulation of FAM26F in pro-inflammatory macrophages we investigated which pathways were involved in activating transcription of the gene. Meanwhile, Ebihara et al. concluded that upon TLR3 stimulation with poly(I:C) mouse bone marrow derived DCs and NK cells up–regulated *Fam26f* expression via the TLR3/TICAM1/IRF3 signalling axis (Ebihara et al., 2010).

We therefore investigated whether the IFNγ receptor and TLR4 (major receptors for IFNγ and LPS, respectively) non-canonical signalling pathways induce *FAM26F* expression in our human macrophage model. Human MDMs were treated with siRNA targeting *MYD88*, *TICAM1* (canonical [NF–κB] and non-canonical TRL4 signalling pathway components respectively) or *STAT1* (downstream of IFNGR) followed by polarisation with IFNγ and/or LPS, knockdown confirmation (**figure 3A**) and assessment of the impact on FAM26F induction (**figure 3B**). Analysis showed that reduced *MYD88* expression did not significantly affect *FAM26F* induction, while *TICAM1* and *STAT1* knockdown both significantly decreased *FAM26F* expression upon activation with LPS or IFNγ (**figure 3B)**. These findings indicate that STAT1 and non-canonical TLR4 signalling are involved in induction of *FAM26F*.

FAM26F regulates STAT1 phosphorylation and chemokine expression

Our findings suggest that induction of FAM26F is associated with IFNγ signalling. We also wished to determine if FAM26F itself regulated IFNγ signalling pathways, in a potential regulatory feedback mechanism. IFNγ–induced signalling is relayed via STAT1, the activity of which in inducing transcription of target genes depends on its phosphorylation. Y701 phosphorylation is required for STAT1 to dimerise, translocate from the cytoplasm to the nucleus and bind DNA to initiate target gene transcription (Ramana et al., 2002). We speculated that FAM26F regulates STAT1 phosphorylation. We inhibited *FAM26F* expression using siRNA, activated the cells with 20 ng/ml IFN γ for 24 h and measured gene expression by qRT–PCR and protein expression by western blotting. We were able to consistently knockdown *FAM26F* gene expression in our model (95.81 ± 0.73% SEM knockdown efficiency, **figure 4A**). *FAM26F* knockdown resulted in a decreased Y701 phosphorylated STAT1 signal compared to non-targeting control siRNA treatment (**figure 4B** and **C**, n = 1). This suggests that FAM26F is regulated by, and is also able to affect, STAT1 signalling. *FAM26F* expression contributes to the regulation of STAT1 phosphorylation and therefore its ability to translocate from the cytoplasm into the nucleus to initiate gene transcription.

A previous report indicated that FAM26F is involved in NK cell activation via cell–to–cell contact by $CD8\alpha^+$ conventional DCs or macrophages, involving IFNγ and leading to reduced volume and metastases of IFNγ–sensitive tumours in mice (Ebihara et al., 2010, Kasamatsu et al., 2014). We therefore tested if FAM26F is involved in regulating the expression of chemokines, which are known chemoattractants and activators of lymphocytes and in many cases are known to be regulated by IFNγ/IFNGR/STAT1. We observed in human MDM that *FAM26F* siRNA knockdown leads to significantly reduced expression of *CCL5*, *CXCL8* and *CXCL11* (**figure 4D**–**F**), while *CXCL9* expression was not statistically significantly altered (**figure 4G**).

FAM26F interacts with LAT in pro-inflammatory THP–1 macrophages and promotes macrophage–T cell interactions

In order to gain insight into the mechanism of activation of FAM26F, we sought to identify FAM26F protein–protein interaction partners. We created a FAM26F–3×FLAG stably expressing THP–1 cell line (**supplementary figure 4**) for use in co–immunoprecipitation. Anti-FLAG beads were used on control and FAM26F–3×FLAG IFNγ+LPS THP–1 lysates to precipitate FAM26F and interacting proteins in two separate experiments (**figure 5A**). We identified peptides of 25 human proteins unique to FAM26F–3×FLAG samples that were shared between the two experiments (**table 2**). Out of these proteins some were of particular interest due to their function and cellular localisation: dermcidin (DCD) among its other functions displays anti-microbial activity (Schittek et al., 2001) and linker for activation of T cells (LAT) is an adapter protein involved in lymphocyte activation (Fuller and Zhang, 2009, Sommers et al., 2004). We were able to confirm interaction of LAT, but not DCD with FAM26F–3×FLAG (n = 1, **figure 5B** and **C**).

Since LAT may provide a linker for macrophage–lymphocyte interactions, and because Fam26f has been implicated in dendritic/macrophage to NK cell interactions (Ebihara et al., 2010, Kasamatsu et al., 2014), we wished to determine whether the FAM26F/LAT expression influences macrophage–lymphocyte binding. We therefore co-cultured fluorescently labelled human T-cells with macrophages, with or without overexpression or knock down of FAM26F. We applied PHK-labelled differentiated Jurkat T cells to differentiated and IFNγ+LPS polarised THP–1 cells overexpressing FAM26F–3×FLAG construct (or control THP-1s). The interaction between THP-1 and Jurkat cells was assessed using fluorescence microscopy and analysed by quantifying cells under contact (**figure 5D**). A higher proportion of Jurkat cells interacted with THP–1s overexpressing FAM26F–3×FLAG compared to control THP-1 cells (**figure 5E**). These data suggest that FAM26F functions in human myeloid and lymphocyte cell lineage interaction due to its association with proteins known to be involved in the process as well as increased proportion of lymphocyte–like cells attaching to FAM26F overexpressing macrophage–like cells upon pro-inflammatory activation.

Discussion

Pro-inflammatory macrophages are an integral part of chronic inflammatory disease progression. In atherosclerosis such cells have long been associated with elevated plaque instability and therefore risk of severe complications. Numerous marker transcripts and proteins have been used to identify pro-inflammatory macrophages in pathologies, but without thorough validation even *in vitro* for polarisation specificity, up–regulation at transcript and protein level, protein localisation to membrane and use across species.

We have identified a novel human pro-inflammatory macrophage marker FAM26F, increased expression of which was specific to $M^{IFN\gamma+LPS}$ at both transcript and protein level. These findings are in agreement with previously published human macrophage transcriptomes (Xue et al., 2014) and proteomics for $M^{IFN\gamma}$ (Brown et al., 2010). We also showed that mouse $M^{IFN\gamma+LPS}$ increased expression of Fam26f compared to M^{un}, while M^{IL-4} and M^{IL-10} did not. In addition, in their mouse atheroma live $CD45^+$ single cell RNA–seq study Kim et al. observed that cells with higher expression of *Fam26f* also displayed increased expression of interferon–stimulated genes (Kim et al., 2018). We were able to identify $CD68^+$/$FAM26F^+$ cells in human carotid artery atherosclerosis and show that human macrophage *in vitro* exposure to simvastatin or atorvastatin did not significantly alter *FAM26F* expression. We therefore propose that FAM26F could be used as a new marker across mouse model and human atherosclerosis to identify pro-inflammatory macrophages.

Similarly to published literature on mouse smooth muscle cells (Chmielewski et al., 2014), we concluded that STAT1 was involved in regulating *FAM26F* expression upon human macrophage stimulation with IFNγ as well as showed that TICAM1 participated in *FAM26F* induction upon LPS challenge. Involvement of murine Ticam1 in induction of *Fam26f* gene expression in DCs and macrophages stimulated with poly(I:C) has been shown before (Ebihara et al., 2010, Kasamatsu et al., 2014). However, following stimulation with poly(I:C) mouse *Ifnar1* (part of the IFNα/β receptor) splenocytes failed to up–regulate expression of *Fam26f* (levels similar to unstimulated), while *Ticam1* or *Irf3* (downstream of *Ticam1*) knockout splenocytes up–regulated *Fam26f* expression to a similar or lower level, respectively (Kasamatsu et al., 2014). Further studies are needed to elucidate if potential involvement of type I IFN signalling in FAM26F induction (especially *in vivo*) is shared among myeloid cells and different activating molecules or is specific to stimulation with double–stranded RNA and its mimics. Interestingly, FAM26F knockdown using siRNA resulted in a lower proportion of STAT1 phosphorylated at Y701, indicating that FAM26F may be involved in a feedback loop that regulates phosphorylation and therefore transcriptional activity of STAT1.

Furthermore, we observed significantly lower expression of *CCL5*, *CXCL8* and *CXCL11* in our FAM26F siRNA knockdown human macrophages. All three genes encode chemokines, which function in leukocyte recruitment, and *CXCL11* in particular is an IFNγ–inducible gene (Griffith et al., 2014, Tokunaga et al., 2018). Regulation of these and other leukocyte attractants could be an additional mechanism of FAM26F bridging innate and adaptive immunities to the previously shown mouse antigen presenting cell–to–cell activation of NK cells to control IFNγ–sensitive tumours (Ebihara et al., 2010, Kasamatsu et al., 2014). Also, in our experiments on macrophage–like IFNγ+LPS FAM26F–3×FLAG THP–1s, FAM26F co-precipitated with LAT (involved in T cell activation) and we are currently performing similar experiments to confirm this finding using our THP–1 cells and Jurkat cells (T cell line). We also used both cell lines to show that increased FAM26F expression in THP–1 macrophages resulted in a higher percentage of Jurkat cells attaching to them compared to the control THP–1 cells. These findings build upon the reports published by Ebihara et al. and Kasamatsu et al. (Ebihara et al., 2010, Kasamatsu et al., 2014) by showing that similarly to mouse cells FAM26F may also be involved in regulating human myeloid and lymphocyte cell interactions.

Our data support the notion that FAM26F could be used in a panel of markers for detection of pro-inflammatory macrophages in research and diagnostics of cardiovascular disease. Future studies should focus on identifying the function of FAM26F, particularly in the interplay between innate and adaptive immunities in chronic inflammatory diseases as well as acute infections, which have been proposed as a risk factor contributing to late stage atheroma destabilisation. Following this FAM26F could be exploited as a new drug target in limiting or enhancing leukocyte recruitment and activation.

Conflict of interest

No conflict of interest.

Financial support

This work was supported by: the Biomedical Research Council (BMRC), Agency for Science, Technology and Research (A*STAR) Research Attachment Programme to HLW, EKT and SCW to support EH and KB; the Royal Embassy of Saudi Arabia, Cultural Bureau to support RA; the University of Sheffield and the NIHR Sheffield Biomedical Research Centre (BRC) / NIHR Sheffield Clinical Research Facility (CRF) to SEF, EKT and JNR to support KK; BL is part of the SIgN Immunomonitoring platform (supported by a BMRC IAF 311006 grant, BMRC transition funds #H16/99/b0/011, BMRC IAF-PP H1901a0024 grant and NRF SIS NRF2017_SISFP09 grant); LMC was funded by a Marie Sklodowska Curie ITN (721532) award from the European Union.

Author contributions

Conception and design: HLW, EKT, SCW, SEF, JNR, MJD, AM. Performed experiments: KB, RA, KK, ÉH, HLW, RMS, DK, LMC, CE. Experimental analysis: KB, RA, KK, ÉH, RMS, BL, MP, LMC, SKS, JNR, CE. Interpretation: KB, ÉH, HLW, EKT, SCW, SEF. Wrote manuscript: HLW, KB, ÉH, RA, CE. Edited manuscript: EKT, SCW.

Acknowledgements

We thank Fiona J Wright and Jonathan Kilby for technical support.

References

AYARI, H. & BRICCA, G. 2013. Identification of two genes potentially associated in iron-heme homeostasis in human carotid plaque using microarray analysis. *Journal of Biosciences,* 38**,** 311-315.

BROWN, J. N., WALLET, M. A., KRASTINS, B., SARRACINO, D. & GOODENOW, M. M. 2010. Proteome bioprofiles distinguish between M1 priming and activation states in human macrophages. *Journal of Leukocyte Biology,* 87**,** 655-662.

CHMIELEWSKI, S., OLEJNIK, A., SIKORSKI, K., PELISEK, J., BLASZCZYK, K., AOQUI, C., NOWICKA, H., ZERNECKE, A., HEEMANN, U., WESOLY, J., BAUMANN, M.& BLUYSSEN, H. A. R. 2014. STAT1-Dependent Signal Integration between IFN gamma and TLR4 in Vascular Cells Reflect Pro-Atherogenic Responses in Human Atherosclerosis. *Plos One,* 9.

COCHAIN, C., VAFADARNEJAD, E., ARAMPATZI, P., PELISEK, J., WINKELS, H., LEY, K., WOLF, D., SALIBA, A. E. & ZERNECKE, A. 2018. Single-Cell RNA-Seq Reveals the Transcriptional Landscape and Heterogeneity of Aortic Macrophages in Murine Atherosclerosis. *Circulation Research,* 122**,** 1661-1674.

EBIHARA, T., AZUMA, M., OSHIUMI, H., KASAMATSU, J., IWABUCHI, K., MATSUMOTO, K., SAITO, H., TANIGUCHI, T., MATSUMOTO, M. & SEYA, T. 2010. Identification of a polyI:C-inducible membrane protein that participates in dendritic cell-mediated natural killer cell activation. *Journal of Experimental Medicine,* 207**,** 2675-2687.

FULLER, D. M. & ZHANG, W. 2009. Regulation of lymphocyte development and activation by the LAT family of adapter proteins. *Immunological Reviews,* 232**,** 72-83.

GRIFFITH, J. W., SOKOL, C. L. & LUSTER, A. D. 2014. Chemokines and Chemokine Receptors: Positioning Cells for Host Defense and Immunity. *Annual Review of Immunology, Vol 32,* 32**,** 659-702.

HUANG, W.-C., SALA-NEWBY, G. B., SUSANA, A., JOHNSON, J. L. & NEWBY, A. C. 2012. Classical Macrophage Activation Up-Regulates Several Matrix Metalloproteinases through Mitogen Activated Protein Kinases and Nuclear Factor-kappa B. *Plos One,* 7.

HUBNER, N. C., REN, S. & MANN, M. 2008. Peptide separation with immobilized pI strips is an attractive alternative to in-gel protein digestion for proteome analysis. *Proteomics,* 8**,** 4862-4872.

KASAMATSU, J., AZUMA, M., OSHIUMI, H., MORIOKA, Y., OKABE, M., EBIHARA, T., MATSUMOTO, M. & SEYA, T. 2014. INAM Plays a Critical Role in IFN-gamma Production by NK Cells Interacting with Polyinosinic-Polycytidylic Acid-Stimulated Accessory Cells. *Journal of Immunology,* 193**,** 5199-5207.

KIM, K., SHIM, D., LEE, J. S., ZAITSEV, K., WILLIAMS, J. W., KIM, K. W., JANG, M. Y., JANG, H. S., YUN, T. J., LEE, S. H., YOON, W. K., PRAT, A., SEIDAH, N. G., CHOI, J., LEE, S. P., YOON, S. H., NAM, J. W., SEONG, J. K., OH, G. T., RANDOLPH, G. J., ARTYOMOV, M. N., CHEONG, C. & CHOI, J. H. 2018. Transcriptome Analysis Reveals Nonfoamy Rather Than Foamy Plaque Macrophages Are Proinflammatory in Atherosclerotic Murine Models. *Circulation Research,* 123**,** 1127-1142.

MALIK, U., JAVED, A., ALI, A. & ASGHAR, K. 2017. Structural and functional annotation of human FAM26F: A multifaceted protein having a critical role in the immune system. *Gene,* 597**,** 66-75.

MURRAY, P. J., ALLEN, J. E., BISWAS, S. K., FISHER, E. A., GILROY, D. W., GOERDT, S., GORDON, S., HAMILTON, J. A., IVASHKIV, L. B., LAWRENCE, T., LOCATI, M., MANTOVANI, A., MARTINEZ, F. O., MEGE, J. L., MOSSER, D. M., NATOLI, G., SAEIJ, J. P., SCHULTZE, J. L., SHIREY, K. A., SICA, A., SUTTLES, J., UDALOVA, I., VAN GINDERACHTER, J. A., VOGEL, S. N. & WYNN, T. A. 2014. Macrophage Activation and Polarization: Nomenclature and Experimental Guidelines. *Immunity,* 41**,** 14-20.

NEWBY, A. C. 2015. Metalloproteinases promote plaque rupture and myocardial infarction: A persuasive concept waiting for clinical translation. *Matrix Biology,* 44-46**,** 157-166.

ORBE, J., FERNANDEZ, L., RODRIGUEZ, J. A., RABAGO, G., BELZUNCE, M., MONASTERIO, A., RONCAL, C. & PARAMO, J. A. 2003. Different expression of MMPs/TIMP-1 in human atherosclerotic lesions. Relation to plaque features and vascular bed. *Atherosclerosis,* 170**,** 269-276.

PARKER, B. L., PALMISANO, G., EDWARDS, A. V. G., WHITE, M. Y., ENGHOLM-KELLER, K., LEE, A., SCOTT, N. E., KOLARICH, D., HAMBLY, B. D., PACKER, N. H., LARSEN, M. R. & CORDWELL, S. J. 2011. Quantitative N-linked Glycoproteomics of Myocardial Ischemia and Reperfusion Injury Reveals Early Remodeling in the Extracellular Environment. *Molecular & Cellular Proteomics,* 10.

RAMANA, C. V., GIL, M. P., SCHREIBER, R. D. & STARK, G. R. 2002. Stat1-dependent and -independent pathways in IFN-gamma-dependent signaling. *Trends in Immunology,* 23**,** 96-101.

RAPPSILBER, J., ISHIHAMA, Y. & MANN, M. 2003. Stop and go extraction tips for matrix-assisted laser desorption/ionization, nanoelectrospray, and LC/MS sample pretreatment in proteomics. *Analytical Chemistry,* 75**,** 663-670.

SCHITTEK, B., HIPFEL, R., SAUER, B., BAUER, J., KALBACHER, H., STEVANOVIC, S., SCHIRLE, M., SCHROEDER, K., BLIN, N., MEIER, F., RASSNER, G. & GARBE, C. 2001. Dermcidin: a novel human antibiotic peptide secreted by sweat glands. *Nature Immunology,* 2**,** 1133-1137.

SOMMERS, C. L., SAMELSON, L. E. & LOVE, P. E. 2004. LAT: a T lymphocyte adapter protein that couples the antigen receptor to downstream signaling pathways. *Bioessays,* 26**,** 61-67.

STOGER, J. L., GIJBELS, M. J. J., VAN DER VELDEN, S., MANCA, M., VAN DER LOOS, C. M., BIESSEN, E. A. L., DAEMEN, M. J. A. P., LUTGENS, E. & DE WINTHER, M. P. J. 2012. Distribution of macrophage polarization markers in human atherosclerosis. *Atherosclerosis,* 225**,** 461-468.

TOKUNAGA, R., ZHANG, W., NASEEM, M., PUCCINI, A., BERGER, M. D., SONI, S., MCSKANE, M., BABA, H. & LENZ, H.-J. 2018. CXCL9, CXCL10, CXCL11/CXCR3 axis for immune activation - A target for novel cancer therapy. *Cancer Treatment Reviews,* 63**,** 40-47.

XUE, J., SCHMIDT, S. V., SANDER, J., DRAFFEHN, A., KREBS, W., QUESTER, I., DE NARDO, D., GOHEL, T. D., EMDE, M., SCHMIDLEITHNER, L., GANESAN, H., NINO-CASTRO, A., MALLMANN, M. R., LABZIN, L., THEIS, H., KRAUT, M., BEYER, M., LATZ, E., FREEMAN, T. C., ULAS, T. & SCHULTZE, J. L. 2014. Transcriptome-Based Network Analysis Reveals a Spectrum Model of Human Macrophage Activation. *Immunity,* 40**,** 274-288.

YAHAGI, K., KOLODGIE, F. D., OTSUKA, F., FINN, A. V., DAVIS, H. R., JONER, M. & VIRMANI, R. 2016. Pathophysiology of native coronary, vein graft, and in-stent atherosclerosis. *Nature Reviews Cardiology,* 13**,** 79-98.

Table 1: Unique up–regulation of proteins in $M^{IFN\gamma+LPS}$

SILAC membrane proteomics data were filtered for Wilcoxon signed–rank test $M^{IFN\gamma+LPS}$ $p < 0.05$. The data were further filtered by selecting only proteins with $M^{IFN\gamma+LPS}$ incorporation fold change > 1 in both donors (A and B) and ordered by average fold change for $M^{IFN\gamma+LPS}$. Proteins uniquely up–regulated in $M^{IFN\gamma+LPS}$ are highlighted.

No.	ID	Gene	$M^{IFN\gamma+LPS}$ p value	Fold change									
				$M^{IFN\gamma+LPS}$		M^{IL-4}		M^{IL-10}		M^{oxPAPC}		M^{CXCL4}	
				A	B	A	B	A	B	A	B	A	B
1	Q5R3K3	FAM26F	0.002	8.437	8.264								
2	P15309	ACPP	0.027	7.100	5.197		1.000		4.023	1.000	4.065	1.000	
3	P51452	DUSP3	0.047	3.204	5.484		3.175		0.687	4.076		2.775	0.764
4	P62829	RPL23	0.018	4.303	3.147					1.000		2.883	
5	B7Z779	TMEM106A	0.026	4.033	2.947	3.485	2.176					2.918	
6	Q92930	RAB8B	0.025	2.724	2.175		1.559		1.374	0.514	1.771	0.600	
7	Q6IQ22	RAB12	0.035	1.841	2.027	0.326	1.679	1.392	0.326	0.717	1.397	1.944	
8	O14879	IFIT3	0.002	1.877	1.746								
9	P18031	PTPN1	0.013	1.794	1.386					0.786		1.256	
10	P48735	IDH2	0.027	1.625	1.527	1.414	0.798	0.305	1.483	1.251	1.455	1.458	1.074
11	P32455	GBP1	0.027	1.554	1.597	1.338	0.864		0.223	0.776	1.068	1.333	
12	Q9BQE5	APOL2	0.025	1.675	1.372	0.948		0.907		1.177	1.161	1.094	
13	Q9NR31	SAR1A	0.050	1.728	1.171	1.504	0.777			0.230	0.230	0.989	1.148
14	Q03518	TAP1	0.037	1.515	1.331	0.210	1.122	0.364	0.548	1.270	1.007	1.101	1.389
15	Q9NQ34	TMEM9B	0.003	1.379	1.347								
16	P14902	IDO1	0.003	1.361	1.340								
17	Q12913	PTPRJ	0.027	1.343	1.253		1.205	0.966	0.670	0.777	1.034	1.005	
18	Q9P0S9	TMEM14C	0.016	1.410	1.145	2.697							
19	Q8WXG1	RSAD2	0.002	1.254	1.276								
20	Q96RQ9	IL4I1	0.007	1.390	1.083							1.020	
21	Q9H0D6	XRN2	0.019	1.265	1.187	1.002	0.987						
22	E9PC70	CD82	0.022	1.300	1.125		1.350			0.998			
23	Q07065	CKAP4	0.038	1.176	1.225	0.666	1.040	0.978	1.118	0.892	1.108	1.183	
24	Q9H3N1	TMX1	0.011	1.177	1.190	1.027	1.015	0.883	1.103	0.939	1.072	1.009	1.140
25	Q03405	PLAUR	0.025	1.141	1.129			0.902	0.914	0.873	1.109	0.946	
26	Q9GZP9	DERL2	0.039	1.137	1.092	0.955	0.923						
27	P04179	SOD2	0.037	1.085	1.142	0.516	1.052		1.051	0.646	0.894	0.903	0.946
28	O15243	LEPROT	0.003	1.138	1.054								
29	Q8TCU6	PREX1	0.033	1.160	1.018		0.965					0.887	

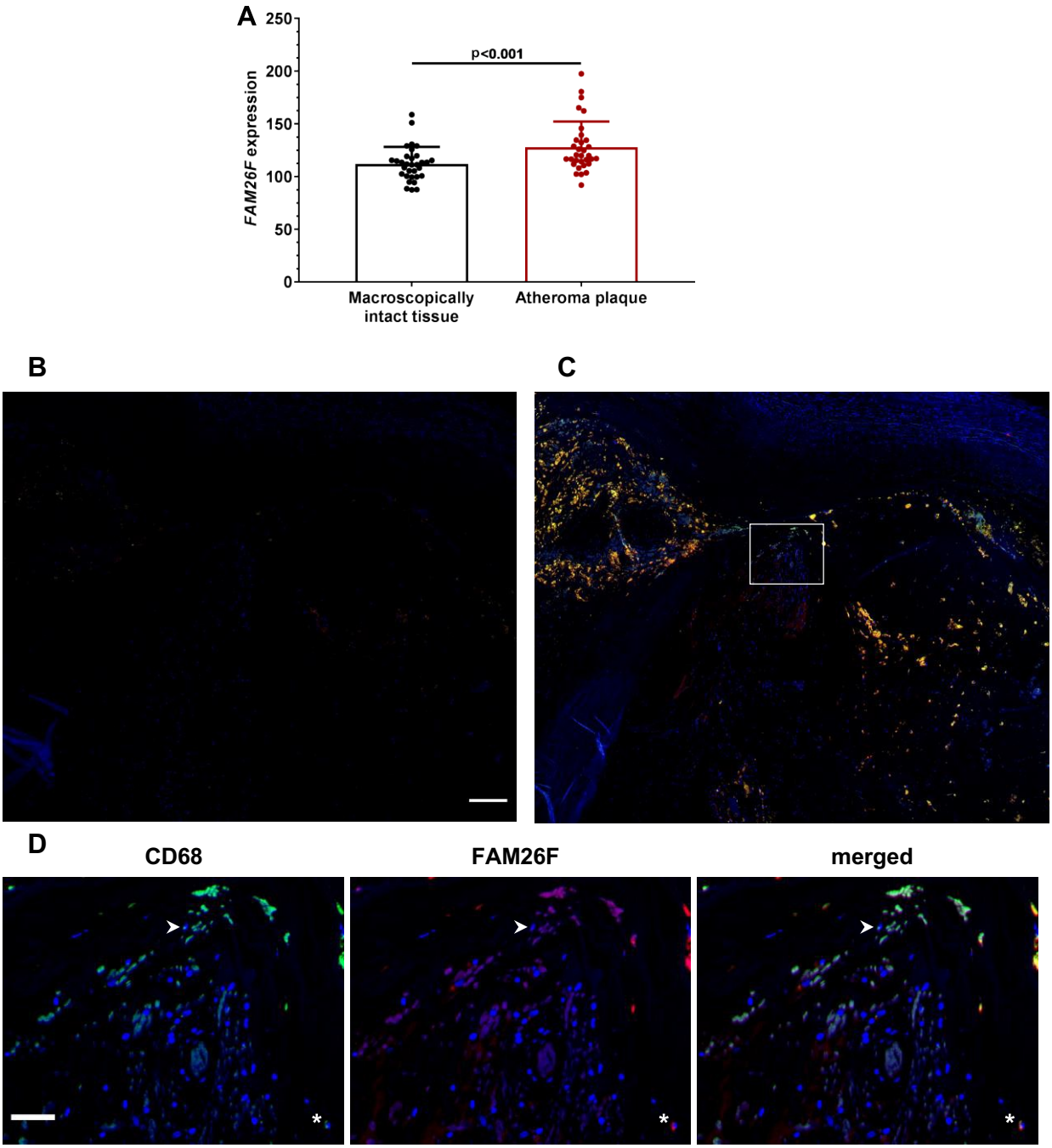

Figure 1: Macrophages express FAM26F in human atherosclerosis.
(**A**) Quantification of GSE43292 data for gene expression in macroscopically normal adjacent and carotid plaque tissue; means ± SEMs, n = 32, paired two–tailed t–test. Immunohistochemistry/immunofluorescence staining of human carotid artery plaque sections for (**B**) mouse (green) and rabbit (red) control IgG and also (**C**) CD68 (pan-macrophage marker, green) and FAM26F (red) ($CD68^{+}FAM26F^{+}$ in yellow), cell nuclei stained with DAPI (blue), scale bar represents 200 µm for both images. (**D**) Enlarged white binding box in (**C**) arrow heads indicate $CD68^{+}FAM26F^{-}$ and asterisks indicate $CD68^{+}FAM26F^{+}$; scale bar represents 50 µm for all images.

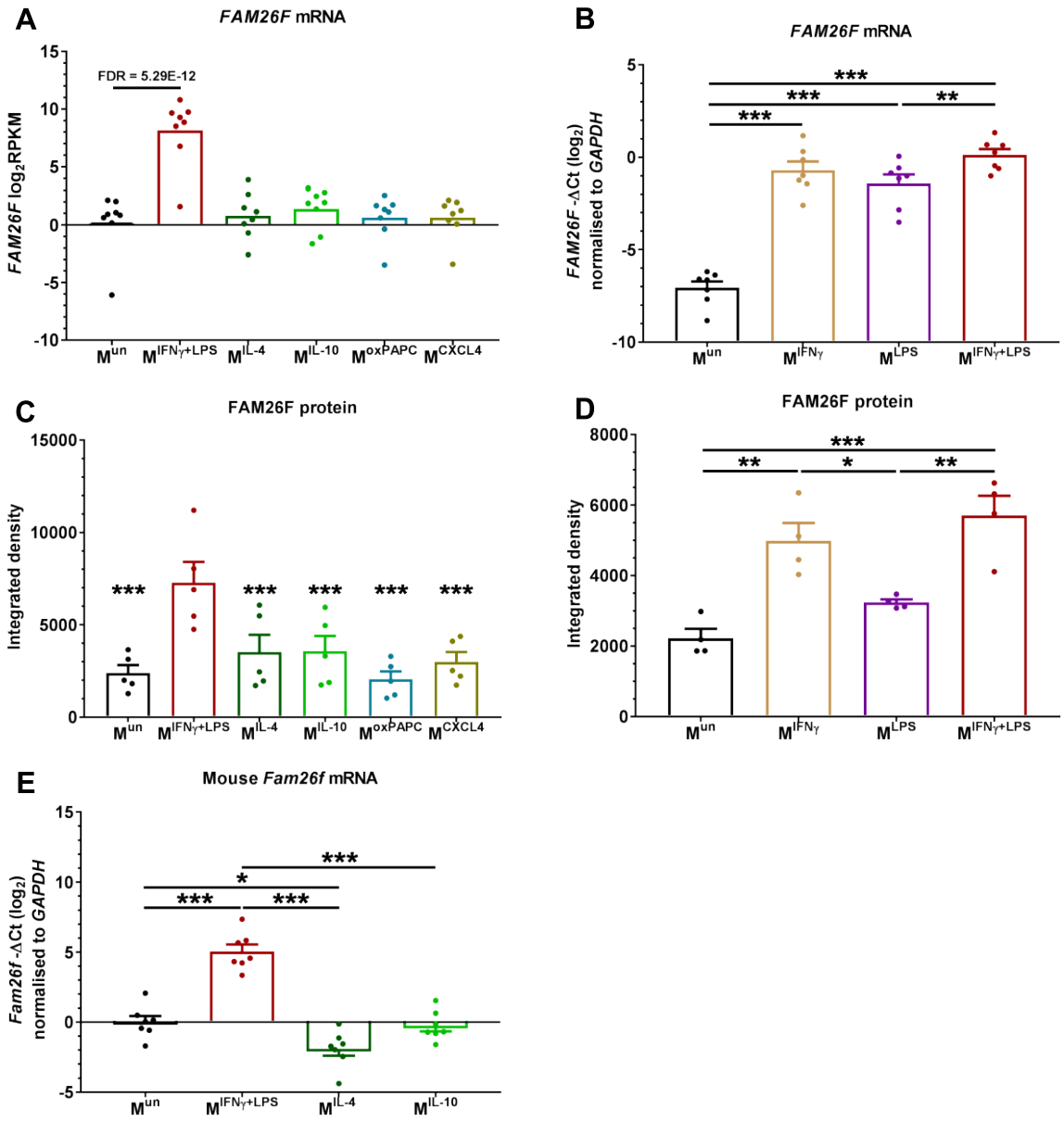

Figure 2: FAM26F is an *in vitro* marker for macrophages activated with IFNγ (and LPS).

(**A**) RNA-seq quantification of *FAM26F* expression among MDM phenotypes compared to M^{un}; n = 8, mean of RPKM (reads per kilobase [of transcript per] million [mapped reads]) and FDR (false discovery rate, Benjamini and Hochberg method) shown. (**B**) qRT–PCR quantification of *FAM26F* gene expression upon stimulation with IFNγ and/or LPS; n = 7. Pooled quantification (10 images/condition, geometric means of integrated densities from each experiment shown as data points) of FAM26F antibody staining (**C**) of MDM phenotypes (n = 5) and (**D**) of unpolarised, IFNγ and/or LPS–activated MDMs (n = 4). (**E**) qRT–PCR quantification of mouse bone marrow derived macrophage *Fam26f* gene expression; n = 7. (**B** – **E**) Means ± SEMs, matched/repeated measures one–way ANOVA with Tukey's post test * $p < 0.05$, ** $p \leq 0.01$, *** $p \leq 0.001$, only significant comparisons are shown (for **C** M^{x} vs $M^{IFN\gamma+LPS}$).

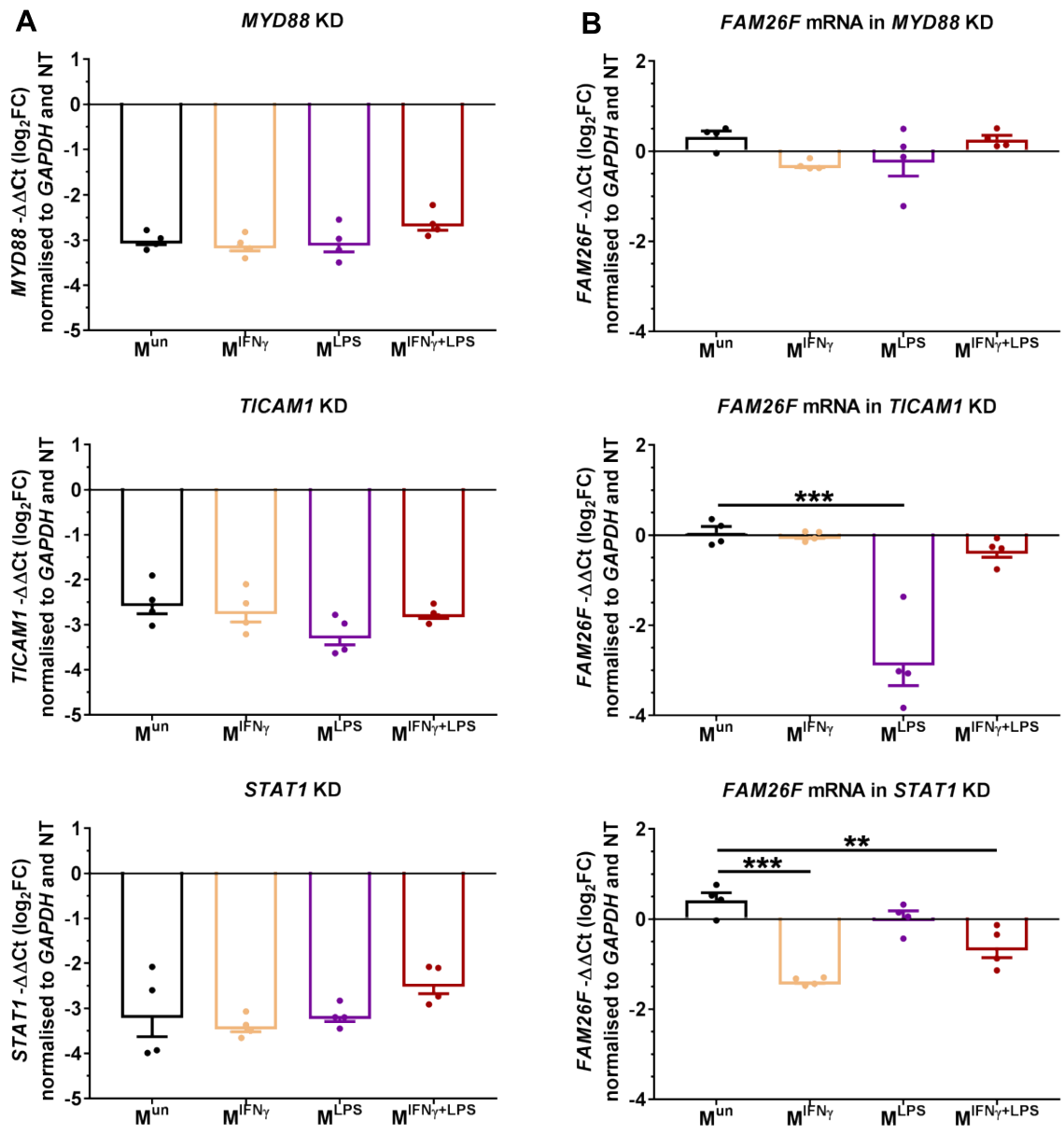

Figure 3: Induction of *FAM26F* gene expression is dependent on STAT1 and TICAM1. (**A**) qRT–PCR quantification of *MYD88*, *TICAM1* and *STAT1* gene siRNA knockdowns in differentially activated human MDMs. (**B**) qRT–PCR quantification of *FAM26F* gene expression in siRNA knockdowns of *MYD88*, *TICAM1* and *STAT1* in differentially activated human MDMs. The data were normalised to *GAPDH* and NT (non-targeting) siRNA using the -ΔΔCt method and shown here in $\log_2$; n = 4, means ± SEMs, matched/repeated measures one–way ANOVA with Dunnett's post test; ** $p \leq 0.01$ *** $p \leq 0.001$ compared to M^{un}.

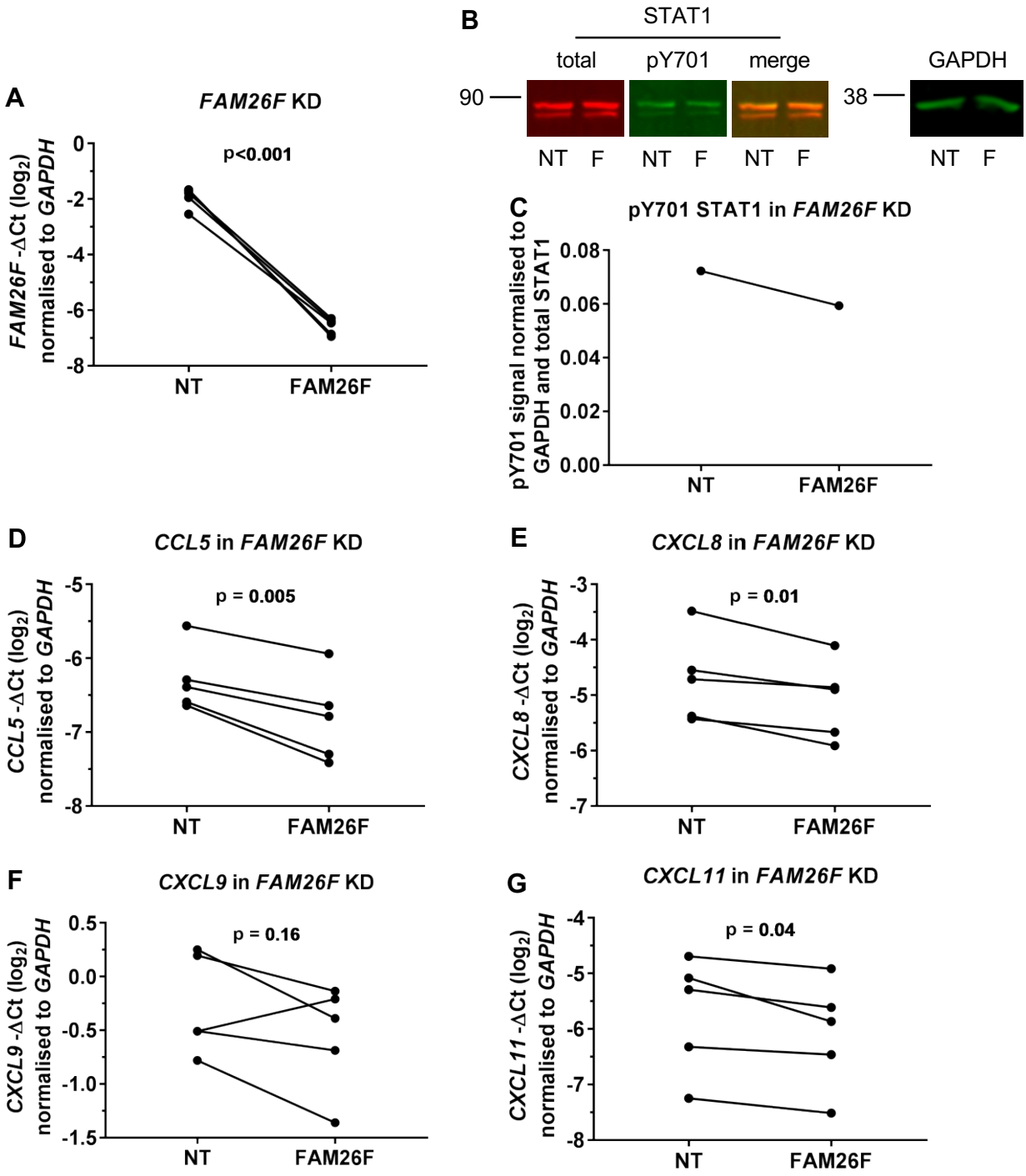

Figure 4: *FAM26F* knockdown attenuates STAT1 phosphorylation and chemokine expression.

(**A**) qRT–PCR quantification of *FAM26F* gene expression in cells treated with non-targeting (NT) or *FAM26F* siRNA, followed by activation with IFNγ. (**B**) Western blot for phosphorylated Y701 and total STAT1, GAPDH; numbers indicate molecular weight standards in kDa. (**C**) Quantification of fluorescence of phosphorylated Y701 STAT1 normalised to GAPDH and total STAT1 (n = 1). (**D**–**G**) qRT–PCR quantification of gene expression in cells treated with non-targeting (NT) or *FAM26F* siRNA, followed by activation with IFNγ. (**A** and **D**–**G**) The data were normalised to *GAPDH* using the -ΔCt method and shown here in $\log_2$; n = 5, lines connect samples from the same donor, paired two–tailed t test.

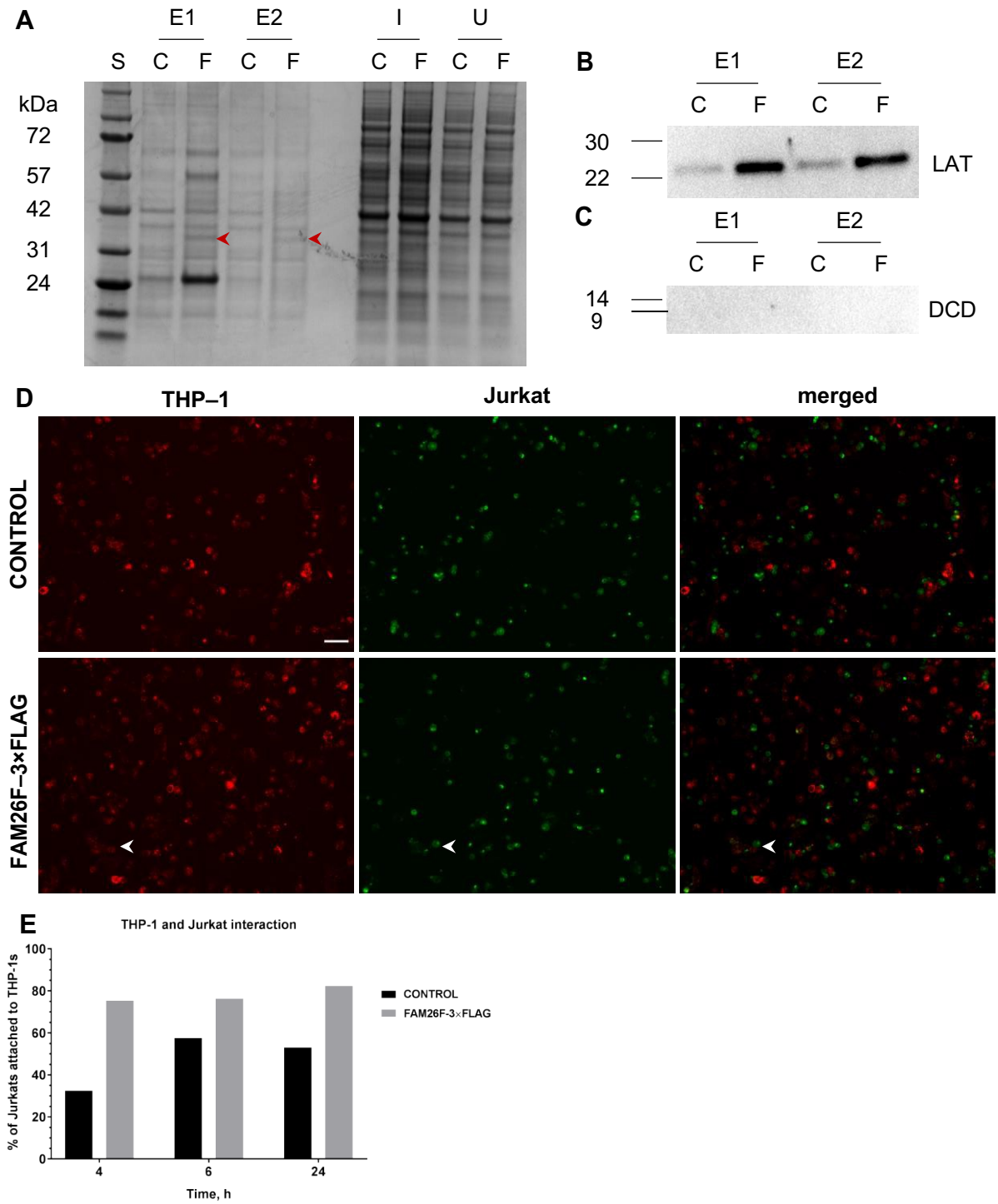

Figure 5: FAM26F regulates macrophage interaction with lymphocytes.
(**A**) Representative Coomassie Blue staining of FAM26F–3×FLAG co-immunoprecipitation; E1 – bound sample elution 1, E2 – bound sample elution 2, I – input sample lysate, U – unbound sample lysate, C – control THP–1s, F – FAM26F–3×FLAG THP–1s, S – molecular weight standards; arrow heads indicate predicted FAM26F–3×FLAG protein molecular weight (~37.3 kDa). Western blots of co-immunoprecipitation samples for (**B**) LAT (linker for activation of T cells, predicted molecular weight ~24.8 – 28.6 kDa) and (**C**) DCD (dermicidin, predicted molecular weight ~8.3 – 12.4 kDa); numbers indicate molecular weight standards in kDa, n = 1. (**D**) Representative images of THP–1 (red) and Jurkat (green) co-culture, scale bar represents 50 µm for all images, arrow head indicate THP–1 and Jurkat interaction. (**E**) Quantification of percentage of Jurkat cells attached to THP–1 cells at 4, 6 and 24 h of co-culture; means of 2 – 4 fields of view, n = 1.

Table 2: Proteins detected only in FAM26F–3×FLAG samples in both co-immunoprecipitation experiments.

UniProt IDs and names are listed for the proteins, peptides of which were detected only in FAM26F–3×FLAG samples in both experiments.

	Identifiers	Proteins
1	sp|P49748|ACADV_HUMAN; tr|G3V1M7|G3V1M7_HUMAN	Acyl-CoA dehydrogenase very long chain
2	sp|Q0VD83|APOBR_HUMAN	Apolipoprotein B receptor
3	sp|Q9BT09|CNPY3_HUMAN	Canopy FGF signaling regulator 3
4	tr|J3QKQ4|J3QKQ4_HUMAN; sp|Q9UGN4|CLM8_HUMAN	CD300a
5	sp|P81605|DCD_HUMAN	Dermcidin
6	sp|P49411|EFTU_HUMAN	Elongation factor Tu, mitochondrial
7	sp|P30040|ERP29_HUMAN; tr|F8VY02|F8VY02_HUMAN	Endoplasmic reticulum protein 29
8	tr|H0YDT8|H0YDT8_HUMAN; sp|Q9NPA0|EMC7_HUMAN	ER membrane protein complex subunit 7
9	tr|D6RBH1|D6RBH1_HUMAN; tr|D6RDX1|D6RDX1_HUMAN; tr|D6RBV2|D6RBV2_HUMAN; sp|Q12907|LMAN2_HUMAN	Lectin, mannose binding 2
10	tr|A0A1W2PQT7|A0A1W2PQT7_HUMAN; sp|O43561|LAT_HUMAN	Linker for Activation of T cells
11	sp|P29966|MARCS_HUMAN	Myristoylated alanine rich protein kinase C substrate
12	sp|P30044|PRDX5_HUMAN	Peroxiredoxin 5
13	sp|Q9UHV9|PFD2_HUMAN	Prefoldin subunit 2
14	tr|F8VR77|F8VR77_HUMAN; sp|Q9UQ80|PA2G4_HUMAN	Proliferation-associated 2G4
15	tr|A0A087WVV1|A0A087WVV1_HUMAN; sp|P49721|PSB2_HUMAN	Proteasome subunit beta 2
16	sp|P13667|PDIA4_HUMAN	Protein disulfide isomerase family A member 4
17	sp|P78527|PRKDC_HUMAN	Protein kinase, DNA-activated, catalytic subunit
18	sp|P61020|RAB5B_HUMAN	RAB5B, member RAS oncogene family
19	sp|P49792|RBP2_HUMAN	RAN binding protein 2
20	tr|J3KRE2|J3KRE2_HUMAN; tr|J3KTF8|J3KTF8_HUMAN; sp|P52565|GDIR1_HUMAN; tr|J3QQX2|J3QQX2_HUMAN	Rho GDP-dissociation inhibitor 1
21	sp|O14828|SCAM3_HUMAN	Secretory Carrier Membrane Protein 3
22	tr|A0A0C4DFV9|A0A0C4DFV9_HUMAN; sp|Q01105|SET_HUMAN; tr|A0A087X027|A0A087X027_HUMAN; sp|P0DME0|SETLP_HUMAN	SET nuclear proto-oncogene
23	sp|P08240|SRPRA_HUMAN	SRP receptor subunit alpha
24	sp|Q9Y320|TMX2_HUMAN	Thioredoxin related transmembrane protein 2
25	sp|O60763|USO1_HUMAN	USO1 vesicle transport factor

Supplementary table 1: qRT PCR primer sequences

All sequences are shown from 5' to 3' ends.

Target	Forward	Reverse
Human		
CCL5	CCTCGCTGTCATCCTCATTGC	TAGGCAAAGCAGCAGGGTGT
CD86	CCCAGACCACATTCCTTGGAT	TCCCTCTCCATTGTGTTGGT
CXCL8	CTCCAAACCTTTCCACCCCAA	ACCCTCTGCACCCAGTTTTC
CXCL9	AGTGCAAGGAACCCCAGTAGT	GTGGATAGTCCCTTGGTTGGTG
CXCL11	GTGTGCTACAGTTGTTCAAGGC	TGCTTTTACCCCAGGGCCTAT
FAM26F	GAGGGCTCGCATCCAAAAGA	GTACTGGCCCTTCGGATTGAA
GAPDH	ATTGCCCTCAACGACCACTTT	CCCTGTTGCTGTAGCCAAATTC
MYD88	TCTTGAACGTGCGGACACAG	TGTGTCTCCAGTTGCCGGAT
STAT1	CTCTGCCCGTTGTGGTGAT	GACAGATTCCTGGGTTCCGC
TICAM1	GCCACCTTCTGCGAGGATTT	CTCAGGCGACAGTCGAAGTT
Mouse		
Fam26f	CAGAAGGTGGAAATGCAGGAGAT	AGCTATCAGAATCCAACCGAAC
Gapdh	TGGCAAAGTGGAGATTGTTGCC	AAGATGGTGATGGGCTTCCCG

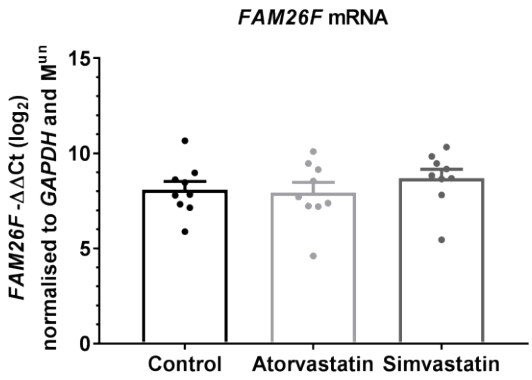

Supplementary Figure 1: Expression of *FAM26F* is not changed by atorvastatin or simvastatin.

qRT–PCR quantification of *FAM26F* expression in human MDMs pre-treated with 1μM atorvastatin or simvastatin 4 h before polarisation in fresh media containing both the statin and IFNγ+LPS. The data were normalised to *GAPDH* and M^{un} using the -ΔΔCt method and shown here in log_2; means ± SEMs, n = 9, matched/repeated measures one–way ANOVA with Dunnett's post test of atorvastatin or simvastatin vs control cells (no statin in the pre-treatment or the IFNγ+LPS polarisation), both comparisons were not significant.

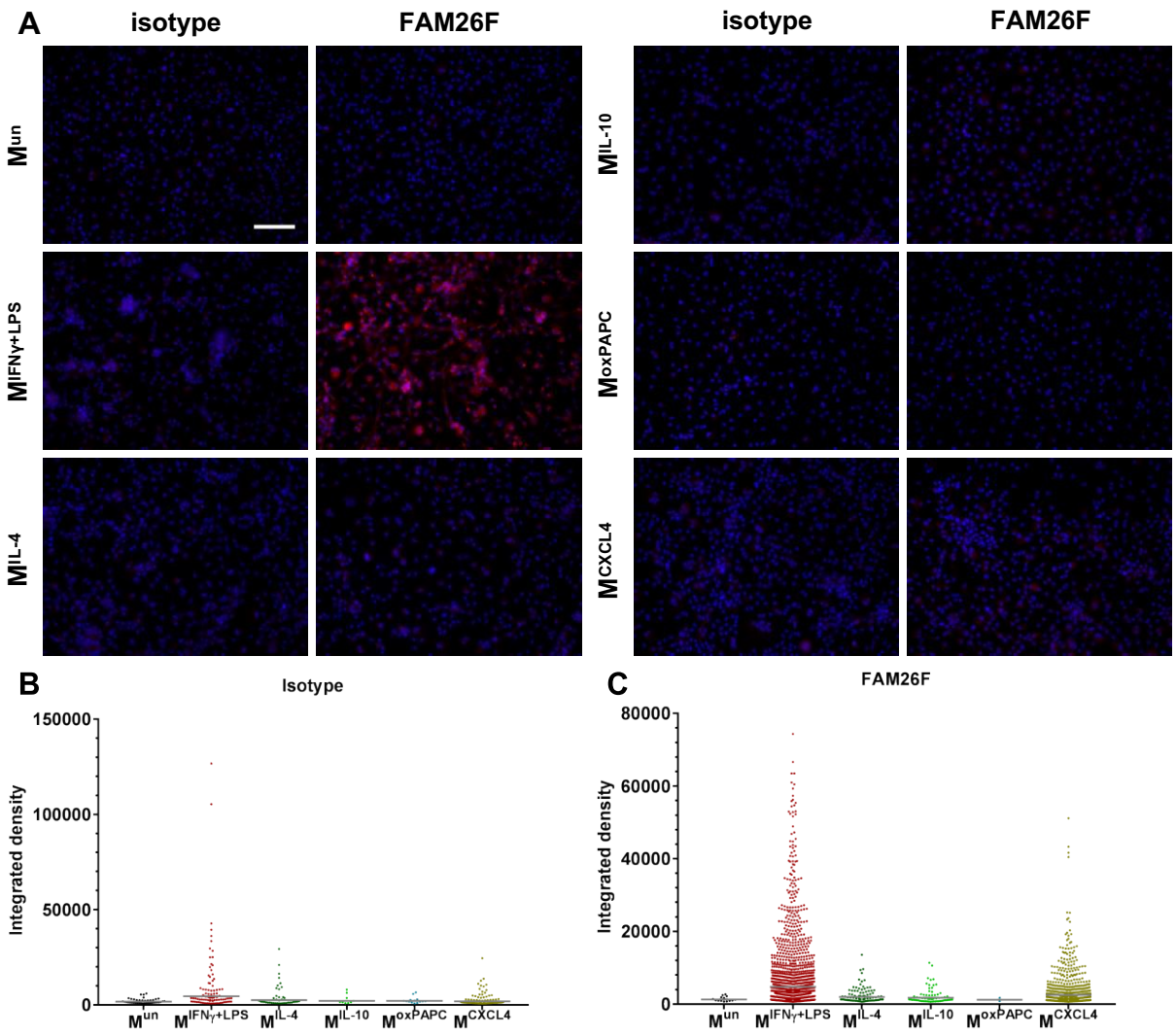

Supplementary figure 2: Representative images and quantification of FAM26F in MDM phenotypes.

(**A**) Representative images of one donor cell staining with DAPI (blue) or isotype/FAM26F antibodies (red), scale bar represents 100 µm for all images. Quantification of (**B**) isotype and (**C**) FAM26F antibody staining in the representative experiment shown; 10 images/condition, geometric means indicated.

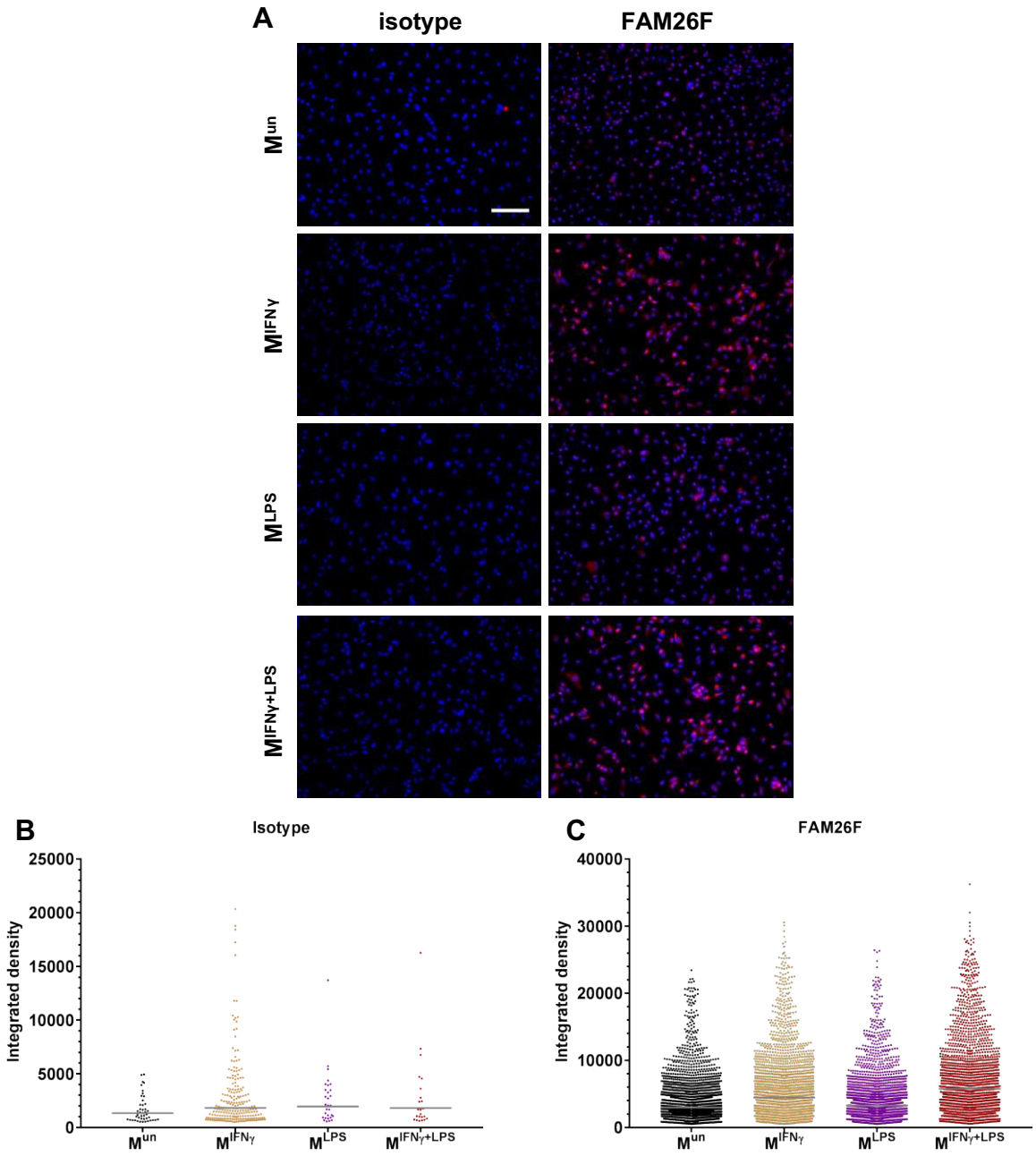

Supplementary figure 3: Representative images and quantification of FAM26F in MDMs activated with IFNγ and/or LPS.

(**A**) Representative images of one donor cell staining with DAPI (blue) or isotype/FAM26F antibodies (red), scale bar represents 100 µm for all images. Quantification of (**B**) isotype and (**C**) FAM26F antibody staining in the representative experiment shown; 10 images/condition, geometric means indicated.